DOCTOR OF PHILOSOPHY

Studies of the dye sensitization of inorganic colloids used in dye-sensitized solar cells

Al-Salihi, Kareem Jumaah Jibrael

Award date:
2013

Awarding institution:
Bangor University

Studies of the dye sensitization of inorganic colloids used in dye-sensitized solar cells

By

Kareem Jumaah Jibrael Al-Salihi

A thesis submitted in fulfilment of the requirements for the degree of Doctor of Philosophy in Bangor University

PhD supervisor - Dr Peter Holliman

PRIFYSGOL
BANGOR
UNIVERSITY

1884

March 2013

Acknowledgements

I would like to express my deep and sincere gratitude to my advisor Dr Peter J. Holliman. He has been the guide in my PhD study for the past several years. His wide knowledge and creativity in science have been of great value to me.

I have to thank the post post doctorates Dr Mathew Davies, Dr Arthur Connil and Dr Eurg for their enormous help when I stepped into this new research domain they taught me a lot in setting up the experiments, operating instruments and explanation the science of results.

I would also like to thank all my friends and colleagues with whom I have had the pleasure to meet and work at the laboratory.

I am also very thankful to the all the technician in school of chemistry, namely Mr Gwynfor Davies , Mr Denis Williams, Mr Nicholas Welsby and Mr Glynne Evans , for allowing me to use the laboratory facilities and resources.

Additionally, I would like to thank Iraqi government especially Ministry of Higher Education and scientific research for supporting me financially to this scholarship.

List of abbreviation

PV	Photovoltaic
DSC	Dye-sensitized solar cell
AM 1.5G	Air Mass 1.5 Global
TCO	Transparent Conductive Glass
FTO	Fluorine-doped Tin Oxide ($F:SnO_2$)
CB	Conduction Band
DSL-18NRT	Titania paste from Dyesol containing ~ 20 nm particles
HOMO	Highest Occupied Molecular Orbital
LUMO	Lowest Unoccupied Molecular Orbital
J-V	Current-Voltage Characteristics
η	Conversion Efficiency power
FF	Fill Factor
J_{sc}	Short-Circuit Current
V_{oc}	Open-Circuit Voltage
NIR	Near-infrared
E_f	Fermi Level Energy
pKb	Base Dissociation Constant
Q_e	Amount of Adsorption
C_e	Equilibrium Concentration
q_{max}	Maximum Amount of adsorption
K_l	Langmuir Constant
K_f and n	Freundlich Constants

Publications

Work in this thesis has been included in the following patent, journal paper and conference proceedings:-

"Method for re-dyeing dye sensitized solar cells", P.J. Holliman, K. Al-Salihi, M. Davies, A. Connell, UK patent GB1201336.3. Filed on 26th January 2012. PCT/GB2013/050171. Filed on 25th January 2013.

"Ultra-fast Co-Sensitization and Tri-Sensitization of Dye-Sensitized Solar Cells with N719, SQ1 and Triarylamine Dyes", P.J. Holliman, M. Mohsen, A. Connell, M.L. Davies, K. Al-Salihi, M.B. Pitak, G.J. Tizzard, S.J. Coles, R.W. Harrington, W. Clegg, C. Serpa, O.H. Fontes, C. Charbonneau, M.J. Carnie, *J. Mat. Chem.*, 2012, **22**(26), 13318-13327.

"Increasing light harvesting in dye sensitized solar cells", P.J. Holliman, M.L. Davies, A. Connell, M. Mohsen, K. Al-Salihi, D. Al-Husenawi, E. Jones, Paper in *Conf. Proceedings - 8th Photovoltaic Science, Applications and Technology Conference – PVSAT-8*, 2-4th April 2012, Northumbria University, Newcastle.

"Low Cost Photovoltaics with "Go Faster" Stripes", P.J. Holliman, E.W. Jones, A. Connell, M. Mohsen, K. Al-Salihi, M.L. Davies, Paper in *Conf. Proceeding - 9th Photovoltaic Science, Applications and Technology Conference – PVSAT-9*, 10-12th April 2013, Swansea University.

Abstract

This thesis involves studies of dye sensitization of dye-sensitized solar cell (DSC) devices using ultra-fast dyeing and ultra-fast desorption. The work includes studies of adsorption isotherms, uptake kinetics and the development of a new method for dye adsorption, desorption and re-dyeing.

The development of a new method of adsorption, desorption and re-dyeing of devices using different desorption solutions with the aim of developing precise dye loading control for different sensitizers. Initially the adsorption of the Ru(II) complex (N719) and the organic dye (SQ1) have been studied on TiO_2 films and the data modelled using Langmuir and Freundlich isotherms. The adsorption data were best represented by the Langmuir model for N719 and by the Freundlich model for SQ1. A new method of ultra-fast dyeing, desorption and re-dyeing has been developed which enables much greater control over dye loading than is possible by passive dyeing. It has been shown that one device can be dyed, desorbed and re-dyed use more than ten times giving the similar performance to the first dyeing. Different alkaline solutions have been tested for desorbing N719 from TiO_2 such as LiOH, NaOH, KOH, Bu_4NOH and *tris*-(hydoxymethy)ethylamine prior to device re-dyeing. Ultra-fast desorption by Bu_4NOH and re-dyeing with the same dyes and also with different dyes has been successfully achieved. The method has been developed to control dye loading by partial dye removal using varying volumes or concentration of Bu_4NOH. A new procedure for the selective removal of dyes has also been developed; N719 by LiOH, SQ1 by dilute Bu_4NOH and D149 by concentrated Bu_4NOH followed by acetone and ethanol. This method has been used to change dyes on the surface and also to quantify dye adsorption in DSC devices.

Ultra-fast co-sensitization of TiO_2 with more than two dyes (N719 plus various organic dyes) using sequential or multiple dyeing on P25 and commercial DSL18NR-T TiO_2 films have been also studied. Sequential ultra-fast co-sensitization with new yellow triphenylamine dye (YD) and N719 yielded η 7.5% which is higher than the individual dyes. Multiple dyeing from a mixed 6% SQ1:N719 solutions gave η 7.1% which is also higher than for the corresponding individual dyes. The best ratio for mixing N719: D149 is 1:3 v/v which yielded η = 8.2%. Co-sensitization with three dyes and four dyes

has been also studied and the devices show improved efficiencies compared to the respective individual dyes.

The rates of adsorption of dyes from mixed dye solutions were studied on TiO_2 using the selective desorption methods developed in chapter three. The kinetics of the adsorption of yellow triphenylamine dye (YD) were studied using ultra-fast and passive dyeing. The results show that adsorption of YD by passive dyeing follows a pseudo second order kinetic model with a rate constant of 9.8×10^{-5} $cm^2.\mu g^{-1}.min^{-1}$ with the TiO_2 surface reaching saturation in *ca.* 350 min. However, ultra-fast dyed YD followed a pseudo-first order model with a rate constant of 11.16×10^{-2} min^{-1} and the surface was reached saturation in 10 min. The experimental data for the ultra-fast co-adsorption of mixed YD: N719 solutions shows YD data can be modelled by both pseudo first order and pseudo second order models but that N719 best fitted with a pseudo first order model. The kinetics adsorption of mixed 5% SQ1:N719 solutions also were studied and the results show both dyes followed both pseudo-first order and pseudo second order models. The effect of dyeing time on the IV device data have also been studied showing that efficiency and photo-current increased with increasing dye loading presumably reflecting higher electron injection into the TiO_2 conduction band.

Table of Contents

Chapter One Introduction

1.1 Area of Study

The work in this PhD thesis is associated with three main areas of research: i) controlling multiple dye loading through the development of a novel method of desorbing and re-dyeing the photo-electrode for dye sensitized solar cells (DSCs) ii) studies of the ultra-fast co-sensitization of TiO_2 photo-electrodes for DSCs and iii) kinetic studies of the co-adsorption of sensitizers on TiO_2 surfaces for DSC devices.

DSCs have been under extensive research since 1991 when a conversion efficiency of 7.1% was first reported.[1] Among the many methods and strategies to optimize DSC efficiency is maximising light harvesting capacity from the visible to the near infrared region of the visible spectrum. Dye-sensitized solar cells are currently the subject of extensive research in the area of renewable energies as low cost photovoltaics. This thesis, contributes to the study and development of a new method for adsorption, desorption and re-dyeing in dye-sensitized solar cells (DSC) devices using ultra-fast dyeing and ultra-fast desorption.

1.2 Introduction of renewable solar energy

The global human population is increasing and this increase is predicted to continue for the foreseeable future.[2] Energy demands are also increasing in all areas of life (e.g. heating, cooling and transportation etc). The demand for the generation electricity is also increasing.[3] In this context, there are two main types of energy sources. Non-renewable energy generally derives from underground sources (e.g. fossil fuels such as coal, oil, natural gas, and nuclear energy).[4] The main disadvantages of non-renewable sources are that they will expire at some point in the future and also that fossil fuels can produce wastes (e.g. $CO_{2(g)}$) which can cause global warming and severe environmental changes.[5] Finally, the prices of fossil fuel energy sources have increased in recent times and this trend is predicted to continue.[6] The other sources of energy are renewable-energy sources. These are produced directly from nature, such as sunlight, wind, tides and geothermal energy.5 The world is increasingly trying to move towards renewable-energy sources because

these avoid the need to rely on any one country to supply raw materials and also they are never going to run out.5 Renewable energy sources can be used in many ways such as large scale applications for heating, cooling and the production of electricity.[7] While energy is necessary to whole areas of life, most primary sources used at present are unsustainable, whilst renewable energy has great potential to meet current and future demands for power.[8] Renewable energy could also play an important role in reducing other pressing problems such as energy security which is a multidimensional concept, including external as well as internal action that is more than sustainability competitiveness and secure supply.7 Figure 1.1 and Table 1.1 demonstrate examples of the potential and progress of renewable energy in the U.S. between 2006 and 2010. Thus, renewable energy consumption rose by 6% to over 8% quadrillion Btu (British Thermal units) from 2006 to 2011 whilst total U.S. energy consumption dropped slightly to nearly 98 quadrillion Btu. The data show that about 90% of the US'S energy comes from fossil fuels, 8% from nuclear, and 9% comes from renewable sources.[9] The biomass share of renewable consumption increased from 49% to 53%, wind increased from 4 to 11%, and conventional hydroelectric decreased from 43 to 31% between 2006 and 2011. Geothermal's share stayed steady at 3% of renewable energy. Likewise the solar share remained about the same at 1%, despite growing rapidly at an average annual rate of 12%.

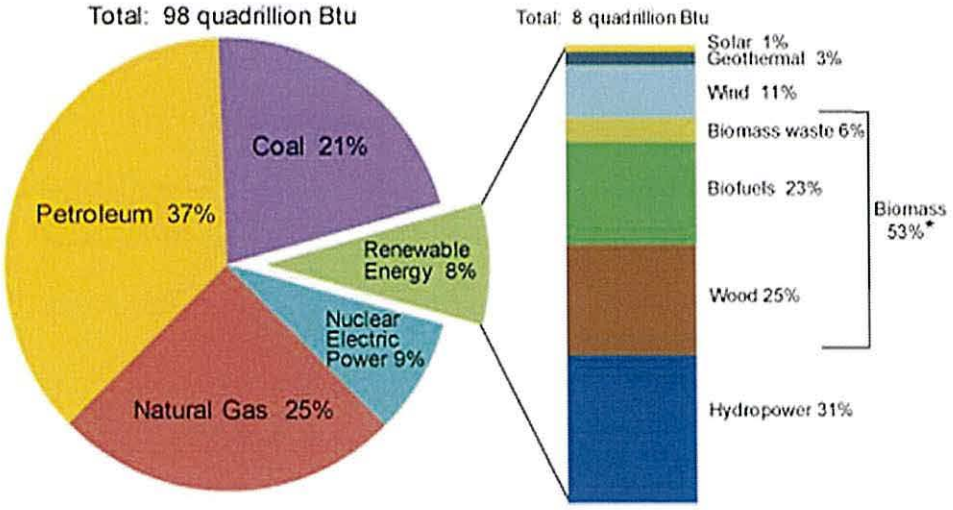

Figure 1.1: Renewable energy consumption in the U.S in 2011.[9]

Table 1.1 US energy consumption by energy source, 2006 -2010 (adapted from reference)

Energy (quadrillion Btu)	2006	2007	2008	2009	2010
Total	99.624	101.362	99.362	94.485	97.892
Fossil Fuels	84.687	86.251	83.54	78.426	81.338
Coal	22.447	22.749	22.385	19.703	20.707
Coal Coke Net Imports	0.061	0.025	0.040	-0.023	-0.006
Natural Gas	22.224	23.702	23.834	23.343	24.667
Petroleum	39.955	39.774	37.28	35.403	35.970
Electricity Net Imports	0.063	0.106	0.113	0.116	0.064
Nuclear Electricity Power	8.215	8.455	8.427	8.356	8.441
Renewable Energy	6.659	6.551	7.191	7.587	8.049
Biomass	3.277	3.503	3.852	3.899	4.295
Biofuels	0.771	0.991	1.372	1.567	1.855
Waste	0.397	0.413	0.436	0.452	0.454
Wood and Derived Fuels	2.109	1.098	2.044	1.881	1.986
Geothermal Energy	0.181	0.186	0.192	0.200	0.212
Hydroelectric Conventional	2.869	2.446	2.512	2.669	2.509
Solar Thermal/PV Energy	0.068	0.076	0.089	0.098	0.109

As stated earlier, over recent decades energy has been consumed at increasing rates to keep up with the development of technology and economies in the world and this is predicted to continue.[10] For example, net electricity consumption is predicted to more than double between 2003 and 2030, and natural gas and renewable energy sources are the only fuels expected to increase their share of total electricity generation over this period.[4] Indeed it has been reported that high world fossil fuel prices will help renewable energy sources to compete commercially in the electric power sector.[11] In this context, solar cells or photovoltaic devices are one of the fastest-growing sources of renewable energy worldwide,[12] replacing fossil fuels due

to the abundance of solar energy and environmental friendliness of PV which means having minimal or no harm on the environment.

1.3 Photovoltaic solar energy

A solar cell or photovoltaic (PV) device is any device that converts sunlight directly into electricity by using photons from the sun's light to excite electrons from ground states to excited states of energy.[13] The photoelectric effect was first observed by Edmond Becquerel[14] in 1839 when he reported the observation of a voltage between electrodes exposed to light and immersed in an electrolyte. In 1873, the photoconductivity of selenium was discovered by Willoughby Smith when he described the effect of light on selenium during the passage of electric current.[15] After three years, another scientist William G. Adams with his student Richard E. Day, discovered that selenium produces electricity when exposed to light.[16] These discoveries were the platform for solar cell devices. The first solar cells were then described by Charles Fritts in 1883 and were made from selenium wafers.[17] In 1905, Albert Einstein published a paper on the theory of the photoelectric effect concerning the production of electrons from radiation.[18] In 1932, Audobert and Stora[19] discovered the photovoltaic effect in cadmium selenide (CdSe), a photovoltaic material still used today. In 1954, the invention of the first modern silicon solar cell was announced at Bell laboratories by Dary Chapin, Calvin S. Fuller and Gerald Pearson.[20] Chapin *et al.* used diffused silicon p-n junctions which consisted of two semiconductors with opposite doping types namely a donor [n-type] and an acceptor [p-type]. These first cells had about 6% efficiency in converting the sun's light to electricity. This was much higher than the best reported selenium cells which typically gave much lower efficiency, typically around 0.5%.[21] Most photovoltaic devices to date have been based on a semiconductor p-n junction. In a p-n junction PV cell, the light absorption and photo-generated carrier transport processes occur side by side throughout the device volume.[22] The different work functions of p- and n-type regions results in a transition region at their interface which also creates an electric field. Optical excitation of the semiconductor with light of energy higher than the bandgap separation of the semiconductor leads to generation of free charge carriers, electrons (e^-) and holes (h^+). In a sandwich structure composed of an n-type

and p-type semiconductor, charge separation occurs due to bending of the bands in the vicinity of the interface. Figure 1.2 shows that conduction band electrons move freely in n-type materials while holes do not. Also holes move freely in p-type materials while electrons do not.[23] The maximum theoretical efficiency of p-n junction solar cells has been calculated by Shockley and Queisser[24] and found to be 30%.

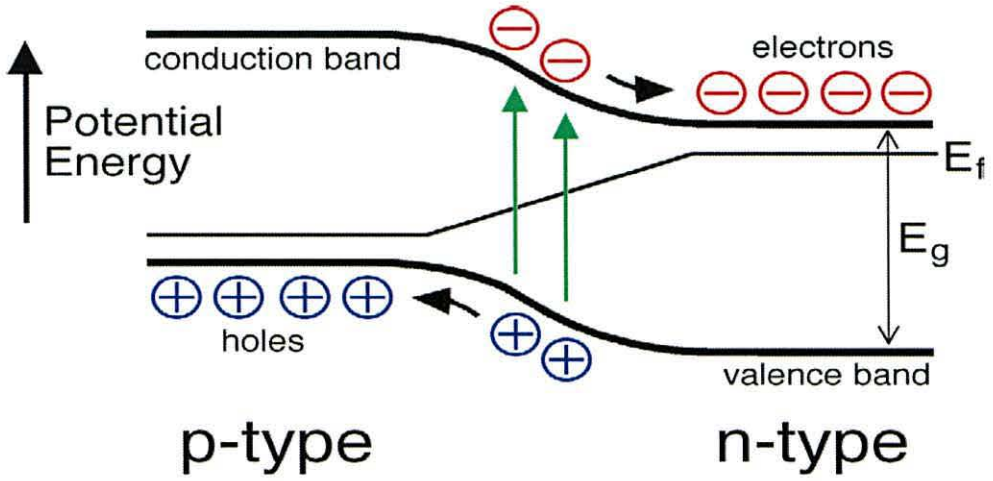

Figure1.2: Essentials of p-n junction solar cell operation.

However, dye sensitized solar cells (DSC), the subject of thesis, operate differently. In the dye sensitized solar cell, photoabsorption excites an electron to a high energy from an adsorbed dye molecule on TiO_2 (a large band gap n-type semiconductor).[23] The excited electron is rapidly injected into the conduction band of TiO_2 and is transported away from the generation site. One reason for studying DSC devices is that the choice of materials and fabrication techniques are key for reducing the cost of solar cells.[25] In addition at present, the cost of electricity produced from photovoltaic device is currently too high to compete with whole-sale electricity without the benefit of government-supported feed-in tariffs.[26] The hope is that DSC devices could be produced commercially at large scale but their efficiency needs increasing which is one aim of this thesis by studying increased spectral response by co-sensitization.

During the past decade several approaches have been suggested to increase conversion efficiency. Martin Green[27] has classified various photovoltaic solar cell into three major categories. First generation solar cells, silicon wafers consist of large area, high quality single layer p-n junction devices such as mono-crystalline silicon.

Despite the high efficiency (*ca.* 17%) with polycrystalline Si solar cells they can have high manufacturing costs and use large amounts of material due to poor light absorption by Si.[28] Also, at low light levels energy can be lost as heat due to recombination processes.[29]

Second generation cells, also called thin film solar cells, use thin deposits of semiconductors such as, cadmium telluride (CdTe) or copper indium gallium disulfide (CIGS).[30] The advantages of second generation cells include; lower manufacturing costs, flexible substrates, lower material usage and thinner films.[31] In addition, third generation solar cells are emerging PV technologies, including polymer solar cells and dye-sensitized solar cells.[32, 33] However, DSC devices suffer from poor spectral response (typically < 650 nm) which limits their efficiency. However, DSCs do have attractive advantages in several aspects such as non-toxic components and potentially lower manufacturing costs.[30]

The cost of solar cells is generally measured in price-per-watt electrical power and is measured under standard test conditions (solar irradiance 1000W.m^{-2}, AM1.5 solar spectrum, perpendicular light incidence and a temperature of 25°C). Figure 1.3 from 2003, shows a graph for possible production costs per unit area together (US \$/m^2) with energy conversion efficiency ranges for the three generations of PV showing costs as US\$/Wp. First generation costs are high and the range between US\$3.0/Wp and US \$ 3.50/Wp with the efficiency between 15-20%.[34] Second generation, thin film technologies are predicted to show lower production costs. The cost ranges between US \$ 50/m^2 to US 120\$/m^2 and costs per watt peak are from US \$ 0.50/Wp to US\$ 3.50/Wp. However the efficiency ranges between 6% and 15% at present.[35] Third generation solar cells have costs predicted to be between US\$ 0.20/Wp and US\$ 0.50/Wp, with costs around US\$ 50/m^2 to US\$ 200/m^2. The graph shows third generation technology is predicted to have much lower overall costs. In addition, DSC devices are beginning to emerge in the market place and remain under active development in laboratories all over the world.[36] However, it should be noted that market conditions change very quickly and this report was in 2003. Since then DSC devices and manufacturing as well as research challenges that must be addressed to continue the rapid commercialization of DSC technology.[37]

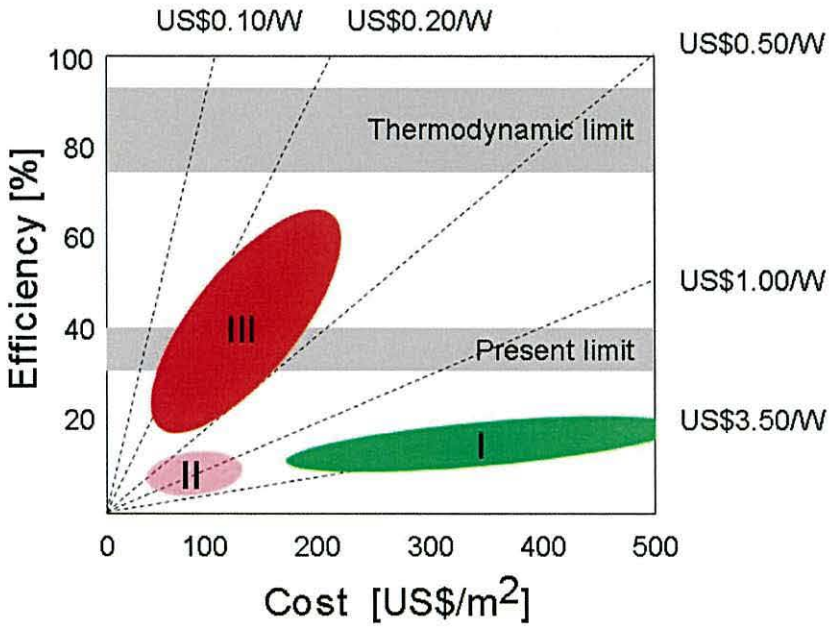

Figure 1.3: Efficiency *versus* cost trade off for the three generations of solar cell technology in 2003: wafers (I), thin films (II), and advanced thin films (III).[38]

The best laboratory efficiencies from various materials and a number of photovoltaic technologies over the last 35 years have been collected by the National Renewable Energy Laboratory (NREL) in the US and the data are plotted in Figure 1.4. The data show two relatively new entries; dye-sensitized solar cells (DSCs) and organic photovoltaic cells.[39] The National Renewable Energy Laboratory have reported the highest efficiency of the first generation multi-junction solar cells reaching over 40% for a three junction GaInP/GaInAs/Ge cell at 240 Suns, under the standard spectrum for terrestrial concentrator solar cells (AM 1.5 D, low aerosol optical depth, 24 W/cm^2, 25°C). By comparison, despite the lower efficiencies of DSCs and organic solar cells, the low cost of these types of solar cells can still make them commercially interesting.[40] In this context, this thesis involving studies of using less dye, more than one dye and faster processes for DSC device manufacturing.

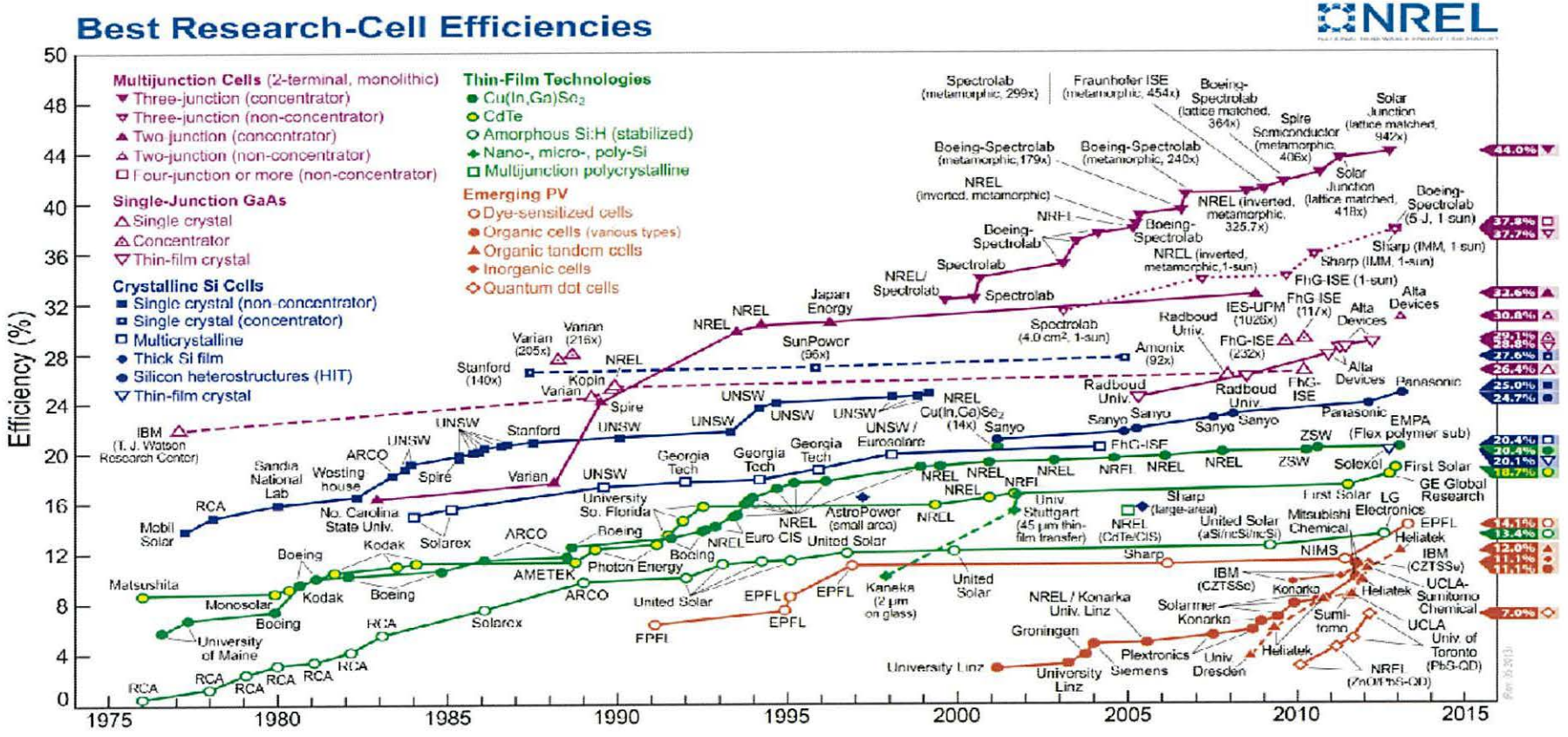

Figure 1.4: Thirty five years evolution in conversion efficiencies of different photovoltaic technologies for laboratory-scale devices. Compiled by Lawrence L. Kazmerski, National Renewable Energy Laboratory (NREL).

1.4 Dye-sensitized solar cells (DSCs)

The dye-sensitized solar cell is a photo-electrochemical solar cell which generally uses a liquid electrolyte and is based on the concept of charge separation at the interface of two materials.[41] The operating principle of a DSC device is similar to photosynthesis in plants but differs in that electricity is produced, whereas plants produce oxygen and sugar, using chlorophyll as sensitizer to harvest photons of light.[42] The story of dye-sensitized solar cells in started in 1970, when chlorophyll molecules were used to inject charge into a wide band gap ZnO semiconductor so that photons were converted into electric current.[43] In 1976, Tsubomura *et al.*[44] achieved up to 1.5% conversion efficiency using an aqueous electrolyte for a sensitized ZnO photo-electrode. These devices had low conversion efficiencies because the devices were based on a flat electrode and had only a monolayer of adsorbed dye leading to low electron injection into the semiconductor. The major breakthrough in DSCs emerged by replacement of the planar electrode by mesoporous nanocrystalline semiconductor films to provide a higher surface area for dye uptake.[45]

Titanium dioxide (TiO_2) is often used as a white pigment because of its brightness and high refractive index.[46, 47] TiO_2 is also the most widely used metal oxide for DSCs because initially low values of the electron diffusion coefficient (10^{-8} to 10^{-4} $cm^2.s^{-1}$) increase with light intensity.[48] In 1972, Fujishima and Honda discovered the phenomenon of the photo-catalytic splitting of water on a TiO_2 electrode.[49] This discovery led to many promising photo-chemical applications of TiO_2 taking advantage of the TiO_2 properties of low cost, low toxicity and excellent optical properties in the visible region.[50] All of these improvements finally led to the announcement by O'Regan and Grätzel,1 in 1991, of a dye sensitized solar cell based on TiO_2 with a conversion efficiency of >7%. Since this report, the published world record DSC efficiency reached over 11% with Ru-bipyridyl dye complexes to sensitize nanocrystalline TiO_2 along with a triiodide/iodide redox couple.[51] However, Yella *et al.* have recently achieved 12.3% with a donor-π-bridge acceptor zinc porphyrin dye as sensitizer and 3-(6-{4-[Bis-(2',4'-bis-hexyloxy-biphenyl-4-yl)-amino]-phenyl}-4,4-bis-hexyloxy-4H-cyclopenta[2,1-b;3,4-b']dithiophen-2-cyano-propionic acid (Y123) as co-sensitizer using a $Co^{(II/III)}$tris(bipyridyl) based redox

electrolyte.[52] This approach of using more than one dye has dramatically improved DSC light absorption to put the power conversion efficiencies into a range that should enable DSCs to become an alternative to conventional p-n junction photovoltaic cells.[53] In this thesis a new method developed for co-sensitization with multiple dyes to improve device performance.

1.4.1 Structure of dye sensitized solar cell

Dye-sensitized solar cells (DSCs), consist of four major components;[54] i) a dye sensitizer, ii) semiconductor nanoparticles of a metal oxide; TiO_2 nanoparticles are generally used although the other wide band gap semi-conductors such as ZnO[55] and Nb_2O_5[56] have also been used, iii) a redox electrolyte such as the iodide/tri-iodide couple iv) and a counter electrode commonly using platinum as a catalyst, because it has sufficient corrosion resistance to the electrolyte and a high rate for the regeneration of reduction of the redox electrolyte [57]. Figure 1.5 shows the arrangement of these components in a typical liquid electrolyte DSC.

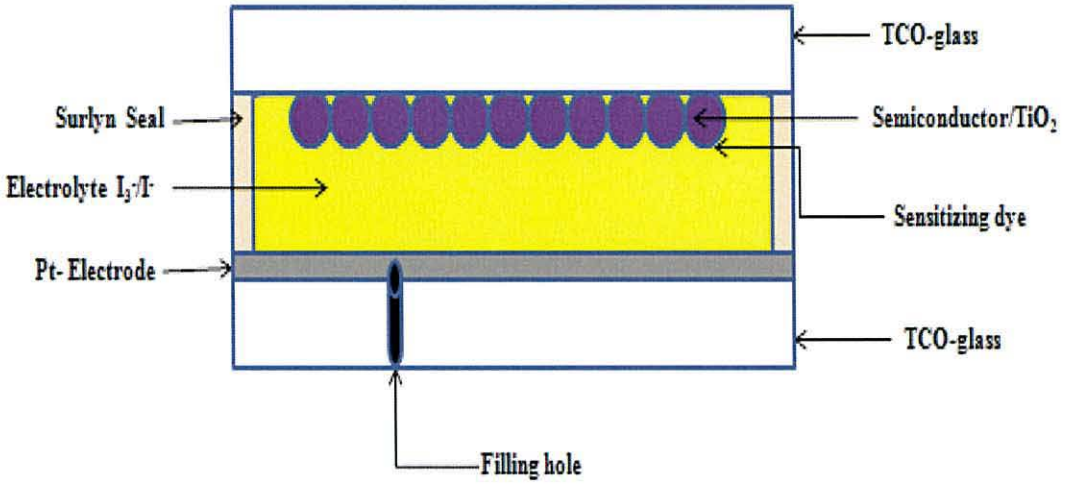

Figure 1.5: Schematic showing typical structure of a liquid electrolyte dye-sensitized solar cell.[58]

DSCs are usually prepared from two transparent conductive glass plates sandwiched together.[59] Typically fluorine-doped tin oxide or tin-doped indium oxide are used as a transparent conducting oxides (TCO). As described above, typically one conducting substrate is coated with a catalyst (e.g. platinum) as the counter electrode

for reduction of the electrolyte redox couple and the other plate is coated with nano-particales of titanium dioxide, which has sensitizing dye adsorbed on the surface. To complete the device liquid electrolyte containing a redox couple (often I^-/I_3^-) is added between the two electrodes providing an electron pathway medium, allowing the charge collected at the counter electrode to be transported back to the dye molecules.[60]

1.4.2 Operation principle of dye sensitized solar cell

Schematic presentations of the key processes taking place in a dye sensitized solar cell are shown in Figure 1.6. Taking the processes in order, 1) sunlight passes through a transparent conductive glass and is absorbed by the dye molecules which are adsorbed on the surface of a wide band gap nano-structured metal oxide surface-usually made up of TiO_2 nanoparticles.[61] The photoelectric chemical process in DSCs can then be expressed in Eqs. 1.1 -1.6. The first reaction that takes place at the anode is the sun light being absorbed by the sensitizer which is adsorbed on the TiO_2 surface, which leads to excited adsorbed dye molecules (D*) by photo excitation , Eq. 1.1.

$$TiO_2/D + hv \rightarrow TiO_2/D^* \qquad Eq.1.1\ Excitation$$

2) Upon light absorption, the excited dye molecule (D*) injects an electron into the conduction band (CB) of TiO_2 also producing a dye cation, Eq. 1.2

$$TiO_2/D^* \rightarrow TiO_2/D^+ + e^-[TiO_2] \qquad Eq.1.2\ Injection$$

3) The injected electron transfers through the mesoporous TiO_2 to arrive at the back contact (or counter electrode) *via* the external load where a catalyst, usually platinum, reduces oxidized iodide (I^-) (Eq. 1.3). In turn the I^-/I_3^- redox couple reduces the exited state dye to complete the circuit.

$$I_3^- + 2e^-[Pt] \rightarrow 3I^- \qquad Eq.1.3\ Regeneration$$

Besides the described pathway of electron migration, loss reactions Eq. 1.4, 1.5, and 1.6 can also occur. For instance, 4) the molecule in the excited state (D*) can decay

to the ground state. However, this is generally rather slow compared to injection into conduction band of TiO_2,[62] Eq. 1.4.

$$TiO_2/D^* \rightarrow TiO_2/D \qquad Eq.1.4\ Relaxation$$

5) Another injected electron loss pathway is that the electron can rapidly recombine with the oxidized dye which can take place without any measurable photocurrent, Eq. 1.5

$$TiO_2/D^+ + e^-(TiO_2) \rightarrow TiO_2/D \qquad Eq.1.5\ Recombination$$

6) The so-called "dark reaction" can also occur during the conversion of light to electricity, as a result of the recombination of injected electrons with the triiodide redox mediator (Eq. 1.6).[63]

$$e^-[TiO_2] + I_2 \rightarrow 2I^- \qquad Eq.1.6\ Back\ Reaction$$

The reactions shown in Equations 1.4, 1.5 and 1.6 enter into a competition with the desired reactions (Equations 1.1-1.3). In a DSC device the voltage generated is equal to the difference between the Fermi level (E_f) of the electron of the solid TiO_2 and the redox potential of the electrolyte. [64] Hence, in most DSC devices, the *V*oc is determined by the Fermi level (E_f) of titania and the redox potential (I_3^-/I^-) of the electrolyte (Fig 1.6). Recombination processes can affect the E_f resulting in lower values for V_{oc}.[65]

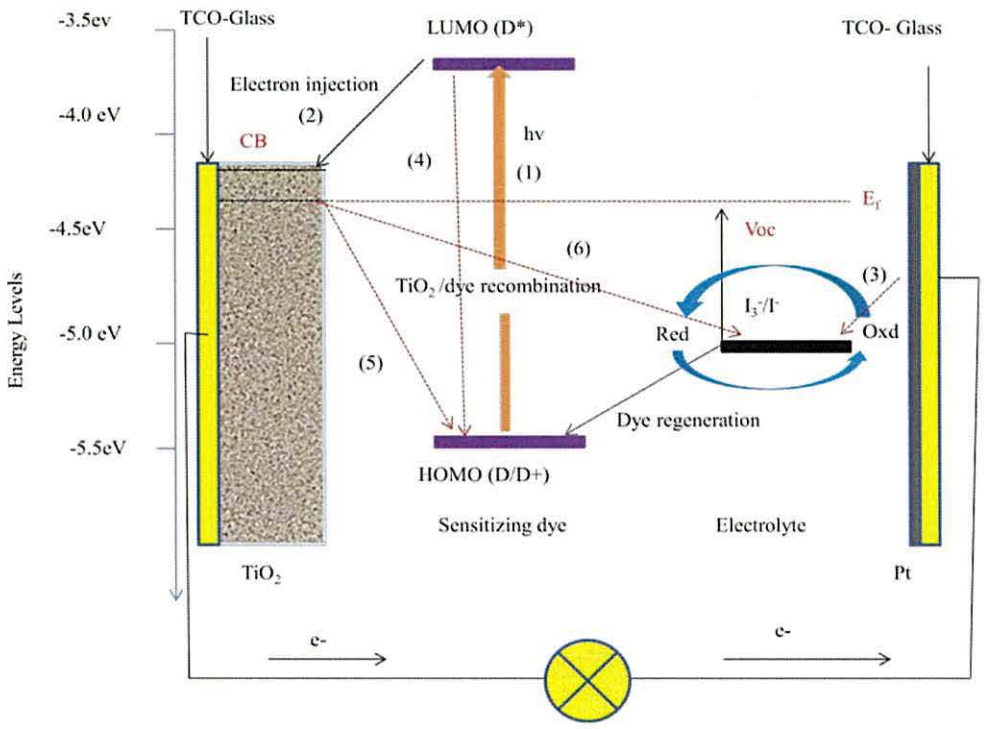

Figure 1.6: Schematic of the key processes taking place during the operation of a dye sensitized solar cell. (Adapted from references[66, 67])

1.4.3 Conversion efficiencies

The conversion efficiency of dye-sensitized solar cells (and any other PV device) is the energy output from the solar cell compared to the input energy from the sunlight. This is affected by the wavelength of light recombination processes, electrical resistance, temperature and the reflection of light.[68] The overall conversion efficiency of solar cells can be expressed as.[69]

$$\eta\ \% = \frac{p_{max}}{p_{light}} = \frac{Jsc\ .Voc\ .\ FF}{P_{in}} \qquad \text{Eq. 1.8}$$

Where (J_{sc}) is the short current–circuit current which is the maximum current from a solar cell which occurs when the voltage across the device is zero, V_{oc} is the open-circuit voltage which is the maximum voltage from a solar cell which occurs when the net current through the device is zero. (P_{in}) is the light power density and the fill factor (FF) is the ratio of the maximum power from the solar cell to the product of V_{oc} and J_{sc} and this can be calculated from:

$$FF = \frac{V_{mp} \cdot I_{mp}}{V_{oc} \cdot J_{sc}} \qquad Eq.1.9$$

Where the maximum power point is P_{max} and the current and voltage at P_{max} (I_{max}, V_{max}) respectively are determined from the I-V curve of the cell as shown in Figure 1.7.

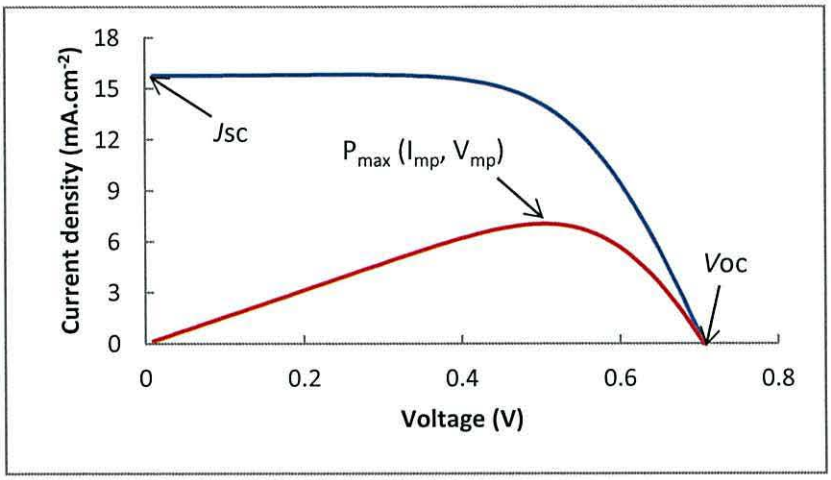

Figure 1.7: Schematic for current density voltage (I-V) characteristic of the photovoltaic structure showing short-circuit current (J_{sc}) and open-circuit voltage (V_{oc}). The maximum power point is also shown. Adapted from

1.5 Factors affecting DSC device solar energy conversion efficiencies

1.5.1 Sensitizers

The molecular structure and energy levels of the dye play an important role as the light harvesting part of dye sensitized solar cells (DSC).[70] The desirable properties for an efficient photo sensitizer are as follows; (1) the light absorption should cover the whole visible and near-IR region. (2) The sensitizer should have suitable anchoring groups such as carboxylic, phosphonic or sulfonic acid groups to strongly bind the dye onto the semiconductor surface. (3) The excited state level (LUMO) of the dye should be higher in energy than the conduction band edge of the metal oxide (usually TiO_2) to enable efficient electron transfer between the excited dye and conduction band (CB), (4) the molar extinction coefficient must be as high as possible to enable the most efficient light harvesting from the smallest amount of

dye, and also (5) the dye should not aggregate on the TiO_2 surface. Finally, (6) the dye should have high thermal and chemical stability to sustain at least 10^8 redox turnovers under normal illumination corresponding to about 20 years of exposure to natural light.[71, 72]

As discussed previously, the sensitizer constitutes a key component of a DSC to harvest sunlight.[73] In the past decades, many dyes have been synthesised and used as sensitizers in DSC. These sensitizers can be divided into two types according to their structure; inorganic dyes such as metal complexes, porphyrins [74, 75] and phthalocyanines[76] and organic dyes including natural organic dyes[77, 78] and synthetic organic dyes.[47] To date, metal complexes have played an important role in the development of DSC technology. In particular, Ru (II) polypyridine complexes have been widely studied as sensitizer molecules for DSCs due to their strong absorption bands in the visible region of the spectrum combined with good charge transfer properties, and thermal and chemical stability. In addition, it has been shown that the metal ligand charge transfer (MLCT) of Ru-bipy dyes can be shifted and provide long emission lifetimes by electron donation.[79 80] Up to now, the most efficient dyes in DSC are the Ru(II)-polypyridine complexes substituted with one or more anchoring carboxyl groups. Table 1.2 shows some common Ru (II) dye complexes which have achieved power conversion efficiencies over 10% in DSCs under standard measurement conditions. The chemical structures of these dyes are shown in Figure 1.9. The first high performance polypyridyl ruthenium complex was *cis*-bis(isothiocyanato)-bis(2,2'-bipyridyl-4,4'-dicarboxylate) ruthenium(II) complex and so-called (N3), leading to the related doubly protonated form, di-tetrabutylammonium *cis*-bis(isothiocyanato)bis(2,2'-bipyridyl-4,4'-dicarboxylate) ruthenium(II) complex (N719). N719 has been found to exhibit outstanding properties such as a broad visible light absorption spectrum and a photo-current conversion efficiency (IPCE) extending to 650 nm. In the (4,4'-dicarboxylic acid-2,2'-bipyridine)(4,4'-di(3-methoxystyryl))-2,2'-bipyridyl] ruthenium (II) complex (Z-910) the metal-to-ligand charge transfer transition is red shifted and shows a higher molar extinction coefficient (16850 $M^{-1}cm^{-1}$, at 543nm) when compared with $Ru(bpy)_3^{+2}$. To further improve the efficiency of DSC devices, the dye *tris*-isothiocyanato-(2,2':6',6''-terpyridyl-4,4',4''-tricarboxylato)ruthenium(II) tris(*tetra*-butylammonium) also known as "black dye" was reported with an IPCE spectrum

covering the whole visible range and into the near IR region up to 920 nm,[81] as shown in Figure 1.8

Table1.2: Maximum literature efficiencies for selected polybipyridyl ruthenium (II) complexes in laboratory DSCs. (These are highly optimal champion cell)

Dyes	J_{sc} (mA.cm^{-2})	V_{oc} (mV)	FF	η%	Ref.
N3	18.20	720	0.73	10.00	82
N719	17.73	846	0.75	11.18	83
Black dye	20.53	720	0.70	10.40	84
Z910	17.20	777	0.76	10.20	85

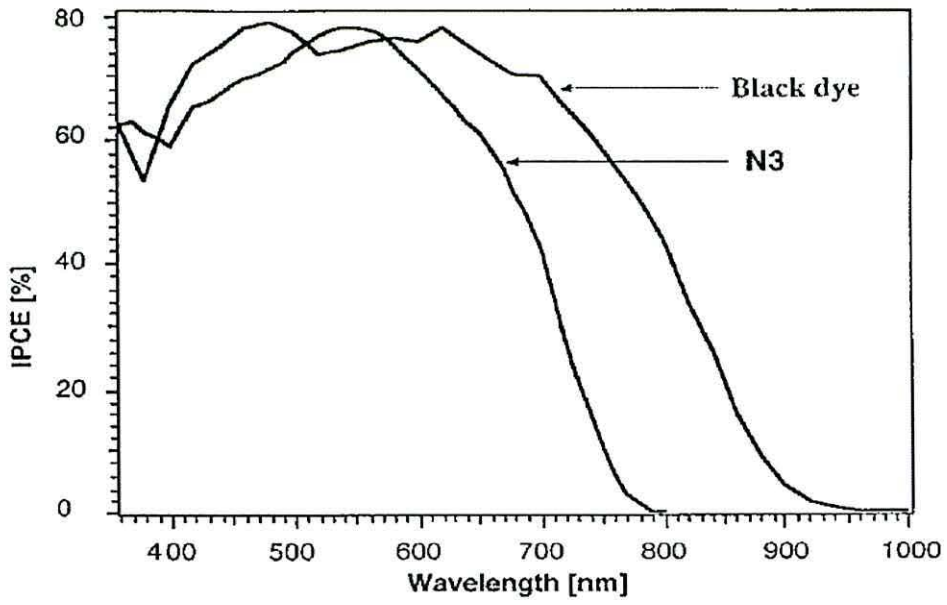

Figure 1.8: IPCE spectrum of the photocurrent response for DSC devices sensitized either by the Ru (II) complex known as black dye or the N3 dye. The data used are from reference.

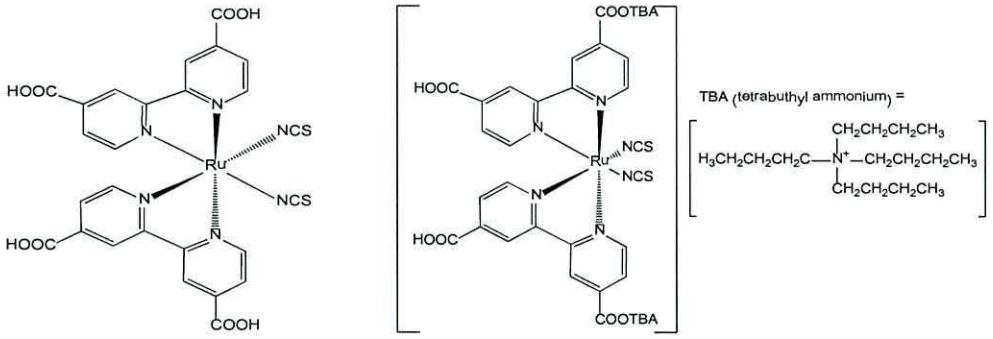

N3 N719

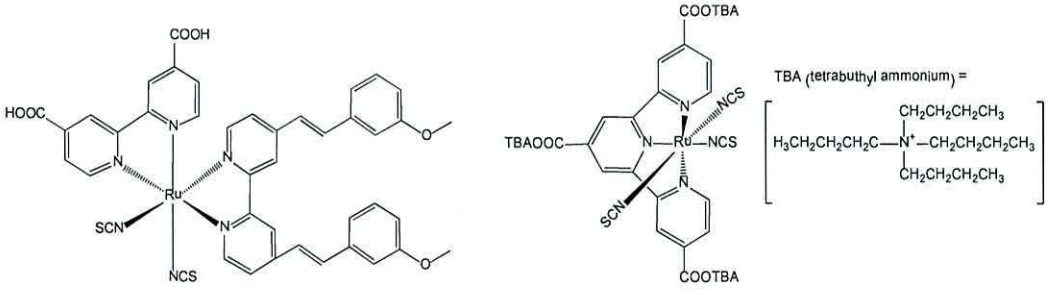

Z910 Black dye

Figure 1.9: Chemical structure of some ruthenium DSC complexes.

However, ruthenium (II) complexes do suffer from some limitations. For instance, they tend to have a low spectral response in the red and infrared regions and also Ru(II) complexes dyes tend to be more expensive than organic dyes. [86] By comparison, organic dyes can be designed with the general structure of donor-π-bridge-acceptor (D-π-A) to help direct electron injection. [87] As such, organic dyes have attracted a lot of attention as alternatives to ruthenium complexes sensitizers because they are generally easier to purify, have higher molar extinction coefficients and can be more flexible to structural modifications.[88] However, the aggregation of organic dyes on TiO_2 films and the recombination of TiO_2 conduction-band electrons with the electrolyte can still be problems for organic dyes relative to the Ru-bipy complexes.[89] During the last few decades various organic dyes for dye-sensitized

solar cells have been developed such as coumarins,[90] merocyanine,[91] indolines,[92, 93] triphenylamines,[94] oligoenes and polyenes,[95] quinoxlines,[96] carbazoles,[97] and squaraines.[98] One example from each organic dye family has been selected to show the varying power conversion efficiencies (Table 1.3). Examples of the structures of an indoline dye (D149), a triphenylamine (TA-ST-CA), a polyene (NKX-2569), a coumarin (NKX-2311), a carbazol (MK-2) and a squarilium dye (SQ1) are shown in Figure 1.10 and the I-V data are summarized in Table 1.3. The organic dyes can also show broad IPCE spectra over the whole visible range extending into the near-IR region up to 650 nm which is the broadest IPCE spectrum in the organic dye based DSCs. However, some kinds of organic dyes also have been used for co-sensitization. For example, the co-sensitization of TiO_2 with SQ1 and JK2 broadens the spectral response to show the IPCE peak efficiencies of 86% and 76% at 530 and 660 nm, respectively, corresponding to the highest absorptions of JK2 and SQ1 as shown in Figure 1.11. In this thesis some these organic dyes were used to develop DSC device performance by ultra-fast dyeing.

Table 1.3: Maximum literature efficiencies for selected organic dyes in dye-sensitized solar cells.

Organic dyes	J_{sc}(mA.cm^{-2})	V_{oc} (mV)	FF	η (%)	Ref.
D149	19.96	653	0.69	9.0	99
TA-St-CA	18.10	743	0.68	9.1	100
NKX-2569	12.90	710	0.74	6.8	101
NKX-2311	14.00	600	0.71	6.0	102
MK-2	10.67	690	0.68	5.0	103
SQ1	10.5	603	0.71	4.5	104

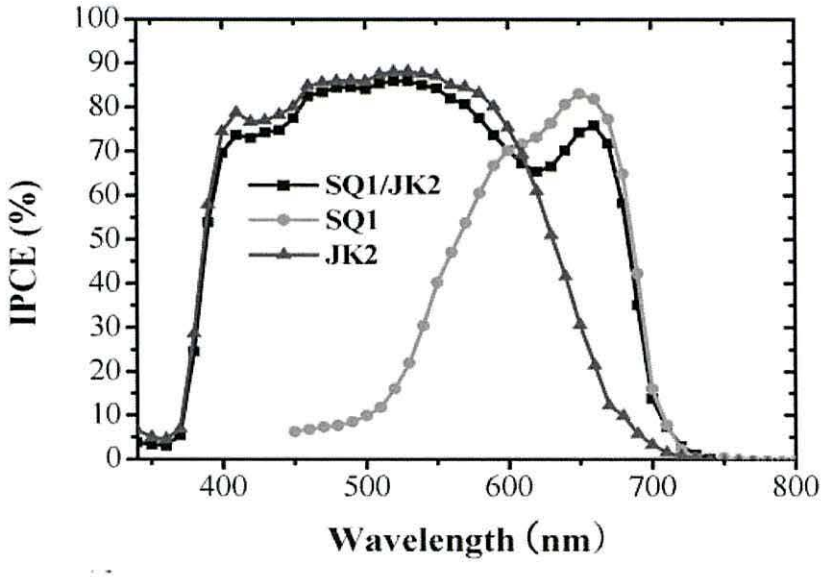

Figure 1.11: Incident photo-current efficiency (IPCE) of cells sensitized with SQ1 (light gray), JK2 (dark gray) and SQ1/JK2 (black). Adapted from reference.[105]

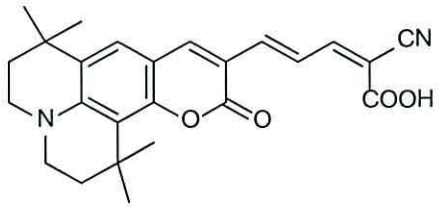

NKX-2311 (Coumarin dye)

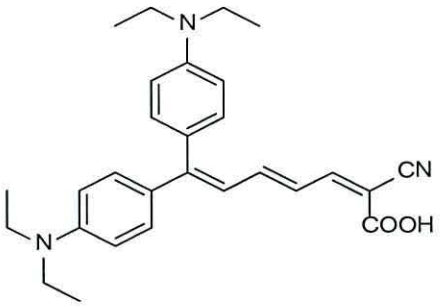

NKX-2569 (Polyene dye)

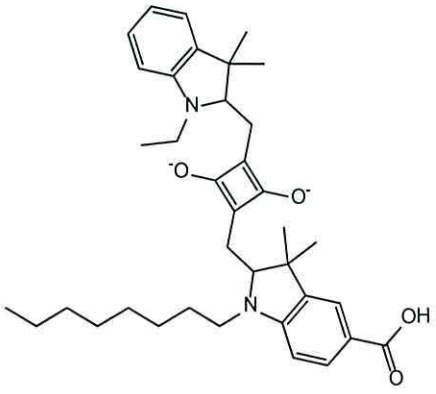

SQ1 (Squaraine dye)

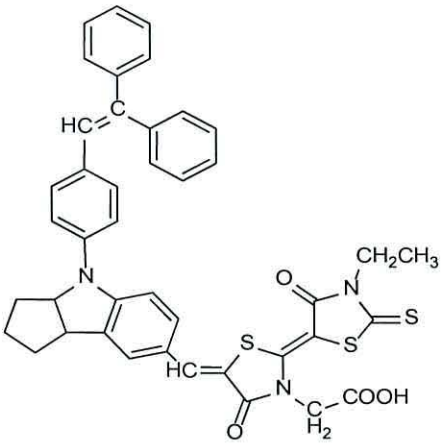

D149 (indoline dye)

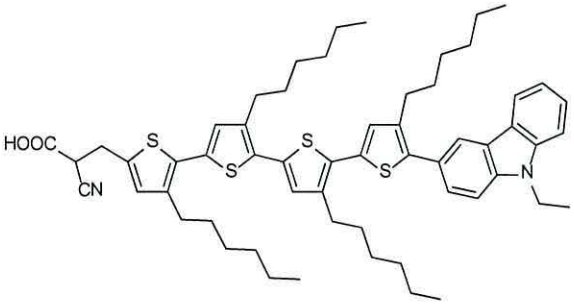

MK-2 (Carbazole dye)

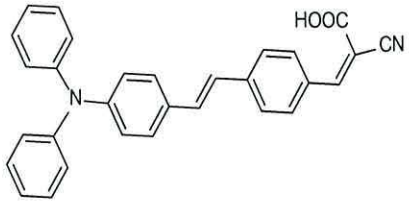

TA-St-CA (Red dye)

Figure 1.10: Chemical structures of selected organic dye sensitizers.

1.5.2 Electrolyte

The electrolyte is another of the main components in DSC devices and plays a vital role in the conversion efficiency and stability of the solar cells.[106] Generally, the electrolyte used in DSCs can be divided into three types: liquid electrolytes, quasi-solid state electrolytes and solid electrolytes.[107] To extend the lifetime of DSC devices, liquid electrolytes should have several properties; such as high thermal and chemical stability, compatibility with the sealing material, low viscosity to reduce any mass transport limitations on the photocurrent and minimal absorption in the visible spectrum.[108] There are two types of liquid electrolytes based on the solvent used; either an organic solvent or ionic liquids. Electrolyte organic solvents can include acetonitrile, valeronitrile, 3-methoxypropionitrile (MPN), ethylene carbonate (EC), or propylene carbonate (PC). By comparison, ionic liquids are materials which consist only of ions and which are liquid below 100 °C. The main advantages of ionic liquid electrolytes include good chemical and thermal stability, low vapour pressure, non-flammability, high ionic conductivity and high solubility for organic and inorganic materials.[109] However, the efficiency of a DSC devices based on ionic liquid electrolytes remains lower in comparison to those using organic solvent based electrolytes because of the lower injection rates of electrons from the dye into the TiO_2, slower dye regeneration by iodide, increased self recombination of the dye, and a small positive shift in the conduction band position within ionic liquid electrolytes.[110]

All DSC liquid electrolytes require a redox couple such as, I_3^-/I^-, Br_3^-/Br^-[111], (SCN^-) /$(SCN)_2$ or $(SeCN^-)/(SeCN)_2$[112] which have all been demonstrated for the successful regeneration of oxidized dyes in DSCs. The redox couple regeneration rates of dye have been reported to decrease in the order $I^- > SeCN^- > SCN^-$, because the equilibrium potentials of SCN/ $(SCN)_2$ is more positive than $SeCN^-/(SeCN)_2$ which is more positive than I_3^-/I^-.[113] Optimization of the electrolyte to enhance the device performance has been reported by the addition of additives such as 4-*tert*-butylpyridine (TBP)[114, 115], guanidinium thiocyanate,[116] and N-methylbenzimidazole (NBBI).[117,118] The addition of these additives decreases recombination rates and improves the open–circuit voltage (V_{oc}), while shifting the conduction band edge of the TiO_2 towards a more negative potential.[119] Although some organic solvents such

as 3-methoxypropioinitrile (MPN) and butyronitrile (BN) have been reported to exhibit good stability during extended tests, some problems still exist for liquid electrolytes such as difficulty of sealing and leakage, and volatilization of the organic solvent.[120] The first time a high efficiency was achieved (η >7 %) for a dye sensitized solar cell based on a solvent-free electrolyte, this was composed of 1-methyl-3-propylimidazolium iodide, 1-methyl-3-ethylimidazolum dicyanamide and lithium iodide combined with an amphiphilic polypyridyl ruthenium sensitizer.[121] Thus, literature work has been carried out on quasi-solid state and solid state electrolytes to try to improve long-term stability and replace liquid electrolytes.[122] For instance, polymer gel electrolytes have been prepared by solidification of a liquid electrolyte into a polymer matrix such as poly-acrylonitrile (PAN),[123] or poly-ethylene glycol (PEG)[124]. However, the efficiency and stability of solid state electrolyte DSC devices are intimately related to the amount and nature of the polymer employed to prepare the electrolyte.[125]

The redox couple (I^-/I^-_3) has been used as the most versatile redox couples for regeneration of the oxidized dye in DSCs and is the redox couple used in this thesis. The mechanism of regeneration of the oxidized dye by a redox couple can be discussed by the following equations:[126]

$$D^* \rightarrow D^+ + e^-[TiO_2] \qquad Eq.1.10$$

$$D^+ + I^- \rightarrow [D \cdots I] \qquad Eq.1.11$$

$$[D \cdots I] + I^- \rightarrow D + I_2^{-\cdot} \qquad Eq.1.12$$

$$I_2^{-\cdot} \rightarrow I_3^- + I^- \qquad Eq.1.13$$

In this thesis, liquid electrolyte based on redox couple triiodide/iodide in acetonitril solvent was used for oxidizing sensitizers with all DSC devices.

1.5.3 Semiconductor

As stated previously, the semiconductor metal oxide plays an important role in improving DSC efficiency mainly by increasing the short circuit current density

(J_{sc}) to lesser a extent, the open circuit voltage (V_{oc}), because the nanostructured metal oxide provide a large surface area for high dye loading and effective sintering ensures good connection between metal oxide grains. [127] Of the wide-bandgap semiconducting metal oxides (TiO_2, ZnO, SnO_2, In_2O_3, Nb_2O_5, WO_3, Ta_2O_5, and ZrO_2),[128] nanocrystalline TiO_2 is the most suitable material in DSCs, due to its low cost, wide availability, non-toxicity and high surface area.[129] Nanocrystalline TiO_2 photo-electrode films are generally made by the doctor blade method or by screen printing by spreading TiO_2 on conductive substrates before sintering at high temperature. [130] Nanocrystalline TiO_2 films can adsorb large amounts of dye. However, the high surface area also increases the possible recombination between electrons in the conduction band of the semiconductor oxide and the electron acceptor in the electrolyte.[131] ZnO has been considered as an appropriate alternative semiconductor in dye sensitized solar cells because ZnO offers a large bandgap (3.37 eV),[132] which is similar to TiO_2, but ZnO also has very high electron mobility compared to TiO_2. ZnO can also be modified to various nanostructures such as nanorods/nanowires as compared to other metal oxides. [133,134] An optimized energy conversion efficiency of 5.34% has been achieved with D205 on a 27μm thick ZnO photo-electrode.[135] Although metal oxides are versatile and easy to adopt in practical terms, metal oxide pastes can be costly for large scale applications. There is thus a growing need to use low cost, renewable and easily available metal oxides for DSC. In this thesis, P25 paste were prepared from P25 TiO_2 (Degussa) and also a commercial TiO_2 paste was used after sintering at 450 ^{0}C and $TiCl_4$ treatment for photo-electrode in DSC devices.

1.5.4 Counter electrode

The counter electrode (CE) performs two important functions in DSCs. The first one is returning electrons from the external circuit back to the electrolyte and then the dye, and the second (related) function is to catalyze the reduction of triiodide to iodide.[136] In DSCs, platinum is widely used as a counter electrode catalyst because it has resistance to the corrosive electrolyte as well as having a high reaction rate for reducing the electrolyte redox couple. The counter electrode is usually prepared by coating a platinum containing material as a solution or paste followed by

thermal decomposition. The price of platinum is high because it is used for various purposes. Carbides, nitrides or oxides of low cost transition metals have also been used as a counter electrode to replace the expensive Pt catalyst in DSCs.[137] Recent research into counter electrodes to replace platinum in DSCs include carbon and the conducting polymer poly (3,4-ethylene-dioxythiophene).[138] However, new materials for the counter electrode are being studied as lower cost alternatives for cheaper and higher performance devices. In this thesis Pt catalyst was used as a counter electrode in DSC devices.

1.6 Adsorption

This thesis focuses on the adsorption of sensitizers on TiO_2 photo-electrodes which plays an important role in DSC. Adsorption is a general term which refers to the accumulation of molecules, ions or atoms of the substance (the adsorbate) on the surface of the other substance (the adsorbent).[139] The adsorption process leads to an increase in the concentration of dissolved substances at the interface of the solid and liquid phases. The molecule contacts the surface of a solid adsorbent in a process which can be characterized by different potentials, such as the dispersion energy, repulsion energy, polarization energy, field dipole energy, field gradient quadrupole energy, sorbate-sorbate energy and acid – base interactions with the active site if the surface contains hydroxyl bridge groups.[140] These electrostatic forces occur between dye molecules and TiO_2 particles caused by their electric charges. In this context, dye adsorption on TiO_2 surface occurs as a result of some of these electrostatic forces. According to the nature of the attractive forces existing between the adsorbate and adsorbent, the adsorption process can be classified into two types; physical adsorption (physisorption) and chemical adsorption (chemisorption). In physical adsorption, the forces involved between the molecules of adsorbate and adsorbent are weak Van der Waal's forces so this is also called Van der Waal's adsorption. In chemisorptions, the interaction forces between the adsorbate and adsorbent are almost the same strength as chemical bond.[141] Some features which are useful to compare between physisorption and chemisorptions are listed in the Table 1.4. The information presented in Table 1.3 indicates some criteria which are helpful in distinguishing between physisorption and chemisorptions. In physisorption, the

adsorbate has a low heat of adsorption (< 40 $kJ.mol^{-1}$). In chemisorptions, the adsorbate molecule undergoes a chemical reaction to bind to certain sites on the sorbent surface with a higher heat of adsorption can be more than 200 $kJ.mol^{-1}$ and only a monolayer adsorption occurs.

Table1.4: Comparison between physical adsorption and chemical adsorption.[142]

	Physisorption	Chemisorption
1.	Forces of attraction are weak (Van der Waal's forces)	It is caused by chemical bond attraction
2.	It is not specific in nature	It is highly specific
3.	It is reversible	It is irreversible
4.	There is a low enthalpy of adsorption usually 20-40 $kJmol^{-1}$	It has a high enthalpy of adsorption more than 200 $kJ.mol^{-1}$
5.	It decreases with increasing temperature	It increases with increasing temperature
6.	It does not require activation energy	It requires activation energy
7.	It increases with increasing surface area	It increases with increasing surface area
8.	Multi-layers of molecules can be formed	It generally, forms monomolecular layers

Physical adsorption equilibrium is usually established very rapidly except when limited by gaseous diffusion in porous adsorbents. However, chemisorptions may be rapid or slow. The occurrence of activation energy for chemisorptions of diatomic molecule with dissociation is illustrated in Figure 1.12. The adsorption mechanism for a gas-solid interface is based on the theory postulated by Langmuir in 1916 where he suggested that the surface of the adsorbent is uniform, adsorbed molecules do not interact with each other and all adsorption occurs through the same mechanism.[143] The curve in Figure 1.12 (i) represents a chemisorption profile and this has a deep potential energy equal to heat of chemical adsorption (ΔH_{ad}). The curve (ii) represents the physical interaction energy between the surface of metal and gas molecules and has lower potential energy equivalence (heat of physical adsorption). The hydrogen molecule approaches the surface and is physically adsorbed at this position and enables the molecules to approach to within this distance of the surface without the large energy necessary for dissociation into H atom. The gas molecules

undergo a transition from curve (ii) to curve (i) if the activation energy barrier to chemisorption is overcome. If this happens on reaching the transition state, the gas molecules dissociate into atoms and bond to the surface. By comparison with gas-solid adsorption, liquid-solid adsorption interactions of the sort studied in this thesis are more complicated. An ideal adsorbed phase is one in which the activity coefficients are unity under all conditions.[144] The gas adsorbed phase equilibrium of a pure component is fully characterized by specifying the temperature and gas phase pressure. However, an additional degree of freedom enters for each additional component. But the adsorption from a liquid onto a solid involves an energetically heterogeneous surface; therefore the adsorption is far from ideal. The adsorptions from solution also have been used for many years for determination of surface area and porosity of certain adsorbent and also it is necessary to understand how a solid behaves in the liquid medium.[145] In this thesis we have considered the significance of two models Freundlich and Langmuir to describe dye adsorption on the TiO_2 surface in DSC devices.

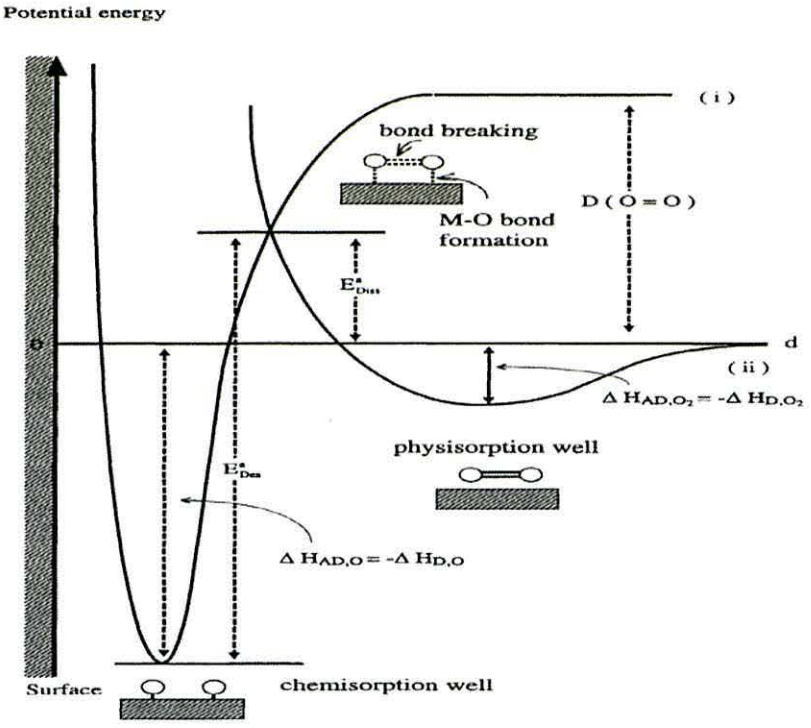

Figure 1.12: The diagram of the potential energy of the dissociative chemisorptions of an O-O molecule, $\Delta H_{AD,O2}$ is the enthalpy of non-dissociative physisorption, $\Delta H_{AD,O}$ enthalpy of chemisorptions at T=0 with activation energy.[146]

1.7 Adsorption isotherms

An adsorption isotherm is defined as the relationship between the equilibrium uptake of a substance with pressure in the gas phase or by concentration in the liquid phase at constant temperature. Theoretical models can be used to describe the type of adsorption including the Freundlich and Langmuir models.[147]

1.7.1 Freundlich isotherm

This isotherm was proposed by Freundlich in 1909 and has been used by many researchers to describe the adsorption of trace quantities of the substances at equilibrium[148] Eq. 1.10. The Freundlich equation describes the behaviour of adsorption from solution when the concentration in solution replaces the gas pressure.

$$\frac{x}{m} = Q_e = \mathrm{K_f}.\, C_e^{\frac{1}{n}} \qquad Eq.\,1.10$$

Where, Q_e is the amount of equilibrium solute sorption per gram of adsorbent ($mg.g^{-1}$), C_e is the equilibrium aqueous concentration of the solute ($mg.L^{-1}$), K_f and n are Freundlich constants which are related to the adsorption capacity and intensity of adsorption, respectively. [149] Evaluation of the parameters in the Freundlich isotherm is accomplished by obtaining a linear form of the isotherm.

1.7.2 Langmuir isotherm

The Langmuir isotherm is the most common model used to describe monolayer chemisorption on distinct, localized adsorption sites. This isotherm is based on some assumption:

1- Molecules are adsorbed at localized sites.

2- All sites are energetically equivalent.

3- The maximum adsorption occurs at equilibrium where no further adsorption can occur.

4- No interactions exist between adsorbate molecules.

The Langmuir equation used for the sorption of a solute from liquid solution is given by :

$$\frac{c_e}{q_e} = \frac{1}{k_l q_{max}} + \frac{c_e}{q_e} \qquad \text{Eq. 1.11}$$

Where, q_{max} is the amount of one layer coverage of adsorbate, k_l is adsorption equilibrium constant and C_e is the equilibrium concentration of adsorbate. The adsorption isotherm indicates how the adsorbed dye molecules distribute between the liquid phase and the solid phase when the adsorption process reaches an equilibrium state.[150] In this thesis, Langmuir and Freundlich models were used to describe physisorption and chemisorptions for the N719 and SQ1 adsorption onto TiO_2 films.

1.8 Dye adsorption and DSC

The performance of DSC devices is affected strongly by the dye adsorption amount and partition coefficient on TiO_2 nanoparticles.[151] Also studying dye adsorption on TiO_2 particles can provide fundamental information concerning adsorption sites, surface structure and the degree of aggregation which is important for optimizing the nanocrystalline cells.[152] A general dyeing procedure consists of immersing photo electrodes in dye solution (10^{-3} to 10^{-4} M) at room temperature with contact times from 16-24 hours to ensure saturate the TiO_2 surface is saturated.[153] A few studies have reported a strong effect of different dye dipping times on photovoltaic performance of the cell.[154] Photoelectron spectroscopy has also been used for a quantitative estimation of dye uptake but this technique is not easily accessible because it is used to indirectly determine the amount of adsorbate molecules and gives only the relative concentrations of the different elements.[155] Dye loading has been found to be crucial for DSC performance by affecting light harvesting which in turn affects the cell short-circuit current J_{sc}.[156] The dye adsorption behaviour also affects the V_{oc} due to movement of the TiO_2 CB and variable charge recombination at the interface between the TiO_2 and electrolyte.[157]

Thus adsorption of dye on TiO_2 has been studied for over 10 years to investigate the nature of the interactions between dye molecules and TiO_2 surfaces.[158] Further understanding of the adsorption mechanism of the semiconductor/adsorbate interface has been widely reported in the literature using vibrational spectroscopy[159], resonance Raman and FTIR spectroscopies,[160, 161, 162] and X-ray absorption spectroscopy was used to investigate the nature of binding on TiO_2 particles.[163,164] These studies suggested that dye adsorption on TiO_2 surfaces is achieved by the formation of ester-like linkages.[165] However, the precise determination of the preferred adsorption mode of a dye on TiO_2 surfaces is difficult because of the large sizes of dyes, dye flexibility, the presence of several anchoring groups, the effect of surface termination and defects.[166] A few methods are known today for quantitative evaluation of total dye loading. The amount of adsorbed dye is typically determined by *ex situ* UV-Vis spectroscopy after dye desorption from the TiO_2 surface by treating the sample with aqueous alcoholic solution of NaOH.[167] More recently, digital imaging and diffuse reflectance UV-Visible spectroscopy have been used for quantitative determination of dye uptake in porous TiO_2 films.[168] The advantages of these new techniques are that they provide rapid *in situ* data by monitoring the colour intensity of dye uptake. An alternative *in situ* method was proposed by Peic *et al.* who used an optical waveguide spectroscopy to study the real-time adsorption of dye in mesoporous nanocrystalline TiO_2 films.[169] However, this works at a fixed wavelength and is not always at the maximum sensitivity. The influence of the anchor and backbone such as perylene dye molecules such as (ID28, ID176, ID505 and ID741) as well as the influence of solvents on the adsorption process have been proposed by Volker *et al.*[170] Based on a vacuum-tight attenuated total reflection infrared (ATR-IR) flow through cell, the experiments showed a significantly lower amount of anhydride dye can be adsorbed on the films, *ex situ* experiments furthermore indicate that the availability of OH groups on the TiO_2 surface may limit adsorption. Also the backbone and base frame of the dye can influence the adsorption time drastically. This also demonstrated that the anchoring group has a strong effect on the adsorption rate also was found that both adsorption and desorption are affected by the solvent.

Literature reports of the studies of adsorption kinetics of the dye uptake in DSCs are more limited. Unpublished work in the laboratories at Bangor suggests mesoporous

TiO_2 films in DSCs are impregnated with dye molecules through a combination of pore diffusion and adsorption/desorption processes. The impregnation starts from the top layer of the film, and then with time it reaches deeper and deeper into the film, until eventually the whole mesoporous TiO_2 film is saturated with dye molecules. In this context the two step kinetics for N3 adsorption on nanocrystalline TiO_2 was first postulated by Fillinger and Parkinson,[171] who suggest that two carboxylic groups are involved in N3 structure in binding on the TiO_2 surface and facilitating charge transfer by electron injection. Efficient charge transfer occurs after anchoring of the sensitizer through carboxylate group onto the surface of the semiconductor. The kinetics of the adsorption Ru(II) complex dyes onto a mesoporous TiO_2 film was studied by Ishihara *et al.*[172] based on diffuse reflectance spectroscopy at room temperature, which suggested that the dye with carboxyl groups exhibited the same kinetics as the dye without carboxyl groups in the period up to 20 minutes.

The adsorption time is very important for speeding up the dye adsorption process. In this context, ultra-fast dye sensitization and co-sensitization to control the dye uptake of different dyes N719 with organic SQ1 dye have been reported, where dye adsorption was completed within 5-10 min when the dye solution concentration was 8.6 mM.[173] The effect of dye concentration on adsorption kinetics has been proposed by Park *et al.*[174] In that work, the quantity of dye loading on TiO_2 surface was measured as a function of immersion time of the TiO_2 film in the dye solution reporting a pseudo-first order adsorption kinetic model. The kinetics of the dynamic dyeing process was investigated from the real time study of dye loading (N3 and N719) under continuous flow conditions on TiO_2 by *in-situ* UV-Vis monitoring upon removal of the dye with aqueous NaOH 0.1 M.[175] More recently, a new spectroscopic tool for fully reliable quantitative evaluation of dye uptake into TiO_2 film has been proposed. This protocol consists of setting a conversion table between the UV-Vis optical spectra of the adsorbed dye after several of dipping times and the absorption of desorbed dye. This studied the adsorption of N719 on TiO_2 from few seconds up to 24 h dipping time, showing a pseudo-first order kinetic model with an observed rate constant of 3.1×10^{-4} s^{-1}. Previous studies to evaluate dye uptake or adsorption kinetics in DSCs have used NaOH solution to desorb ruthenium dyes. However, using NaOH solution has some disadvantages. Firstly, the TiO_2 film can

be damaged if the film is left in NaOH solution for a long time. Secondly, it is difficult to removing organic dye from TiO_2 surfaces by NaOH solution.

To improve DSCs, recent research efforts continue to try fill the gap between the recent efficiency achievements and the Shockely-Queiser limit of applies of p-n junction η = 32%. Co-sensitization is an effective approach to improve DSC device performance by using two or more dyes together to harvest light at different wavelengths. This is because it's difficult for one dye to absorb all the light from 350-940 nm. Therefore a combination of multiple dyes can be used to harvest the whole spectrum from the visible and near infrared regions. In the past, co-sensitization of organic dyes was preferred to ruthenium complex dyes because of the higher molar extinction coefficients of organic dyes which require smaller surface areas to co-sensitize thinner DSC films.[176] Guo *et al.*[177] investigated co-sensitizing a mixture of cyanine dyes on TiO_2 nanocrystalline solar cells generating the highest photoelectric conversion yield of 3.4%. Zhang *et al.*[178] combined three organic dyes to co-sensitize TiO_2 electrodes which led to a wide 400- 700 nm spectral response and found that all three dyes behaved better in triple sensitization than as individual dyes and a high efficiency up to 6.5% was achieved. The Grätzel group demonstrated co-sensitization of two organic dyes; squarylium (SQ1) and bisthiophene (JK2) on a TiO_2 electrode to give η = 6.4% under 1.5 AM sun light at 100 $mW.cm^{-2}$ irradiation which is higher than that of the individual dyes (η = 3.78% for SQ1, η = 6.02 % for JK2).[179] The effect of molar ratio of mixing dyes for co-sensitization has been proposed by Hua *et al.*[180] who used a mixture of trimethinecyanine (A) and pentamethinecyanine (B) to sensitize nanocrystalline TiO_2 solar cells and found a molar ratio (A:B= 3:1) generated the highest efficiency giving 3% . Ogura *et al.*[181] significantly, enhanced photocurrent such that the device performance by a combination of black dye with the indoline dye (D131) achieved a power conversion efficiency of 11%. Two mechanisms were suggested for this co-sensitization; one electron transfer was independent from each dye to the TiO_2 electrode, the second was the dissociation mechanisms in which each dye works mutually. Yella *et al.* have recently achieved 12.3% with a donor-π-bridge acceptor zinc porphyrin dye as sensitizer and Y123 as a co-sensitizer using a $Co^{(II/III)}$tris(bipyridyl) based redox electrolyte. A stepwise approach to enhance the V_{oc} and J_{sc} has been designed for co-sensitization of the zinc porphyrin sensitizer

(LD12) with a spirally configured organic dye (CD5), which showed that upon co-sensitization, the performance of the device improved to yield η = 9% which was greater than either individual dye made from LD12 η = 7.5 % and for CD5 η = 5.7 % in separate devices under the same conditions of fabrication. The co-sensitization of LD12 with CD5 on TiO_2 film was achieved *via* a stepwise approach: the TiO_2 electrode was immersed in the LD12 solution for 3 h and then immersed in the CD5 for 2 h.[182] Passive dyeing was used with all previous researches in co-sensitization method. More recently, Holliman *et al.*[183] have applied ultra-fast co-sensitization of three dyes into TiO_2 in 5 minutes. Using N719, SQ1 and a new dye of triarylmine dye (YD) gives an efficiency of 7.5% which is higher than that of individual DSCs.

In spite of progress in co-sensitization with some organic co-sensitization properties and understanding the mechanisms of co-adsorption of DSCs with different dyes are still needed.

1.9 The aim of project

Efficiency improvements rely on the development of new combinations of dyes, redox couples, and photoanodes in DSC. However, low cost and sustainable manufacturing of DSC modules also depends on the use of high-throughput roll-to roll processing and inexpensive abundant materials. From our review there no reports for re-dyeing DSC devices in the literature This thesis work has focused on the adsorption, desorption and re-dyeing of dye sensitizers on nanocrystalline TiO_2 in DSC devices. One challenge has been to study if it is possible to desorb and re-dye a device either better or with similar performance to the first dyeing. The advantage of this approach should be that it is possible to re-use the device after re-dyeing to reduce times the cost and time of dyeing in DSCs. Another aim of this work is to study ultra-fast co-sensitization to enhance the overall conversion efficiency of DSC by developing selective dye removal from DSC devices. This is linked to how to control the dye loading in DSC to improve device performance. Another area of this work has been to use the new method of selective dye removal for studying co-adsorption kinetics of the sensitizers on TiO_2 nanoparticles in DSCs.

1.10 References

[1] B. C. O'Regan, M. Grätzel, *Nature*, 1991, **353**, 737-739.

[2] I. Pilatowsky, R. J. Romero, C. A. Isaza, S. A. Gamboa, P. J. Sebastian W. Rivera, in *Cogeneration Fuel Cell Sorption Air Conditioning Systems*, 2011, Springer-Verlag London Limited, p 10.

[3] J. Klimstra, M. Hotakainen, in *Smart Power Generation,* 1989, 3rd Edition Avain Publishers, Helsinki, 80-129.

[4] L. Henrik , in *Renewable Energy Systems*, 2010, Elsevier Inc., p7.

[5] M. S. Dresselhaus, I. L. Thomas, *Nature*, 2001, **414**, 332-337.

[6] J. A. Palz, D. C. Lendrum, T. Holloway, J. A. Foley, *Nature*, 2005, **438**, 310-317.

[7] G. K. Tusher, P. A. Mark, in *Energy Resources and Systems/Renewable resource*, 2011,Volume 2, Springer Science –Business Media B. V.

[8] P. Balraju, M. Kumar, M. S. Roy, G. D. Sharma, *Synthetic Metals*, 2009, **159**, 1325-1331.

[9] U.S. DOE-0384, Energy Information Administration (EIA) (2011), Monthly Review September 2011, www.eia.gov/aer.

[10] E. A. Rosa, T. Dietz, *Nature Climate Change*, 2012, **2**, 581-586.

[11] P. Brow, G. Whitney, *U.S. Renewable Electricity Generation: Challenges, Congressional Research Service*, 2011, R41954.

[12] E. F. Fuchs, M. A. S. Masoum, in *Power Conversion of Renewable Energy*, 2011, Springer Science Business Media, p 87.

[13] S. J. Fonash, in *Solar Cell Device Physics*, 2010, 2nd edition, Academic Press Elsevier Burlington USA, p2.

[14] A. E. Becquerel, *Comptes Rendus,* 1839, **9**, 561.

[15] W. Smith, *Nature*, 1873, **7**, 303.

[16] W. G. Adams; R. E. Day, *Proc. R. Lond.*, 1876, **25**, 113-117.

[17] C. Fritts, *American Journal of Science*, 1883, **26**, 465-472.

[18] A. Einstein, *Annalen der Phesik*, 1905, **17**, 132-148.

[19] R. Audobert, C. Stora, *Comptes Rendus*, 1932, **194**, 1124.

[20] D. M. Chapin, C. S. Fuller, G. L. Pearson, *Journal of Applied Physics*, 1954, **25**, 676-677.

[21] M. Telkes, *Journal of Applied Physics*, 1947, **18**, 1116-1127.

[22] B. A. Gregg, M. C. Hanna, *Journal of Applied Physics*, 2003, **93**, 3605-3614.

[23] M. A. Green, *Physica E*, 2002, **14**, 11-17.

[24] W. Shockley, H. J. Queisser, *Journal of Applied Physics*, 1961, **32**, 510-519.

[25] M. Grätzel, *Accounts of Chemical Researches*, 2009, **42**,1788-1798.

[26] C. M.H. Keske, S. G. Evans,T. Iverson, *The Electricity Journal*, 2012, **25**, 1-9.

[27] M. A. Green, D. Jordan, *Progress In Photovoltaics:Research and Applications*, 1998, **6**, 169-180.

[28] K. A. Münzer, K. T. Holderman, R. E. Schlosser, S. Sterk, *IEEE Transactions on Electron Devices*, 1999, **46**, 2055-2061.

[29] N. Keren, A. Berg, P. J. M. Van Kan, H, Levanon, I. Ohad, *Plant Biology*, 1997, **94**, 1579-1584.

[30] K. L. Chopra, P. D. Paulson, V. Dutta, *Progress in Photovoltaics: Research and Applications*, 2004, **12**, 69-92.

[31] A. Barnett, D. Kirkpatrick, C. Honsberg, D. Moore, M. Wanlass, K. Emery, R. Schwartz, D. Carlson, S. Bowden, D, Aiken, A. Gray, S. Kurtz, L. Kazmerski, M. Steiner, J. Gray, T. Davenport, R. Buelow, L. Takacs, N. Shatz, J. Bortz, O. Jani, K. Goossen, F. Kiamilev, A. Doolittle, I. B. Unger, G. Schmidt, E. Christensen, D. Salzman, *Progress In Photovoltaics: Research and Applications*, 2009, **17**, 75-83.

[32] G. F. Brown, J. Wu, *Laser and Photonics Reviews*, 2009, **3**, 394-405.

[33] S. E. Shaheen, D. S. Ginley, G. E. Jabbour, *MRS Bulletin*, 2005, **30**, 10-19.

[34] M. J. Kerr, A. Cuevas, P. Campbell, *Progress In Photovoltaics: Research and Applications*, 2003, **11**, 97-104.

[35] G. W. Crabtree, N. S. Lewis, *Physics Today*, 2007, **60**, 37-42.

[36] P. Kumar, S. Chand, *Progress In Photovoltaics: Research and Applications*, 2012, **20**, 377-415.

[37] J. B. Baxter, *Journal of Vacuum Science and Technology A,* 2012, **30**, 020801-020819

[38] M. A. Green, in *Third Generation Photovoltaics/Advanced Solar Energy Conversion*, 2006 Springer – Vertag Berlin Heidelberg, p7.

[39] L. M. Peter, *Philosophical Transactions of the Royal Society A*, 2011, **369**, 1840-1856.

[40] R. R. King, D. C. Law, K. M. Edmondson, C. M. Fetzer, and G. S. Kinsey, *Applied and Physics Letters*, 2007, **90**, 183516.

[41] M. Grätzel, *Journal of Photochemistry and Photobiology C: Photochemistry Reviews,* 2003, **4**, 145-153.

[42] D. A. Bryant, N. U. Frigaard, *Trends in Microbiology*, 2006, 14, 488-496.

[43] H. Tributsch, M. Calvin, *Photochemistry and Photobiology*, 1971, **14,** 1-49.

[44] H. Tsubomura, M. Matsumura, Y. Nomura, T. Amamiya, *Nature*, 1976, **261**, 402-403.

[45] B. C. O'Regan, J. E. Moser, M. Grätzel, *Journal of Physical Chemistry*, 1990, **94**, 8720-8726.

[46] G. Pfaff and P. Reynders, *Chemical Reviews*, 1999, **99**, 1963-1981.

[47] X. Chen, and S. S. Mao, *Chemical Reviews*, 2007, **7**, 2891-2859.

[48] L. Dlozik, O. Iluperama, I. Lauermann, L. M. Peter, E. A. Ponomarev, G. Redmond, N. J. Shaw, I. Uhlendorf, *Journal of Physical Chemistry B*, 1991, **101**, 10281-10287

[49] A. Fujishima, K. Honda, *Nature*, 1972, **238**, 37-38.

[50] M. I. Baraton, *The Open Nanoscience Journal*, 2011, **5,** 64-77.

[51] M. K. Nazeeruddin, F. D. Angelis, S. Fantacci, A. Selloni, G. Viscardi, P. Liska, S. Ito, B. Takeru, M. Grätzel, *Journal of American Chemical Society*, 2005, **127**, 16835.

[52] A. Yella, H. W. Lee, H. N. Tsao, C,Yi, A. K. Chandirn, M. K. Nazeeruddin, E. W. G. Diau, C. Y., Yeh, S. M. Zakeeraddjn, M. Grätzel, *Science*, 2011, **334**, 629- 634.

[53] B. E. Hardin, H. J. Snaith and M. D. McGehee, *Nature Photonics*, 2012, **6**, 162-169.

[54] J. B. Baxter, E. S. Aydil, *Applied Physics Letters*, 2005**, 86**, 053114.

[55] M. Grätzel, *Chemistry of Materials*, 1994, **6**, 686-691.

[56] K. Sayama, H. Sugihara, H. Arakawa, *Chemistry of Materials*, 1998, **10**, 3825-3832.

[57] G. P. Smestad, M. Grätzel, *Journal of Chemical Education*, 1998, **75**, 752-756.

[58] A. Hauch, A. Georg, *Electrochimica Acta*, 2001, **46**, 3457-3466.

[59] Y. Tachibana, J. E. Moser, M. Grätzel, D. R. Klug, J. R. Durrant, *Journal of Physical Chemistry*, 1996, **100**, 20056-20062.

[60] T. N. Murakami, M. Grätzel, *Inorganica Chimica Acta*, 2008, **361**, 571-580.

[61] M. Grätzel, *Journal of Photochemistry and Photobiology A: Chemistry*, 2004, **164**, 3-14.

[62] J. E. Moser, M. Wolf, F. Lenzmann, M. Grätzel, *Zeitschrift für Physikalische Chemie Bd*, 1999, **212,** S. 85-92.

[63] M. Hilgendorff, V. Sundström, *Journal of Physical Chemistry B*, 1998, **102**, 10505-10514.

[64] M. Grätzel, *Progress In Photovoltaics: Research and Applications*, 2003, **4**, 145-153.

[65] W. Bagienski, M. C. Gupta, *Solar Energy Materials and Solar Cells*, 2011, **95**, 933-941.

[66] M. S. Dresselhaus, I. L. Thomas, *Nature*, 2001, **414**, 332-337.

[67] Y. Takahashi, H. Arakawa, H. Sugihara, K. Hara, A. Islam, R. Katoh, Y. Tachibana, M. Yanagida, *Inorganica Chimica Acta*, 2000, **310**, 169-174.

[68] L. Antonio, H. Steven, in *Handbook of Photovoltaic Science and Engineering*, 2003, John Wiley & Son's ltd, pp 60-100.

[69] K. Kalyanasundaram in *Dye-Sensitized Solar Cells*, 2010, First edition, EPFL press, Lausanne Switzerland, p20.

[70] K. L. Wu, C. H. Li, Y. Chi, J. N. Clifford, L. Cabau, E. Palomares, Y. M. Cheng, H.A. Pan, P. T. Chou, *Journal of American Chemical Society*, 2012, **134**, 7488-7496.

[71] A. Hagfeld, G. Boschloo, L. Sun, L. Kloo, H. Petterson, *Chemical Reviews*, 2010, **110**, 6595-6663.

[72] A. Mishra, M. K. R. Fisher, P. Bauerle, *Angewandte Chemie International Edition*, 2009, **48**, 2474-2499.

[73] M. Katono, T. Bessho, S. Meng, R. H. Baker, G, Rothenberger, S. M. Zakeeruddin, E. Kaxiras, M. Grätzel, *Langmuir, 2011*, **27**, 14248-14252

[74] C. W. Lee, H. P. Lu, C. M. Lan, Y. L. Huang, Y. R. Liang, W. N. Yen, Y. C. Liu, Y. S. Lin, E. W. G. Diau, C. Y. Yeh, *Chemistry A European Journal*, 2009, **15**,1403-1412.

[75] W. M. Campbell, K. W. Walsh, K. C. Gordon, L. Schmidt-Mende, M. K. Nazeeruddin, Q. Wang, M. Grätzel, D. L. Officer, *Journal of Physical Chemistry C*, 2007, **111**, 11760-11762.

[76] M. G. Walter, A. B. Rudine, and C. C. Wamser, *Journal of Porphyrins and Phthal*ocyanines, 2010, **14**, 760-792.

[77] K. Tennakone, A. R. Kumarasinghe, G. R. R. A.Kumara, K. G. U. Wijantha and P.M. Sirimanne, *Journal of Photochemistry and Photobiology A: Chemistry*, 1997, **108**, 193-195.

[78] H. Zhou, L. Wu, Y. Gao, T. Ma, *Journal of Photochemistry and Photobiology A: Chemistry,* 2011, **219**, 188-194.

[79] Y. Qin and Q. Peng, *International Journal Photoenergy*, 2012, **ID 291579**, 21pages, doi:10.1155/2012/291579.

[80] J. Xu, H. Wu, X. Jia, D. Zou, *Chemical Communications*, 2012, **48**, 7793-7795.

[81] A. Hagfeldt, M. Grätzel, *Accounts of Chemical Research*, 2000, **33**, 269-277.

[82] M. K. Nazeeruddin, A. Kay, I. Rodicio, R. Humphry-Baker, E. Muller, P. Liska, N. Vlachopoulos, M. Grätzel, *Journal of American Chemical Society*, 1993, **115**, 6382-6390.

[83] M. K. Nazeeruddin, F. D. Angelis, S. Fantacci, A. Selloni, G. Viscardi, P. Lisk, S. Ito, B. Takeru, M. Grätzel, *Journal of American Chemical Society,* 2005, **127**, 16835-16847.

[84] Y. Chiba, A. Islam. Y. Watanabe, R. Komiya, N. Koide, L. Han, *Japanese Journal of Applied Physics*, **45**, L638-L640.

[85] P. Wang, S. M. Zakeeruddin, J. E. Moser, R. Humphry-Baker, P. Comte,V. Aranyos, A. Hagfeldt, M. K. Nazeeruddin, Grätzel, *Advanced Materials*, 2004, **20**, 1806-1811.

[86] L. M. Goncalves, V. D. Z. Bermudez, H. A. Ribeiro, A. M. Mendes, *Energy Environmental and Science*, 2008, **1**, 655-667.

[87] A. O. Adeloye, T. O. Olomola, A. I. Adebayo, P. A. Ajibade, *International Journal of Molecular Sciences,* 2012, **13**, 3511-3526.

[88] Z. Chen, F. Li, C, Huang, *Current Organic Chemistry,* 2007, **11**, 1241-1258.

[89] H. Choi, S. O. Kang, J. Ko, G. gao, H. S. Kang, M. Kang, M. K. Nazeeruddin, M. Grätzel, *Angewandte Chemie International Edition*, 2009, **48**, 1-5.

[90] X. Zhang, J. Zhang, Y. Xia, *Journal of Photochemistry and Photobiology A: Chemistry*, 2008, **194**, 167-172.

[91] R. Abe, K. Sayama, H. Arakawa, *Chemical Physics Letters*, 2002, **362**, 441-444.

[92] S. Ito, H. Miura, S. Uchida, M. Takata, K. Sumioka, P. Liska, P. Comte, P. Pech, M. Grätzel, *Chemical Communications*, 2008, 5194-5196.

[93] T. Horiuchi, H. Miura, K. Sumioka, S. Uchida, *Journal of American Chemical Society*, 2004, **126**, 12218-12219.

[94] W. Xu, B. Peng, J. Chen, M. Liang, F. Cai, *Journal of Physical Chemistry C*, 2008, **112**, 874-880.

[95] K. Hara, M. Kurashige, S. Ito, A.Shinpo, S. Suga, K. Sayama, H. Arakawa, *Chemical Communications*, 2003, 252-253.

[96] D. W. Chang, H. J. Lee, J. H. Kim, S. Y. Park, S. Park, L. Dai and J. Baek, *Organic Letters,* 2011, **13**, 3880-3883.

[97] E. M. Barea, C. Zafer, B. Gultekin, B. Aydin, S. Koyuncu, S. Icli, F. F.Santiago, and J. Bisquert, *Journal of Physical Chemistry C*, 2010, **114**, 19840-19848.

[98] T. Inoue, S. Pandey, N. Fujikawa, Y. Yamaguchi, S. Hayase, *Journal of Photochemistry and Photobiology A: Chemistry,* 2010, **213**, 23-29.

[99] S. Ito, S. M. Zakeeruddin, R. H. Baker, P. Liska, R. Charvet, P. Comte, M. K. Nazeeruddin, P. Pechy, M. Takata, H. Miura, S. Uchida, M. Grätzel, *Advanced Materials*, 2006, **18**, 1202-1205.

[100] S. Hwang, J. H. Lee, C. Park, H. Lee, C. Kim, C. Park, M. H. Lee, W. Lee, J. Park, K. Kim, N. G. Park, C. Kim, *Chemical Communications*, 2007, 4887-4889.

[101] K. Hara, T. Sato, R. Katoh, A. Furube, T. Yoshihara, M. Murai, M. Kurashige, S. Ito, A. Shinpo, S. Suga, H. Arakawa, *Advanced Functional Materials*, 2005, **15**, 246-252.

[102] K. Hara, Y. Tachibana, Y. Ohga, A. Shinpo, S. Suga, K. Sayama, H. Sugihara, H. Arakawa, *Solar. Energy Materials and Solar Cells*, 2003, **77**, 89-103.

[103] Z. S. Wang, N. Koumura, Y. Cui, M. Takahashi, H. Sekiguchi, A. Mori, T. Kubo, A. Furube, K. Hara, *Chemistry of Materials*, 2008, **20**, 3993-4003.

[104] J. H. Yum, P. Walter, S. Huber, D. Rentsch, T. Geiger, F. Nüesch, F. D. Angelis, M. Grätzel, M. K. Nazeeruddin, *Journal of American Chemical Soc*iety, 2007, **129**, 10320-10321.

[105] J. H. Yum, S. R. Jang, P. Walter, T. Geiger, F. Nüesch, S. Kim, J. KO, M. Grätzel, M. K. Nazeeruddin, *Chemical Communications*, 2007, **44**, 4680-4682.

[106] S. Kambe, S. Nakade, T. Kitamura, Y. Wada, S. Yanagida, *Journal of Physical Chemistry B*, 2002, **106**, 2967-2972.

[107] J. Wu, Z. Lan, S. Hao, P. Li, J. Lin, M. Huang, L. Fang, Y. Haung, , *Pure and Applied Chemistry*, 2008, **80**, 2241-2258.

[108] Z. Yu, N. Vlachopoulous, M. Gorlov, L. Kloo, *Dalton Transactions*, 2011, **40**, 10289-10303.

[109] Y. Zhou, *Current Nanoscience*, 2005, **1**, 35-42.

[110] F. Fabregat-Santiago, J. Bisquert, E. Palomares, L. Otero, D. Kuang, S. M. Zakeeruddin, M. Grätzel, *Journal of Physical Chemistry C*, 2007, **111**, 6550-6560.

[111] K. Hara, T. Horiguchi, T. Kinoshita, K. Sayama, H. Arakawa, *Solar Energy Materials and Solar Cells*, 2001, **70**, 151-161.

[112] P. Wang, S. M. Zakeeruddin, J. E. Moser, R. Humphry-Baker, and M. Grätzel, *Journal of American Chemical Society*, 2004, **126**, 7164-7165.

[113] G. Oskam, B. V. Bergeron, G. J. Meyer, P. C. Searson, *Journal of Physical Chemistry B*, 2001, **105**, 6867-6873.

[114] S. Y. Huang, G. Schlichthorl, A. J. Nozik, M. Grätzel, and A. J. Frank, *Journal of Physical Chemistry B*, 1997, **101**, 2576-2582.

[115] G. Boschloo, L. Haggman, A. Hagfeldt, *Journal of Physical Chemistry B*, 2006, **110**, 13144-13150.

[116] N. Kopidakis, N. R. Neale, A. Frank, *Journal of Physical Chemistry B*, 2006, **110**, 12485-12489.

[117] T. Stergiopoulos, E. Rozi, C. Karagianni, P. Falaras, *Nanoscale Research Letters,* 2011, **6**, 307.

[118] A. F. Nogueira, C. Longo, M. A. De Paoli, *Coordination Chemistry Reviews,* 2004, **148**, 1455-1468.

[119] G. Boschloo, A. Hagfeldt, *Accounts of Chemical Research*, 2009, **42**, 1819-1826.

[120] I. Chung, B. Lee, J. He, R. P. H. Chang, M. G. Kanatzidis, *Nature*, 2012, **485**, 486-490.

[121] P. Wang, S. M. Zakeeruddin, J. Moser, M. Grätzel, *Journal of Physical Chemistry B*, 2003, **107**, 1380-13285.

[122] E. Stathatos, P. Lianos, U. L. Stangar, B. Orel, *Advanced Materials*, 2002, **14**, 353-357.

[123] F. Cao, G. Oskam, P. C. Searson, *Journal of Physical Chemistry*, 1995, 99. 17071-17073.

[124] J. Wu, S. Ho, Z. Lan, J. Lin, M. Huang, Y, Huang, L. Fang, S. Yin, T. Sato, *Advanced Functional Materials*, 2007, **17**, 2645-2652.

[125] G. L. D. Gregorio, R. Agosta, R. Giannuzi, F. Martina, L. D. Marco, M. Manca, G. Gigli, *Chemical Communications*, 2012, **48**, 3109-3111.

[126] A. Y. Anderson, P. R. F. Barnes, J. R. Durrant , B. C. O'Regan, *Journal of Physical Chemistry C*, 2011, **115**, 2439-2447.

[127] K. Park, Q. Zhang, B. B. Garcia, X. Ahou, Y. H. Jeong, G. Cao, *Advanced Materials,* 2010, **22**, 2329-2332.

[128] R. Jose, V. Thavasi, S. Ramakrishna, *Journal of the American Ceramic Society*, 2009, **92**, 289-301.

[129] K. Sayama, H. Sugihara, H. Arakawa, *Chemistry of Materials,* 1998, **10**, 3825-3832.

[130] S. Ito, P. Chen, P. Comte, M. K. Nazeeruddin, P. Liska, P. Pechy, M. Grätzel, *Progress in Photovoltaics : Research and Applications,* 2007,**15,** 603-612.

[131] J. R. Jennings, Q. Wang, *Journal of Physical Chemistry C*, 2010, **114**, 1715-1724.

[132] A. Mang, K. Reimann, St. Rübenacke, *Solid State Communications*, 1995, **95**, 251-254.

[133] E. M. Kaidashev, M. Lorenz, H. V. Wenckstern, A. Rahm, H. C. Semmelhack, K. H. Han, G. Benndorf, C. Bundesmann, H. Hochmuth, M. Grundmann, *Applied Physics Letters,* 2003, **82**, 3901-3903.

[134] H. M. Cheing, W. H. Chiu, C. H. Lee, S. Y. Tsai, W. F. Hsieh, *Journal of Physical Chemistry C*, 2008, **112**, 16359-16364.

[135] H. M. Cheng, W. F. Hseih, *Energy and Environmental Science*, 2010, **3**, 442-447.

[136] A. Hauch, A. Georg, *Electrochemica Acta*, 2001, **46**, 3457-3466.

[137] M. Wu, X. Lin, Y. Wang, L. Wang, W. Guo, D. Qi, X. Peng, A. Hagfeldt, M. Grätzel, T. Ma, *Journal of American Chemical Soc*iety, 2012, **134**, 3419-3428.

[138] T. N. Murakami, M. Grätzel, *Inorganic Chimica Acta*, 2008, **361**, 572-580.

[139] W. A. Adamson, in *Physical Chemistry of Surfaces*, 1982, 4th ed., John Wiley & Sons, New York, p548.

[140] L. T. Zhuravlev, *Colloids and Surfaces A: Physicochemical and Engineering Aspects*, 2000, **173**, 1-38.

[141] P. B. Balbuena, K. E. Gubbins, *Langmuir*, 1993, **9**, 1801-1814.

[142] P. Atkins, J. D. Paula, in *Physical Chemistry*, 2006, Oxford University Press, p917.

[143] I. Langmuir, *Journal of American Chemical Society*, 1918, **40**, 1361-1403.

[144] M. Murthi, R. Q. Snurr, *Langmuir*, 2004, **20**, 2489-2497.

[145] F. Rouquerol, J. Rouquerol, K. Sing, in *Adsorption by Powders and Porous Solids*, 1999, Academic press London, p118.

[146] H. E. Avery, in *Basic Reaction Kinetics and Mechanisms*, 1974, Macmillan Press LTD, London, p 121.

[147] Z. Xu, J. G. Cai, B. C. Pan, *Journal of Zhejiang University Science A (Applied Physics and Engineering),* 2013, **14**,155-176.

[148] W. Roger Jr, M. Sclar, *Journal of Physical Chemistry*, 1932, **36**, 2284-2291.

[149] J. J. Kipling, in *Adsorption from Solution of Non-Electrolytes*, 1965, Academic Press INC. London, p 24.

[150] S. Sohn, D. Kim, *Chemosphere*, 2005, **58**, 115-123.

[151] P. Wen, M. Xue, Y. Ishikawa, H. Itoh, Q. Feng, *Applied Materials and Interfaces*, 2012, **4**, 1928-1934.

[152] Y. Lu, D. J. Choi, J. Nelson, O. B. Yang, B. A. Parkinson, *Journal of the Electrochemical Society*, 2006, **158**, E131-E137.

[153] E. D. Orto, L. Raimondo, A. Sassella, A. Abboto, *Journal of Materials Chemistry*, 2012, **22**, 11364-11369.

[154] M. K. Nazeerudin, F. D. Angelis, S. Fantacci, A. Selloni, G. Viscardi, P. Liska, S. Ito, B. Takeru, M. Grätzel, *Journal of American Chemical Society*, 2005, **127**, 16835-16847.

[155] T. Marinado, M. Hahlin, X. Jiang, M. Quintana, E. M. J. Johansson, E. Gabrielsson, S. Plogmaker, D. P. Hagberg, G. Boschloo, S. M. Zakeeruddin, M. Grätzel, H. Siegbahn, L. Sun, A. Hagfeldt, H. Rensmo, *Journal of Physical Chemistry C*, 2010, **114**, 11903-11910.

[156] H. A. Harms, N. Tetreault, V. Gusak, B. Kasemo, M. Grätzel, *Journal of Physical Chemistry and Chemical Physics*, 2012, **14**, 9037-9040.

[157] Y. Liang, B. Peng, J. Chen, *Journal of Physical Chemistry C*, 2010, **114**, 10992-10998.

[158] S. P. Bates, G. Kresse, M. J. Gillan, *Surface Science*, 1998, **409**, 336-349.

[159] P. Falaras, *Solar Energy Materials and Solar Cells*, 1998, **53**, 163-175.

[160] A. H. Goff, S. Joiret, P. Falaras, *Journal of Physical Chemistry B*, 1999, **103**, 9569-9575.

[161] H. Greijer, J. Lindgren, A. Hagfeldt, *Journal of Physical Chemistry B*, 2001, **105**, 6314-6320.

[162] C. P. Leon, L. kador, B. Peng, M. Thelakkat, *Journal of Physical Chemistry B*, 2006, **110**, 8723-8730.

[163] V. Shklover, Y. E. Ovchinnikov, L. S. Braginsky, S. M. Zakeeruddin, M. Grutzel, *Chemistry of Materials*, 1998, **10**, 2533-2541.

[164] A. Kay, M. Grätzel, *Chemistry of Materials*, 2002, **14,** 2930-2935.

[165] K. E. Lee, M. A. Gomez, S. Elouatik, G. P. Demopoulos, *Langmuir*, 2010, **26**, 9575-9583.

[166] N. Martsinovich, A. Troisi, *Energy and Environmental Science*, 2011, **4**, 4473-4495.

[167] Z.S. Wang, H. Kawauchi, T. Kashima, H. Arakawa, *Coordination Chemistry Reviews*, 2004, **248**, 1381-1389.

[168] T. Watson, P. Holliman, D. Worsley, *Journal of Materials Chemistry*, 2011, **21**, 4321-4325.

[169] A. Peic, D. Staff, T. Risbridger, B. Menges, L. M. Peter, A. B. Walker, P. J. Cameron, *Journal of Physical Chemistry C*, 2011, **115**, 613-619.

[170] B. Volker, F. Wolzl, T. Burgi, D. Lingenfelser, *Langmuir*, 2012, **28**, 11354-11363.

[171] A. Fillinger, B. A. Parkinson, *Journal of the Electrochemical Society*, 1999, **146**, 4559-4564.

[172] T. Ishihara, J. Tokue, T. Sano, Q. Shen, T. Toyoda, N. Kobyashi, *Japanese Journal of Applied Physics*, 2005, **44**, 2780-2782.

[173] P. J. Holliman , M. L. Davies, A. Connell, B. V. Velasco, T. M. Watson, *Chemical Communications*, 2010, **46**, 7256-7258.

[174] C. R. Lee, H. S. Kim, I. H. Jang, J. H. Im, N. G. Park, *Applied Materials and Interfaces,* 2011, **3**, 1953-1957.

[175] I. Concina, E. Frison, A. Braga, S. Silverstrini, M. Maggini, G. Sberveglieri, A. Vomiero, T. Carofiglio, *Chemical Communications*, 2011, **47**, 11656-11658.

[176] J. J. Cid, J. H. Yum, S. R. Jang, M. K. Nazeeruddin, E. M. Ferrero, E. Palomares, J. Ko, M. Grätzel, T. Torres, *Angewandte Chemie International Edition*, 2007, **46**, 8358-8362.

[177] M. Guo, P. Diao. Y. J. Ren, F. Meng, H. Tian, S. M. Cai, *Solar Energy Materials & Solar Cells*, 2005, **88**, 23-35.

[178] Y. Chen, Z. Zeng, C. Li, W. Wang, X. Wang, B. Zhang, *New Journal of Chemistry*, 2005, **29**, 773-776.

[179] D. Kuang, P. Walter, F. Nuesch, S. Kim, J. Ko, P. Comte, S. M. Zakeeruddin, M. K. Nazeeruddin, M. Grätzel, *Langmuir,* 2007, **23**, 10906-10909.

[180] W. Wu, F. Meng, J. Li, X. Teng, J. Hua, *Synthetic Metals*, 2009, **159**, 2028-1033.

[181] R. Y. Ogura, S. Nakane, M. Morooka, M. Orihashi, Y. Suzuki, K. Noda, *Applied Physics Letters*, 2009, **94**, 073308-1 -073308-3.

[182] C. M. Lan, H. P. Wu, T. Y. Pan, C. W. Chang, W. S. Chao, C. T. Chen, C. L. Wang, C. Y. Lin, E. W. G. Diau, *Energy and Enivironmental Science*, 2012, **5**, 6460-6464.

[183] P. J. Holliman, M. Mohsen, A. Connell, M. L. Davies, K. AL-Salihi, M. B. Pitak, G. J. Tizzard, S. J. Coles, R. W. Harrington, W. Clegg, C. Serpa, O. H. Fontes, C. Charbonneau, M. J. Carnie, *Journal of Materials Chemistry*, 2012, **22**, 13318-13327.

Chapter Two Experiment and Methods

2.1 Experimental Part

The initial part of this chapter contains a detailed description of the materials and instruments used for each specific experiment. The second part of this chapter focuses on the device manufacture and the experiments which are related to desorption and re-dyeing of sensitizers for DSC, ultra-fast co-sensitization and experiments which are related to the kinetics of sensitizer adsorption on TiO_2 photo-electrodes for DSCs.

2.2 Materials

2.2.1 Conductive glass

Fluorine-doped transparent conducting oxide (TCO) was sourced from NSG-Pilkington. This TEC-15 glass has a characteristic, resistivity 15 Ω/sq, transmission 83% at 550 nm and glass thickness 3.2 mm.[1]

2.2.2 TiO_2 paste

The TiO_2 paste used in this thesis was either a commercial paste; DSL 18NR-T (Dyesol) or a P25 TiO_2 paste which was prepared according to the procedure in the literature.[2] This paste used 20% wt% of P25 TiO_2 (Degussa) mixed with ethyl cellulose (Aldrich) in anhydrous terpineol (Aldrich). This was prepared by dissolving ethyl cellulose in terpineol, and adding P25 powder and stirring for 24 hr. Finally the paste was homogenized for 30 minutes followed by sonication for 15 minutes. The paste was characterized by TGA to determine the ratio of TiO_2 in the paste, typically using 0.6 mg of paste and heating from 30-650 °C at a rate 10 °C/min. The TiO_2 ratio was typically about 20% (wt) in the paste.

2.2.3 Counter electrode

The platinum catalyst was used as counter electrodes in this thesis, which were prepared by thermal decomposition of platinum. Usually, 40 μl to 10 mM solution of

hexachloroplatinic (IV) acid hydrate (Aldrich) in anhydrous isopropanol was put on clean FTO glass. Coated electrodes were sintering at 400 °C for 30 min. It was then gradually cooled to room temperature and used for device manufacturing.

2.2.4 Redox electrolyte

The electrolyte triiodide/iodide redox couple mediator was used with all DSC devices in this thesis. The electrolyte was prepared by dissolving mixing different components 0.1 M lithium iodide, 0.05 M iodine and 0.6 M dimethyl propyl imidazolium iodide (Sigma-Aldirch) in dry acetonitrile and methoxypropionitrile solvents.

2.2.5 Chemicals

All chemical reagents (puriss grade) were used without further purification. Tetra-butyl ammonium hydroxide (98%), acetonitrile, methoxypropionitrile, tert-butanol were purchased from Sigma Aldrich.

2.2.6 Sensitizers

The dye sensitizers used were *cis*-bis(isothiocyanato)bis(2,2'-bipyridyl-4,4'-dicarboxylato)-ruthenium(II)-bis-terta-butylammonium, (N719) (Dyesol Ltd), the indoline dyes D131 and (D149) (Mitsubushi), and SQ2 (Solaronix Ltd). SQ1 and YD were prepared by Dr Arthur Connell and Moneer Mohsen at Bangor University.[3]

2.3 Instruments

2.3.1 UV-Vis Spectroscopy

UV-Vis spectroscopy is a useful technique employed to measure the amount of light absorption by a sample. The light absorption by a sample depends upon the wavelength of light, so UV-visible spectrophotometers use monochromatic light. The instrument operates by passing a beam of light from the UV-Vis lamp sources (a deuterium lamp for UV light, and a tungsten lamp is used as a source for visible

light), through a sample and measuring the intensity of light reaching a detector. A general schematic of UV-Vis Spectrometer is shown in Figure 2.1.

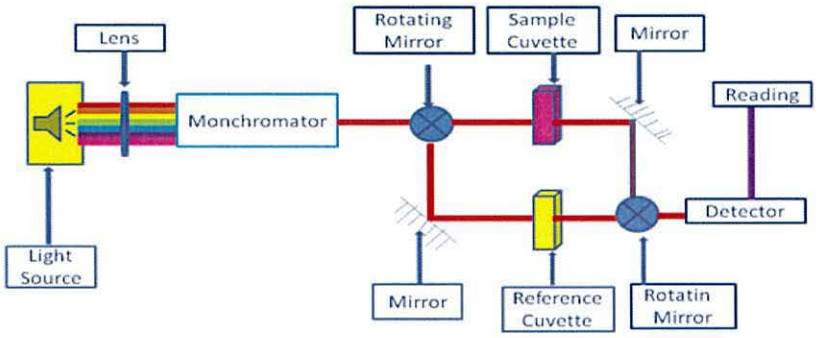

Figure 2.1: Diagram showing the principle working double beam UV/Vis-Spectrophotometer. Redrawn from[4]

UV-Vis light absorption is due to electronic transitions in the sample. The electron promotion will be from a ground state otherwise known as the highest occupied molecular orbital (HOMO) to excited states. Generally valence electrons are the only ones whose energies permit them to be excited by UV-Vis radiation.[5] There are four types of electronic transitions that are possible, ($n \rightarrow \pi^*$), ($\pi \rightarrow \pi^*$), ($n \rightarrow \sigma^*$) and ($\sigma \rightarrow \sigma^*$). The energy of these electronic transitions is generally in the following order.[6] ($n \rightarrow \pi^*$) < ($\pi \rightarrow \pi^*$) < ($n \rightarrow \sigma^*$) < ($\sigma \rightarrow \sigma^*$)

To illustrate these energy levels, Figure 2.2 shows the hypothetical energy diagram of electronic transitions in an organic molecule:

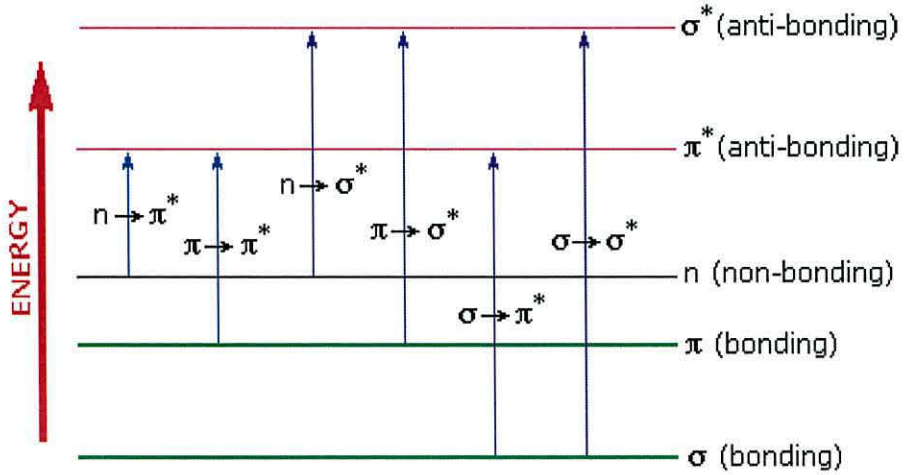

Figure 2.2: Hypothetical diagram of electronic transitions in organic molecule. Redrawn from.[4]

The transition n → σ* is high in energy, typically with a corresponding wavelength of 150-250 nm. Most UV-Vis spectra involve the transitions n → π* and π → π* and the transitions π→ π* are generally more intense than n → π* because n → π* band is usually at longer wavelength since the transition energy is lower.[7]

Based on Beer's law, the absorption of light by the sample is proportional to the concentration of absorbing molecules and Lambert's law tells us that the fraction of radiation absorbed is dependent on the path length. Combining these two laws gives the Beer-Lambert law.[8]

$$A = \log_{10} \frac{I_o}{I} = \varepsilon lc \qquad \text{Eq 2.1}$$

Where

A is the absorbance

I_o is the intensity of the radiation

I is the intensity of the transmitted radiation

Ɛ is the molar extinction coefficient in $mol^{-1}.L.cm^{-1}$

l is the path length of the absorbing solution in cm

C The concentration of absorbing species in $mol.L^{-1}$

The most common application of Beer-Lambert equation is to determine the concentration of a chromophore in solution. In practice, the Ɛ can be determined at the maximum absorbance λ_{max} by measuring a series of known concentrations of dye solution or standards. The absorbances of the standard solutions are then used to prepare a calibration curve.

2.3.2 I-V measurments

The current-voltage characteristics for the DSC devices were measured using a Keithley 2400 source meter in the voltage range (0-1 V at a maximum current 0.2A).

This was connected with a class AAB (ABET solar) simulator a 450 W xenon light source to give an irradiance of one sun (AM 1.5 spectrum).

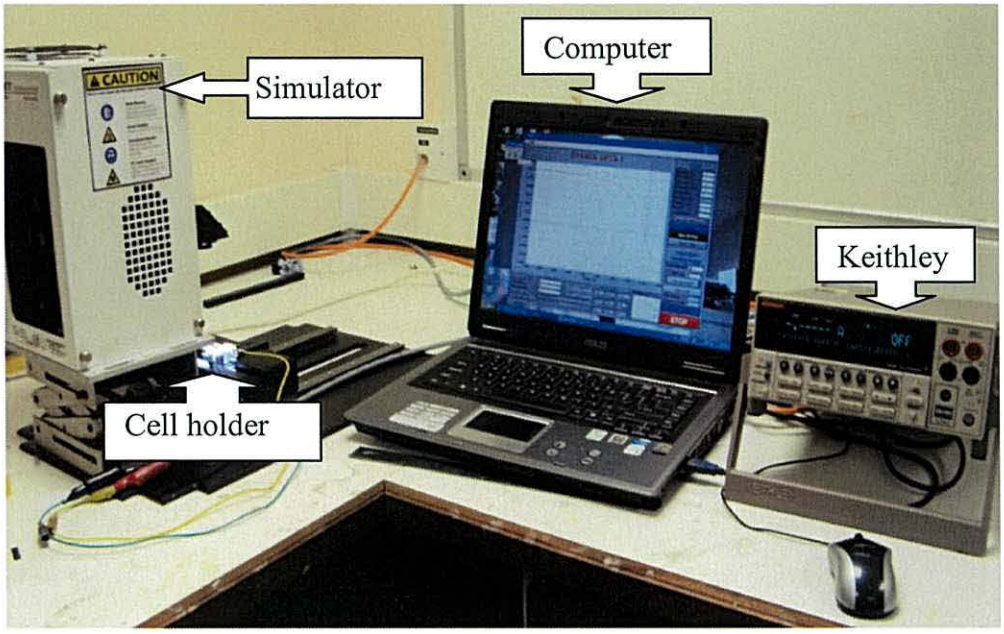

Figure 2.3: Photograph of Keithley Source-meter and I-V measurement system

2.3.3 Thermogravimetry (TGA)

Thermo gravimetric analysis (TGA) is based on the measurement of mass loss of materials as a function of temperature. A thermogrvimetric curve is obtained from a plot of mass change against temperature (T). During a TGA measurement, about 0.5 mg of TiO_2 paste was accurately weighed and then run in a nitrogen atmosphere and was heated from 25-650 °C at a rate of 10°C/min using an SDT Q600 instrument (TA Instruments).

2.3.4 External quantum efficiency (EQE) measurements

All the EQE for the samples were measured in Swansea University by Dr Mathew Davies. A QEX10 Quantum Efficiency Measurement system used a xenon arc lamp source, monochromator, filter and reflective optics to provide stable monochromatic light. The machine was calibrated with Si reference cell. In general, samples measured at range 300-800 nm with data measuring every 10 nm.

2.3.5 Digital Camera

All photographs for the devices in this thesis were taken using a Sony digital camera (12.1 mega pixels, 6.2-18.6 mm optical 3x).

2.3.6 Fast dyeing technique

Ultra-fast dyeing was used for dyeing DSC devices and the experimental design is shown in Figure 2.4. In general, this method involved first sealing the two electrodes together and then injecting or pumping a dye solution through the device cavity. Full details of the dyeing experiments are given in the following section.

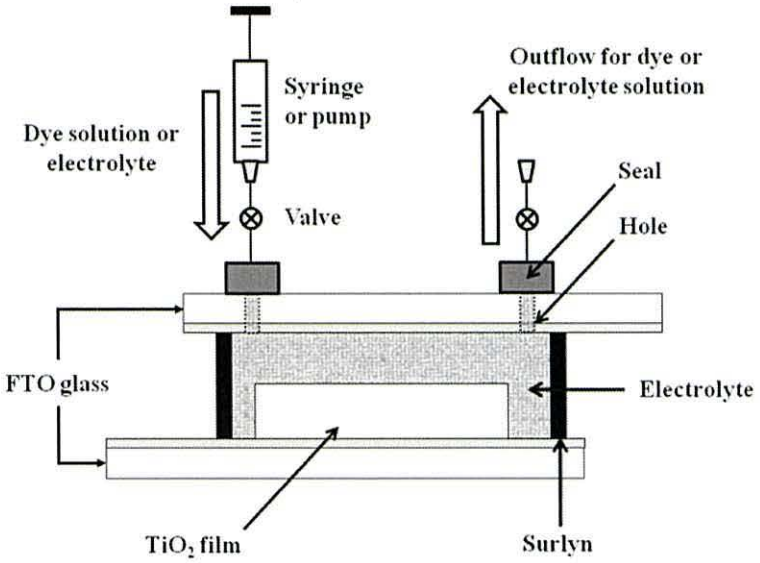

Figure 2.4 Schematic of the design of the dye-sensitized solar cell used in these studies showing pumping procedure. Taken from the reference[9]

2.4 Experiments Relating to Chapter 3 – Adsorption –Desorption and Re-dyeing

2.4.1 Molar extinction coefficient (Ɛ).

The molar extinction coefficients (Ɛ) for the dyes used were obtained by measuring UV-Vis spectra using a series of varying dye concentrations. To do this, stock solutions of dye were prepared by dissolving an exact amount of dye in a known volume of solvent. The solutions were then diluted into the working range of the

spectrometer and the absorbance values were recorded at the wavelength maximum for each dye using a ATI Unicom UV/Vis Spectrophotometer. The calibration curves were plotted between absorbance and dye concentrations to find the molar extinction coefficient (ε) from the slope using Beer Lambert equation (Equation 2.1).

2.4.2 Adsorption isotherm experiments

To make TiO_2 films, glass microscope slides (3 cm x 1.5 cm) were washed with isopropanol and dried in air and two layers of P25 colloid were printed onto microscope slides glass using a doctor blade method. The layer thickness was defined by a Scotch tape™ spacer (2 cm x 0.5 cm). The resulting TiO_2 film electrodes were sintered at 450 ^{o}C for 30 min after each TiO_2 layer had dried at room temperature. All batch adsorption experiments were carried out under dark conditions at *ca.* 20 ^{0}C. A stock solution of N719 was prepared (100 mg.L^{-1}) and then diluted to the appropriate concentration at the range (5-60 mg.L^{-1}). A stock solution of the other dye (SQ1) was also prepared (10 mg.L^{-1}) and then diluted to the appropriate concentration in the range (0.1 – 1.2 mg.L^{-1}). Adsorption was achieved by adding sintered TiO_2 films (2 cm x 0.5cm) into 20 ml of dye solution of a known concentration in a sealed pot and leaving this to stand for 8 hours at room temperature. After 8 hours the films were taken out and the absorbance of the desorbed dye solutions was measured at 532 nm for N719 and at 636 nm for SQ1, using a UV-Vis spectrometer. The adsorbed dye amount on the TiO_2 (mg.cm^{-2}) at equilibrium (Qe) was calculated from the following equation.[10]

$$Qe = \frac{(C_i - C_e) * V}{A} \qquad \text{Eq 2.2}$$

Where C_i and C_e are the initial and equilibrium dye concentration (mg.L^{-1}) V is the volume (litre), and A is the area of film (cm^2).

2.4.3 Device Manufacture

For the working electrode, conductive glass (TEC-15, NSG Pilkington) (3 cm x 1.5 cm) was washed with isopropanol and dried in air and two layers of P25 colloid were printed onto the conductive side of the glass using a doctor blade method. The layer

thickness was defined by a Scotch tape™ spacer. The resulting TiO_2 film electrodes were sintered at 450 °C for 30 min after each TiO_2 layer deposition. The films were then immersed in an aqueous solution of $TiCl_4$:THF_2 (15mM, Aldrich) for 30 min at 70 °C, after then re-sintered at 450 °C for 30 min.

For the counter electrode, two holes were drilled *ca.* 2 cm apart through conductive glass (TEC-15, Pilkington) (3 cm x 1.5 cm) and the glass was washed with isopropanol and dried in air. Then the conductive side of the glass was coated with an aqueous solution of H_2PtCl_6 (40 μL of 5mM, Aldrich) and the electrodes were sintered at 400 °C for 30 min.

Devices were then assembled by first placing a Surlyn™ (DuPont) gasket around the TiO_2 photo-electrode and then placing the platinised counter electrode on top of this and sealing at 120 °C with gentle pressure for 2 min. Finally, prior to the sensitization procedures described below, contacts were made onto the working and counter electrodes using conductive silver paint (Agar).

2.4.4 Investigation of SQ1 and N719 sorption from mixed dye solution by passive dyeing

From stock solutions of N719 (1.5 mM) and SQ1 (0.25mM) a series of different ratios of SQ1:N719 were prepared in the range (5 %, 10 %, 20 %, 40 %, 50 %, 60 % and 80 % c/c) in 10 ml volumes and labelled (a to j). A number of double layer TiO_2 films (1 x 2cm) were also prepared and sintered at 450 °C for 30 minutes. After the TiO_2 films cooled, each film was placed in a pot of mixed dye solution. After 24 hours, the films were taken out and washed with ethanol. The UV-Vis spectrum for each dyed film was measured using a ATI Unicam UV/Vis Spectrophotometer. Each film was then immersed in *tetra*-butyl ammonium hydroxide solution (1% by weight prepared by dissolving 1 g of *tetra*-butyl ammonium hydroxide in 100 ml of a 50:50 V/V ethanol:water solution). The absorbances for the desorbed dye solutions were measured on the same spectrometer and the desorbed amounts of the dyes were determined using the molar extinction coefficient of each dye.

2.4.5 Studies of dye desorption by different alkali solutions.

The TiO_2 electrode of a sealed DSC device was dyed with the Ru-bipy dye N719 (Dyesol) by pumping dye solution (1ml, 2.8mM) through the device cavity at a flow rate of 100 μL min^{-1} for 10 minutes using the fast dyeing technique described previously[8] and this was labelled Device A. After the device performance had been measured, the N719 dye was desorbed using a solution of KOH (150 μL, 100mM). The device cavity was then washed sequentially with ethanol, 0.1 M $HCl_{(aq)}$, and filled with I_3^-/I^- electrolyte. This device was labelled Device A1 and the device performance was re-measured and the efficiency was found to have dropped significantly confirming dye removal. After the electrolyte was removed from the device cavity, this was again rinsed with ethanol in the same manner as described above and the same device was re-dyed with N719 (1 ml, 2.8 mM) and fresh electrolyte was added; the resulting device was labelled B. After the device performance had been measured, the N719 dye was desorbed using a solution of NaOH (150 μL, 100 mM) The device cavity was then washed sequentially with ethanol, 0.1 M $HCl_{(aq)}$, and filled with I_3^-/I^- electrolyte. This device was labelled Device B1. After electrolyte removal in the same manner as described above, the same device was re-dyed with N719 (1 ml, 2.8 mM) and fresh electrolyte was added; the resulting device was labelled C. After the device performance had been measured, the N719 dye was desorbed using a solution of LiOH (150 μL, 100 mM). The device cavity was then washed sequentially with ethanol, 0.1 M $HCl_{(aq)}$, filled with I_3^-/I^- electrolyte. This device was labelled Device C1. After the electrolyte removal in the same manner as described above the same device was re-dyed with N719 (1 ml, 2.8 mM) and fresh electrolyte was added; the resulting device was labelled D. After the device performance had been measured, the N719 dye was desorbed using a solution of Bu_4NOH (200 μL, 40 mM). The device cavity was then washed sequentially with ethanol, 0.1 M $HCl_{(aq)}$, and filled with I_3^-/I^- electrolyte. This device was labelled Device D1. After the electrolyte removal in the same manner as described above the same device was re-dyed with N719 (1 ml, 2.8 mM) and fresh electrolyte was added; the resulting device was labelled E. After the device performance had been measured, the N719 dye was desorbed using a solution of tris(hydoxymethyl)ethylamine (THMA) (300 μL, 40 mM). The device cavity was

then washed sequentially with ethanol, 0.1 M $HCl_{(aq)}$, and filled with I_3^-/I^- electrolyte. This device was labelled Device E1. After the electrolyte removal, the same device was re-dyed with N719 (1 ml, 2.8 mM) and fresh electrolyte was added; the resulting device was labelled F.

2.4.6 Dark current measurement

The TiO_2 electrode of a sealed DSC device was dyed with the Ru-bipy dye N719 (Dyesol) by pumping dye solution (1ml, 0.5 mM) through the device cavity at a flow rate of 100 μL min^{-1} for 10 minutes using the fast dyeing technique described previously and this was labelled Device A. The device performance was measured under light and also in a dark when the device was covered by black paper. N719 was desorbed using a solution of *tetra*-butyl ammonium hydroxide solution (1% by weight g/ml). The device cavity was then washed sequentially with de-ionized water, 0.1 M $HCl_{(aq)}$, water, ethanol and acetone and then filled with I_3^-/I^- electrolyte. This device was labelled Device B and the performance was re-measured again under light and in the dark. After electrolyte removal using 200 μl ethanol, the device was then re-dyed with N719 (1 ml, 0.5 mM) then filled with I_3^-/I^- electrolyte and this was labelled Device C and the performance was measured again under light and in a dark. Dyeing desorption and re-dyeing with the same solutions and measuring under light and in the dark were repeated three times.

2.4.7 Device error

A numbers of TiO_2 electrodes of a sealed DSC device were prepared and dyed with Ru-bipy dye N719 (Dyesol) by pumping dye solution (1ml, 2.8 mM) through the device cavity at a flow rate of 100 μL min^{-1} for 10 minutes using the fast dyeing technique described previously. Each device was filled with I_3^-/I^- electrolyte then the device performance was measured.

2.4.8 Desorption and re-dyeing the Ru-bipyridyl Dye - N719

The TiO_2 electrode of a sealed DSC device was dyed with the Ru-bipy dye N719 (Dyesol) by pumping dye solution (1ml, 2.8 mM) through the device cavity at a flow

rate of 100 μL min^{-1} for 10 minutes using the fast dyeing technique described previously and this was labelled Device A. After the device performance had been measured, the N719 dye was desorbed using a solution of *tetra*-butyl ammonium hydroxide solution (1% by weight g/ml). The device cavity was then washed sequentially with de-ionized water, 0.1 M $HCl_{(aq)}$, water, ethanol and acetone and then filled with I_3^-/I^- electrolyte. This device was labelled Device A1 and the performance was re-measured and the efficiency was found to have dropped significantly confirming dye removal. Finally the electrolyte was removed from the device cavity which was again rinsed with de-ionized water, 0.1 M $HCl_{(aq)}$, de-ionized water, ethanol and acetone in the same manner as described above and the same device was re-dyed with N719 (1 ml, 2.8 mM) and fresh electrolyte was added; the resulting device was labelled A1-R. Desorption and re-dyeing cycles were then repeated using the same procedure and showing the same trends in device efficiency. These devices were labelled A2 (desorbed TiO_2) and A2-R (N719 re-dyed for the second time). The photographs of TiO_2 devices (2x0.5 cm) were taken to illustrate the colour changes taking place during the dyeing, desorption and re-dyeing cycles using the Ru-bipyridyl dye N719.

2.4.9 Desorption and re-dyeing the Ru-terpyridyl Dye – "Black dye"

The TiO_2 electrode of a sealed DSC device was dyed with the Ru-terpyridyl dye "Black dye" (Dyesol) by pumping dye solution (1 ml, 0.28 mM) through the device cavity at a flow rate of 100 μL min^{-1} for 10 minutes using the fast dyeing technique described previously and this was labelled Device B. After the device performance had been measured (Table 3.9), the "Black dye" dye was desorbed using *tetra*-butyl ammonium hydroxide solution (1% by weight in 1:1 ethanol-water solution). The device cavity was then washed sequentially with de-ionized water, 0.1 M $HCl_{(aq)}$, de-ionized water, ethanol and acetone and then filled with electrolyte. This device was labelled Device B1 and the performance was re-measured and the efficiency was found to have dropped significantly confirming dye removal. Finally the electrolyte was removed from the device cavity which was again rinsed with de-ionized water, 0.1 M $HCl_{(aq)}$, de-ionized water, ethanol and acetone and the same device was re-dyed with "Black dye" (1 ml, 2.8 mM) and fresh electrolyte was added; the resulting device was labelled B1-R. The desorption and re-dyeing cycle was then repeated

using the same procedure and showing the same trends in device efficiency. These devices were labelled B2 (desorbed TiO_2) and B2-R ("Black dye" re-dyed for second time).

2.4.10 Desorption and re-dyeing with the organic dye SQ1

The TiO_2 electrode of a sealed DSC device was dyed with SQ1 (1 ml, 0.28 mM) by pumping dye solution through the device cavity at a flow rate of 100 $\mu L\ min^{-1}$ for 10 minutes using the fast dyeing technique described previously and this was labelled Device C. After the device performance had been measured (Table 3.10), the SQ1 dye was desorbed using a solution of *tetra*-butyl ammonium hydroxide solution (1% by weight prepared by dissolving 1 g of *tetra*-butyl ammonium hydroxide in 100 ml of a (1:1) V/V ethanol:water solution). The device cavity was then washed sequentially with de-ionized water, 0.1 M $HCl_{(aq)}$, de-ionized water, ethanol and acetone and then filled with I_3^-/I^- electrolyte. This device was labelled Device C1 and the performance was re-measured and the efficiency was found to have dropped significantly confirming dye removal (Table 3.10). Finally, the electrolyte was removed from the device cavity which was again rinsed with de-ionized water, 0.1 M $HCl_{(aq)}$, de-ionized water, ethanol and acetone and the same device was re-dyed with SQ1 and fresh electrolyte was added; the resulting device was labelled C1-R. Photographs of TiO_2 devices (2x0.5 cm) were taken to illustrate the colour changes taking place during the dyeing desorption and re-dyeing cycles using SQ1.

2.4.11 Desorption and re-dyeing with the organic dye D149

The TiO_2 electrode of a sealed DSC device was dyed with the organic dye D149 by pumping dye solution (1ml, 0.5 mM) through the device cavity at a flow rate of 100 $\mu L\ min^{-1}$ for 10 minutes using the fast dyeing technique described previously and this was labelled Device D. After the device performance had been measured (Table 3.11), the D149 dye was desorbed using aqueous *tetra*-butyl ammonium hydroxide solution (1% by weight in 1:1 ethanol-water solution). The device cavity was then washed sequentially with de-ionized water, 0.1 M $HCl_{(aq)}$, de-ionized water, ethanol and acetone and then filled with electrolyte. This device was labelled Device D1 and the performance was re-measured and the efficiency was found to have dropped

significantly confirming dye removal. Finally the electrolyte was removed from the device cavity which was again rinsed with de-ionized water, 0.1 M $HCl_{(aq)}$, de-ionized water, ethanol and acetone in the same manner as described above and the same device was re-dyed with D149 (0.5 mM) and fresh electrolyte was added; the resulting device was labelled D1-R.

2.4.12 Desorption and re-dyeing with different dyes

A sealed TiO_2 photo-electrode was dyed with SQ1 (1 ml, 0.28 mM) using the fast dyeing technique described above and this was labelled Device E. After the device performance had been measured and the data summarized in Table 3.12, the SQ1 dye was desorbed using *tetra*-butyl ammonium hydroxide solution (1% by weight in 50:50 ethanol-water solutions). Finally the same device was re-dyed with N719 (1 ml, 2.8 mM) and fresh electrolyte was added; the resulting device was labelled E1-R.

2.4.13 Changing the orders of dyeing N719 and SQ1

A sealed TiO_2 photo-electrode was dyed with the Ru-bipy dye N719 (1ml, 2.8 mM) using the fast dyeing technique and this was labelled Device F. After the device performance had been measured (Table 3.13), the N719 dye was desorbed using aqueous *tetra*-butyl ammonium hydroxide solution (1% by weight in 50:50 ethanol-water solution). Finally the same device was re-dyed with SQ1 (1ml, 0.28 mM) and fresh electrolyte was added; the resulting device was labelled F1-R.

2.4. 14 Desorption and re-dyeing using mixed dye solutions.

A mixed dye solution containing N719 and SQ1 was prepared by mixing 4300 μL of N719 solution (2 mM) with 700μL of SQ1 solution (0.4 mM) to give an overall ratio SQ1:N719 of 3%:97% (conc. to conc.). The TiO_2 electrode of a sealed DSC device was then dyed by pumping this mixed N719:SQ1 solution through the device cavity at a flow rate of 100 μL min^{-1} for 10 minutes using the fast dyeing technique described previously and this was labelled Device G. After the device performance had been measured (Table 3.14), the dyes were desorbed using aqueous *tetra*-butyl ammonium hydroxide solution (1% by weight in 50:50 ethanol-water solution). The

device cavity was then washed sequentially with de-ionized water, 0.1 M $HCl_{(aq)}$, de-ionized water, ethanol and acetone and then filled with electrolyte. This device was labelled Device G1 and the performance was re-measured and the efficiency was found to have dropped significantly confirming dye removal. The concentration of N719 dye desorbed from the TiO_2 photo-electrode was also measured using UV-visible spectroscopy and the data are shown in Table 3.14. Finally, the electrolyte was removed from the device cavity which was again rinsed with de-ionized water, 0.1 M $HCl_{(aq)}$, de-ionized water, ethanol and acetone in the same manner as described previously and the same device was re-dyed with mixed N719:SQ1 dye solution and fresh electrolyte was added; the resulting device was labelled G1-R.

2.4.15 Effect of Bu_4NOH concentration on dye desorption

A TEC glass device was prepared with a P25 colloid sintered onto the working electrode and Pt sintered on to the counter electrode. The two electrodes were then sealed together with a Surlyn gasket and the device photo-electrode was then dyed with N719 solution (1ml, 1 mM). The dye was partially desorbed using 100µl of different concentrations of *tetra*-butyl ammonium hydroxide (4, 8, 20 or 40 mM). In between each desorption, the device cavity was rinsed as described previously before re-dyeing with a solution of N719. I-V data were measured after each dyeing step.

2.4.16 Effect of varying volumes of Bu_4NOH on dye desorption

A TEC glass device was prepared with a double layer of P25 colloid sintered onto the photo-electrode and Pt sintered on to the counter electrode. The two electrodes were then sealed together with a Surlyn gasket and the device photo-electrode was then dyed with N719 (1 ml, 1 mM) solution. The dye was partially desorbed using different volumes of 4 mM *tetra*-butyl ammonium hydroxide (100 to 1000 µl). In between each desorption, the device cavity was rinsed as described previously before re-dyeing with a solution of N719. I-V data were measured after each dyeing and desorption step.

2.4.17 Studies of partial dye removal and re-dyeing

The TiO_2 electrode of a sealed DSC device was dyed with N719 by pumping dye solution (1 ml, 2.8 mM) through the device cavity at a flow rate of 100 μL min^{-1} for 10 minutes using the fast dyeing technique described previously and this was labelled Device H. After the device performance had been measured, the N719 dye was partially desorbed using aqueous *tetra*-butyl ammonium hydroxide solution (0.001% by weight in 50:50 ethanol-water solution). The device cavity was then washed sequentially with de-ionized water, 0.1 M $HCl_{(aq)}$, de-ionized water, ethanol and acetone and then filled with electrolyte. This device was labelled Device H1 and the performance was re-measured. The amount of partial N719 removal was then measured using UV-Vis spectroscopy. The electrolyte was then removed from the device cavity which was again rinsed with water, 0.1 M $HCl_{(aq)}$, water, ethanol and acetone in the same manner as described above and the same device was re-dyed with SQ1 (1 ml, 0.28 mM) and fresh electrolyte was added; the resulting device was labelled H1-R. The electrolyte was then removed from the device cavity which was again rinsed with de-ionized water, 0.1 M $HCl_{(aq)}$, de-ionized water, ethanol and acetone in the same manner as described above and the same device was re-dyed with N719 (300μl, 2.8 mM) and fresh electrolyte was added; the resulting device was labelled H2-R.

2.4.18 Study of repeated partial desorption and re-dyeing with different dyes

The TiO_2 electrode of a sealed DSC device was dyed with N719 by pumping dye solution (1ml, 2.8 mM) through the device cavity at a flow rate of 100 μL min^{-1} for 10 minutes using the fast dyeing technique described previously followed by I_3^-/I^- electrolyte and this was labelled Device A. After the device performance had been measured, the N719 dye was desorbed using aqueous *tetra*-butyl ammonium hydroxide solution (1% by weight in 50:50 ethanol-water solution). The device cavity was then washed sequentially with de-ionized water, 0.1 M $HCl_{(aq)}$, de-ionized water, ethanol and acetone and then re-filled with electrolyte. This device was labelled Device B and the performance was re-measured and the efficiency was found to have dropped significantly confirming N719 dye removal. The electrolyte was then removed from the device cavity which was again rinsed with water, 0.1 M $HCl_{(aq)}$, water, ethanol and acetone in the same manner as described above. The same

device was re-dyed with N719 (1 ml, 2.8 mM) and then N719 partially removed using 20 μl of *tetra*-butyl ammonium hydroxide solution before fresh electrolyte was added; the resulting device was labelled C. The electrolyte was then removed from the device cavity with ethanol, and N719 was then partially removed by pumping Bu_4NOH (100 μl, 8 mM) Device D. To the same device, SQ1 (1.5 ml, 0.25 mM) was then added followed by added fresh electrolyte the resulting device was labelled E. The total dye loading was then removed using Bu_4NOH (200 μl, 40 mM), then electrolyte was added and the device measured Device F. Again the same device was re-dyed with N719 (1 ml, 2.8 mM) followed by adding an electrolyte and the I-V was measured. After removing I_3^-/I^- electrolyte by ethanol N719 was partially removed using Bu_4NOH (25 μl, 1 mM) giving Device H. Again the amount of desorbed dye was measured by UV-Vis spectrophotometer. SQ1 (1 ml, 0.25 mM) was added giving (Device I). After the I-V was measured the total dyes were desorbed by Bu_4NOH (200 μl, 40 mM) giving Device J. In the same manner, the amounts of both desorbed dyes were measured by UV-Vis spectroscopy. The device was then re-dyed with N719 (1 ml, 2.8 mM) giving Device K. After measuring the I-V, N719 was partially removed by Bu_4NOH (50 μl, 1 mM) followed by adding electrolyte giving Device L and the electrolyte was then removed and N719 added (1 ml, 2,8 mM) giving Device M and the I-V was then re-measured.

2.4.19 Study of the selective removal of N719

A TEC glass device was prepared with a P25 colloid sintered onto the working electrode and Pt sintered on to the counter electrode. The two electrodes were then sealed together with a Surlyn gasket and the device photo-electrode was then dyed with N719 solution (1 ml, 2.5 mM) followed by I_3^-/I^- electrolyte and the I-V was measured. After the electrolyte was flushed out by 100 μL of ethanol and rinsing, SQ1 was added (300 μL, 2.8 mM) by pumping through the device cavity the cell was measured. The cell was washed with 100 μL of ethanol. N719 was then removed by LiOH (50 μL, 100 mM), and SQ1 was then removed by *tetra*-butyl ammonium hydroxide (100 μL, 4 mM). The UV/Vis spectrum was taken for each desorbed solution. The device was again rinsed with water, 0.1 M $HCl_{(aq)}$, water, ethanol and acetone before being re-dyed with SQ1 (1 ml, 2.8 mM) followed by filling with I_3^-/I^- electrolyte and the I-V of the device was measured. The electrolyte was then

removed from the device cavity which was again rinsed with de-ionized water, 0.1 M $HCl_{(aq)}$, de-ionized water, ethanol and acetone in the same manner as described above and the same device was dyed with N719 (1 ml , 2.5 mM) and fresh electrolyte was added and measured the device. I-V data were measured after each dyeing and desorption step.

2.4.20 Selective removal of N719 and D149

A TEC glass device was prepared with a P25 colloid sintered onto the working electrode and Pt sintered on to the counter electrode. The two electrodes were then sealed together with a Surlyn gasket and the device photo-electrode was then dyed with N719 solution (1 ml, 1 mM). The dye was partially desorbed using *tetra*-butyl ammonium hydroxide (50 μL, 4 mM) before adding D149 dye solution (250 μL, 0.5 mM). The N719 dye was then selectively removed using LiOH (200 μl, 100 mM) before re-dyeing with N719. In between desorption, the device cavity was rinsed as described previously. I-V data were measured after each dyeing and desorption step.

2.4.21 Selective removal of N719, SQ1 and D149

A TEC glass device was prepared with a P25 colloid sintered onto the electrode and Pt sintered on to the counter electrode. The two electrodes were then sealed together with a Surlyn gasket and the device photo-electrode was then dyed with SQ1 solution (300 μL, 0.34 mM), followed by I_3^-/I^- electrolyte and this was labelled Device A. After electrolyte removal and rinsing, N719 was added (500 μL, 1 mM), followed by I_3^-/I^- electrolyte and this was labelled Device B. After electrolyte removal and rinsing D149 was added (200 μL, 0.5 mM), followed by I_3^-/I^- electrolyte and this was labelled Device C. After electrolyte removal and rinsing, N719 dye was selectively removed by pumping LiOH (100 μL, 100 mM) through the device cavity followed by HCl (50 μL, 100 mM), and re-filling with I_3^-/I^- electrolyte and this was labelled Device D. After electrolyte removal and rinsing the SQ1 was desorbed by pumping Bu_4NOH (100 μL, 1 mM) through the device cavity followed by adding I_3^-/I^- electrolyte and this was labelled Device E. After electrolyte removal and rinsing, the D149 was desorbed by pumping Bu_4NOH (100 μL, 8 mM) followed by pumping

acetone (100 μL), and then ethanol (100 μL) and the device was labelled F. I-V data were measured after each dyeing and desorption step.

2.5 Dye Experiments Relating to Chapter 4 - Co-Sensitization

2.5.1 Co-sensitization of Hf-SQ1with N719

A TEC glass device was prepared with a P25 colloid sintered onto the working electrode and Pt sintered on to the counter electrode. The two electrodes were then sealed together with a Surlyn gasket and the device photo-electrode was then sequentially dyed with 3-[(1-ethyl-1,3-dihydro-3,3-dimethyl-2H-indol-2-ylidene)methyl]-4-hydroxy-cyclobutene-1,2-dione otherwise known as half SQ1 (HfSQ1) dye (300μL, 5mM), filling with I_3^-/I^- electrolyte, and then the I-V was measured. After electrolyte removal with 100μL ethanol and rinsing the device, N719 (500 μL, 2.8 mM) was added and the cell was measured. The electrolyte was then removed from the device cavity with 100 μL ethanol. Then all the dyes were completely removed using *tetra*-butyl ammonium hydroxide (250 μL, 40 mM) followed by passing $HCl_{(aq)}$, (100 μL. 100 mM) through the device cavity. Then the device was re-dyed with N719 (500 μL, 2.8 mM) before re-filling with I_3^-/I^- electrolyte and measuring the cell. Hf-SQ1 (300 μL, 5 mM) was then added followed by I_3^-/I^- electrolyte and the cell measured. I-V data were measured after each dyeing and desorption step.

2.5.2 Studies of controlling dye loading in co-sensitized devices

A TEC glass device was prepared with a P25 colloid sintered onto the working electrode and Pt sintered on to the counter electrode. The two electrodes were then sealed together with a Surlyn gasket and the device photo-electrode was then dyed with N719 solution (1 ml, 1 mM), followed by I_3^-/I^- electrolyte and this was labelled Device A. Then dye was partially desorbed using *tetra*-butyl ammonium hydroxide (100 μl, 2 mM) and more I_3^-/I^- electrolyte was added and this was labelled Device B. The device cavity was rinsed as described previously before re-dyeing with a solution of HfSQ1 dye (1 ml, 0.1 mM) followed by I_3^-/I^- electrolyte addition and this was labelled Device C. Dye was then completely removed by Bu_4NOH (200 μl,40

mM) followed by I_3^-/I^- electrolyte and this was labelled Device D . The device cavity was rinsed again before re-dyeing with N719 (1 ml, 1mM) followed by I_3^-/I^- electrolyte addition and this was labelled Device E. N719 was then partially removed by pumping Bu_4NOH (200 µl, 4 mM) followed by I_3^-/I^- electrolyte addition and this was labelled Device F. SQ1 (500 µl, 0.5 mM) in 5mM CDCA was then added followed by I_3^-/I^- electrolyte and this was labelled Device G. Again dye was then completely removed by Bu_4NOH (200 µl, 40 mM) followed by I_3^-/I^- electrolyte addition and this was labelled Device H. The device was re-dyed again with N719 (1 ml, 1mM) followed by I_3^-/I^- electrolyte addition and this was labelled Device I. After partial dye removal, a mixed half SQ1 and SQ1 solution was prepared in 1:1 v/v ratio (1 ml of 0.5 mM SQ1 and 1 ml of 0.1 mM HfSQ1) was followed by I_3^-/I^- electrolyte addition and this was labelled Device K. After removal of all dyes using Bu_4NOH (200 µl, 40 mM), the device was redyed with Hf-SQ1 (1 ml, 0.1 mM) followed by I_3^-/I^- electrolyte addition and this was labelled Device N. N719 (1 ml, 1 mM) was then added followed by I_3^-/I^- electrolyte and this was labelled Device O. The I-V data were measured for each adsorption and desorption step.

2.5.3 Co-sensitization using SQ1:SQ2 mixtures

A TEC glass device was prepared with two layers of DSL-18NRT TiO_2 colloid sintered onto the working electrode followed by a TiO_2 scattering layer and Pt was deposited on the counter electrode as described previously. The two electrodes were then sealed together with a Surlyn gasket and the device photo-electrode was then dyed with 700 µL of a mixed solution containing SQ1 (0.22 mM) and SQ2 (0.33 mM) in 10 mM CDCA, followed by I_3^-/I^- electrolyte addition. The dyes were then completely removed by pumping Bu_4NOH (300 µl, 40 mM) and then $HCl_{(aq)}$ (100 µL , 100 mM) through the device cavity followed by 100µL ethanol, to neutralize and clean the TiO_2 surface. The device was then re-dyed with the same mixed dye solution followed by I_3^-/I^- electrolyte addition and measured the cell. The I-V data were measured at each dyeing and desorption step.

2.5.4 Co-sensitization by sequential dyeing of SQ1 and SQ2

A TEC glass device was prepared with two layers of DSL-18NRT TiO_2 colloid sintered onto the working electrode and Pt sintered on to the counter electrode as described previously. The two electrodes were then sealed together with a Surlyn gasket and the device photo-electrode was then dyed with SQ1 (700 µl, 0.34 mM with 10 mM Chenodeoxycholic acid (CDCA)) followed by I_3^-/I^- electrolyte addition. After electrolyte removal by pumping 100 µl ethanol, SQ1 was partially removed by pumping Bu_4NOH (100 µl, 1 mM) through the device cavity followed by $HCl_{(aq)}$ (50 µL, 100mM). Again I_3^-/I^- electrolyte was added the cell I-V data were measured. The electrolyte was removed and SQ2 (500 µl, 1 mM) was added before re-filling with I_3^-/I^- electrolyte. The I-V data were measured at each step and for the following six days. The above procedure was repeated using another device but changing the order of dyeing; first dyeing with SQ2 (500 µl, 1mM) and after desorption, re-dyeing with SQ1 (200 µl, 0.34 mM).

2.5.5 SQ1 Dyeing, Partial and Selective removal and N719 re-dyeing.

A TEC glass device was prepared with two layers of DSL-18NRT TiO_2 colloid sintered onto the working electrode followed by a TiO_2 scattering layer and Pt was sintered on to the counter electrode as described previously. The two electrodes were then sealed together with a Surlyn gasket and the device photo-electrode was then dyed with SQ1 (300 µl, 0.34 mM) dye solution containing 5 mM CDCA. The dye was partially desorbed using *tetra*-butyl ammonium hydroxide (200 µl, 1mM) and the device cavity was washed by $HCl_{(aq)}$ (50 µl, 100mM) followed by 100 µl ethanol, before adding N719 dye (150 µl, 1 mM) in 5 mM CDCA. The N719 dye was then selectively removed using LiOH (100 µl, 100 mM). The device was then re-dyed again with N719 (1 ml, 1 mM). In between desorptions, the device cavity was rinsed as described previously. I-V data were measured after each dyeing and desorption step.

2.5.6 Co-sensitized sequence of N719 the SQ1

A TEC glass device was prepared with two layers of DSL-18NRT TiO_2 colloid sintered onto the working electrode and Pt was sintered on to the counter electrode as described previously. The two electrodes were then sealed together with a Surlyn gasket and the device photo-electrode was then dyed with N719 (1 ml, 1 mM) containing 5mM MCDCA. The dye was partially desorbed using *tetra*-butyl ammonium hydroxide (50μL, 4mM), and the device cavity was then rinsed, before adding SQ1 dye (10 μl, 0.24 mM). The N719 dye was then selectively removed by pumping LiOH (100 μL, 100 mM) through the device cavity followed by rinsing and re-filling with I_3^-/I^- electrolyte. After electrolyte removal and rinsing, the device was then re-dyed with N719 (1 ml, 1 mM). In between each desorption, the device cavity was rinsed as described previously. The I-V data were measured after each dyeing and desorption step.

2.5.7 Co-sensitization with 6% SQ1:N719

A TEC glass device was prepared with two layers of DSL-18NRT TiO_2 colloid sintered onto the working electrode and Pt was sintered on to the counter electrode as described previously. The two electrodes were then sealed together with a Surlyn gasket and the device photo-electrode was then dyed with a mix of 6% SQ1:N719 by concentration, which was prepared by mixing 1 ml of 0.1 mM SQ1 with 4 ml of 1.5 mM N719 along with 5 mM CDCA. The final concentrations each dye in a mixing dyes solution were found by measuring the absorbance of the dye solutions after diluting 100 times using UV/Vis spectroscopy. The cell was measured after filling with I_3^-/I^- electrolyte. The dyes were removed using *tetra*-butyl ammonium hydroxide (200 μl, 40mM) and the absorbance of the desorbed solution was measured to determine the amount of adsorbed each dye. Again the device was re-dyed with the same 6% SQ1:N719 dye solution after washing the device by $HCl_{(aq)}$ (50μL, 100mM) and 100μL of ethanol followed by rinsing and re-filling with I_3^-/I^- electrolyte and the I-V was measured.

2.5.8 Co-sensitization with single Yellow dye YD

A TEC glass device was prepared with two layers of DSL-18NRT TiO_2 colloid sintered onto the working electrode and Pt was sintered on to the counter electrode as described previously. The two electrodes were then sealed together with a Surlyn gasket and the device photo-electrode was then dyed with the yellow triphenylamine dye, 4-[2-(4-diphenylaminophenyl)vinyl]benzoic acid] (YD) (1.5 ml , 2.5 mM) containing 5 mM CDCA. The device was then re-filling with I_3^-/I^- electrolyte. The I-V data were measured. The dye loaded was then desorbed using Bu_4NOH (200 µL, 40 mM).

2.5.9 Co-sensitization of YD and N719

A TEC glass device was prepared with two layers of DSL-18NRT TiO_2 colloid sintered onto the working electrode and Pt was sintered on to the counter electrode as described previously. The two electrodes were then sealed together with a Surlyn gasket and the device photo-electrode was then dyed with yellow triphenylamine dye (YD), (1.5 ml , 2.5 mM) containing 5 mM CDCA. The device was then filing with I_3^-/I^- electrolyte then the cell was measured. Thereafter the electrolyte was removed by Bu_4NOH (200µL, 40mM). N719 (1ml, 1mM) was added followed by re-filling with I_3^-/I^- electrolyte and the cell measured. After one, day the dyes were desorbed and measured using ATI Unicam UV-Vis spectroscopy. A similar experiment was repeated with another device but changing the order of dyeing, the device dyed was first with N719 and then added YD was added and the I-V was measured.

2.5.10 Co-sensitization of SQ1 and YD

A TEC glass device was prepared with two layers of DSL-18NRT sintered onto the working electrode and Pt was sintered on to the counter electrode as described previously. The two electrodes were then sealed together with a Surlyn gasket and the device photo-electrode was then dyed with SQ1 (500µL, 0.25 mM containing 5 mM CDCA), then YD (1 ml, 2.5 mM with 5 mM CDCA), followed by filling with I_3^-/I^- electrolyte. The I-V data were measured at each dyeing step. The dyes loading were desorbed by Bu_4NOH (200µL, 40mM) and the dye loadings were measured

using the UV-Vis using and depending on the molar extinction coefficient of each dye.

2.5.11 Sensitization using D149

A TEC glass device was prepared with two layers of DSL-18NRT TiO_2 colloid sintered onto the working electrode and Pt was sintered on to the counter electrode as described previously. The two electrodes were then sealed together with a Surlyn gasket and the device photo-electrode was then dyed with D149 (1.5ml, 0.5mM with 5 mM CDCA) using ultra-fast dyeing. The device was then filing with I_3^-/I^- electrolyte and this was labelled Device A the I-V -V data were measured.

2.5.12 Co-sensitization of YD with D149

A TEC glass device was prepared with two layers of DSL-18NRT TiO_2 colloid sintered onto the working electrode and Pt was sintered on to the counter electrode as described previously. The two electrodes were then sealed together with a Surlyn gasket and the device photo-electrode was then dyed with YD (1ml, 2.5mM with 10 mM CDCA) using ultra-fast dyeing followed by I_3^-/I^- electrolyte and this was labelled Device B. After measurement, the electrolyte was then removed by passing 100μL ethanol through the device cavity. D149 (1ml, 0.5 mM) in 10 CDCA was then added through the device cavity followed by re-filling with I_3^-/I^- electrolyte. After the device holes were sealed carefully, and the I-V was measured. The device was the left and was labelled Device D, and after five days was labelled Device E.

2.5.13 Sequential co-sensitization of N719:D149 (10:1)

A TEC glass device was prepared with two layers of DSL-18NRT TiO_2 colloid sintered onto the working electrode and Pt was sintered on to the counter electrode as described previously. The two electrodes were then sealed together with a Surlyn gasket and the device photo-electrode was dyed with N719 (1ml, 1mM with 10 mM CDCA) using ultra-fast dyeing. The device was then measured after filling with I_3^-/I^- electrolyte. The electrolyte was then removed by passing 100μL ethanol through the device cavity. Dye was partially removed by Bu_4NOH (100 μL, 1mM) followed by

rinsing and re-filling with I_3^-/I^- electrolyte the device was re-measured. The electrolyte was then removed by passing 100μL ethanol through the device cavity and D149 (100μL, 0.5 mM with 10 CDCA) was then added followed by re-filling with I_3^-/I^- electrolyte, and the device was re-measured. N719 was then selectively removed with LiOH (200μL, 100mM). The device was then measured after re-filling with I_3^-/I^- electrolyte. After electrolyte removal and rinsing, the device was re-dyed with N719 (1ml, 1mM) followed by re-filing with I_3^-/I^- electrolyte. The holes of the device were then sealed carefully, the device aged and the I-V was measured.

2.5.14 Co-sensitization of a mixed solution of N719:D149 (1:1 v/v)

A TEC glass device was prepared with two layers of DSL-18NRT TiO_2 colloid sintered onto the working electrode and Pt was sintered on to the counter electrode as described previously. The two electrodes were then sealed together with a Surlyn gasket and the device photo-electrode was then dyed with 1.5 ml of a mix N719:D149 solution which was prepared by mixing N719 (1 ml, 1 mM) with D149 (1ml, 0.5 mM) to 60 % D149:N719 by concentration ratio, using ultra-fast dyeing. The device was measured after filing with I_3^-/I^- electrolyte. The dye loadings were desorbed by Bu_4NOH (200μL, 40mM) followed by 200μL of acetone and 100μl of ethanol. The device cavity was washed with $HCl_{(aq)}$ (100μL, 100 mM) followed by 100μL ethanol. The device was the re-dyed with the same N719:D149 dye solution followed by re-filling with I_3^-/I^- electrolyte and the I-V was measured.

2.5.15 Co-sensitization of a mixed solution of N719:D149 (1:2) (v/v)

A TEC glass device was prepared with two layers of DSL-18NRT TiO_2 colloid sintered onto the working electrode and Pt was sintered on to the counter electrode. The two electrodes were then sealed together with a Surlyn gasket and the device photo-electrode was then dyed with 1.5 ml of a mixed N719:D149 solution which was prepared by mixing N719 (1 ml, 1 mM) with D149 (2ml, 0.5 mM with 10 mM CDCA) to give 50 % N719: D149 by concentration ratio, using ultra-fast dyeing. The device was measured after filling with I_3^-/I^- electrolyte. The electrolyte was then removed by 100μL ethanol. N719 was the selectively removed by LiOH (100μL, 100mM) followed by filling with I_3^-/I^- electrolyte and re-measured the I-V of the

device. After electrolyte removal and rinsing, the device was re-dyed with N719 (1ml, 1mM with 10 CDCA). The I-V data were measured and are listed in Table 4.16. This experiment was repeated with another device dyeing with a mix of N719:D149 (1:3V/V) corresponding to 16 % N719:D149 by concentration ratio and the I-V were measured at each dyeing step.

2.5.16 Co-sensitization using a mixed solution of three dyes (N719:D149:SQ1)

A TEC glass device was prepared with two layers of DSL-18NRT sintered onto the working electrode and Pt was sintered on to the counter electrode. The two electrodes were then sealed together with a Surlyn gasket and the device photo-electrode was then dyed with a mixed solution of N719:D149:SQ1 which was prepared by mixing N719 (1 ml, 1 mM), D149 (1ml, 0.5 mM), and SQ1 (100μL, 0.25mM) with 10 mM CDCA followed by filling with I_3^-/I^- electrolyte and the I-V data were measured at each dyeing step.

2.5.17 Sequential co-sensitization with three dyes (N719:D131:SQ1)

A TEC glass device was prepared with two layers of DSL-18NRT TiO_2 colloid sintered onto the working electrode and Pt was sintered on to the counter electrode. The two electrodes were then sealed together with a Surlyn gasket and the device photo-electrode was then dyed with N719 dye solution (1ml, 1 mM), followed by filling with I_3^-/I^- electrolyte. After electrolyte removal and rinsing, N719 was partially desorbed using *tetra*-butyl ammonium hydroxide (50 μl, 4 mM) and the device re-fillied with I_3^-/I^- electrolyte and measured. After electrolyte removal and rinsing the device was selectively using LiOH (100μL, 100mM) filling with I_3^-/I^- electrolyte and measured the devices. After electrolyte removal and rinsing the device was then re-dyed with mix of D131:SQ1. I-V data were measured after each dyeing and desorption step.

2.5.18 Sequential dyeing and desorption of (N719: YD: SQ1)

A TEC glass device was prepared with double layers of DSL-18NRT sintered onto the working electrode and Pt was sintered on to the counter electrode. The two

electrodes were then sealed together with a Surlyn gasket and the device photo-electrode was then dyed with SQ1 (500μL, 0.34 mM with 5 mM CDCA), followed by filling with I_3^-/I^- electrolyte. After electrolyte removal by 100 μL ethanol and rinsing, YD was added (1ml, 0.25 mM with 5mM CDCA) followed by re-filling with I_3^-/I^- electrolyte. Again the electrolyte was removed with 100 μL ethanol and rinsing. N719 was then added (1ml, 1 mM) in 5mM CDCA, and the device re-filled with I_3^-/I^- electrolyte. The I-V data were measured at each dyeing step. N719 was then desorbed by LiOH (200 μL, 100mM) and diluted in 3ml of 100 mM LiOH. Also SQ1 and YD were desorbed by Bu_4NOH (200μL, 40mM) and diluted in 5 ml of Bu_4NOH. The absorbance of the desorbed dye solutions were measured using UV-Vis spectroscopy.

2.5.19 Sequential ultra-fast co-sensitization of YD and N719:D149

A TEC glass device was prepared with two layers of DSL-18NRT TiO_2 colloid sintered onto the working electrode and Pt was sintered on to the counter electrode. The two electrodes were then sealed together with a Surlyn gasket and the device photo-electrode was then dyed with YD (1.5 ml, 1.2mM with 10 mM CDCA) followed by filling with I_3^-/I^- electrolyte. The electrolyte was removed by passing 100μL of ethanol through the device and rinsing. Then 1ml of a mix of N719:D149 which was prepared by mixing N719 (1ml, 1mM with 10 mM CDCA) with D149 (1ml, 0.5 mM with 10 mM CDCA) was added followed by filling with I_3^-/I^- electrolyte and the I-V was measured at each dyeing step.

2.5.20 Sensitization with the triarylamine red dye (RD)

A TEC glass device was prepared with double layers of DSL-18NRT paste sintered onto the working electrode and Pt was sintered on to the counter electrode. The two electrodes were then sealed together with a Surlyn gasket and the device photo-electrode was then dyed with triarylamine red dye (RD) (1 ml, 1.5mM with 5 mM CDCA) followed by filling with I_3^-/I^- electrolyte and the I-V data was measured. The electrolyte was then removed after one day by passing 100 μL ethanol through the device. The dye was removed with Bu_4NOH (200μL, 40mM). The absorbance of

desorbed dye was measured at 412 nm using UV-Vis spectroscopy and the dye loading was determined using Beer's –Lambert Law.

2.5.21 Sequential co-sensitization with YD, then RD, then N719

A TEC glass device was prepared with a double layer of DSL-18NRT paste sintered onto the working electrode and Pt was sintered on to the counter electrode. The two electrodes were then sealed together with a Surlyn gasket and the device photo-electrode was then dyed with YD (1 ml, 1.2 mM with 10 mM CDCA) followed by filling with I_3^-/I^- electrolyte. The electrolyte was removed by passing 100 µL of ethanol through the device and rinsing. Then RD was added (300 µL, 1.5 mM with 10 mM CDCA) followed by re-filling with I_3^-/I^- electrolyte. Again the electrolyte was removed with 100µL ethanol and rinsing. N719 (1 ml, 1 mM with 10 mM CDCA) was then added and the device re-filled with I_3^-/I^- electrolyte. The I-V data were measured at each dyeing step. The dye loadings were then removed; N719 was removed first with LiOH (100 µL, 100 mM) and diluted into 3ml for measuring by UV-vis spectroscopy. Then both YD and RD were removed by Bu_4NOH (200 µL, 40 mM). Also pictures of the device were taken after each dyeing step using a digital camera.

2.5.22 Co-Sensitization with a mixed solution of four dyes (N719:D149:YD: SQ1)

A TEC glass device was prepared with a double layer of DSL-18NRT TiO_2 colloid sintered onto the working electrode and Pt was sintered on to the counter electrode. The two electrodes were then sealed together with a Surlyn gasket and the device photo-electrode was then dyed with a mixed (N719:D149: YD: SQ1 solution with10 mM CDCA). This was prepared by mixing N719 (1 ml, 1 mM), D149 (1 ml, 0.5 mM), YD (1 ml, 1.2 mM) and SQ1 (100 µL, 0.25 mM) solutions with 10 mM CDCA. After dyeing, the device was filled with I_3^-/I^- electrolyte and the I-V data were then measured.

2.5.23 Co-sensitization of four dyes and studies of selective removal

A TEC glass device was prepared with two layers of DSL-18NRT TiO_2 colloid sintered onto the working electrode and Pt was sintered on to the counter electrode. The two electrodes were sealed together with a Surlyn gasket and the device photo-electrode was then dyed with N719 (1 ml, 1 mM) followed by an electrolyte labelled Device A. The electrolyte was the removed by 100µl ethanol and then 200µl of a mix of three dyes D149: YD: SQ1 was prepared by mixing D149 (1ml, 0.5mM) with YD (1ml, 1.2mM) and SQ1 (100µl, 0.25mM). This was added giving Device B. N719 was then selectively removal with LiOH (100 µl, 100 mM) giving Device C. Again the device was re-dyed with N719 (1 ml, 1 mM) giving Device D. The I-V data were measured at each dyeing step.

2.5.24: Co-Sensitization with a mix of D131:SQ1 followed by a mix of D149:N719

A TEC glass device was prepared with two layers of DSL-18NRT TiO_2 colloid sintered onto the working electrode and Pt was sintered on to the counter electrode. The two electrodes were then sealed together with a Surlyn gasket and the device photo-electrode was then dyed with a 1ml of a mixed solution of SQ1:D131 which was prepared by mixing SQ1 (1 ml, 0.25 mM with 10mM CDCA) with D131 (1 ml, 0.5 mM with 10 mM CDCA) followed by electrolyte and labelled Device A. The electrolyte was removed by 100 µl ethanol then added a mix of N719:D149 (1:2) which was prepared by mixing N719 (1ml, 1mM) with D149 (2 ml, 0.5 mM with 10 mM CDCA) labelled Device B.

2.6 Experiments Relating to Chapter Five (Adsorption kinetics)

The kinetics of two types of dyeing technique were studied. The kinetics of dye adsorption on TiO_2 films by passive dyeing technique and the kinetics of dye adsorption on photo-electrodes by ultra-fast dyeing.

2.6.1 Adsorption kinetics by passive dyeing

2.6.1.1 Effect of contact time

Batch experiment was carried out by using a several TiO_2 films (0.5 x 1cm) which were prepared using two layers of TiO_2 colloid sintered at 450 °C for 30 minutes. The films were placed in a container containing 1.2 mM of YD, at room temperature, and the time was measured using a stop watch. Films were removed at fixed intervals (10, 20, 30,....., 1440) minutes. Desorption was carried by immersing each TiO_2 film loaded with YD in Bu_4NOH (10 ml, 40 mM). The absorbance was then measured for each desorbed dye solution using UV-vis spectroscopy.

2.6.1.2: Adsorption kinetics by ultra-fast dyeing

In general, the adsorption kinetics by ultra-fast dyeing were measured on devices containing two holes in the counter electrode. The dye solution was passed through the cell from one hole and collected from another hole for fixed time intervals. After adding dye solution for a measured time, the cell was cleaned by 100µL ethanol followed by desorption of the dye using different alkaline solutions. The absorbance of each desorbed dye solution was measured at λ_{max}.

2.6.1.3 Kinetic study for ultra-fast adsorption Yellow dye adsorbed on TiO_2.

A TEC glass device was prepared with two layers of TiO_2 DSL-18NRT sintered onto the working electrode and Pt was sintered on to the counter electrode. The two electrodes were then sealed together. The device was pump dyed with YD (1.5 mM) for fixed time periods followed by adding an electrolyte before the I-V was measured. The electrolyte was then removal by passing 100µl ethanol through the device cavity followed by YD desorption by Bu_4NOH (200 µl, 40 mM). The amount of desorbed dye was then measured using UV-Vis spectroscopy. After washing and rinsing the device the dyeing, measurement and desorption steps were repeated across a range of a dyeing times (1-10 minutes) to try to saturate the TiO_2 with dye.

2.6.1.4 Kinetic study of a co-adsorbed mix of N719:YD on TiO_2 films.

A DSC device was prepared in the same manner as for the previous experiment. A mixed solution of N719:YD (1:1) was prepared by mixing N719 (1 ml, 1 mM) with YD (1 ml, 1.2 mM). The N719:YD (1:1) v/v solution was pump dyed through the device for 1 minute followed by electrolyte and the I-V was measured. The electrolyte was then removed by passing 100µl ethanol through the device. N719 was then selectively removal by LiOH (100 µl, 100 mM) and the remaining YD was desorbed by Bu_4NOH (200 µl, 40 mM). The amounts of desorbed dyes were measured separately using UV-Vis spectroscopy. The experiment was repeated with dyeing times ranging from 1-12 min.

2.6.1.5 Kinetic study for mix of (5% SQ1: 95%N719) on TiO_2 film.

A DSC device was prepared as the same manner as for the previous experiment. A mixed dye solution of (5% SQ1: N719 c/c) was prepared by mixing SQ1 (2 ml, 0.25 mM) with N719 (3 ml, 2 mM). A mixed of 5% SQ1:N719 solution was pump dyed through a device for 1 minute followed by electrolyte and the I-V was then measured. The electrolyte was then removed by passing 100µl ethanol through the device. N719 was then selectively removal by LiOH (100 µl, 100 mM) and remaining SQ1 was desorbed by Bu_4NOH (200 µl, 40 mM). The amounts of desorbed dyes were measured separately using UV-Vis spectroscopy.

2.7 References

1 www.pilkington.com/TEC-glass./ Accessed 5 March , 2013.

2 S. Ito, P. Chen, P. Comte, M. K. Nazeeruddin, P. Liska, P. Pechy, and M. Gratzel, *Progress in Photovoltaics: Research and. Applicaions*, 2007, **15**, 603-612.

3 P. J. Holliman, M. Mohsen, A. Connell, M. L. Davies, K. AL-Salihi, M. B. Pitak, G. J. Tizzard, S. J. Coles, R. W. Harrington, W. Clegg, C. Serpa, O. H. Fontes, C. Charbonneau, M. J. Carnie, *Journal of Materials Chemistry*, 2012, **22**, 13318-13327.

4 http://www.le.ac.uk/spectraschool/sias/IntroductionUV-Vis Spectroscopy.pdf/ Accessed 3 March 2013.

5 C. Reichardt, *Chemical Reviews*, 1994, **94**, 2319-2358.

6 B. Valeur, in *Molecular Fluorescence*, 2001, Wiley-VCH Verlag GmbH, p21

7 D. Rendell, in *Fluorescence and Phosphorescence*, 1987, John Wiley and Sons, New York, p5

8 D. A. Skoog, in *Principles of Instrumental Analysis*, 1985, 3th Edition, Sunders College Publishing, USA, p162.

9 P. J. Holliman , M. L. Davies, A. Connell, B. V. Velasco, T. M. Watson, *Chemical Communications*, 2010, **46**, 7256-7258.

10 W. A. Adamson, in *Physical Chemistry of Surface*, 1982, 4th ed., John Wiley & Sons, New York, P 548.

Chapter Three - Ultra-fast selective dyeing, desorption and re-dyeing for highly controlled sensitization of dye sensitized solar cell photo-electrodes

3.1 Introduction

In this chapter, highly versatile adsorption-desorption and re-dyeing procedures will be described for dye sensitized solar cells which have a number of key advantages; for example control over dye loading, the ability for large numbers of dyes to be tested, faster processing and uses it low cost materials and techniques. The adsorbed dye plays the vital role in electron injection into the conduction band (CB) of TiO_2.[1] Anchoring groups (generally carboxylates) are responsible for dye adsorption onto the TiO_2 surface and facilitate the injection of the excited electron into the conduction band of the TiO_2.[2] The carboxyl groups can interact with metal ions by physical adsorption *via* hydrogen bonding or by chemisorption on the TiO_2 surface with a unidentate linkage, a bidentate linkage or a bridging linkage.[3] Bidentate adsorption has been found more favourable over monodentate for organic dyes (perylene chromophores) molecules on TiO_2 nanocrystals.[4] The dye adsorption is important for enhancing DSCs performance and it has been found that the quantity of dye adsorption and the dye adsorption equilibrium constant on TiO_2 surface can affect the performance of DSCs.[5]

3.2 Aim of study

The main aim of this section of the work is how to control dye loading on TiO_2 nanoparticles by re-dyeing the devices after dye desorption in DSCs. The other aim of this work is to find a method to study sensitizer adsorption on TiO_2 without device damage.

3.3 Result and discussion

3.3.1 Molar extinction coefficient

The molecular structures of di-tetrabutylammonium cis-bis(isothiocyanato)bis(2,2'-bipyridyl-4,4'-dicarboxylate) ruthenium(II) complex (N719), 2-((5-carboxy-3,3-

dimethyl-1-1-octylindolin-2-yl)methyl)-4-((1-ethyl-3,3-dimethylindolin-2-yl)methyl)cyclobuta-1,3-diene-1,3-(olate) (SQ1), 2-((2E,5Z)-5-((4-(4-(2,2-diphenylvinyl)-1,2,3,3a,4,8b-hexahydrocyclopenta[b]indol-7-yl)methylene)-3',4,4',5-tetrahydro-2'H,3H-[2,5'-bithiazolydine]-3-yl)acetic acid (D149) and (E)-4-(4-(diphenylamino)styryl)benzoic acid (YD) are shown in Figure 3.1

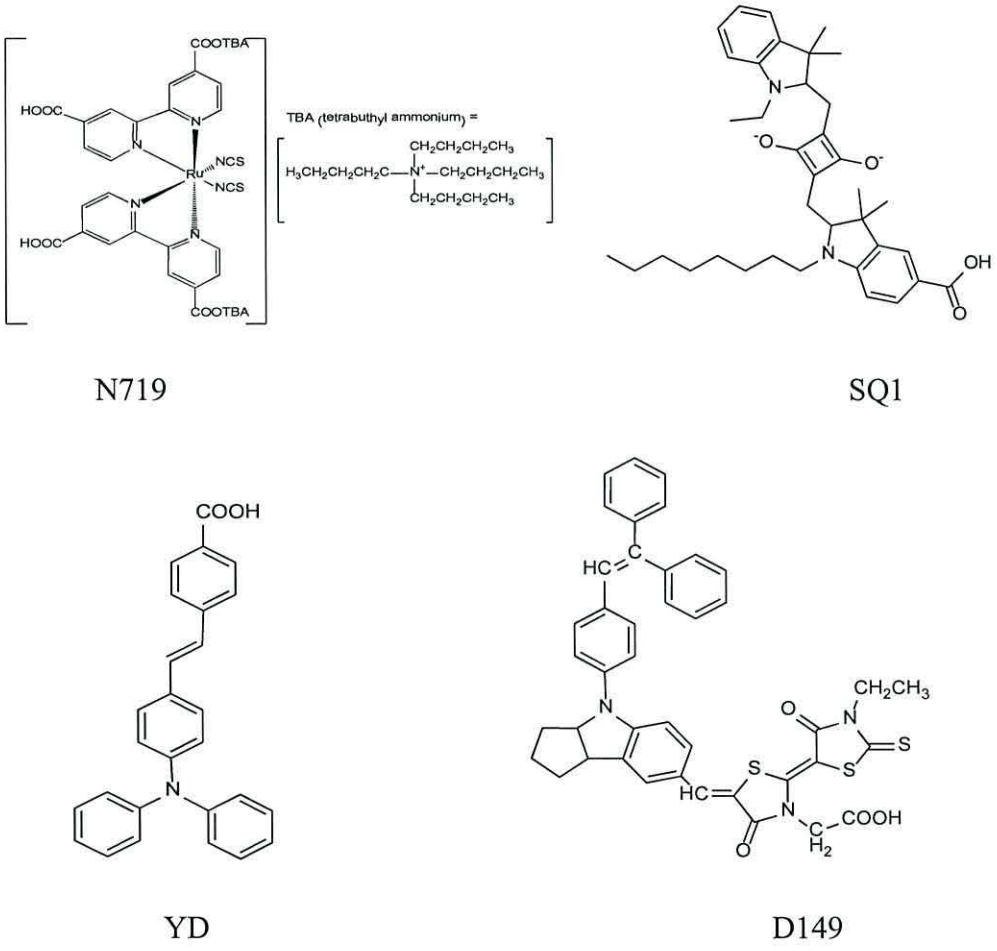

N719 SQ1

YD D149

Figure 3.1: Molecular structures of N719, SQ1, YD and D149

For this study, we used four dyes from different families; Ru-(bipyridyl) complex dyes (e.g. N719) which are efficient DSC dyes, the organic dye SQ1 which absorbs light towards the NIR region, the D149 indoline dye which is a high efficiency organic dye and YD-a novel dye. Figure 3.2 show the UV-Vis spectrum for each of these dyes in different solvents. Figure 3.2a shows the maximum absorption of (0.05 mM) N719 in *tert*-Butanol:Acetonitrile (1:1) at 532 nm. The maximum absorption of (0.01 mM) SQ1 in ethanol is at 636 nm as shown in Figure 3.2b, and the maximum

absorption of (0.25 mM) YD in ethanol at 380 nm is shown in Figure 3.2c. Figure 3.2d shows the maximum absorption of (0.25 mM) D149 in *tert*-Butanol:Acetonitrile (1:1) at 532 nm. Stock solutions of these dyes were used (100 $mg.L^{-1}$ of N719, 10 $mg.L^{-1}$ of SQ1, 50 $mg.L^{-1}$ of D149 and 50 $mg.L^{-1}$ YD) to prepare standard dye solutions whose concentrations were determined by dilution. Then the absorbance of standard dye solutions for each dye at given wavelength were determined using a UV-visible spectrophotometer. A calibration curve for each dye was prepared by plotting the absorbances of known concentration *versus* concentration are shown in Figures 3.3a-f. The molar extinction coefficients of N719, SQ1, D149 and the yellow triphenylamine dye (YD) were determined from the calibration curve for each dye giving a slope equal to the molar extinction coefficient (ε). The data were then compared with the molar extinction coefficients of these dyes in the literature, as shown in Table 3.1 These molar extinction coefficients were then used along with the Beer – Lambert equation to measure dye loading on the TiO_2 photo-electrodes.

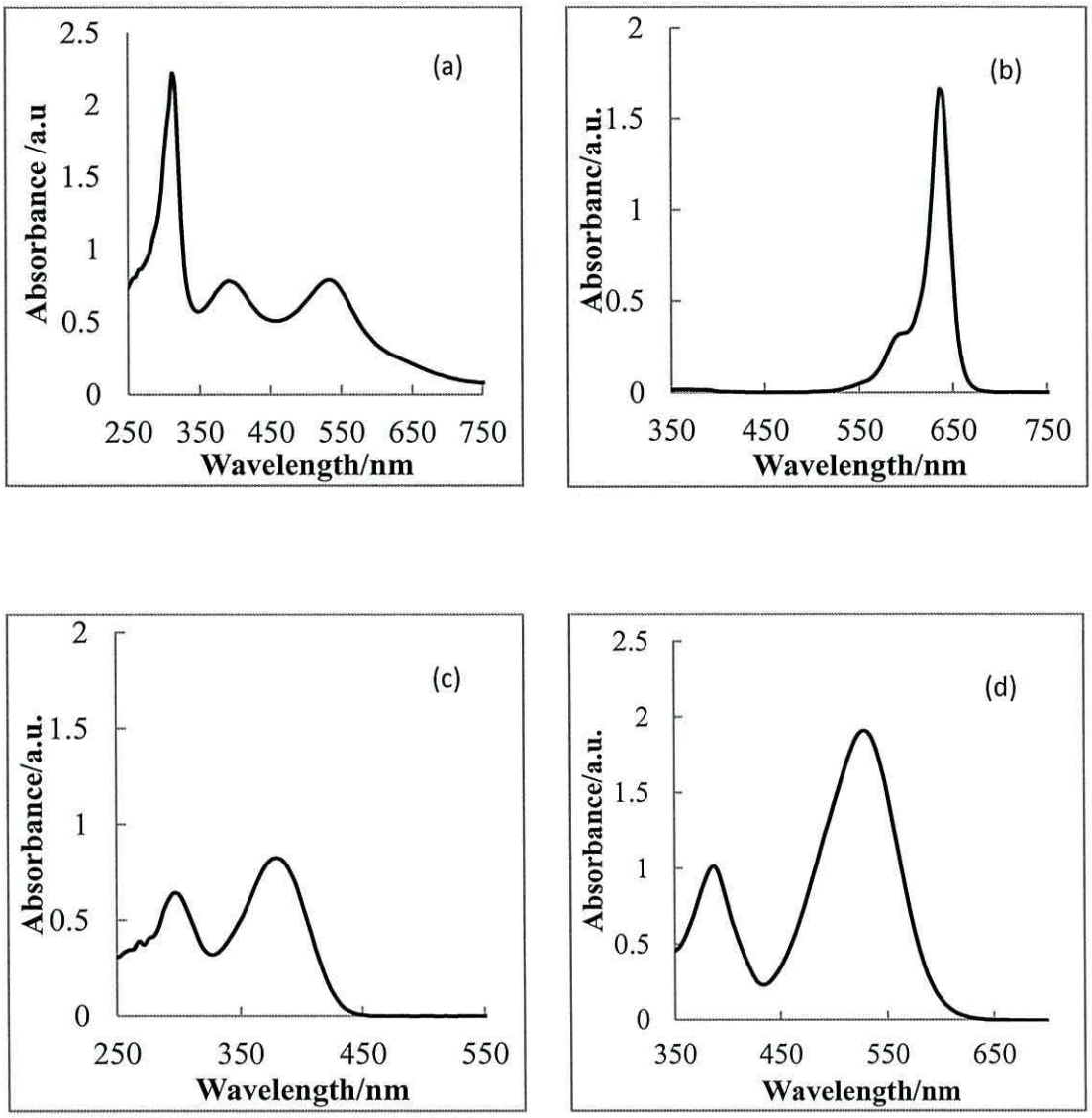

Figure 3.2: UV-Vis spectra for (a) 0.05 mM N719 in ethanol, (b) 0.01 mM SQ1 in ethanol, (c) 0.25 mM YD in ethanol and (d) 0.25 mM D149 in *tert*-butanol:acetonitrile (1:1).

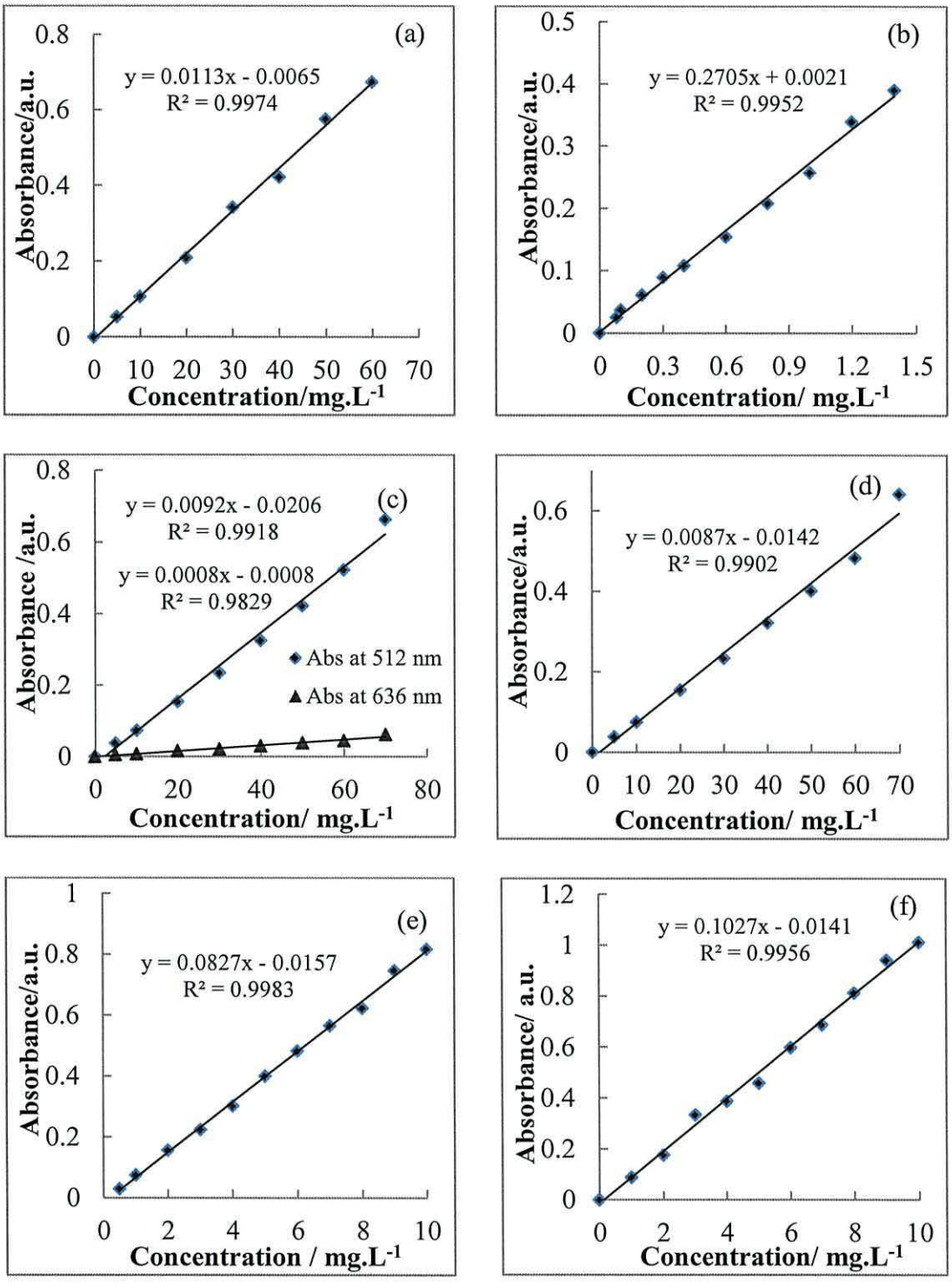

Figure 3.3: Calibration curve data of absorbance *versus* concentration for (a) N719 dye in ethanol at 532 nm. (b) SQ1 dye in ethanol at 636 nm. (c) N719 in *tert*-butanol ammonium hydroxide solution at 512 nm and at 636 nm. (d) N719 dye in 0.1 molar of LiOH at 504 nm and 636 nm. (e) YD dye in ethanol at 384 nm. (f) D149 dye in *tert*-butanol: acetonitrile (1:1) at 532 nm.

Table 3.1: The experimental molar extinction coefficient of the dyes used in this chapter.

Dye	Solvent	λ_{max}/nm	This work Ɛ/ $M^{-1}.cm^{-1}$	Lit. Ɛ/ $M^{-1}.cm^{-1}$	Ref.
N719	Ethanol	532	13300 ±300	14000	6
N719	Bu_4NOH(0.04M)	512	10900 ±100	-	
N719	Bu_4NOH (0.04M)	636	950 ± 200	-	
N719	LiOH (0.1M)	504	9500 ± 500	-	
SQ1	Ethanol	636	1569001±150	158500	7
D149	t-BuOH:MeCN	526	77600 ±200	68700	8
YD	Ethanol	384	32300 ± 200	32300	9

The data show the extinction coefficients of these organic dyes are higher than the molar extinction coefficient of Ru-(bipy) dye N719, which is also blue-shifted in alkaline medium. The blue shift of 15 nm is due to an increasing solvent polarity which leads to n–π* being shifted to shorter wavelengths (blue shift).[10] The reason due to the distraction of double bonds which decrease the extent of delocalization of the electronic system concerned, hence shifting the frequency of light absorbed toward the UV region.[11] The molar extinction coefficient of N719 in 0.04 M of *tert*-butanol ammonium hydroxide at 512 nm was ~11,000 $M^{-1}cm^{-1}$ and in 0.1 mM LiOH at 504 nm was found to be ~10,000 $M^{-1}.cm^{-1}$. The molar extinction coefficient of N719 was believed to decrease because of the phenomenon of solvatochromism which is the cumulative effect of all solvent-solute interactions.[12] The Ɛ of N719 in 0.04 M Bu_4NOH at 636 nm also was found to be ~1000 $M^{-1}cm^{-1}$. This was calculated to reduce the error for calculation of SQ1 in mixed N719:SQ1 solutions because the UV-Vis spectrum of N719 overlaps with SQ1 spectra at 636 nm as shown the UV-Vis spectrum in Figure 3.4. The molar extinction coefficient for the organic dyes SQ1 in ethanol at 636 nm, D149 in *tert*-Butanol: Acetonitrile (1:1) at 532 nm and YD in ethanol 384 nm were measured to be 156, 900, 77,600 and 32,300

M^{-1} cm^{-1} respectively. The results show the molar extinction coefficients of all used organic dyes are higher than N719.

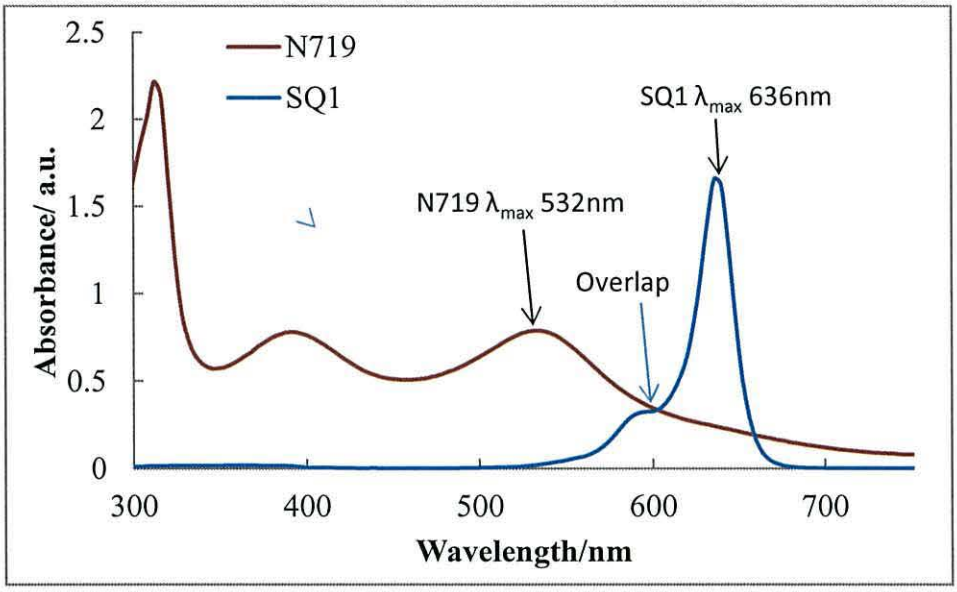

Figure 3.4: UV-Vis spectra for 0.1 mM N719 in *tert*-butanol:acetonitrile(1:1) and 0.05 mM SQ1 in ethanol shows N719 spectrum overlaps with SQ1 spectrum at 636 nm.

3.3.2 Adsorption isotherms

Dye adsorption isotherms were measured for N719 and SQ1 and the data were analyzed using two common models (Langmuir and Freundlich isotherms) to describe the adsorption characteristics.[13] The amount of dye loadings for each of N719 and SQ1 on the TiO_2 surface were calculated by desorption in alkali solution. Here the dyes were desorbed by Bu_4NOH (5 ml, 40 mM) from the surfaces of the TiO_2 films. The concentrations at equilibrium and the amounts of dye adsorption on TiO_2 surface were calculated by dye desorption and the data are summarized in Table 3.2. The amount of adsorbed dye on the TiO_2 surface was calculated by Equation 3.1.

$$Q_e = \frac{C_e}{A} x\, V \qquad 3.1$$

Where Q_e the amount of adsorbed dye ($mg.cm^{-2}$), C_e equilibrium concentration of adsorbed dye ($\mu g.ml^{-1}$), V volume of alkaline used for desorption (ml) and A is the

surface area of TiO_2 film. The Langmuir and Freundlich isotherms are valid in describing the adsorption behaviour either as chemisorptions of a monolayer of adsorbed molecules on an adsorbent surface or of the physisorption for multi-layers of dye molecules on a TiO_2 surface.[14] Figure 3.5a and Figure 3.5b show the adsorption isotherms of N719 and SQ1, respectively. The isotherm shape was obtained by plotting the amount of adsorbed dye per 1 cm^2 of TiO_2 film *versus* the dye concentrations at equilibrium at room temperature. The adsorption isotherm shape of N719 is L-type according Giles's classification of isotherm systems which is indicative of molecules adsorbed flat on a surface.[15] Figure 3.5b for the SQ1 the adsorption isotherm shows an S-shape which, according Giles's classification of isotherms, is indicative of vertical orientation of adsorbed molecules at the surface. The results in Tables 3.2 and 3.3 show the data for the different adsorption isotherms for N719 and SQ1 onto TiO_2. The reason for the different adsorption behaviour is due to the variety of adsorption configurations of dye molecules.[16] For example, N719 has two anchoring groups with a octahedral shape of ligands about a Ru central atom and is bigger than SQ1 which has a linear shape and includes only one anchor group.

Table 3.2: Adsorption isotherm data for the adsorption of various concentration of N719 dye on TiO_2 films (0.5 x 2 cm) at 24 hours.

C_i / mg.L^{-1}	C_e / mg.L^{-1}	Q_e /mg.cm^{-2}	Log C_e	Log Q_e	C_e/Q_e
5	3.75	0.025	0.57	-1.602	150.0
10	7.41	0.052	0.87	-1.283	142.5
20	15.50	0.090	1.19	-1.045	172.2
30	24.50	0.110	1.39	-0.958	222.7
40	32.66	0.149	1.51	-0.835	223.7
50	41.80	0.164	1.62	-0.785	254.8
60	50.26	0.194	1.70	-0.710	259.1

Table 3.3: Adsorption isotherm data for the adsorption of various concentration of SQ1 dye on TiO_2 films (0.5 x 2) cm at 24 hours.

C_i / mg.L^{-1}	C_e / mg.L^{-1}	Q_e /mg.cm^{-2}	Log C_e	Log Q_e	C_e/Q_e
0.1	0.07	0.0006	-1.154	-3.221	11.66
0.2	0.11	0.0018	-0.795	-2.744	61.11
0.3	0.19	0.0022	-0.657	-2.657	86.36
0.4	0.26	0.0028	-0.585	-2.552	92.85
0.6	0.39	0.0042	-0.408	-2.376	92.85
0.8	0.51	0.0058	-0.292	-2.236	87.93
1.0	0.67	0.0066	-0.174	-2.180	101.50
1.2	0.85	0.0073	-0.070	-2.154	116.40

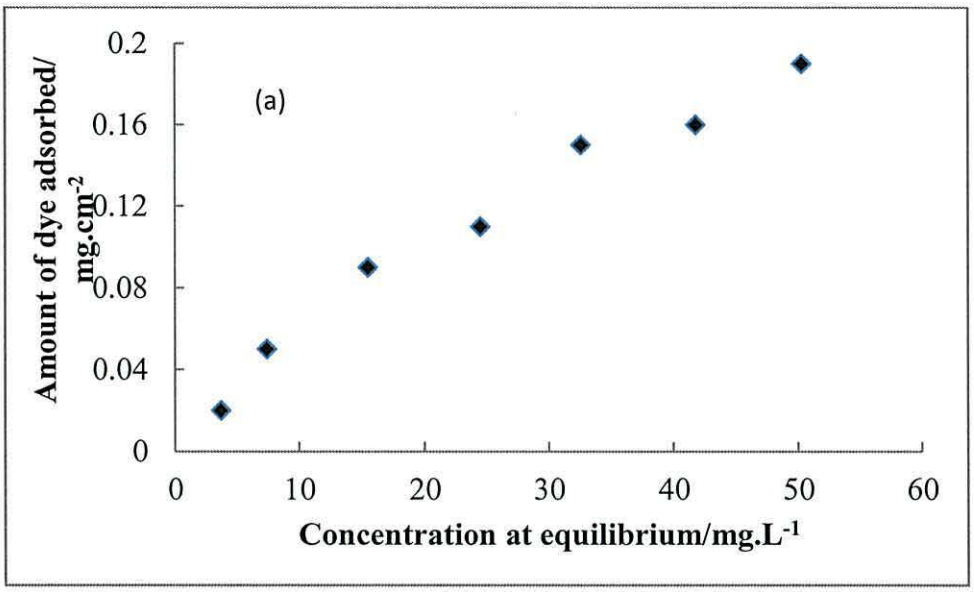

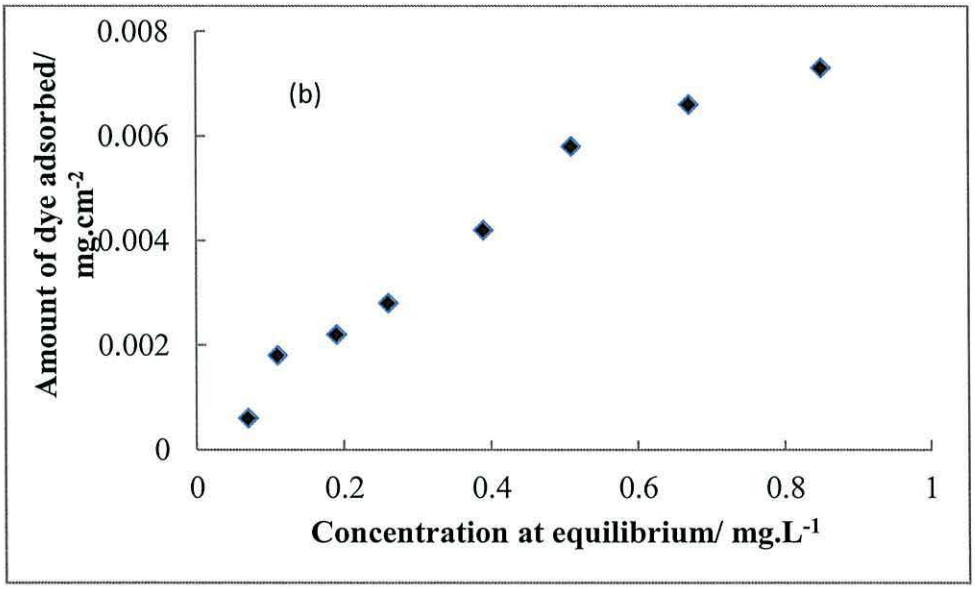

Figure 3.5: The variation of the amount adsorbed dye *versus* the equilibrium concentration at room temperature for the adsorption of (a) N719 and (b) SQ1, on TiO_2 films for 24 hours.

Linear Langmuir and Freundlich models were then plotted for both N719 and SQ1 adsorption data. The Langmuir isotherm was used in the form:[17]

$$\frac{c_e}{q_e} = \frac{1}{k_l q_{max}} + \frac{c_e}{q_{max}} \qquad \text{Eq. 3.2}$$

Where C_e is the equilibrium concentration (mgL^{-1}), q_e the amount of dye adsorbed ($mg.cm^{-2}$), q_{max} is a constant that reflects a complete monolayer coverage of the dye on a TiO_2 surface ($mg.cm^{-2}$) and k_l is adsorption equilibrium constant that is related to the strength of sorption. The Langmuir isotherm plots for N719 and SQ1 sorption are given in Figures 3.6a and Figure 3.6b respectively, and the corresponding constants are listed in Table 3.4. The linearized Freundlich isotherm was used in form:[18]

$$\frac{x}{m} = Q_e = K_f . C_e^{\frac{1}{n}} \qquad Eq. 3.3$$

Where, n is a constant characteristic of the intensity of the dye onto the adsorbent and K_f is a constant indicative of the adsorption capacity related to the bond energy of weak Van der Waals forces.[19] The Freundlich plots for N719 and SQ1 sorption on TiO_2 films are given in Figures 3.7a and 3.7b respectively, and the Freunedlich isotherm parameters are also listed in Table 3.4. As can be seen from the data, the Langmuir and Freundlich models show a closer fit with the N719 adsorption with R^2 values of 0.94 and 0.98, respectively. This indicates that the adsorption process could be described by these models. For N719, this assumes that adsorption takes place at specific homogeneous sites on the TiO_2 surface with a maximum monolayer capacity q_{max} obtained as 0.372 $mg.cm^{-2}$ using Langmuir model.[20] The Freundlich isotherm parameters K_f and n indicate effective binding of N719 molecules and TiO_2 particles. The Freundlich isotherm fits the experimental data of the SQ1 sorption better than Langmuir isotherm. The large value of K_f indicates the maximum amount of dye adsorption which may due multi-layer adsorption formed or the SQ1 aggregate on more heterogeneous TiO_2 surface.

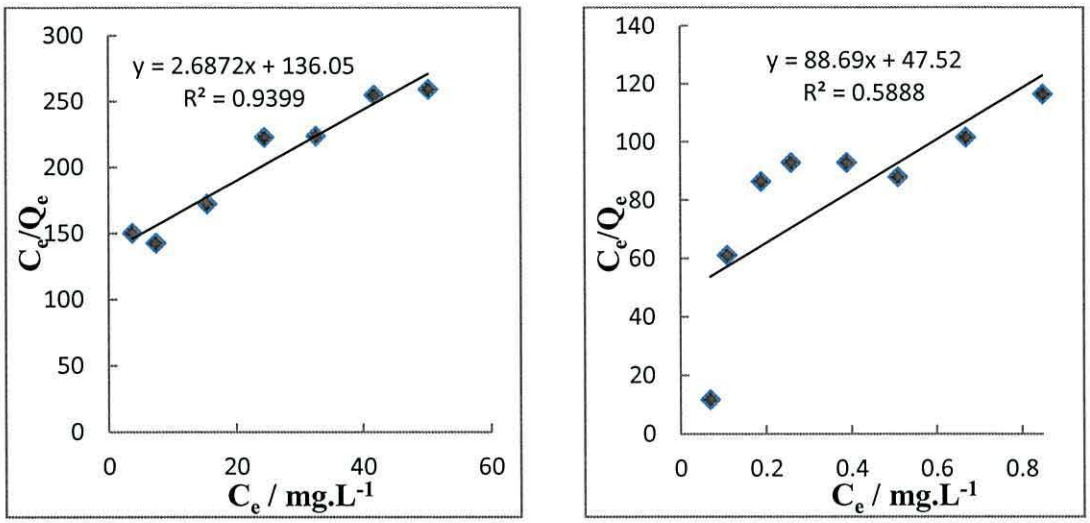

(a) (b)

Figure 3.6: The graphs presented the data of C_e/Q_e plotted *versus* concentration at equilibrium (C_e) according the Langmuir model for the adsorption of (a) N719 on TiO_2 and (b) SQ1 on TiO_2.

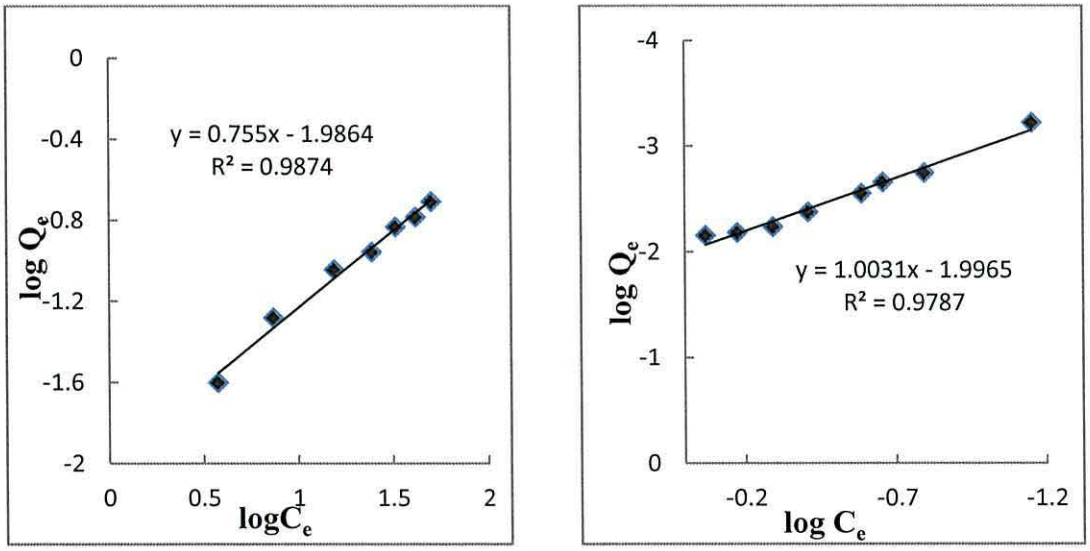

(a) (b)

Figure 3.7: Graphs of log Q_e plotted *versus* Log C_e according to the Freundlich model for the adsorption of (a) N719 on TiO_2 and (b) SQ1 on TiO_2.

Table 3.4: Freundlich and Langmuir isotherms constants for the adsorption N719 and SQ1 by TiO_2 films.

Dye	Freundlich Constants			Langmuir Constants		
	K_f	n	R^2	q_m/ mg.cm^{-2}	K_L	R^2
N719	0.01	1.324	0.9874	0.372	365	0.9399
SQ1	99.19	0.996	0.9787	0.011	4320	0.5888

3.3.3 Investigation of desorption process.

An initial study was carried out into dye desorption using of *tetra*-butyl ammonium hydroxide (Bu_4NOH) to remove the adsorbed dye on a TiO_2 surface. Normally, NaOH has been used to desorb dyes for the evaluation of dye uptake.[21] Also the *pseudo* first-order adsorption kinetics of N719 dye on TiO_2 has been investigated by desorption using aqueous NaOH solutions.[22] However, NaOH solution has some disadvantages in dye removal from TiO_2 surfaces. Firstly, is not possible to leave the TiO_2 film in NaOH solutions for long periods because this leads to TiO_2 film damage. Secondly, it is less easy to remove organic dyes using NaOH. To solve this problem *tetra*-butyl ammonium hydroxide has been studied here. Initially the effect of varying concentrations ratio of mixing SQ1:N719 while maintaining the adsorbate volume and the area of TiO_2 film constant were studied as follows. A number of TiO_2 films (dimension 1cm x 2cm) after sintering at 450 °C for 30 minutes were placed in sealed glass bottles containing a series of different ratios of SQ1:N719 (80%, 60%, 50%, 40%, 20%, 10% and 5%) labelled a-j which were prepared by mixing a specific volume of each dye from the stock solution (2 mM N719) and (0.34 mM SQ1) as shown Figure 3.8. After 24 hours, the films were taken out and the pictures of TiO_2 films a to j in Figures 3.6 show an indication of dye uptake. It should be noted that this was competitive adsorption from solutions containing both N719 and SQ1. As a comparison, a reference TiO_2 film is shown on the right. It can

be seen that the colour of films changes from blue (film a) to dark red (film j) which is suggests that the amount of SQ1 loading decreases with decreasing amount of SQ1 in the initial dye mixture.

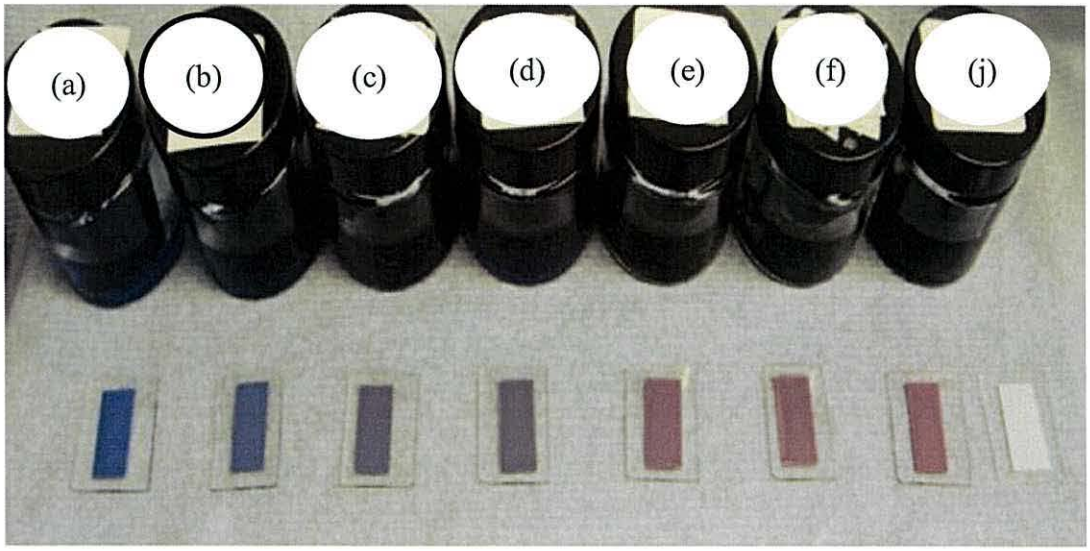

Figure 3.8: Photographs of TiO_2 films (1cm x 2cm) after immersion for 24 hr in 20 ml of various ratios of SQ1:N719 (a) 80% SQ:N719 (b) 60% SQ1:N719 (c) 50% SQ1:N719 (d) 40% SQ1:N719 (e) 20% SQ1:N719 (f) 10% SQ1:N719 (j) 5% SQ1:N719 in ethanol and *tert*-butanol:acetonitrile (1:1) solvents with a TiO_2 film shown on the far right for comparison.

The UV-Vis absorbances of the TiO_2 films after dye adsorption were measured. Figure 3.9 shows the UV-Vis spectra of TiO_2 films with different dyes with peaks at 636 nm due to SQ1 and 530 nm due to N719.

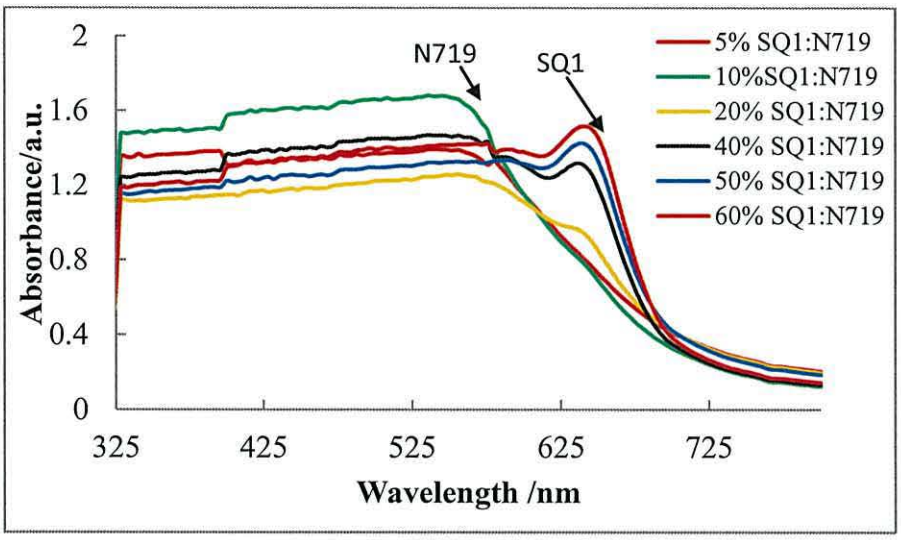

Figure 3.9: UV-Vis spectra of transparent TiO_2 films showing differing amounts of SQ1 and N719 adsorbed from mixed dye solutions of various ratios of % SQ1:N719.

The UV-visible spectra shows both N719 and SQ1 were adsorbed on the TiO_2 surfaces in different ratios. To investigate the amount of each dye which is adsorbed on the TiO_2 films, the dyes were desorbed using *tetra*-butyl ammonium hydroxide $(Bu_4NOH)_{(aq)}$. After washing each film by ethanol to remove the dye molecules which were not adsorbed on the TiO_2 surfaces, the TiO_2 films were immersed in 5 ml of 40mM $(Bu_4NOH)_{(aq)}$ for 3 minutes. The dyes appeared to be completely desorbed from the TiO_2 surfaces in 1-3 minutes. Thereafter, the absorbances were measured for the TiO_2 films and no peaks were found due to SQ1 or N719. For instance Figure 3.10 shows the UV-Vis spectra of a TiO_2 film after desorption.

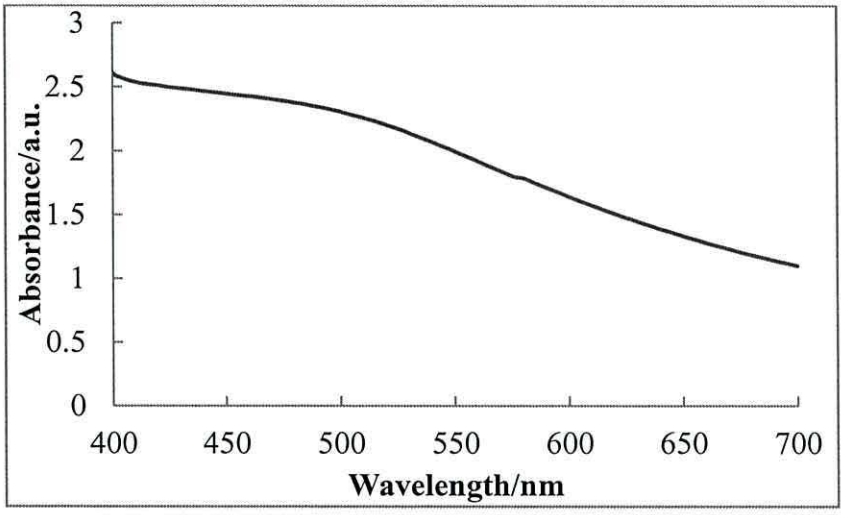

Figure 3.10: UV-Vis spectra of TiO_2 film after desorbed 50% SQ: N719 by *tetra*-butyl ammonium hydroxide (5 ml, 40 mM).

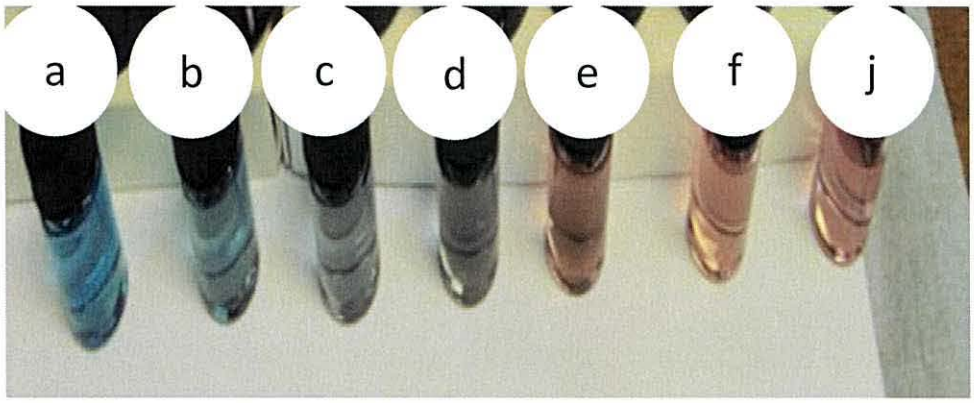

Figure 3.11: Photographs of dye solutions desorbed from TiO_2 by Bu_4NOH (5ml, 40mM) from various initial dye ratios of SQ1:N719 (a) 80% SQ: N719 (b) 60% SQ1:N719 (c) 50% SQ1:N719 (d) 40% SQ1:N719 (e) 20% SQ1:N719 (f) 10% SQ1:N719 (j) 5% SQ1:N719.

The desorbed dyes solution were collected in a separate vials and labelled a to j corresponding to the initial concentration of mixed SQ1:N719 as shown in Figure 3.10. By comparison, Figure 3.11 shows pictures of desorbed dye solutions. As can be seen clearly through the changes of colour from a to j, the amount of desorbed SQ1 decreases along with an increasing amount of desorbed N719. The absorbances of the desorbed dye solutions were also measured and Figure 3.12 shows the UV-Vis spectra of the desorbed dye solution with peaks at 636 nm due SQ1 and 512 nm due to N719. The amount of dye uptake was evaluated by measuring the absorbance at the specific wavelengths and then using the relevant molar extinction coefficient for each dye and the data are summarised in Table 3.5.

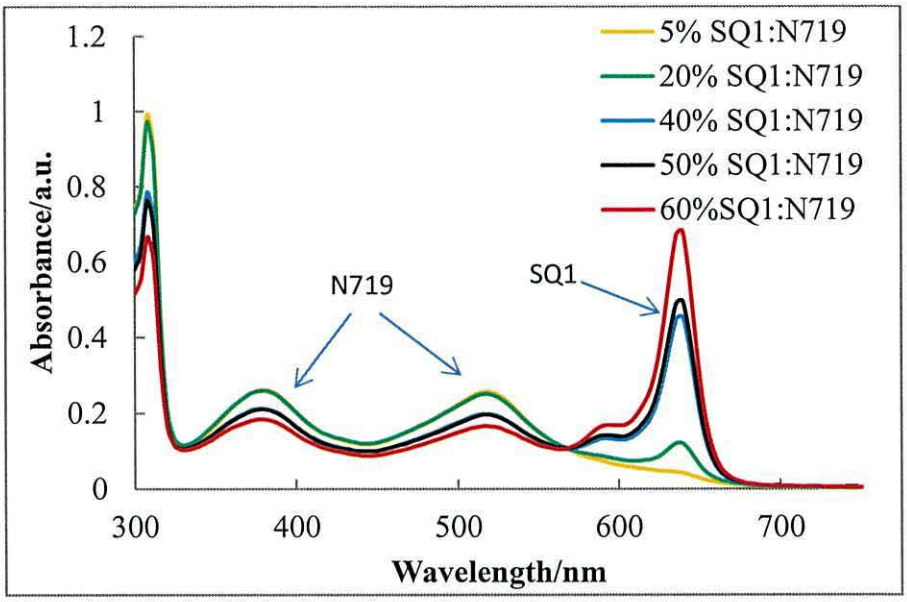

Figure 3.12: UV-Vis Spectra of various initial ratios of (SQ1:N719) after being desorbed by Bu_4NOH (5 ml, 40 mM) from TiO_2 films (1 cm x 2 cm).

Table 3.5: The amount of desorbed N719 and SQ1 by *tetra*-butyl ammonium hydroxide (5ml, 40 mM) from TiO_2 films (1cm x 2 cm).

Initial dye conc. %C/C	Amount of dye desorbed N719 /μg.cm^{-2}	Amount of dye desorbed SQ1 /μg.cm^{-2}
5% SQ1:N719	161.25 ± 3	1.05 ± 1
10% SQ1:N719	155.50 ± 5	2.23 ± 1
20% SQ1:N719	161.87 ± 8	4.91 ± 1
40% SQ1:N719	158.12 ± 6	8.28 ± 2
50% SQ1:N719	125.62 ± 2	10.59 ± 2
60% SQ1:N719	118.12 ± 1	12.42 ±2

3.3.4 Ultra-fast desorption by various alkali solutions and re-dyeing with N719 dye.

Ultra-fast dyeing has been successfully demonstrated for reducing the dyeing time and the amount of dye solution required to dye DSC devices.[23] It is also known that the performance of DSCs is affected strongly by dye adsorption behaviour on the

surface of TiO_2 electrodes.[24] More detail about ultra-fast dyeing will be discussed in Chapter four. This chapter instead focuses on desorption and re-dyeing to control dye loading. In this work, various alkaline solutions have been investigated for the selective removal of dyes adsorbed using ultra-fast dyeing along with the device re-dyeing. To the best of our knowledge, no studies have reported on evaluating dye uptake by ultra-fast dyeing, dye desorption and re-dyeing the device to control dye uptake. Table 3.6 shows the various alkaline solutions with pk_b values of the bases that have been used for dye removal.

Table 3.6: The values of selected base dissociation constants.[25]

Name	Formula	pK_b value
Potassium hydroxide	KOH	-0.3
Sodium hydroxide	NaOH	0.5
Lithium hydroxide	LiOH	0.2
tetra-butylammonium hydroxide	Bu_4NOH	0.3
tris-(hydoxymethy)ethylamine	THAM	8.0

In these experiments, ultra-fast dyeing of N719 (1 ml, 1 mM) on TiO_2 electrodes has been investigated. Figure 3.13 shows the I-V data for a TiO_2 device dyed with N719 and then desorbed with various alkali solutions before re-dyeing with N719 (1 ml, 1 mM). Figure 3.14 shows the I-V data for the TiO_2 device after each step of desorption by different alkali solutions. The detailed photovoltaic parameters of the devices after sensitizing, desorbing, and re-dyeing by different alkali solutions are summarized in Table 3.7. Firstly, the device was ultra-fast dyed with N719 (1ml, 1mM) Device A, giving $\eta = 4.57\%$ with (J_{sc} =10.05 $mA.cm^{-2}$, V_{oc} = 0.70V and FF = 0.65) on black background, but when a white paper was placed under the device the J_{sc} increased by 1 $mA.cm^{-2}$, because more light was reflected by the white background which lead to an increase in η of about 0.4% although the V_{oc} and FF were not affected. After the N719 was removed by KOH (150 µL, 100 mM), Device A1, and after re-filling with I_3^-/I^- electrolyte and washing sequentially with de-ionized water, 0.1 M $HCl_{(aq)}$, ethanol the device performance was re-measured and

the efficiency had dropped to 0.3 %. The parameters all decreased (J_{sc}= 0.74 $mA.cm^{-2}$, V_{oc} = 0.58 and FF = 0.54) indicating N719 removal which was observed clearly in Figure 3.14a and b which shows that the TiO_2 film became white after N719 desorption. The amount of desorbed N719 was then determined by UV-Vis spectroscopy giving 162 $\mu g/cm^{-2}$.

In the same manner as described above with the same device, the process of re-dyeing with N719 after desorption was repeated in sequence using NaOH (150 µL, 100 mM), LiOH (150 µL, 100 mM), *tetra*-butyl ammonium hydroxide (200 µL, 40 mM) and *tris*-(hydoxymethy)ethylamine (THMA) (300 µL, 40 mM). Figure 3.15a - 3.15e show the pictures of the device at each stage which indicate the process of desorption and re-dyeing, which may give some indication of the ability of the alkali solution for removing N719 from the TiO_2 colour after desorption and also from the desorbed N719 in vials. The I-V data in Table 3.7 show that the FF and V_{oc} remain constant during the re-dyeing and desorption processes. However, the J_{sc} from the first dyeing with N719 increased from 10.04 $mA.cm^{-2}$ after five re-dyeing and desorption cycles by five different alkali solutions reaching 13.23$mA.cm^{-2}$ and this led to an increase in efficiency from 4.9 % to 6.0 %. The reason for this may due to more dye molecules being adsorbed because the TiO_2 surface becomes more activated during the washing by $HCl_{(aq)}$, after each desorption neutralizes the surface. Desorption by alkali solutions were applied to gain further insight into the effect of adsorption behaviour on the cell performances with re-dyeing the device.

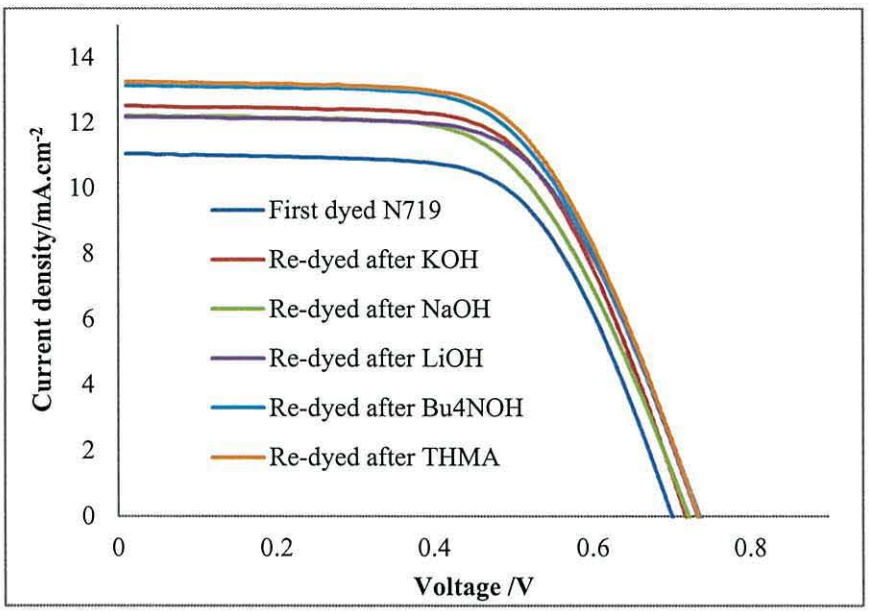

Figure 3.13: Photocurrent density-voltage characteristics under AM 1.5 full sunlight (100 mW.cm^{-2}). The data show a device ultra-fast dyed with N719, then devices which have been treated with alkali shown and then re-dyed with N719.

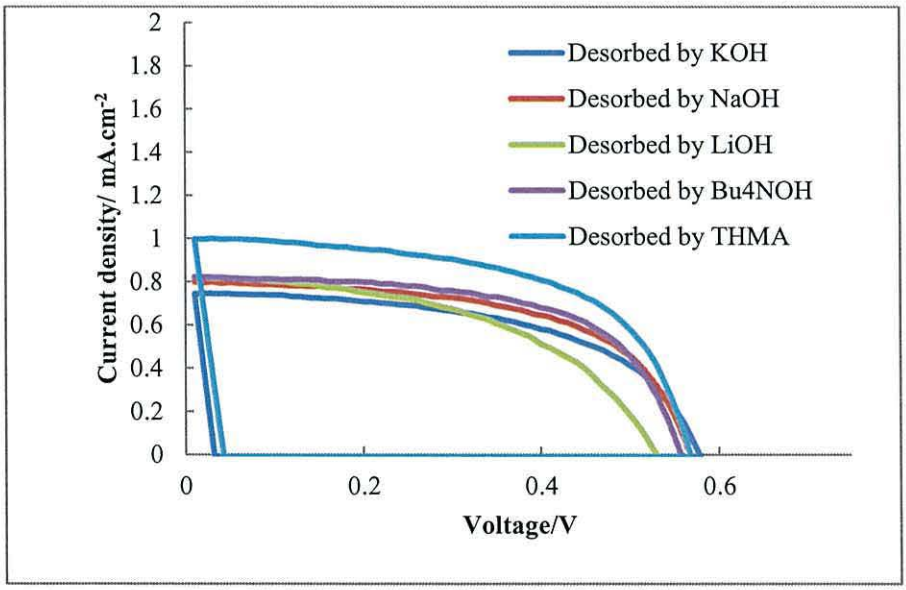

Figure 3.14: Photocurrent density-voltage characteristics of various DSC devices as shown Figure 3.12 under AM 1.5 full sunlight (100 mW.cm^{-2}), after N719 desorption by different the alkaline solution

Table 3.7: I-V data of a 1 cm^2 device of TiO_2 dyed with N719 and then desorbed with different alkaline solutions and re-dyed with N719. (Approximate errors on devices are ± 10% of the values shown).

Device		Background	η(%)	V_{oc} /V	J_{sc} /mA.cm^{-2}	FF
A	Dyed with N719	Black	4.6	0.70	10.05	0.65
		White	4.9	0.70	11.04	0.64
A1	Desorbed by KOH		0.3	0.58	0.74	0.55
B	Re-dyed N719	Black	5.6	0.75	11.26	0.66
		White	5.8	0.75	12.18	0.63
B1	Desorbed by NaOH		0.3	0.57	0.80	0.58
C	Re-dyed N719	Black	5.1	0.72	11.31	0.62
		White	5.3	0.72	12.21	0.61
C1	Desorbed by LiOH		0.2	0.53	0.81	0.48
D	Re-dyed N719	Black	5.1	0.72	11.45	0.62
		White	5.7	0.72	12.51	0.63
D1	Dsorbed by *tetra*-butyl ammonium hydroxide		0.3	0.56	0.82	0.60
E	Re-dyed N719	Black	5.5	0.74	11.92	0.63
		White	5.9	0.73	13.14	0.61
E1	Desorbed by tres(hydoxymethy)ethylamine (THAM)		0.3	0.57	0.99	0.58
F	Re-dyed N719	Black	5.6	0.73	12.17	0.63
		White	6.0	0.73	13.26	0.62

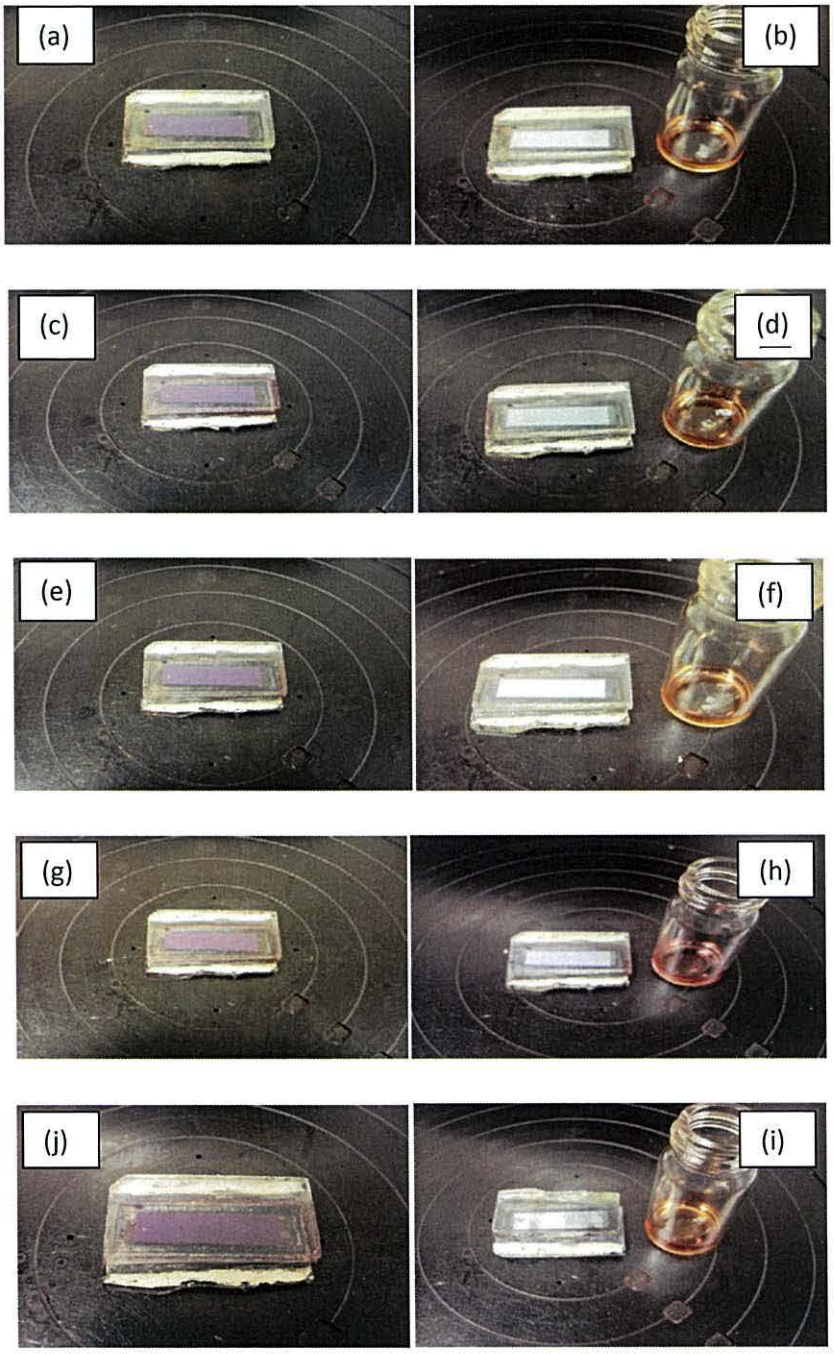

Figure 3.15: Photographs of a P25 device dyed with N719 (1 ml, 1 mM) and desorbed with different alkali solutions (a) dyed with N719 (1 ml, 1 mM) (b) desorbed by KOH (200 µL,100 mM), (c) re-dyed with N719 (d) desorbed by NaOH (200 µL,100 mM) (e) re-dyed with N719 (f) desorbed by LiOH (200µL,100mM), (g) re-dye with N719, (h) desorbed by Bu_4NOH (200 µL,40 mM), (j) re-dye with N719, (i) desorbed by *tris*-(hydroxylmethyl)ethylamine (300 µL,40 mM) also showing desorbed dye solution.

3.3.5 Dark current measurement

Dark current for a device dyed with N719 then desorbed and the re-dyed were studied as a comparison with DSC devices under light. Because the large surface area enhances dye loading of the photo-electrode leading to enhanced photon absorption surface defects, which act as recombination centres at the TiO_2/dye/electrolyte interface, can significantly affect the overall DSC performance. Figure 3.16 shows the I-V data for DSC device under light and Figure 3.17 shows the I-V data in the dark the data are summarized in Table 3.8. This experiment was carried out by measuring the P25 device after filling with I_3^-/I^- electrolyte under light giving η 0.3 % with (J_{sc} = 0.61 mA.cm^{-2}, V_{oc} = 0.77 V and FF = 0.64). For the same device, when measured in the dark, the efficiency dropped to 0.1% and both of J_{sc} and V_{oc} was decrease to 0.28 mA.cm^{-2} and 0.73V respectively. After electrolyte removal and rinsing, the device was dyed with N719 (1 ml, 0.5 mM) giving η 4.6 % with (J_{sc} = 9.64 mA.cm^{-2}, V_{oc} = 0.76 V and FF = 0.63) under illumination. And when the device was measured in the dark the η dropped to 0.1% and both J_{sc} and V_{oc} decreased to 0.29 mA.cm^{-2} and 0.60V respectively. The device was then desorbed with Bu_4NOH (100 µl, 40 mM) and measured under illumination and gave 0.3 % which is in line with the initial device TiO_2. When this measured in the dark gave η of 0.1 % with decreased J_{sc} to 0.28 mA.cm^{-2} and V_{oc} to 0.58 V. The amount of dye loading was measured was to be 156 µg.cm^{-2} using UV-Vis spectroscopy. After electrolyte removal and rinsing, the processes were repeated in the same manner and the result shows an increased recombination of photogenerated carriers can lead to a significant loss in J_{sc} and V_{oc}, consistent low efficiency 0.1% in dark saturation current and electric field reduction at the interface of TiO_2/dye/electrolyte leading to worsened fill factor. Suggests that the dye molecules it takes time to absorb photons, so it might also take time for dye molecules to transfer those excited electrons to the carrier molecules.

Table3.8: The I-V data of 1 cm^2 P25 device were measured under illuminated and in dark current, dyed with N719 (1ml, 0.5mM), and desorbed with Bu_4NOH (100 µl, 40 mM) and the re-dyed with the same N719 dye solution. (Approximate errors on devices are ± 10% of the values shown).

Device	η (%)	V_{oc} (V)	J_{sc} /mA.cm^{-2}	FF	Amount of desorbed N719 /µg.cm^{-2}
TiO_2 only	0.3	0.77	0.61	0.64	
TIO_2 in the dark	0.1	0.73	0.28	0.66	
Dyed with N719	4.6	0.76	9.64	0.63	
Dyed with N719 in the dark	0.1	0.60	0.29	0.70	
Desorbed N719	0.3	0.79	0.62	0.64	156
Desorbed N719 in the dark	0.1	0.58	0.28	0.72	
Dyed N719	5.0	0.76	9.58	0.62	
Dyed N719 in the dark	0.1	0.60	0.29	0.71	
Desorbed N719	0.3	0.80	0.60	0.65	174
Desorbed N719 in the dark	0.1	0.73	0.28	0.66	
Re-dyed N719	4.8	0.75	9.75	0.59	
Re-dyed N719 in the dark	0.1	0.58	0.28	0.72	161

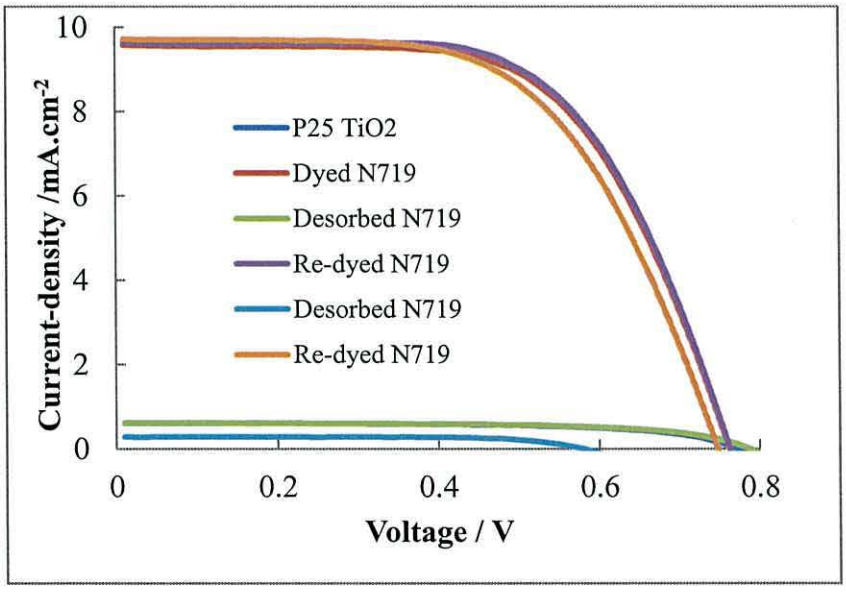

Figure3.16: I-V data were measured under one sun light (1.5 AM) for 1 cm^2 P25 device dyed with N719 (1 ml, 0.5 mM) desorbed with Bu_4NOH (100 µL, 40 mM) then e re-dyed with same N719 dye solution.

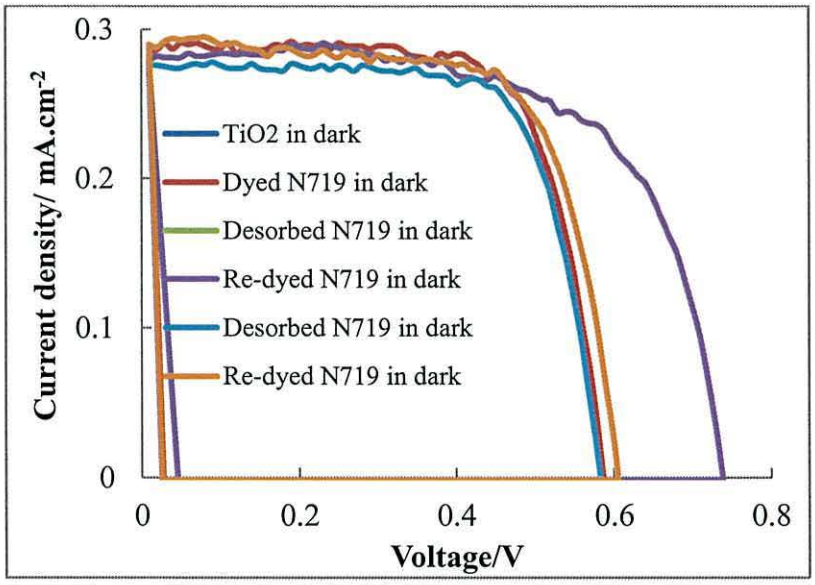

Figure 3.17: I-V data were measured in dark of 1 cm^2 P25 device dyed with N719 (1 ml, 0.5 mM) desorbed with Bu_4NOH (100 µl, 40 mM) then re-dyed with same N719 dye solution.

3.3.6 Device errors

Through this work the errors have been estimated for repeated device re-dyeing with N719 (1ml, 2.8 mM) and the data are listed in Table 3.9. For the series of cells measurements of a given dye quantity (x) were used to calculate the mean ($\overline{X}$), and the standard deviation σ_x. The mean is defined as;[26]

$$\overline{X} = \frac{1}{N}\sum_{i=1}^{N} x_i \qquad \text{Eq. 3.4}$$

Where x_i is the result of the i^{th} measurement and N is the number of measurements. The standard deviation is given by

$$\sigma_x = \left(\frac{1}{N}\sum_{i=1}^{N}(x_i - \overline{x})^2\right)^{\frac{1}{2}} \qquad Eq. 3.5$$

Then the standard deviation of the the mean is

$$\sigma_{\bar{x}} = \frac{\sigma_x}{\sqrt{N}} \qquad Eq. 3.6$$

Table 3.9: The I-V data of P25 devices dyed with N719 (1 ml, 2.8 mM) desorbed by Bu4 NOH (200 µl, 40 mM) and re-dyed with the same N719 dye solution.

Device	η (%)	V_{oc} (V)	J_{sc} /mA.cm^{-2}	FF
a	3.7	0.72	10.38	0.40
b	5.3	0.77	8.64	0.62
c	4.6	0.76	8.96	0.54
d	4.1	0.78	7.06	0.63
e	4.1	0.75	8.57	0.64
f	5.1	0.79	8.04	0.64
g	4.8	0.76	8.14	0.58
h	5.4	0.73	9.07	0.66
Average	4.64	0.76	8.61	0.59
SD	0.58	0.02	0.90	0.09
Error	4.6 ± 0.5	0.76 ±0.03	8.61 ± 0.3	0.59 ± 0.03

3.3.5 Desorption from the device by Bu_4NOH

Tetra-butyl ammonium hydroxide is strong base that is used often under phase-transfer conditions to effect alkylations and deprotonations.[27] In addition dyes neutralized by Bu_4NOH should give lipophilic salts of the conjugate base. The early experiments suggested that Bu_4NOH is a suitable alkali to desorb both Ru complexes and organic dyes from the DSCs devices dyed using the ultra-fast method. To further test this, the desorption of various dyes using Bu_4NOH was studied.

3.3.5.1 Desorbing and Re-dyeing the Ru-bipyridyl (N719)

Table 3.10 shows the photovoltaic parameters of a device dyed with Ru-bipy dye N719 (1 ml, 2.8 mM) for 10 min at flow rate 100 µL min the device giving η of 4.5 % with (J_{sc} = 11.06 mA.cm^{-2}, V_{oc} = 0.78V and FF = 0.52); typical for a 0.95 cm^2 TiO_2 photo-electrode. N719 was then desorbed by pumping Bu_4NOH (200µL, 40mM) through the device cavity followed by rinsing and re-filling with I_3^-/I^- electrolyte giving η of 0.3% in line with N719 removal (Device A1). After electrolyte removal and rinsing, the device was re-dyed with N719 (Device A1-R), showing similar performance to the first dyeing. Again the N719 was removed by Bu_4NOH (200 µL, 40 mM) in the same manner, (Device A2) giving η 0.4% slightly higher than the first desorption which might suggest the amount of Bu_4NOH was not

enough to remove N719 completely. The processes of the dyeing desorption and re-dyeing can be clarified by the pictures of the device for each step. Figure 3.18 shows four pictures of the device. Fig 3.18a represents the device before dyeing, with a white TiO_2 film. After the device was dyed with N719, (Fig 3.18b) a dark purple colour covered the TiO_2. When N719 was removed by Bu_4NOH the device colour changed to white, indicating the ability of Bu_4NOH to desorb N719. When an electrolyte was added for photovoltaic measurement (Fig 3.18c) the device shows the yellow colour of I_2. Finally, after electrolyte removal, the device was re-dyed with N719 (Fig 3.18d) again the dark purple indicating adsorption of N719.

Table 3.10: Photovoltaic parameters for a 0.95 cm^2 TiO_2 device dyed, desorbed using Bu_4NOH (200 μL, 40 mM) and re-dyed using with N719 (1 ml, 2.8 mM). (Approximate errors on devices are ± 10% of the values shown).

Device		η (%)	V_{oc} (V)	J_{sc} / $mA.cm^{-2}$	FF
A	Dyed with N719	4.5	0.78	11.06	0.50
A1	After desorption	0.3	0.58	0.95	0.64
A1-R	Re-dyed with N719	4.5	0.77	10.96	0.53
A2	After desorption	0.4	0.60	0.98	0.65

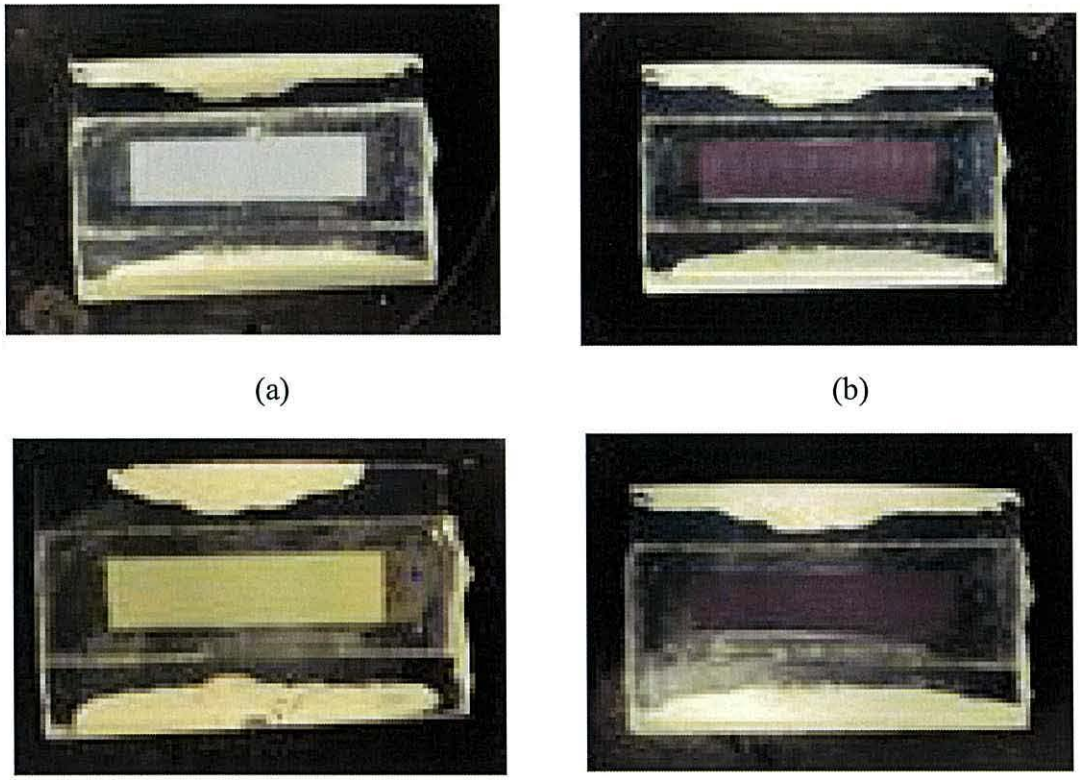

(a) (b)

(c) (d)

Figure 3.18: Photographs of a TiO_2 device (2x0.5 cm) showing the dyeing, desorption and re-dyeing cycle using the Ru-bipy dye N719 (a) the device before dyeing (b) dyed with N719 (c) added an electrolyte after dye removal by Bu_4NOH (d) Re-dyed with N719

3.3.5.2 Re-dyeing the Ru-terpyridyl Dye – "Black dye"

The re-dyeing by Bu_4NOH was tested with another Ru complex dye (black dye) that has three carboxyls as anchoring groups as shown the chemical structure in Figure 3.19.

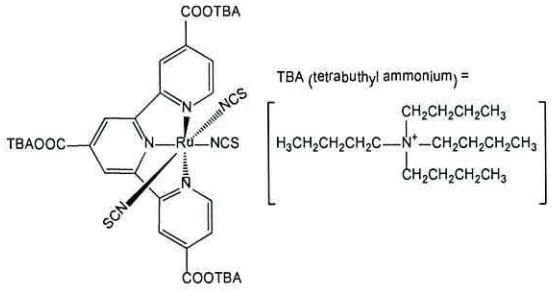

Figure 3.19: Chemical structure of *tris*-isothiocyanato-(2,2':6',6''-terpyridyl-4,4',4''-tricarboxylato)ruthenium(II) tris(*tetra*-butylammonium) (black dye)

Table 3.11 shows the I-V data of a device dyed and re-dyed with black dye after desorption with Bu_4NOH. Device B for a 1 cm^2 TiO_2 photo-electrode was pump dyed with Ru-terpyridyl "black dye " (1ml, 0.28 mM) for 10 min at a flow rate 100μL/min giving η of 2.2% and (J_{sc} = 5.08 $mA.cm^{-2}$, V_{oc} = 0.66 V and FF = 0.65). The dye was then desorbed (Device B1) by pumping Bu_4NOH (200μL, 40mM) through the device cavity followed by rinsing and re-filling with I_3^-/I^- electrolyte giving η of 0.3% in line with black dye removal. The device was then re-dyed with "black dye" (Device B1-R) showing similar performance to the first dyeing. This process was repeated with dye removal (Device B2) and with re-dyeing Device B2-R giving η 2% which is slightly less than the first dyeing which may be due to the fill factor dropping slightly. The observation of colours on the TiO_2 photo-electrode also gives an indication of dye adsorption and desorption. Figure 3.20 shows the pictures of the device (a) before dye adsorption showing the white colour of TiO_2. When the black dye was adsorbed on TiO_2 surface the colour changes to teal colour (Fig 3.17b). After dye removal, the white colour of the TiO_2 appears again. Fig 3.17c also shows a faint yellow due to I_2 electrolyte. The I-V data and pictures show the ability of Bu_4NOH to remove Ru-terpyridyl "black dye "

Table 3.11: Photovoltaic parameters for 1 cm^2 TiO_2 device dyed, desorbed and re-dyed with Ru-terpyridyl "black dye" (1 ml, 0.28 mM). Desorbed was by Bu_4NOH (200 μL, 40 mM). (Approximate errors on devices are ± 10% of the values shown).

Device		η (%)	V_{oc} (V)	J_{sc} /$mA.cm^{-2}$	FF
B	Dyed with black dye	2.2	0.66	5.08	0.65
B1	Desorbed by Bu_4NOH	0.3	0.57	0.74	0.63
B1-R	Re-dyed with black dye	2.2	0.68	5.23	0.62
B2	Desorbed by Bu_4NOH	0.2	0.56	0.74	0.57
B2-R	Re-dyed with black dye	2.0	0.66	4.99	0.61

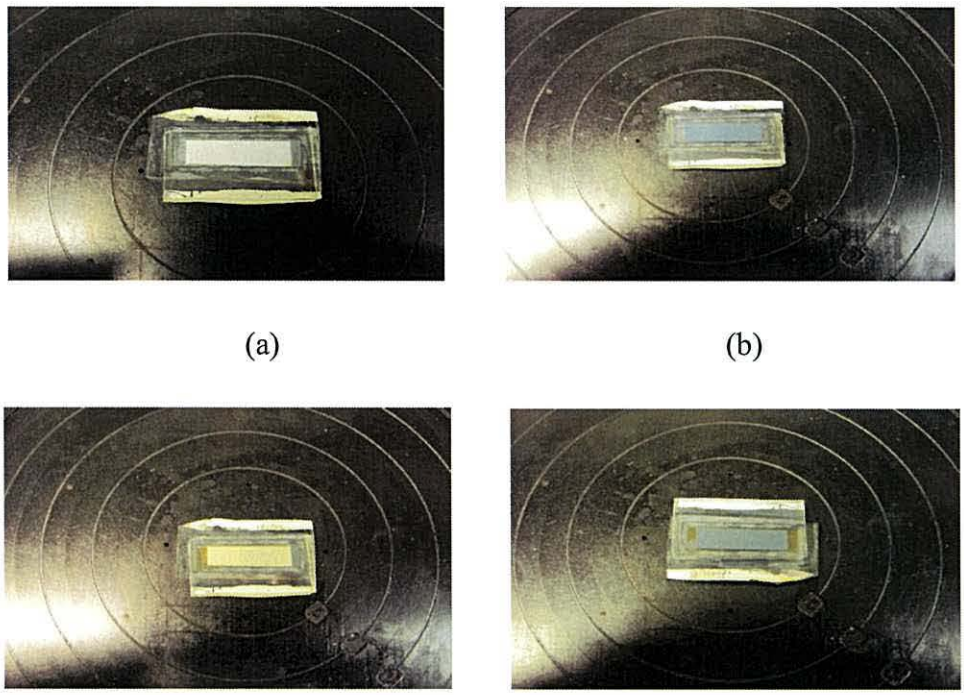

(a) (b)

(c) (d)

Figure 3.20: Photographs of device (2x0.5 cm) showing the dyeing, desorption and re-dyeing cycle using the Ru-terpyridyl dye "Black dye" (a) the device before dyeing (b) dyed with black dye (c) after adding an electrolyte after dye removal by Bu_4NOH and (d) re-dyed with black dye.

3.3.5.3 Re-dyeing with an organic dye

The re-dyeing procedure was then tested with an organic dye and the data are summarized in Table 3.12. Device C was pump dyed with SQ1 (500 μL, 0.28 mM) for 10 min giving η of 1.3%. SQ1 was then desorbed by pumping Bu_4NOH (200 μL, 40 mM) through the device cavity followed rinsing and re-filling with I_3^-/I^- electrolyte giving 0.3% (Device B1). After electrolyte removal and rinsing, the device was re-dyed with SQ1. The resulting device B1-R shows a higher efficiency than first dyeing η of 1.7 % due to an increase in J_{sc} = 4.54 mA.cm^{-2} with constant V_{oc} = 0.64V. However, the fill factor dropped to 0.57 which may due to some factors such as the crocodile clip connection with the device, on the silver paste on each electrode or may be the platinium of counter electrode was influenced by alkali or acid solutions during the device processing. Figure 3.21 shows the photographs of the adsorption and desorption processes for SQ1. Fig 3.21a shows a white colour of the device before dye adsorption. The organic dye SQ1 has one carboxylic group attached directly to the chromophore as shown the structure in Figure 3.1. After the

SQ1 dye (blue) was pumped through the device the TiO_2 photo-electrode changes to blue colour (Fig 3.21b) which indicates adsorbed dye molecules on the TiO_2 surface. When the dye was desorbed by pumping Bu_4NOH (200 μL, 40 mM) through the device cavity the white colour of TiO_2 re-appears, while the I_3^-/I^- electrolyte changed the colour to pale yellow (Fig 3.21c). The device was then re-dyed with SQ1 after washing and rinsing (Fig 3.21d) and again the TiO_2 film became blue colour as result of adsorbed SQ1 molecules. These data show the ability of Bu_4NOH to desorb the organic dye SQ1 without damaging the internal components of the device so allowing re-dyeing to take place.

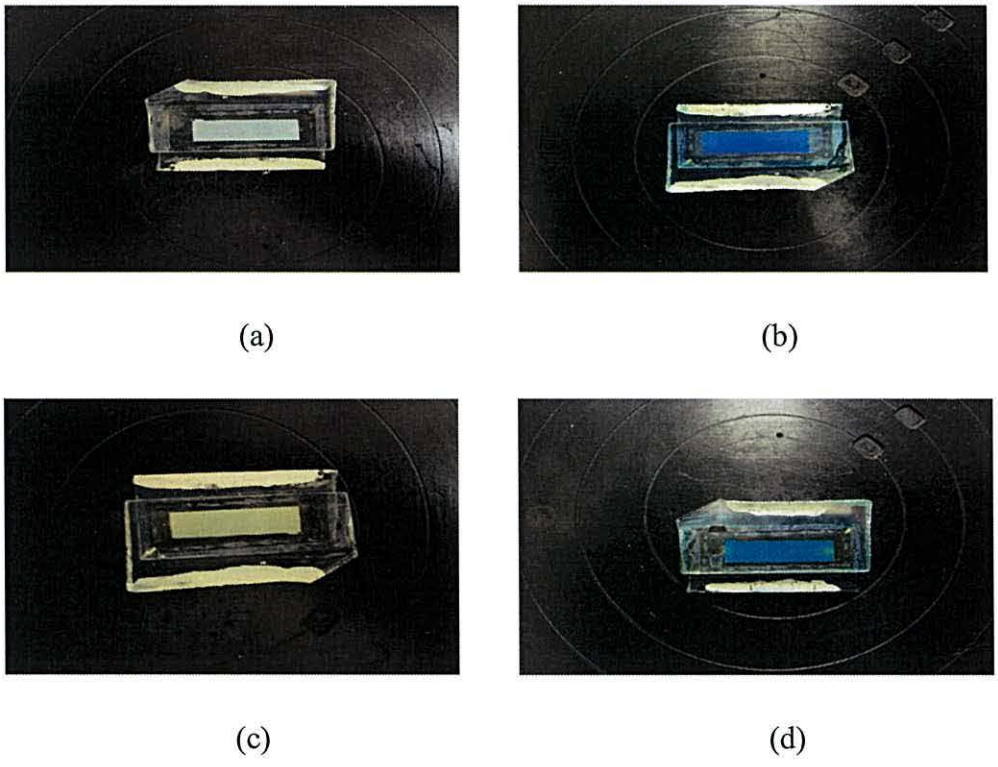

Figure 3.21: Photographs of TiO_2 devices (2x0.5 cm) showing the dyeing, desorption and re-dyeing cycle using the NIR dye SQ1 (a) the device before dyeing (b) dyed with SQ1 (c) after adding an electrolyte after dye removal by Bu_4NOH and (d) re-dyed with SQ1.

Table 3.12: Photovoltaic parameters for a 0.86 cm^2 P25 device dyed and re-dyed with the squaraine dye SQ1 (500 μL, 0.28 mM) Desorption was by Bu_4NOH (200μL, 40mM). (Approximate errors on devices are ± 10% of the values shown).

Device		η(%)	V_{oc} (V)	J_{sc}/mA.cm^{-2}	FF
C	dyed with SQ1	1.3	0.64	3.03	0.68
C1	desorbed by Bu_4NOH	0.3	0.64	0.78	0.60
C1-R	re-dyed with SQ1	1.7	0.64	4.54	0.57

3.3.5.4 Re-dyeing the organic dye D149

The re-dyeing procedure has been tested with another type of organic dye, the indoline D149 dye which has light absorption at the same wavelengths as N719. Table 3.13 shows the photovoltaic parameters of the device dyed and re-dyed with D149 (1ml, 0.5mM) after being desorbed by Bu_4NOH. To do this, first the device was pump dyed with indoline dye D149 (1 ml, 0.5 mM) for 10 min at a flow rate of 100μL/min giving η of 4.0 % (Device D). The D149 was then desorbed by pumping Bu_4NOH (0.5 ml, 40 mM) through the device cavity followed by rinsing and re-filling with I_3^-/I^- electrolyte giving η of 0.4% (Device D1) which is slightly higher than the 0.3% measured for other blank devices which might indicate a small amount of D149 still on TiO_2 surface which might indicate that a more concentrated solution of Bu_4NOH is needed to remove all dye molecules. After washing and rinsing, the device was then re-dyed with D149 (D1-R). The efficiency dropped to 3.5% with the same J_{sc} =10.62 mA.cm^{-2} and V_{oc} = 0.75V but, the fill factor had decreased which may due to the connection of the device or the counter electrode being affected by the desorber solution. Figure 3.22 shows photographs during the processes. When the device was dyed with D149 the colour changes from white (Fig 3.22a) to dark violet (Fig 3.22b) because of adsorbed D149 on TiO_2. The dye was taken off by Bu_4NOH (Fig 3.22c) which shows a yellow colour of TiO_2 because of the electrolyte added for the device. Finally, the device was re-dyed with D149 (Fig 3.22d) and again the device changed to dark violet. The I-V data and photographs show the ability of Bu_4NOH to remove dye (in this case D149) without damaging the device components allowing for re-dyeing.

Table 3.13: Photovoltaic parameters for a 1 cm^2 P25 device dyed and re-dyed with indoline dye D149 (1 ml, 0.5 mM). Desorption was by Bu_4NOH (500 μL, 40 mM). (Approximate errors on devices are ± 10% of the values shown).

Device		η (%)	V_{oc} (V)	J_{sc} /mA.cm^{-2}	FF
D	Dyed with D149	4.0	0.76	10.67	0.50
D1	Desorbed by Bu_4NOH	0.4	0.61	1.11	0.65
D1-R	Re-dyed with D149	3.3	0.75	10.62	0.44

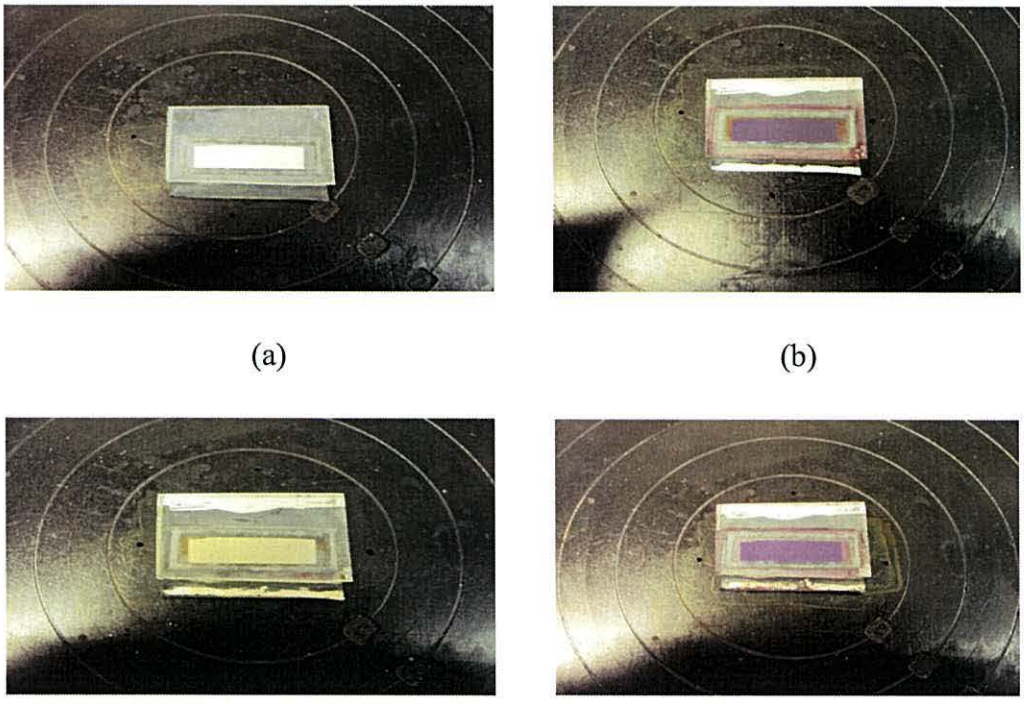

(a) (b)

(c) (d)

Figure 3.22: Photographs of a TiO_2 device (2 x 0.5 cm) showing a dyeing, desorption and re-dyeing cycle using the organic dye D149 (a) the device before dyeing (b) dyed with D149 (c) after adding an electrolyte after dye removal by Bu_4NOH and (d) Re-dyed with D149.

The data in Tables 3.10-3.13 show that Bu_4NOH could be a favourable alkali to desorb both Ru-complexes and organic dyes, without any detrimental effectes on the device performance which could then lead to successful re-dyeing of DSC devices.

3.3.5.5 Re-dyeing with different dyes

Changing the adsorbed dye in the same device has also been studied to see if it is possible to change the spectral response of the same device. To test this, Device E was pump dyed with SQ1 (1 ml, 0.28 mM) for 10 min giving η of 1.6% (Table 3.14). The organic dye SQ1 was then desorbed by pumping Bu_4NOH (200 µl, 40 mM) through the device cavity followed by rinsing and neutralizing the photo-electrode by 50 µL HCl (0.1 M). After re-dyeing with N719 (1 ml, 2.8 mM) giving Device E1-R, the efficiency had increased to 4.0 % with a big increase in J_{sc} to over 9.79 $mA.cm^{-2}$ along with increased in V_{oc} to 0.77V. These data show it is possible to replace SQ1 from the device by N719 without any negative influence on the device performance.

Table 3.14 I-V data for 1.0 cm^2 P25 devices first dyed with SQ1 (1 ml, 0.28 mM) and then re-dyed with N719 (1 ml, 2.8 mM). (Approximate errors on devices are ± 10% of the values shown).

Sample	Dye	η (%)	V_{oc} (V)	J_{sc} /mA cm^{-2}	FF
E	SQ1	1.6	0.65	3.70	0.68
E1-R	N719	4.0	0.77	9.79	0.53

The procedure was also tested by dyeing with N719 first. Device F was pump dyed with N719 (1 ml, 2.8 mM) for 10 min giving η of 4.4% (Table 3.15). N719 was then desorbed by pumping Bu_4NOH (200 µl, 40 mM) through the device cavity followed by rinsing and neutralizing the photo-electrode by 50µL HCl (0.1 M). The device was then re-dyed with SQ1 (1 ml, 0.28 mM) giving Device F1-R where the efficiency had dropped to 1.9 % which is in line with SQ1 performance. The data in Tables 3.12 and 3.13 shows that one adsorbed dye could be replaced with a different dye in the same device.

Table 3.15: I-V data for 0.95 cm^{-2} P25 device first dyed with N719 (1 ml, 2.8 mM) and then re-dyed with SQ1 (1 ml, 0.28 mM) after desorption by Bu_4NOH (200 µl, 40 mM). (Approximate errors on devices are ± 10% of the values shown).

Sample	Dye	η (%)	V_{oc} (V)	J_{sc} mA cm^{-2}	FF
F	N719	4.4	0.79	11.05	0.50
F1-R	SQ1	1.9	0.64	4.61	0.64

3.3.5.6 Dyeing, Desorbing and re-dyeing of multiple dyes

Removing multiple dyes from a co-sensitized device with a mixed SQ1:N719 has also been studied. For this purpose, a solution of SQ1:N719 was prepared to give an overall molar ratio 3%: 97%. The dye solution was pump dyed through a 1 cm^2 TiO_2 photo- electrode for 10 min (Device G) giving η of 5.0 % (Table 3.16). The SQ1:N719 dyes were then desorbed by pumping Bu_4NOH (200 µl, 40 mM) through the device cavity (Device G1) followed by rinsing and re-filling with I_3^-/I^- electrolyte giving η = 0.3 %. The desorbed amount of each dye was measured to be 202µg.cm^{-2} for N719 with 1 µg.cm^{-2} for SQ1 by UV-Vis spectroscopy. After the electrolyte was removed and the cavity rinsed, the device was re-dyed with the same mixed dye solution (Device G1-R) giving similar device performance to the initial dyeing. However, the amount of dye desorbed was higher after re-dyeing which might be due to the activation of TiO_2 particles by washing and neutralizing with hydrochloric acid. Figure 3.23 shows photographs of the dyeing and desorption processes. Fig 3.23a shows a white of TiO_2 device before adsorption whilst Fig 3.23b shows the device after pump dyeing SQ1:N719 showing the TiO_2 film changes to dark red because the TiO_2 surface becomes covered by N719 and SQ1 molecules. Because of the small amount of SQ1 adsorbed, it is difficult to see the SQ1 colour from the picture. After dye removal, the colour changes to white (Fig 3.23c) while the I_2 electrolyte in the device gives a pale yellow colour. Finally, when the device was re-dyed with 3% SQ1:N719 the device colour becomes dark red again as shown in (Fig 3.23d).

Table 3.16: I-V data for a 1cm^2 P25 device dyed and then re-dyed with 3% SQ1:N719. Desorption was by Bu_4NOH (200 µl, 40 mM). (Approximate errors on devices are ± 10% of the values shown).

Device		η(%)	V_{oc} (V)	J_{sc} /mA.cm^{-2}	FF	Desorbed N719 µg.cm^{-2}	Desorbed SQ1 µg.cm^{-2}
G	Dyed with 3%SQ1:N719	5.0	0.78	10.23	0.63	202	1
G1	Desorb by Bu_4NOH	0.3	0.59	0.78	0.63	-	-
G1-R	Re-dyed with 3% SQ1:N719	5.0	0.8	10.33	0.61	240	1

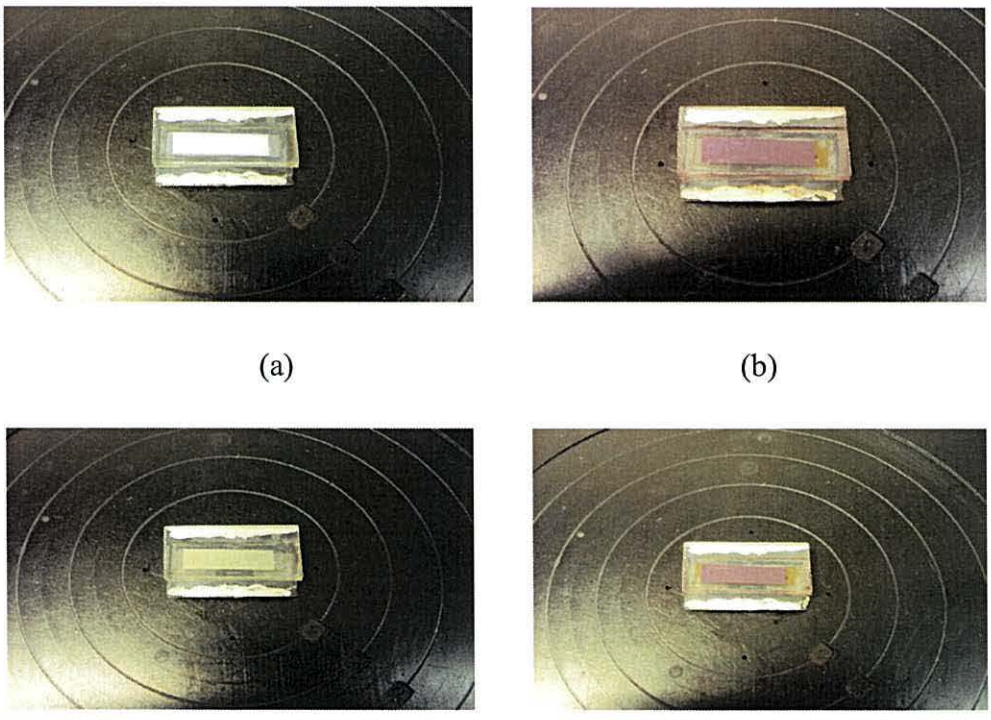

(a) (b)

(c) (d)

Figure 3.23: Photographs of front of a P25 device (2x0.5 cm) showing the dyeing, desorption and re-dyeing cycle for a co-sensitized device using a dye mixture of 3% SQ1: N719 (a) the device before dyeing (b) dyed with 3% SQ1:N719 (c) after adding an electrolyte after dye removal by Bu_4NOH (d) Re-dyed with 3% SQ1:N719.

3.3.6 Effect of Bu_4NOH concentration on dye desorption

The influence of Bu_4NOH concentrations on dye removal from TiO_2 photo electrodes has also been investigated to study whether lower concentrations of Bu_4NOH can partially remove adsorbed dye. To test this, the volume of alkali was fixed (100 µl) and the Bu_4NOH concentration was varied and the same photo-electrode was dyed, desorbed and re-dyed. Figure 3.24 shows the I-V curves for a device after dyeing and desorption steps in normal illumination and on a white background to study the effects of dye removal on device performance.

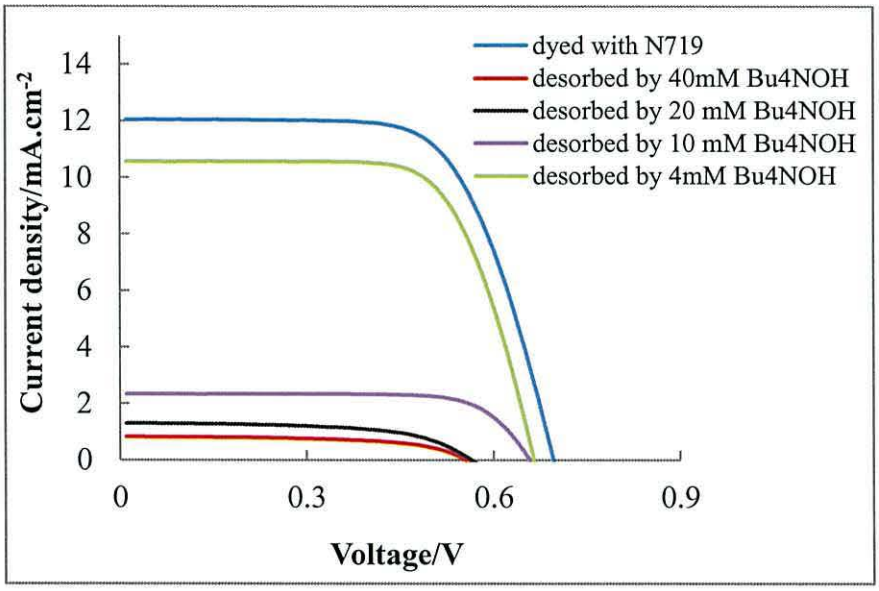

Figure 3.24: Photocurrent density-voltage characteristics under AM 1.5 full sunlight (100 $mW.cm^{-2}$), after desorption by various concentration of Bu_4NOH solution.

The data are summarized in Table 3.17. Device A was pump dyed with N719 (1 ml, 2.8 mM) for 10 min giving η of 4.9 % under normal illumination (AM 1.5). The device was then desorbed by Bu_4NOH (100 µL, 40 mM) giving Device A1 which, after rinsing and refilling with I_3^-/I^- electrolyte, showed the efficiency dropped to 0.3 % with both of V_{oc} and J_{sc} decreasing to 0.59 V and 0.81 $mA.cm^{-2}$ respectively , which is in line with N719 removal.

Table 3.17: I-V data of a 1cm^2 of P25 device dyed and re-dyed with N719 (1 ml, 2.8 mM) and desorbed with different concentration of Bu_4NOH at constant volume. (Approximate errors on devices are ± 10% of the values shown).

Device	η (%)	V_{oc} (V)	J_{sc} /mA.cm^{-2}	FF
A Dyed with N719	4.9	0.80	12.05	0.51
A1 Desorbed by 40mM Bu_4NOH	0.3	0.59	0.81	0.68
B Re-dyed with N719	5.0	0.77	11.87	0.55
B1 Desorbed by 20 mM Bu_4NOH	0.4	0.6	0.85	0.69
C Re-dyed with N719	4.9	0.77	11.3	0.57
C1 Desorbed by 10 mM Bu_4NOH	0.9	0.64	2.21	0.64
D Re-dyed with N719	4.7	0.76	11.26	0.55
D1 Desorbed by 4 mM Bu_4NOH	4.2	0.76	10.02	0.56
E Re-dyed with N719	4.9	0.77	10.35	0.61

The data means that all of the N719 was removed by 40 mM of Bu_4NOH because the device gives η 0.3 % which in line with P25 device before dyeing. After the electrolyte was removed, the device was re-dyed with N719 dye solution (1 ml, 2.8 mM) giving Device B showing a similar performance to the first dyeing. The device was then desorbed by Bu_4NOH diluted to 20 mM giving η of 0.4% (Device B1) which is slightly higher compared with the efficiency after the first desorption. This may suggest a very small amount of dye molecules still remain on the TiO_2 surface. Again after washing and rinsing, the device was re-dyed with N719 (Device C) giving η of 4.9 %. The device was then desorbed by 10 mM of Bu_4NOH giving η of 0.9 % with J_{sc} = 2.21 mA.cm^{-2} and V_{oc} = 0.60 V which does indicate some remaining remaining N719 on TiO_2 which is higher than the amount of dye than after the first or second desorbing. This means 10 mM of Bu_4NOH was unable to remove all N719 dye from TiO_2 surface. Again the device re-dye with N719 (Device D) giving η of 4.7 % with J_{sc} = 11.26 mA.cm^{-2}. The device was then desorbed by 4 mM Bu_4NOH giving η 4.2 % and J_{sc} = 10.02 mA.cm^{-2} which is only slight drop, due

to more N719 remaining on TiO_2. These data show that the desorbing of N719 from TiO_2 surface is affected by the concentration of Bu_4NOH.

3.3.7 Effect of volume of Bu_4NOH at constant concentration.

Following an investigation of Bu_4NOH concentration, a study was carried out varying the volume of alkali. To do this, different volumes of Bu_4NOH at a constant concentration (4 mM) were used to remove adsorbed N719. Figure 3.25 shows the I-V curves for a device after removing N719 by different volumes of Bu_4NOH and the photovoltaic parameters with the amount of desorbed dye are summarized in Table 3.18. To start with, Device A in Table 3.16 was pump dyed with the Ru-bipy dye N179 (1 ml, 2.8 mM) for 10 min giving η of 4.6 %. The dye was then desorbed by 1000 µL of 4 mM Bu_4NOH (Device B) giving η of 1% with small J_{sc} = 2.15 $mA.cm^{-2}$ and the partial removal of N719 was calculated as 132 $\mu g.cm^{-2}$. After washing and rinsing, the device was re-dyed with N719 (Device C) giving slightly higher η of 4.7 % and J_{sc} of 11.21 $mA.cm^{-2}$ with similar V_{oc} = 0.78 V and FF = 0.61 compared with first dyeing which may due to the activation of TiO_2 surface after washing and neutralizing by dilute hydrochloric acid. The device was then desorbed with 750 µL of Bu_4NOH (Device D) giving η of 1.9% which means the remaining adsorbed N719 dye should be higher than the amount remaining on Device B. The amount of desorbed dye was measured as 127.5 $\mu g.cm^{-2}$ which is lower which supports this. The device was re-dyed with N719 (Device E) giving η of 5.1 %. The device was then desorbed by 500 µL of Bu_4NOH (Device F) giving higher η of 2.7 % and higher J_{sc}= 5.52 $mA.cm^{-2}$ than Device D. The amount of desorbed dye was measured and gave 121.2 $\mu g.cm^{-2}$ which was slightly lower than the previous desorption. Again after washing and rinsing, the device was re-dyed with N719 (Device G) giving η of 4.9% showing similar performance to the first re-dyeing. The device was then desorbed by 250µL of Bu_4NOH (Device H) giving η of 3% which was again higher than the previous desorption. The partially desorbed dye was measured and gave 92.5 $\mu g.cm^{-2}$. Finally, the device was re-dyed with N719 (Device I) showing a similar performance to the first re-dyeing. Again the device was desorbed but this time by 100µL of Bu_4NOH (Device L) showing similar performance to the first dyeing. However, 71.3$\mu g.cm^{-2}$ of N719 was desorbed by 100µL of Bu_4NOH from the TiO_2 device. These data suggest it is possible to control of dye uptake by desorbing with varying volumes of a dilute concentration of Bu_4NOH.

Table 3.18: The I-V data of 1 cm^2 of P25 device dyed with N719 (1 ml, 2.8 mM) and desorbed with different volumes of 4mM Bu_4NOH. (Approximate errors on devices are ± 10% of the values shown).

Device with N719	η(%)	V_{oc} (V)	J_{sc} /$mAcm^{-2}$	FF	Volume of Bu_4NOH/μL	Amount of desorbed dye/$\mu g.cm^{-2}$
A First dyeing	4.6	0.78	10.10	0.59		
B Desorbed dye	1.0	0.66	2.15	0.72	1000	132.0 ± 10
C Re-dyed	4.7	0.78	11.21	0.61		
D Desorbed dye	1.9	0.68	3.93	0.73	750	127.5 ± 15
E Re-dyed	5.1	0.74	11.22	0.61		
F Desorbed dye	2.7	0.69	5.52	0.70	500	121.2 ± 20
G Re-dyed	4.9	0.75	10.79	0.61		
H Desorbed dye	3.0	0.69	6.29	0.70	250	92.5 ± 12
I Re-dyed	4.8	0.74	11.09	0.59		
L Desorbed dye	4.6	0.74	10.26	0.60	100	71.3 ± 8

From the data in Table 3.18 varying of volumes of Bu_4NOH at fixed concentration was plotted with each of the amount of desorbed N719 dye (Figure 3.26a), efficiency (Figure 3.26b), J_{sc} (Figure 3.26c) and V_{oc} (Figure 3.26d) for the device dyed with N719 (1 ml, 2.8 mM) . The results also shows that more dye loading can be removed with using large amount of alkaline solution and a small amount of dye desorbed when using small amount of alkali solution at a fixed concentration of alkali solution. Both of η and J_{sc} decrease with increased volume of Bu_4NOH at fixed concentration because a dye loading on TiO_2 was decreased. But V_{oc} was very slightly changed with the volume of Bu_4NOH.

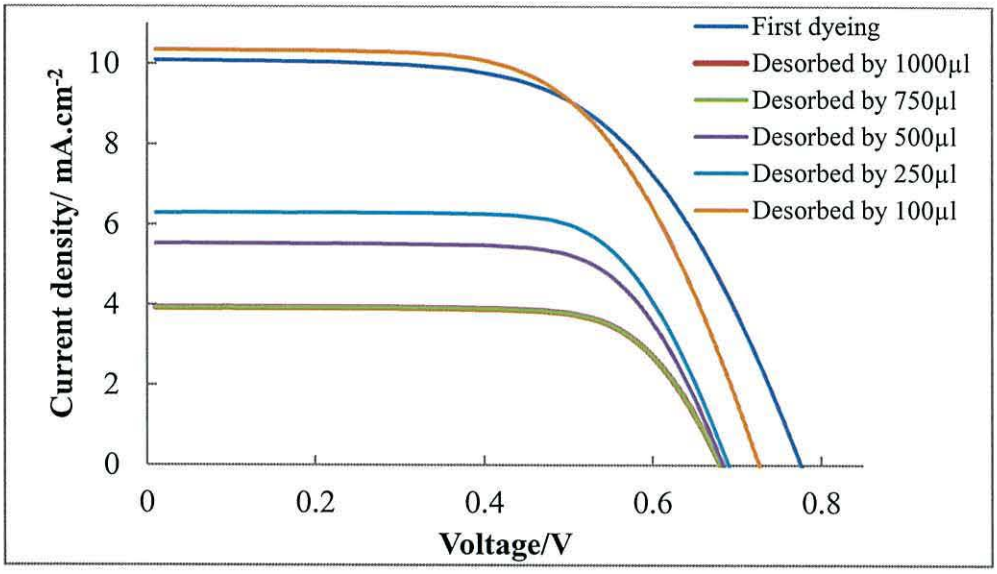

Figure 3.25: Photocurrent density-voltage characteristics under AM 1.5 full sunlight (100 $mW.cm^{-2}$), for a device dyed with N719 after desorption by different volume of 4 mM Bu_4NOH solution.

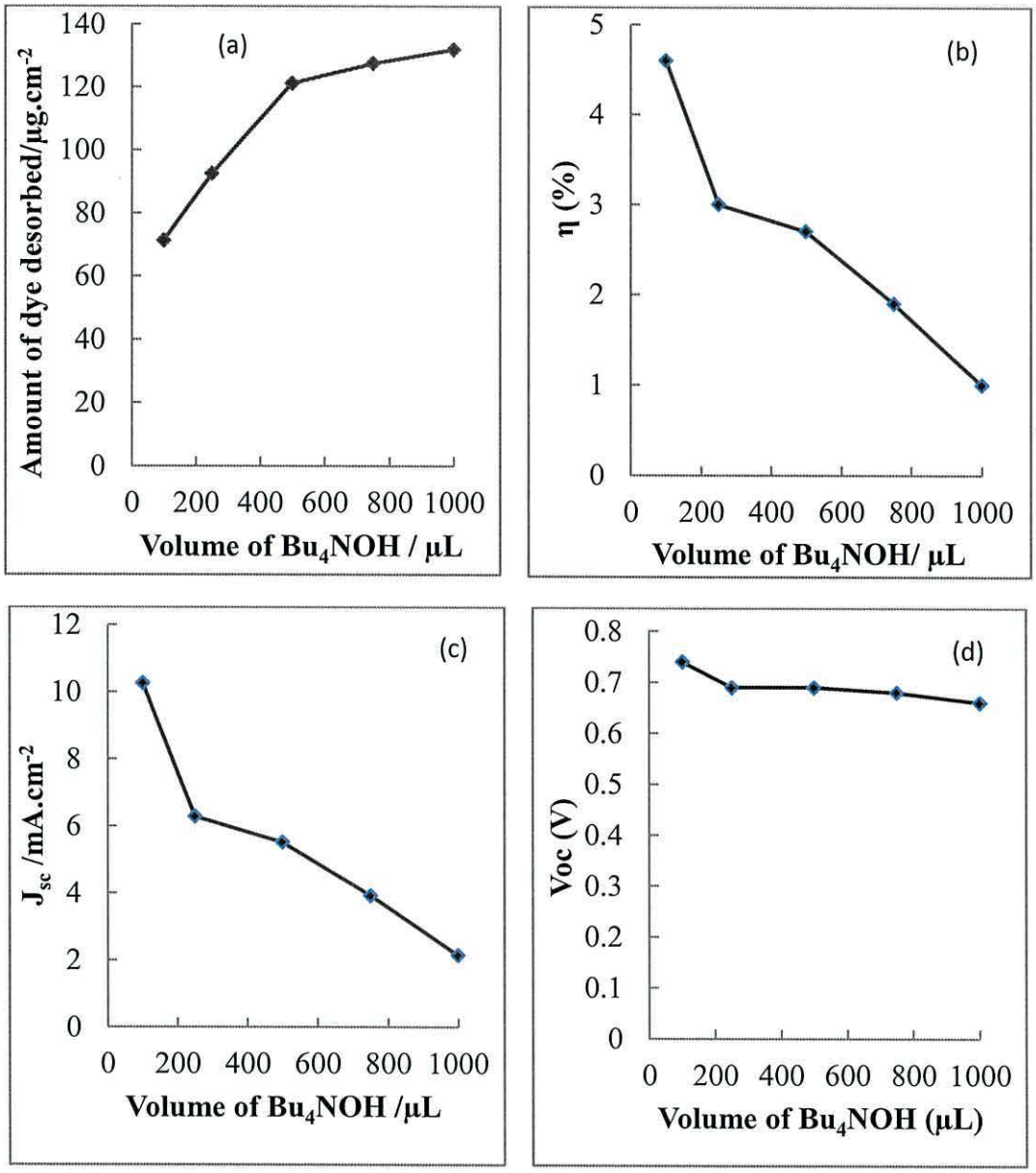

Figure3.26: Plot various volumes of 4 mM Bu_4NOH (µL) *versus* (a) amount of desorbed dye (µg.cm^{-2}), (b) η (%) (c) J_{sc} (mA.cm^{-2}) and (d) V_{oc} (V) used for P25 device dyed with N719 (1ml, 2.8 mM).

3.3.8 Studies of partial dye removal and re-dyeing

The next step was to study if dyes can be partially removed from a photo-electrode to make space for other dyes as was suggested might be possible from the previous data. Figure 3.27 shows the I-V data for a device dyed with N719, then partially removed, then SQ1 added and then N719 added. The photovoltaic parameters are summarized in Table 3.19. In detail Device H was pump dyed with N719 dye (1 ml, 2.8 mM) giving efficiency 4.5% with parameters V_{oc} =0.76 V, J_{sc} = 9.33 mA.cm^{-2}

and FF = 0.62. N719 was then partially desorbed by Bu_4NOH (100 µl, 1 mM) and after re-filling with I_3^-/I^- electrolyte, (Device H1) the efficiency dropped to 3% with decreasing J_{sc} to 7.58 $mA.cm^{-2}$ because of a decrease in the amount of adsorbed dye on TiO_2 surface. The amount of desorbed N719 was measured to be 80 $\mu g.cm^{-2}$ by UV-Vis spectroscopy. After electrolyte removal and rinsing, SQ1 (1 ml, 0.28 mM) was added, giving Device H1-R. The performance efficiency increased to 3.5% which may be due to SQ1 molecules adsorbing on unoccupied sites on the TiO_2 surface. N719 (300 µl, 2.8 mM) was then added (Device H2-R) giving η 4.7% which is slightly higher than the first dyeing with N719 possibly because of the two dyes on the TiO_2. The device was then desorbed by Bu_4NOH (200 µl, 40 mM) and the amount of each dye was measured to be 159 $\mu g.cm^{-2}$ for N719 and 13 $\mu g.cm^{-2}$ for SQ1 by UV-Vis spectroscopy. Figure 3.28 shows the devices after each process. Before adsorption (Figure 3.28a) shows white TiO_2. When adsorbed by N719 (Figure 3.28b) the colour changes to dark red. There was not a big difference in a device colour after partial removal of N719 (Figure 3.28c) because only small amount of N719 was desorbed by Bu_4NOH. But when adding SQ1 (Figure 3.28d) the device shows a blue colour. Finally, when N719 was added the colour changed to the dark purple (Figure 3.28e) because more N719 was also adsorbed on the TiO_2 surface.

Table 3.19: I-V data for 0.9 cm^2 of P25device after partial removal of N719 and re-dyed with SQ1 and then N719. (Approximate errors on devices are ± 10% of the values shown).

Device	Process	η (%)	V_{oc}(V)	J_{sc} /$mA.cm^{-2}$	FF	Desorbed N719 $\mu g.cm^{-2}$	Desorbed SQ/ $\mu g.cm^{-2}$
H	Dyed N719	4.6	0.76	9.33	0.62		
H1	Partial N719 removal	3.0	0.71	7.58	0.56	80	
H1-R	Added SQ1	3.5	0.71	7.85	0.67		

H2-R	Added N719	4.7	0.76	9.48	0.65	159	13

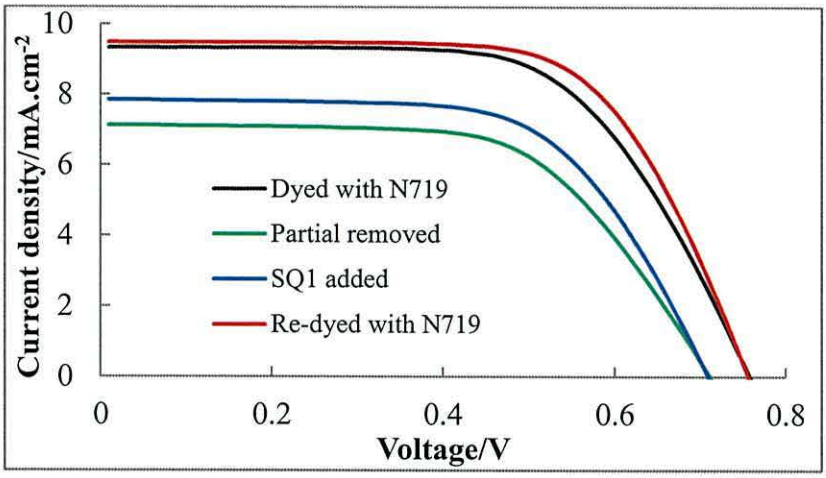

Figure 3.27: Photocurrent density-voltage characteristics under AM 1.5 full sunlight (100 $mW.cm^{-2}$), for a device dyed with N719 (1ml, 2.8mM) followed by partial removal by Bu_4NOH (100µl, 1mM) and then the addition of SQ1 (1ml, 0.28mM) then N719.

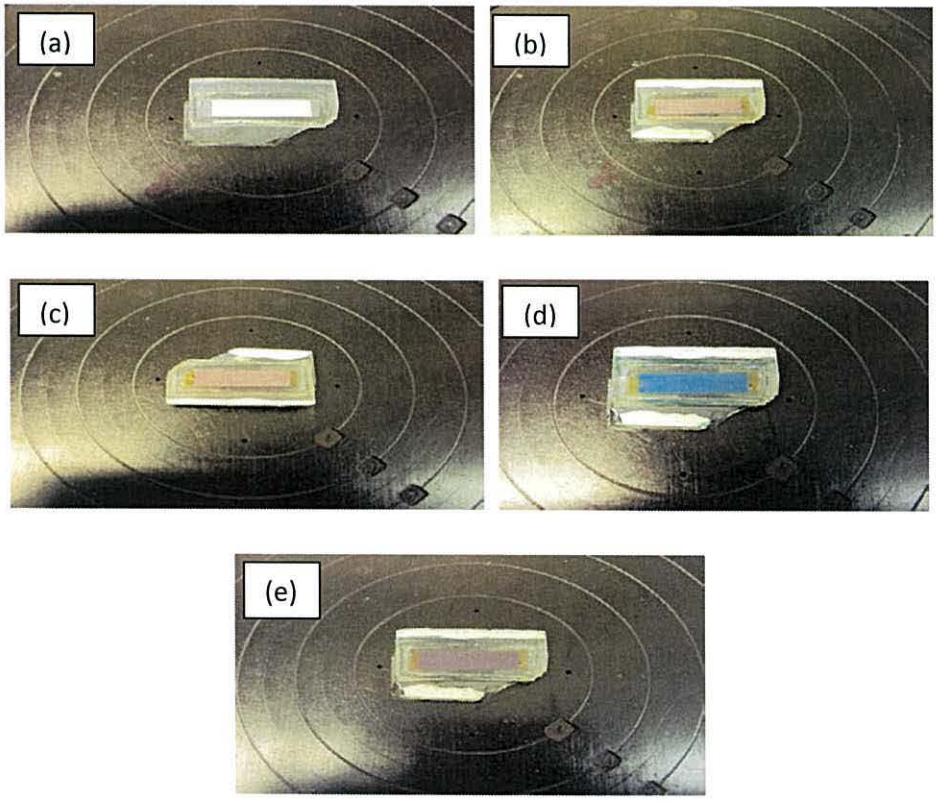

Figure 3.28: Photographs of front of P25 a device (2 x0.5 cm) showing dyeing with N719, partial desorption of N719 and then re-dyeing (a) the device before dyeing (b)

dyed with N719 (1 ml, 1 mM) (c) partial removal of N719 by Bu_4NOH (100 µl, 8 mM) (d) after adding SQ1 (1 ml, 0.25 mM) and (e) Re-dyed with N719 (1 ml, 1 mM).

3.3.9 Study of repeated partial desorption and re-dyeing with different dyes

The next experiment was designed to test if the dyeing, desorption and re-dyeing cycles could be repeated on the same device. To do this, a TiO_2 device was dyed with N719, desorbed and re-dyed with SQ1 in repeated cycles as shown in Table 3.20. Device A was dyed with Ru-bipy N719 (1 ml, 2.8 mM) giving η of 5.0 % with parameters J_{sc} = 10.64 mA.cm^{-2}, V_{oc} = 0.77V. The device was then desorbed by pumping Bu_4NOH (200 µl, 40 mM) through the device cavity (Device B) giving 0.3% which is in line with N719 removal. The amount of desorbed N719 dye was measured to be 185 µg.cm^{-2} by UV-Vis spectroscopy. After electrolyte removal and rinsing, the device was then re-dyed with N719 Device C giving η of 4.5% which is lower than the first dyeing. However, the J_{sc} and V_{oc} were increased to 11.21 mA.cm^{-2} and 0.79 V but the fill factor had dropped to 0.51 which may due to more dye molecules loading on TiO_2 surface. However, it should be remembered that this device had not been aged which often means the fill factor increases as the electrolyte fills the TiO_2 pores more efficiently. The dye was then partially removed by Bu_4NOH (100 µl, 8 mM) giving Device D. The performance was re-measured and the efficiency was found to have dropped to 2.2% and J_{sc} to 5.02 mA.cm^{-2} because only a small amount of N719 was still adsorbed on the TiO_2 particles. The amount of N719 desorbed was measured to be 116 µg.cm^{-2}. SQ1 (1.5 ml, 0.25 mM) was then added (Device E) and the η dropped to 1.5% with decreasing J_{sc} and V_{oc} (3.28 mA.cm^{-2} and 0.59 V). One possible reason for this could have been dye aggregation which could have lead to quenching of dye photo-excited states by electron transfer.[28] All dyes were desorbed using Bu_4NOH (200 µl, 40 mM) and the device was then measured (Device F) giving 0.3 % in line with N719 and SQ1 removal. The amount of each was measured to be 30 µg.cm^{-2} for N719 and 13 µg.cm^{-2} for SQ1 by UV-Vis spectroscopy. After washing and rinsing, the device was then re-dyed with N719 (Device G) giving η of 4.5 % showing similar performance to the first re-dyeing with N719. After removing a small amount of N719 using Bu_4NOH (25 µl, 1 mM), Device H, the η had dropped to 3.8% with J_{sc} = 8.08

$mA.cm^{-2}$, V_{oc} = 0.70V and FF = 0.67. The amount of partial N719 removal was measured as 79 $\mu g.cm^{-2}$. After this, SQ1 (1 ml, 0.25 mM) was added (Device) giving η of 4.0 % with an increase J_{sc} to 9.82 $mA.cm^{-2}$ but both V_{oc} and FF dropped to 0.68 V and 0.59 respectively. The device was then desorbed by Bu_4NOH (Device J) and the η dropped to 0.3 % and the desorbed amount of each dye was measured to be 95 $\mu g.cm^{-2}$ for N719 and 22 $\mu g.cm^{-2}$ for SQ1. Again after washing and rinsing the device was re-dyed with N719 (Device K) giving η of 4.6% with a big increase in J_{sc} (12.31 $mA.cm^{-2}$) because of the large amount of N719 loaded on the TiO_2. N719 was then partially removed by Bu_4NOH (50 µl, 1 mM) giving η of 4.0 % (Device L). The amount of N719 desorbed was measured giving 104 $\mu g.cm^{-2}$. Finally, N719 (1 ml, 2.8 mM) was added Device M giving η of 4.7 % showing similar performance to the initial re-dyeing. The results showing that the desorbing and re-dye cycle could be repeatedly applied on the same device with highly control of dye uptake. Also N719/SQ1 data suggest that dye aggregation and dye arrangement on the surface may strongly affect η and J_{sc}.

Table 3.20:I-V data for 1 cm^2 of TiO_2 device showing re-dyeing with SQ1 and N719 along with partial desorption and re-dyeing. (Approximate errors on devices are ± 10% of the values shown).

Device	Process	η (%)	V_{oc} (V)	J_{sc} / $mA.cm^{-2}$	FF	Amount of desorbed N719/$\mu g.cm^{-2}$	Amount of desorbed SQ1/$\mu g.cm^{-2}$
A	Dyed with N719	5.0	0.77	10.64	0.61	-	-
B	All dye desorbed	0.3	0.58	0.74	0.60	185	-
C	Re-dyed with N719	4.5	0.79	11.21	0.51	-	-
D	Partial dye removed	2.2	0.78	5.02	0.57	116	
E	SQ1 Added	1.5	0.65	3.28	0.72	-	-
F	All dyes desorbed	0.3	0.59	0.69	0.65	30	13
G	Re-dyed with N719	4.5	0.77	11.27	0.52	-	-
H	Partial dye removed	3.8	0.70	8.08	0.67	79	-
I	SQ1Added	4.0	0.68	9.82	0.59	-	-
J	All dyes desorbed	0.3	0.57	0.74	0.63	95	22
K	Re-dyed with N719	4.6	0.76	12.31	0.49	-	-
L	Partial dye removed	4.0	0.70	8.72	0.66	104	-
M	Re-dyed with N719	4.7	0.75	11.77	0.53	225	-

3.3.10 Studies of selective dye removal

Following the earlier experiments showing successful dye desorption using Bu_4NOH and re-dyeing, studies of selective dye removal were attempted using different desorption solutions to try to further control dye loading.

3.3.10.1 Study of the selective removal of N719

To start with, $LiOH_{(aq)}$ was studied to selectively desorb N719. Table 3.21 shows I-V data measured after each dyeing and desorption step. Initially N719 (1 ml, 2.5 mM) was pump dyed though a 1 cm^2 DSL18NRT photo-electrode cell cavity (Device A) giving η 5.8 %. After the electrolyte was removed by 100 µL ethanol and rinsing, SQ1 was added (300 µl, 0.28 mM) by pumping through the device cavity, (Device B) and the efficiency dropped to 5.1% with J_{sc} decreasing from 10.7 $mA.cm^{-2}$ to 9.2 $mA.cm^{-2}$. The drop in efficiency could have been due to the aggregation of SQ1, which may have quenched the N719 excited state. N719 was then selectively desorbed by LiOH (50 µL, 100 mM) pumped through the device cavity and, when the device was measured, (Device C) the η again had dropped to 0.65% which was due to a only small amount of SQ1 remaining on the surface of the TiO_2. Figure 3.29a shows the UV-Vis spectrum for desorbed N719 by LiOH which shows two peaks at 504 nm and 364 nm which are due to N719 dye. The spectrum indicates that the desorbed solution contains only N719 and no SQ1. The desorbed amount of N719 was measured to be 63.7µg.cm^{-2}. The remaining SQ1 was then desorbed from the device by (Bu_4NOH 100µl, 4mM) and measured by UV-Vis spectroscopy giving a spectrum as shown in Figure 3.29b showing the maximum absorbance at 636nm which is due to SQ1. The spectrum does not show any peaks for N719 confirming selective dye desorption. The amount of desorbed SQ1 was then measured to be 11.8 µg.cm^{-2}. The UV-Vis spectra for both desorbed N719 and SQ1are the same as those for the pure dyes shown in Figure 3.30. After washing and rinsing the device was then re-dyed with SQ1 (300 µl, 0.28 mM), Device D, giving η of 2.1 %. After the electrolyte was removed and the device cavity rinsed N719 (1 ml, 2.8 mM) was then added (Device E) and then the η increased to 5.2 % and J_{sc} also increased from 4.47 $mA.cm^{-2}$ to 9.75 $mA.cm^{-2}$ showing similar performance to Device B which co-sensitized with N719 and SQ1.

Table 3.21: I-V data of 1 cm^2 DSL-18NRT dyed with N719 (1 ml, 2.8 mM) followed by adding SQ1 (300 µl, 2.8 mM) and selective removal of N719 by LiOH (100 µl, 100 mM) and SQ1 desorbed by Bu_4NOH (100 µl, 4 mM). (Approximate errors on devices are ± 10% of the values shown).

Device	η (%)	V_{oc} (V)	J_{sc} / $mA.cm^{-2}$	FF
A Dyed with N719	5.9	0.78	10.77	0.63
B Added 300µL SQ1	5.1	0.74	9.25	0.67
C Desorbed N719 by LiOH	0.7	0.61	1.42	0.68
D Re-dyed with SQ1	2.3	0.66	4.47	0.71
E Added 1ml N719	5.2	0.73	9.75	0.66

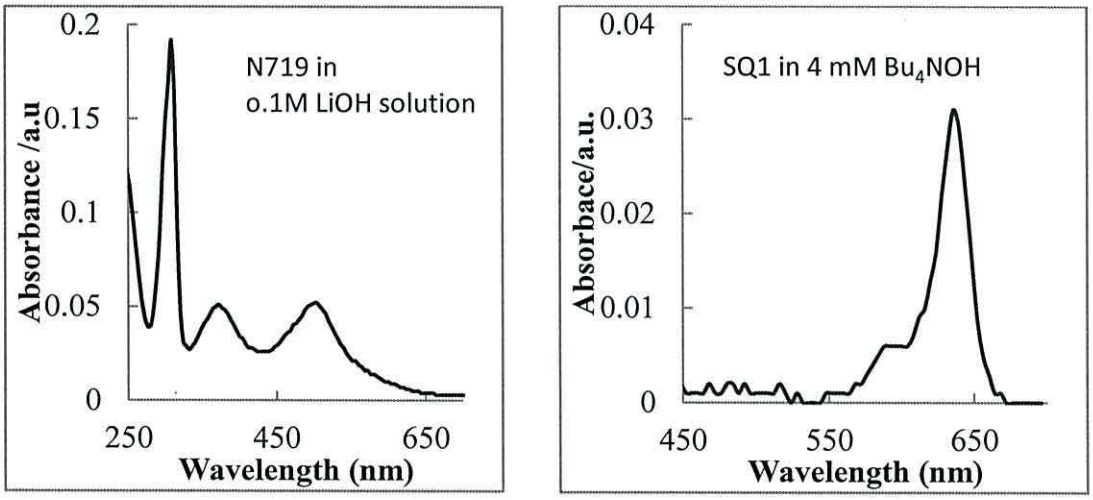

(a) (b)

Figure 3.29: UV/Vis Spectra of selectively desorbed dye solutions (a) N719 by LiOH (50 µL, 0.1 M), and (b) SQ1 desorbed by Bu_4NOH (100 µl, 4 mM).

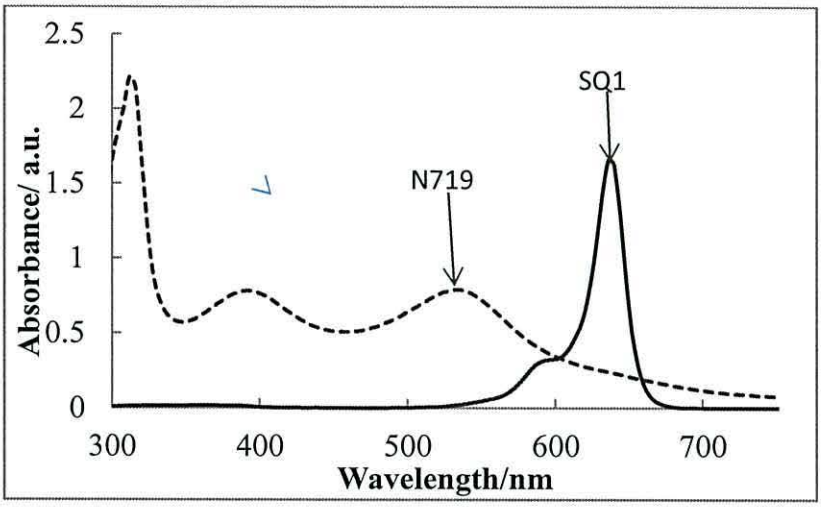

Figure 3.30: UV/Vis Spectra of neat 0.06 mM N719 (.....) in ethanol and 0.1 mM SQ1 (—) in ethanol.

3.3.10.2 Selective removal of N719 and re-dyeing with D149

Selective dye removal was then tested using N719 and D149. Both dyes have a maximum light absorption at the same wavelength (λ_{max} = 532 nm) as shown in Figure 3.31 which shows the UV-Vis spectrum for 0.1 mM N719 in ethanol and 0.25 mM D149 in *tert*-butanol:acetonitrile (1:1). Figure 3.32 shows I-V data and the photovoltaic parameters are summarized in Table 3.22. Device A was initially dyed with N719 (1ml, 1mM) in 5mM CDCA for 10 min giving η of 5.1 % with J_{sc} = 11.3 mA.cm^{-2}, V_{oc} = 0.81V and FF = 0.56. After electrolyte removal and rinsing, the N719 was partially desorbed by Bu_4NOH (50 µL, 4 mM) giving Device B. The efficiency had dropped to 3.6 % with J_{sc} decreasing to 10.16 mA.cm^{-2} presumably due to decreasing amount of adsorbed dye molecules on photo-electrode. The partial amount of desorbed N719 was measured by UV-Vis spectroscopy to be 116 µg.cm^{-2}. Again after electrolyte removal and rinsing, D149 (250 µL, 0.5 mM) in 5 ml CDCA was added (Device C) slightly increasing η to 3.8 % with J_{sc} increasing to 11.82 mM.cm^{-2} but V_{oc} dropping to 0.65V because the device now contained both N719 and D149 molecules and D149 gives a lower V_{oc} than N719.[29] N719 was then selectively desorbed by LiOH (200 µL, 100 mM) giving Device D lowering efficiency to 2.9 % with decreasing J_{sc} to 8.28 mA.cm^{-2} and V_{oc} to 0.60 V due to the remaining D149 on the TiO_2 surface. The amount of desorbed N719 was then measured to be 106 µg.cm^{-2} as show the UV-Vis spectra in (Figure 3.33a). The

remaining D149 was then desorbed by Bu_4NOH (300 µl, 40 mM) followed by 0.5 ml acetone and the D149 desorbed was measured by UV-Vis spectroscopy (Figure 3.33b) to be 22 $\mu g.cm^{-2}$. After washing and rinsing, the device re-dyeing with N719 (1 ml, 1 mM), Device E, and the η increased to 5.9 % which may due the activation of TiO_2 surface leading to form a monolayer of adsorbed dye molecules.

Table 3.22: I-V data for 1 cm^2 of TiO_2 device showing selective removal of N719 (1ml, 1mM) along with partial desorption and adding D149 (250 µl, 0.5 mM) selectively removed N719 by LiOH (100 µl, 100 mM). (Approximate errors on devices are ± 10% of the values shown).

Device	η (%)	V_{oc} (V)	J_{sc} /mA.cm^{-2}	FF
A Dyed with N719	5.1	0.81	11.30	0.56
B Partial dye removed	3.6	0.63	10.16	0.57
C D149 added	3.8	0.65	11.82	0.50
D Selective N719removal	2.9	0.60	8.27	0.58
E Re-dyed with N719	5.9	0.80	11.70	0.51

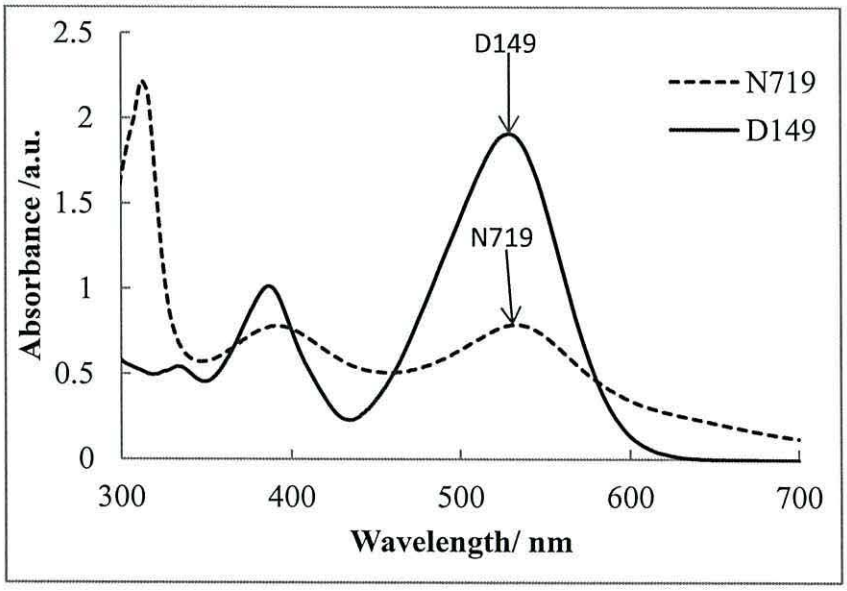

Figure 3.31: UV-Vis spectrum of neat 0.05 mM N719 (....) in ethanol and 0.25 mM D149 (—) in tert-butanol:acetonitrile (1:1)

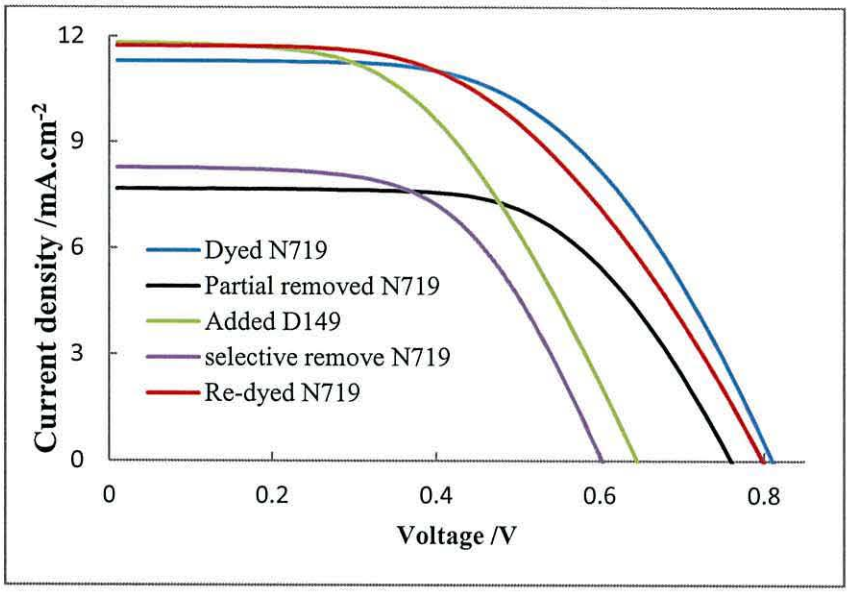

Figure 3.32: Photocurrent density-voltage characteristics under AM 1.5 full sunlight (100 mW.cm^{-2}), for a device dyed with N719 (1ml, 1mM) partial removed by Bu_4NOH (100µl, 1mM), after D149 (250µl, 0.5mM) then selectively removal N719 using LiOH (100 µl, 100 mM) then after N719 was added (1ml, 1mM).

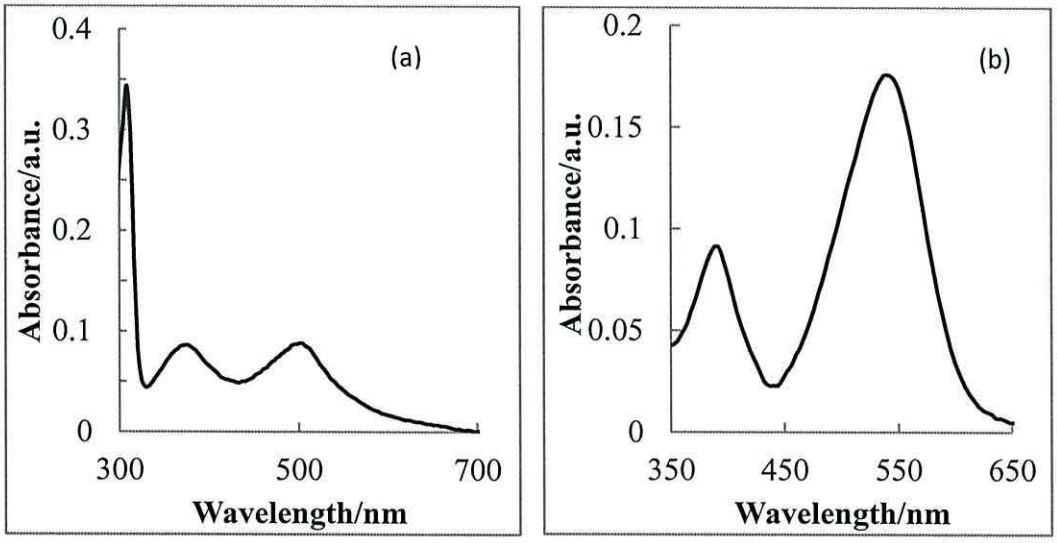

Figure 3.33: UV-Vis spectra for desorbed dye solution (a) N719 desorbed by 100 mM LiOH, and (b) D149 desorbed by Bu_4NOH (200 µl, 40 mM) followed by acetone and ethanol.

3.3.10.3 Selective removal of N719, SQ1 and D149

An experiment was then designed to see if multiple dyes can be selectively desorbed from a photo electrode. To test this, a device was sequentially dyed with SQ1, N719 and D149 and the UV-Vis spectrum for each neat dye is shown Figure 3.34a. The photovoltaic parameters are summarized in Table 3.23. Device A was pump dyed with SQ1 (300 µl, 0.28 mM) giving η 2.3% with J_{sc} of 6.38 mA.cm^{-2} and V_{oc} 0.60V. After electrolyte removal with ethanol, N719 was added (500 µl, 1 mM) giving Device B with η to 4.8% with a greater photo current than Device A. This might be due to the co-sensitization of N719 and SQ1.[23] The electrolyte was removed in the same manner and D149 (200µl, 0.5mM) was then added (Device C), giving η 5.5% with similar J_{sc} and V_{oc} as Device B. Then, N719 was selectively removed using LiOH (100 µl, 100 mM) giving Device D, and efficiency dropped to 0.8% with a big decrease in J_{sc} = 1.44 mA.cm^{-2} due to the remaining SQ1 and D149 on the TiO_2 surface. The UV-Vis spectrum of the desorbed N719 is shown in Figure 3.34b. This shows a spectrum similar to the UV-Vis spectrum of N719 neat in Figure 3.34a. This suggests that only N719 was desorbed by LiOH. The amount of N719 was then measured to be 132.5µg.cm^{-2}. Secondly, SQ1 was selectively desorbed by Bu_4NOH (100 µl, 1 mM) giving η of 1.3 % with slightly increased J_{sc} to 3.7 mA cm^{-2} Device E, which is due to remaining D149 on the TiO_2 surface. The UV-Vis spectrum for the desorbed SQ1 Figure 3.25c shows a spectrum similar to the neat SQ1 dye as shown in Figure 3.32a. The amount of desorbed SQ1 was measured to be 1.2 µg.cm^{-2}. Finally, D149 was then desorbed by Bu_4NOH (100 µl, 40 mM) followed by 200µl acetone, and 100 µl ethanol. The UV-Vis for the desorbed D149 was measured (Figure 3.34d) showing a similar UV-Vis spectrum to pure D149 as shown in Figure 3.34a. The amount of desorbed D149 was measured to be 3.9µg.cm^{-2}. External quantum efficiency (EQE) measurements were used to study spectral response. The EQE spectrum of the co-sensitization of SQ1+N719+D149 and after selective removal of N719 and SQ1 are shown in Figure 3.35. The spectral response of the co-sensitization with three dyes SQ1, N719 and D149 (green line) ends at about 700 nm. The change in EQE between 600 and 700 nm is attributed to SQ1 photoresponse with a peak EQE_{max} of about 20% at 640 nm and a rather broad peak that centres at 550 nm yielding a maximum EQE of 40%. The EQE for SQ1+D149 is significantly reduced (black line) after selective removal of N719. The EQE generated below 400 nm after all dyes were removed is a result of light absorption by the titania. Figure

3.36 shows photographs of the device dyed with three dyes then selective desorption of each dye. At first, the device dyed with SQ1 (Figure 3.36a) shows the blue colour of SQ1. When N719 was added (Figure 3.36b) the device colour became dark violet. D149 was then added and the device became dark red (Device C). When N719 was removed by LiOH, the device colour appears dark blue-red (Figure 3.36d). This photograph also shows a vial containing a red solution of desorbed N719. Next SQ1 was selectively removed by Bu_4NOH leaving a red colour of D149 on TiO_2, (Figure 3.36e) which also shows a vial containing a blue solution of SQ1. Finally, D149 was desorbed by Bu_4NOH and acetone leaving a white device of TiO_2. A red solution of desorbed D149 was collected in a vial as shown in (Figure 3.36f). The results suggest that sequential selective removal of N719, SQ1 and D149 has been successfully achieved. The procedure is important for the performance of DSCs by changing different dyes into co-sensitization in the same device.

Table 3.23: I-V data for a P25 TiO_2device sequentially dyed with SQ1 (300 µl, 0.28 mM)), N719 (500 µl, 1 mM) and D149 (200 µl, 0.5 mM) followed by the sequentially selective removed N719 by LiOH (100µl, 100mM), SQ1 by Bu_4NOH (100 µl, 1mM) and D149 by Bu_4NOH (100 µl, 40 mM) followed by 200 µl acetone and 100 µl ethanol. (Approximate errors on devices are ± 10% of the values shown).

Device		η (%)	V_{oc} (V)	J_{sc} / mA.cm^{-2}	FF	Amount of selectively desorbed dye/µg.cm^{-2}
A	Dyed with SQ1	2.3	0.60	6.39	0.61	
B	N719 added	4.8	0.68	13.47	0.53	
C	D149 added	5. 5	0.69	13.36	0.59	
D	Desorbed N719	0.8	0.78	1.44	0.67	132.5
E	Desorbed SQ1	1.3	0.61	3.72	0.60	1.2
F	Desorbed D149	0.3	0.57	0.84	0.62	3.9

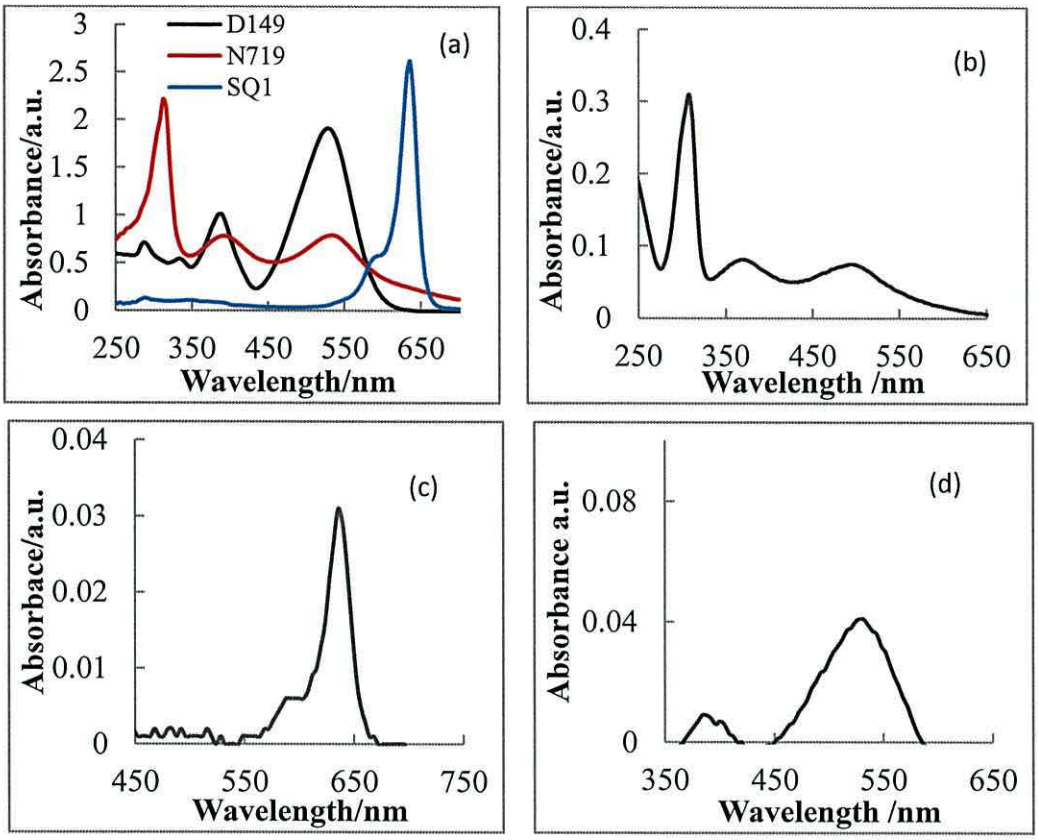

Figure 3.34: UV-Vis spectra for neat (a) (0.5 mM) N719 (red), (0.2 mM) D149 (black) and (0.1 mM) SQ1 (blue) dyes before adsorption, (b) N719 desorbed with 0.1M LiOH, (c) SQ1 desorbed with 1mM Bu_4NOH, and (d) D149 desorbed D149 by 40mM Bu_4NOH and acetone

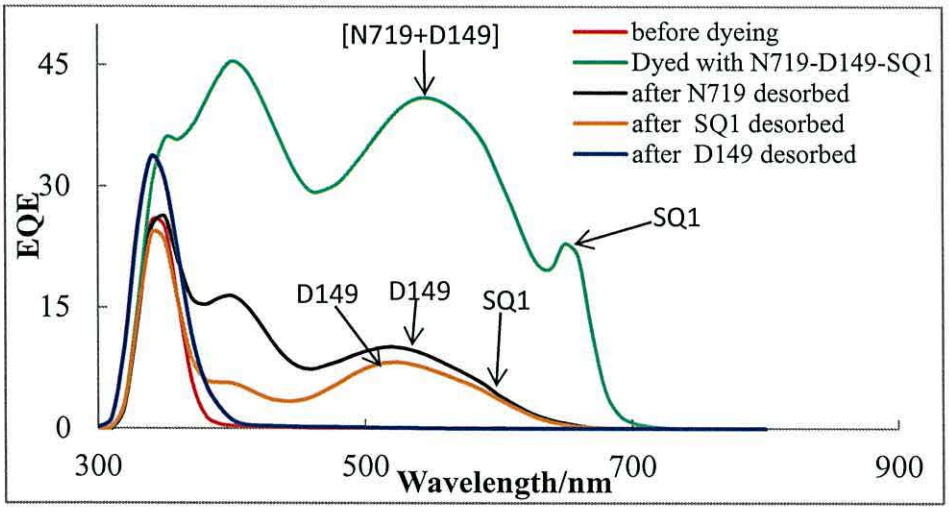

Figure 3.35: External quantum efficiency *versus* wavelength for a device containing SQ1+N719+D149 then after selective removal N719 and then after selectively removal of SQ1 as well as the TiO_2 after the removal of all dyes.

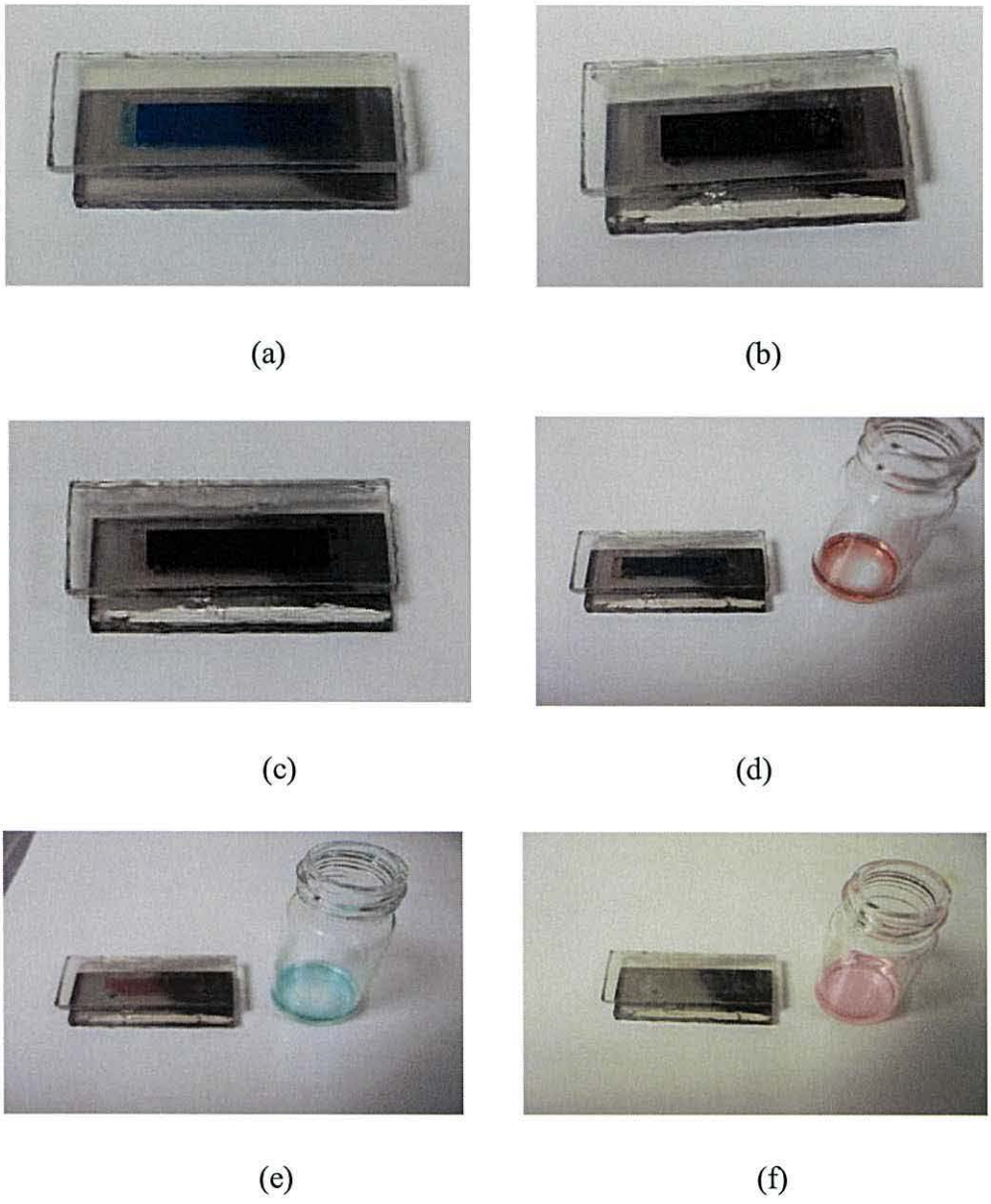

Figure 3.36: Photographs of TiO_2 device (2 x 0.5 cm) showing cycles of dyeing with SQ1, then N719 and then D149 selective removal of N719, SQ1 and D149 (a) dyed with SQ1 (300 μL, 2.8 mM), (b)dyed with N719 (500 μL, 1 mM), (c) dyed with D149 (200 μL, 0.5 mM), (d) N719 desorbed by LiOH (100 μL, 100 mM), (e) SQ1desorbed by Bu_4NOH (100 μL, 2 mM), (f) D149 desorbed D149 by Bu_4NOH (200 μL, 40 mM) and 200 μL acetone. The solutions in the vials show the desorbed solution as follows (d) desorbed N719, (e) desorbed SQ1 and (f) desorbed D149.

3.4 Conclusions

In summary, the data in this chapter show a novel adsorption, desorption and re-dyeing method which can be used to control dye uptake. Mesoporous TiO_2 was prepared and the adsorption of N719 and SQ1 dyes on the as-prepared TiO_2 was studied. The equilibrium data have been analyzed using Langmuir and Freundlich isotherms and characteristic parameters for each isotherm have been determined. The Freundlich isotherm has been shown to give the best agreement for the SQ1 adsorption and the Langmuir isotherm fits better for the adsorption of N719. Desorption and ultra-fast re-dyeing through DSCs device has also been studied using different alkali solutions. Bu_4NOH has been used as the best alkaline for desorbing both of Ru-bipyridyl and organic dyes from the TiO_2 devices because of the ability to remove both Ru(II) complexes and organic dyes from TiO_2 devices without any damage to the TiO_2 films. The procedure was then developed to remove only partial amounts of dye by controlling the volume and concentration of Bu_4NOH. Ultra-fast re-dyeing with the same dye or different dyes into the same device was then studied and found to be successful. A new method for the highly selective removal of multiple dyes N719, SQ1 and D149 from a photo-electrode was also studied. The result of this shows that there is potential to reduce the amount of dye used within a photo-electrode with relatively less effect on device performance with obvious benefits for reducing cost. The method is also very versatile enabling ultra-fast re-dyeing for a wide range of DSC dyes leading to ultra-fast multiple sensitizations of metal oxide photo-electrode films. Selective removal also has been concluded for co-adsorption of different dyes on TiO_2.

3.5 References

[1] P. Persson, S. Lunnell, *Solar Energy Materials and Solar Cells*, 2000, **63**, 139

[2] Z. Zhang, S. M. Zakeeruddin, B. C. O'Regan, R. H. Baker, M. Grätzel, *Journal of Physical Chemistry B*, 2005, **109**, 2818

[3] A. Vittadini, A. Selloni, F. P. Rotzinger, M. Grätzel, *Journal of Physical Chemistry B*, 2000, **104**, 1300-13006.

[4] P. Person, M. J. Lundqvist, R. Ernstorfer, W. A. Goddard, F. Willing, *Journal of Chemical Theory and Computation*, 2006, **2**, 441-451.

[5] P. Wen, M. Xue, Y. Ishikawa, H. Itoh, Q. Feng, *Applied Materials and Interfaces*, 2012, **4**, 1928-1934.

[6] P. Wang, C. Klein, R. Huphry-Baker, S. M. Zakeeruddin, M. Grätzel, *Journal of American Chemical Society*, 2005, **127**, 808-809.

[7] J. H. Yum, P. Walter, S. Huber, D. Rentsch, T. Geigar, F. Nuesch, F. De Angelis, M. Grätzel, M. K. Nazeeruddin, *Journal of American Chemical Society,* 2007, **129**, 10320-10321.

[8] S. Ito, S. M. Zakeeruddin, R. Humphry-Baker, P. Liska, R. Charvet, P. Comte. M. K. Nazeeruddin, P. Pechy, M. Takata, H. Miura, S. Uchida, M. Grätzel, *Advanced Materials*, 2006, **18**, 1202-1205.

[9] P. J. Holliman, M. Mohsen, A. Connell, M. L. Davies, K. AL-Salihi, M. B. Pitak, G. J. Tizzard, S. J. Coles, R. W. Harrington, W. Clegg, C. Serpa, O. H. Fontes, C. Charbonneau, M. J. Carnie, *Journal of Materials Chemistry*, 2012, **22**, 13318-13327

[10] B. Z. Shan, Q. Zhao, N. Goswami, D. M. Eichhorn, D. P. Rillema, *Coordination Chemistry Reviews*, 2001, **211**, 117-144.

[11] D. M. Manuta, A. J. Lees, *Inorganic Chemistry*, 1986, **25**, 3212-3218.

[12] E. Buncel, S. Rajagopal, *Accounts of Chemical Research*, 1990, **23**, 226-231.

[13] W. A. Adamson, in *Physical Chemistry of Surfaces*, 1982, 4th ed., John Wiley & Sons, New York, p548.

[14] I. Frank, D. Marx, M. Parrinello, *Journal of American Chemical Society*, 1995, **117**, 8037-8038.

[15] C. H. Giles, A. P. DeSilva, and I. A. Easton, *Journal of Colloidal and Interface Science*, 1974, **47**, 766-778.

[16] N. Martsinovich, A. Troisi, *Energy and Environmental Science*, 2011, **4**, 4473-4495.

[17] Y. S. Ho, G. Mckay, *Adsorption Journal of the International Adsorption Society*, 1999, **5**, 409-417.

[18] B. Bai, Y. Wu, R. B. Girgg, Journal of *Physical Chemistry C*, 2009, **113**, 13772-13779.

[19] I. Efremenko, M. Sheintuch, *Langmuir*, 2006, **22**, 3614-3621.

[20] F. O. Okeola, O. E. Odebunmi, *Advances in Environmental Biology*, 2010, **4**, 329-335.

[21] T. Watson, P. J. Holliman, D. Worsley, *Journal of Materials Chemistry*, 2011, **21**, 4321-4325.

[22] C. R. Lee, H. S. Kim, I. H. Jang, J. H. Im, N. G. Park, *Applied Materials and Interfaces*, 2011, **3**, 1953-1957.

[23] P. J. Holliman, M. L. Davies, A. Connell, B. V. Velasco, T. M. Watson, *Chemical Communications*, 2010, **46**, 7256-7258.

[24] P. Wen, M. Xue, Y. Ishikawa, H. Itoh, Q. Feng, *Applied Materials and Interfaces*, 2012, **4**, 1928-1934.

[25] D. R. Lide, in *CRC Handbook of Chemistry and Physics*, 2010, 90th Edition, Taylor and Francis, Boca Raton FL. 8-49.

[26] T. Yamane, in *Statistics an Introductory Analysis*, 1967, Harper and Row, London, p59-64.

[27] A. B. Woodside, Z. Huang, D. C. Poulter, *Organic Synthesis Collective*, 1993, **8**, 616.

[28] S. Tatay, S. A. Haque, B. O'Regan, J. R. Durrant, W. J. H. Verhees, J. M. Kroon, A. Vidal-Ferran, P. Gavina, E. Palomares, *Journals of Materials Chemistry*, 2007, **17**, 3037-3044.

[29] Y. Ren, Y. Z. Zheng, J. Zhao, J. F. Chen, W. Zhou, X. Tao, *Electrochemistry Communications*, 2012, **16**, 57-60.

Chapter Four Ultra-Fast Co-sensitization

4.1 Introduction

The development of sensitizing dyes to broaden the spectral response from the visible to the near infrared region has been one of the key issues for dye sensitized solar cells.[1] The optimal sensitizer for solar cell application should be panchromatic; that is that it absorbs all the photons from the visible to the near–infrared region.[2] DSCs based on ruthenium complexes have been preferred choice for many years.[3] However, the problem with the ruthenium complexes is the difficulty of further improvement in the conversion efficiency, because of their low molar extinction coefficients (ε = 10,000 - 20,000 $M^{-1}.cm^{-1}$ at 550 nm) and low spectral response in the near-IR region.[4,5] Several groups have studied co-sensitization with two or more dyes including metal-free organic dyes such as JK-2 with SQ1,[6] triple dye sensitization using yellow merocyanin, red hemicyanine, and blue squarylium cyanine dyes,[7] or a zinc prophyrin sensitizer (LD12) with an organic dye (CD5).[8] The reason for using organic dyes in co-sensitization is because of their generally higher molar extinction coefficients which allow sufficient light absorption even with lower amounts of each dye.[9] Co-sensitization uses more than one dye having a broad absorption of visible, near-infrared and infra-red light.[10] Previous approaches for the co-adsorption of multiple dyes onto the DSC electrodes have achieved only limited success.2 For instance, slow dyeing procedures in co-sensitization have been used by several researchers. However, recently a new technique of ultra-fast dye sensitization and co-sensitization has been applied successfully in Bangor University.[11] The diagram of the ultra-fast technique by first sealing the photo-electrode and counter electrode together to create a sealed cavity around the photo-electrode and then pumping a dye solution through a one hole from in back of counter electrode to other hole was shown in chapter two.

In this chapter, different co-sensitization methods have been studied to improve the photovoltaic performance of DSCs such as; 1) studying mixed dye solutions loaded directly on to the TiO_2 2) stepwise co-sorption of different dyes 3) using selective dye desorption of co-sensitization in the device of DSCs. The key issue is controlling dye loadings using ultra-fast dyeing.

4.2 Aim of the study

The aim of this study is to improve DSC performance using ultra-fast sensitization to sensitize titania with more than one dye in <10 minutes. Also, to develop co-sensitizing methods using selective desorption for changing the adsorbed dyes to help control dye loadings and spectral response.

4.3 Results and discussion

Co-sensitizing using multiple dyes has been shown as a promising approach to improve DSC performance. Many dye combinations have been trialled for cosensitization such as; a ruthenium complex with an organic dye,[12] metal free organic dye, phthalocyanine with organic dye and dye sensitization with different dyes in separate layers,[13] all of which have been reported to show enhanced photovoltaic performance relative to their individual single-dye system. This chapter looks at different aspects of ultra-fast co-sensitization such as the sequence of dyeing, and changing the dye molecule from the adsorbed site to improve cell performance. The ultra-fast co-sensitization by two dyes, three dyes and four dyes have been studied in this chapter using N719, SQ1, Hf-SQ1, D149, D131, RD, and YD dyes.

4.3.1 Co-sensitization with N719 and Hf-SQ1

The molecular structure of the organic dye 3-[(1-ethyl-1,3-dihydro-3,3-dimethyl-2H-indol-2-ylidene)methyl]-4-hydroxy-cyclobutene-1,2-dione otherwise known as half – squarilium Hf-SQ1 dye is shown in Figure 4.1.

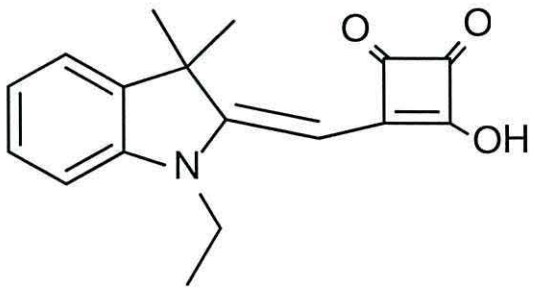

Figure 4.1: Molecular structure of Hf-SQ1.

The absorption maximum of Hf-SQ1 is 420 nm which overlaps with the second absorption band of N719 at ~400 nm as shown in Figure 4.2. The I-V curves of sensitization of a P25 device with Hf-SQ1 and N719 individually and the co-sensitization of both dyes using ultra-fast dyeing are shown in Figure 4.3. The corresponding photo-voltaic parameters (short-circuit photocurrent density J_{sc} ($mAcm^{-2}$), open-circuit voltage V_{oc} (v), fill factor (FF) and efficiency η (%) are presented in Table 4.1.

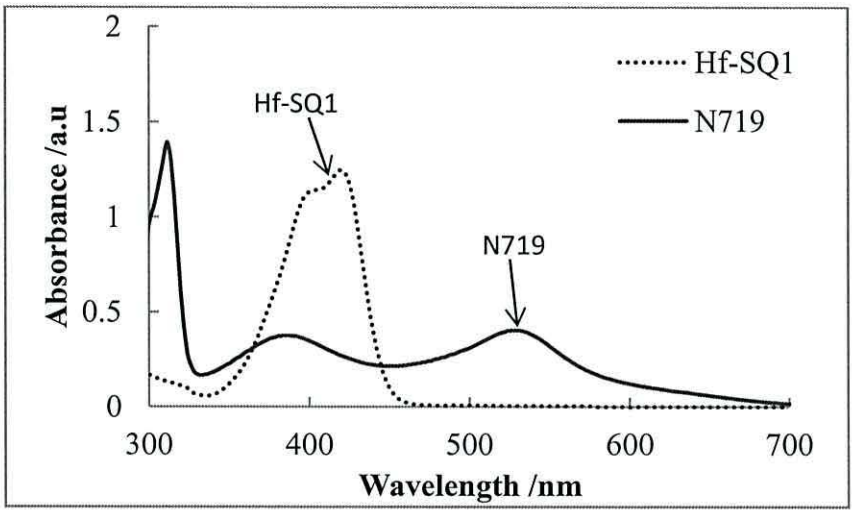

Figure 4.2: UV-Vis Spectra for 0.1 mM N719 in *tert*-butanol: acetonitrile and 5 mM Hf-SQ1in ethanol.

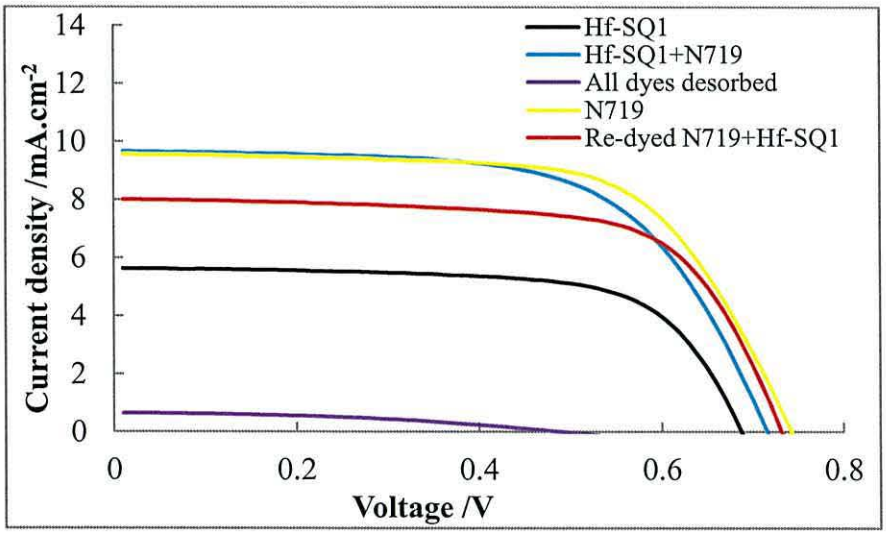

Figure 4.3: Photocurrent density-voltage characteristics under AM 1.5 full sunlight (100 $mW.cm^{-2}$), for a device co-sensitized with N719 (500 µl, 2.8 mM) and Hf-SQ1 (300 µl, 5 mM) desorbed and re-dyed with N719 and Hf-SQ1.

Device A was initially dyed with a single dye by pumping Hf-SQ1 (300 μl, 5 mM) giving η 2.9 % with parameters (J_{sc} = 5.32 mA.cm^{-2}, V_{oc} =0.69, and FF = 0.68). The electrolyte was then removed by ethanol and N719 (500 μl, 2.8 mM) was then added to give Device B. The co-sensitization of the cell shows an increase in η to 4.7% with a greater J_{sc} than the Hf-SQ1 alone. The total dye were then desorbed by Bu_4NOH (200 μl, 40 mM) and the absorbance of the solution measured Figure 4.4 shows UV-Vis spectra of the desorbed solution of N719 and Hf-SQ1. A blue shift was observed for N719 from 532 nm to 512 nm, because the dye is solvatochromic, the solvent in which the absorbing N719 is dissolved affects the N719 peak resulting from (n → π*) transitions which are shifted to shorter wavelength (blue shift).[14] However, the Hf-SQ1 peak at 420 nm didn't show any shift. The sequence of dyeing was then changed so the device was first dyed with N719 (500 μl, 2.8 mM), Device C, giving η of 5.1 % with the similar J_{sc} to Device B but after adding Hf-SQ1 (300 μl, 5 mM) giving Device D the η dropped to 4.6% and J_{sc} decreased to 8.75 mA.cm^{-2}. The change in the colour of the device illustrates the dye adsorption behaviour. Thus Figures 4.5a to 4.5d, show pictures of the device during the process, (a) shows the white TiO_2 device before adsorption and when the device dyed with Hf-SQ1 the colour changes to yellow which means the TiO_2 particles are covered by Hf-SQ1 molecules. N719 was then added and the colour of the device changes to dark red with disappearance the yellow colour of Hf-SQ1 (Figure 4.5c) because the layer of N719 molecules dominates Hf-SQ1 molecules. But when Hf-SQ1 is added to N719 the colour of the device remains dark red (Figure 4.5f) which suggests a low loading of Hf-SQ1 relative to N719. The results show that dyeing with Hf-SQ1 and then N719 is better than using N719 then Hf-SQ1 for co-sensitization, which suggests that the order of dyeing in co-sensitization is important.

Table 4.1: I-V data of a P25 device sequentially sensitized with Hf-SQ1 (300 µl, 5 mM) and N719 (500 µl, 2.8 mM) and after desorbing and re-dyeing with different dyeing sequences. (Approximate errors on devices are ± 10% of the values shown).

Device		η (%)	Voc (V)	J_{sc} /mAcm^{-2}	FF
A	Dyed with 300µL Hf-SQ1	2.9	0.69	5.63	0.68
B	Added 500µL N719	4.7	0.72	9.66	0.62
C	After total dye desorption	0.2	0.49	0.64	0.41
D	Re-dyed with 500 µL N719	5.1	0.74	9.57	0.66
E	After adding 300 µL Hf-SQ1	4.6	0.73	8.75	0.68

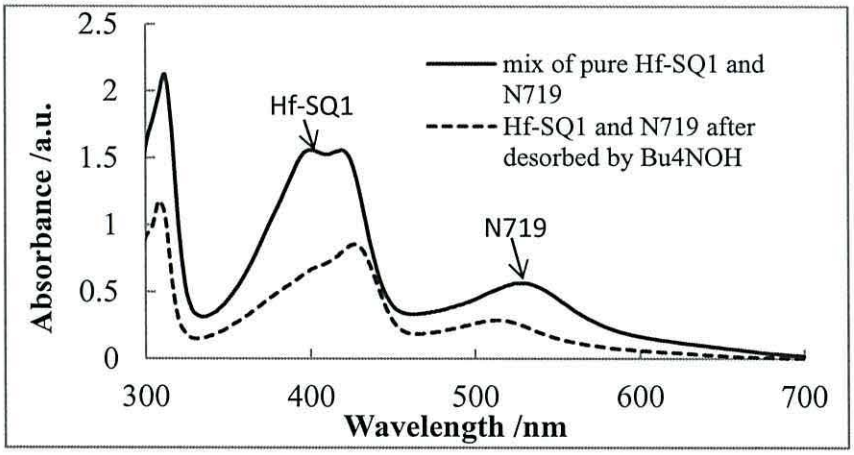

Figure 4.4: UV-Vis spectra for a mixed of N719 (2.8 mM) and Hf-SQ1(0.5 mM) solutions (solid line) before adsorption and solution desorbed by Bu_4NOH (200 µl, 40 mM, dashed line).

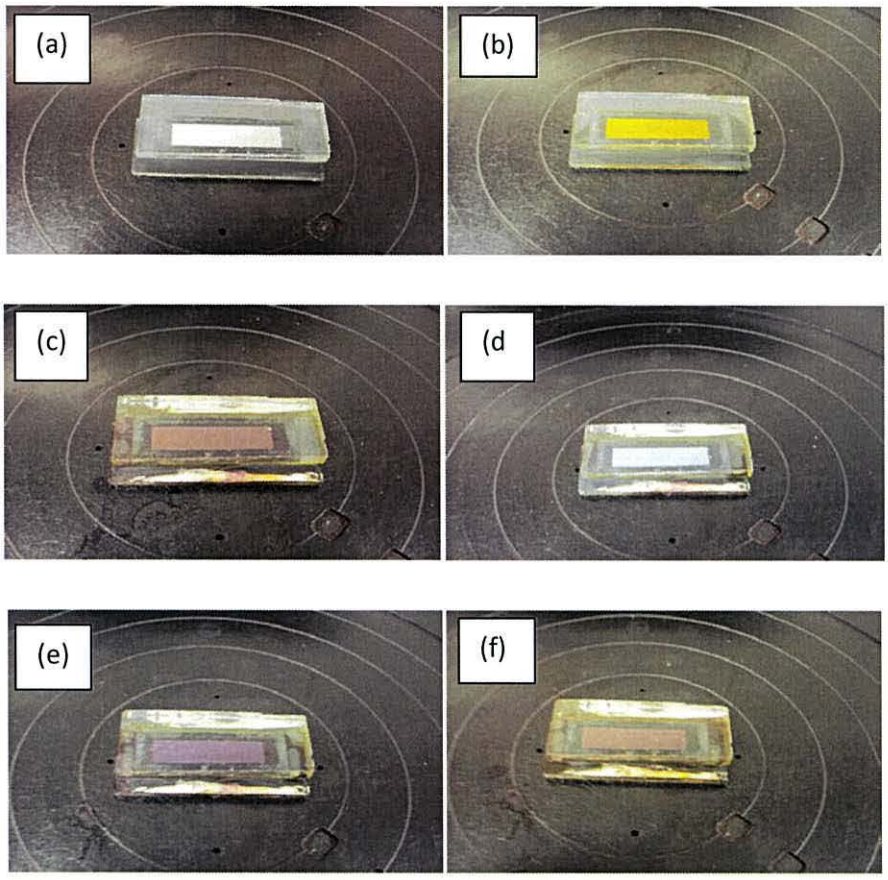

Figure 4.5: Photographs of a P25 device sensitized with Hf-SQ1 and N719 before and after desorption by 40 mM of Bu_4NOH (a) before dyeing (b) dyed with Hf-SQ1 (300 μL, 5 mM) (c) N719 added (500 μL, 2.8 mM) (d) all dyes desorbed by Bu_4NOH (200 μL,40 mM) (e) re-dyed with N719 (500 μl, 2.8 mM) and (f) after adding Hf-SQ1(300 μL,5 mM).

4.3.2 Studies of controlling dye loading

Controlling the dye loadings when co-sensitizing N719 with Hf-SQ1 has been studied by dye desorption and re-dyeing to study the accurate control of loading different dyes. Table 4.2 shows I-V data for a 1 cm^2 TiO_2 photo-electrode. Firstly the device was dyed with N719 (1 ml, 1 mM, Device A) giving η of 4.3 % with parameters (J_{sc}= 8.6 $mAcm^{-2}$, V_{oc} = 0.79V and FF = 0.64). N719 was then partially removed by pumping Bu_4NOH (100 μl, 2 mM) through the device cavity followed by re-filling I_3^-/I^- electrolyte (Device B). The re-measured device gave η = 2.1 % with a decreased J_{sc} of 4.13$mA.cm^{-2}$ due only a smaller amount of N719 remaining on the TiO_2 surface. Hf-SQ1 dye was then added (1 ml, 0.1 mM, Device C) to give η = 3.2% which is higher than Hf-SQ1 alone (which gave η of 2.6% in a previous

experiment). Device C shows improvement in cell performance as a result of co-sensitizing TiO_2 with Hf-SQ1and a small amount of N719. All the dyes were removed by Bu_4NOH (200 µl, 40 mM, Device D). After re-dyeing the device with N719 and then partial removal again by pumping Bu_4NOH (200 µl, 2 mM, Device F) η dropped to 0.8%. SQ1 (500 µl, 0.25 mM) was then added (Device G) giving η of 2% similar to the efficiency for SQ1 alone. Again all the dyes were removed using Bu_4NOH (200 µl, 40 mM, Device H) and η dropped to 0.3%. The process was then repeated by re-dyeing with N719 (Device I) giving η 4.6%. Partial N719 was then removed using Bu_4NOH (100 µl, 2 mM, Device J) and η dropped to 3%. Then a mix of Hf-SQ1:SQ1 (0.5 mM: 0.24 mM in 1:1 volume ratio) was added Device K and η slightly increased to 3.5%. The results show that the device performance by co-sensitizationTiO_2 with N719 and Hf-SQ1 is higher than Hf-SQ1 alone but the device performance is to less than N719 alone. These dyes were chosen for co-sensitization because they absorb light at different wavelengths.

Table 4.2: I-V data of 1 cm^2 P25 device dyed with N719 then co-sensitized with Hf-SQ1 and N719 desorbed and re-co-sensitized with N719 and Hf-SQ1/SQ1. (Approximate errors on devices are ± 10% of the values shown).

Device		η (%)	V_{oc} (V)	J_{sc} /mAcm^{-2}	FF
A	Dyed with N719	4.3	0.79	8.60	0.64
B	Partial N719 removal	2.1	0.72	4.13	0.70
C	Re-dyed with half SQ1	3.2	0.69	7.14	0.66
D	After all dyes desorbed	0.3	0.61	0.77	0.67
E	Re-dyed with N719	4.4	0.78	9.37	0.60
F	Partial N719 removal	0.8	0.64	1.78	0.69
G	SQ1 added	2.0	0.66	5.34	0.58
H	After all dyes desorption	0.3	0.56	0.80	0.65
I	Re-dyed with N719	4.6	0.76	9.34	0.63
J	Partial N719 removal	3.0	0.71	7.58	0.56
K	Added mix (SQ1+Hf-SQ1)	3.5	0.71	7.85	0.63
L	Total dyes desorption	0.3	0.58	0.85	0.65
M	Re-dyed with Hf-SQ1	2.6	0.62	6.71	0.61
N	N719 added N719	4.8	0.76	9.49	0.66

4.3.3 Comparison between P25 and commercial TiO_2 DSL-18NRT pastes

The photo-electrodes which were used for the devices in all previous experiments were made from P25 paste consisting of 74 wt. % anatase and 24 wt.% rutile.[15] The P25 is less transparent compared to the commercial TiO_2 DSL-18NRT paste. To test this, three films from each paste were prepared using one layer of Scotch tape. The films were then sintered at 450 °C, for 30 minutes. One film from each paste was left without dyeing; a second film was immersed in (1mM) N719 dye solution and the last one was immersed in SQ1 dye solution. After 24 hours the transmittance and absorbance were measured for each film using a UV-Vis spectrophotometer. Figures 4.6a shows the transmittances of a P25 film as a reference, P25 dyed with N719, and P25 dyed with SQ1 and Figure 4.6(b) shows similar data for DSL-18NRT films. At the same time the data was considered in absorbance as shown in Figure 4.7(a) and Figure 4.7(b). The UV-Vis spectra show more than 80% of the light at wavelength 650 nm transmitted through DSL-18NRT, but only about 30% of the light transmitted through TiO_2 p25 using a glass slide as a blank reference .

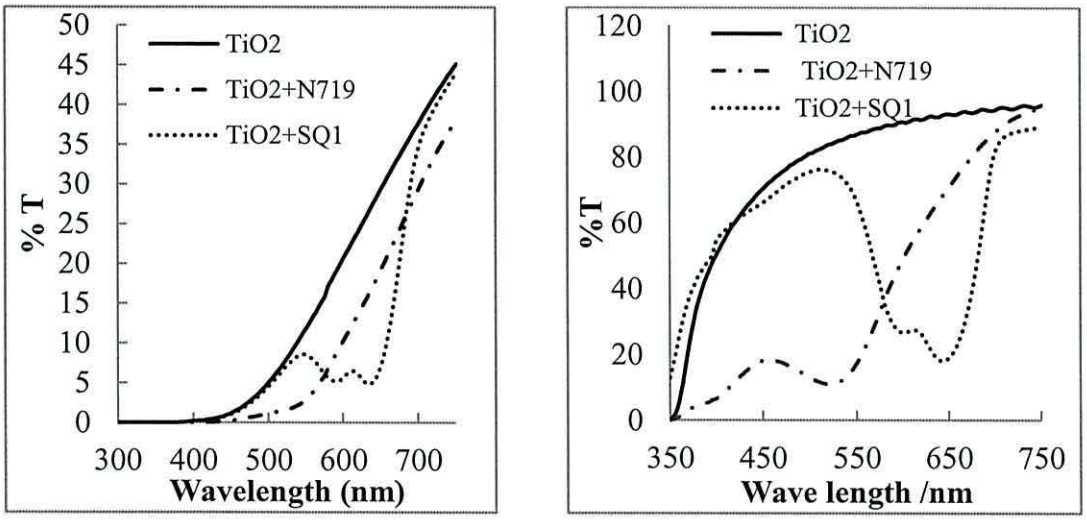

(a) (b)

Figure 4.6: Transmittance UV-Vis spectra of (a) (solid line) only P25 film, (dotted line) after SQ1adsorbed and (dashed line) after N719 adsorbed N719 and (b) (solid line) only DSL-18NRT films (dotted line) after SQ1 adsorbed and (dashed line) after N719 adsorbed.

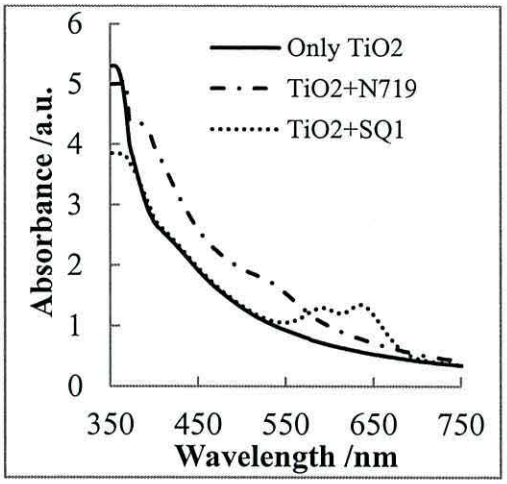

(c)

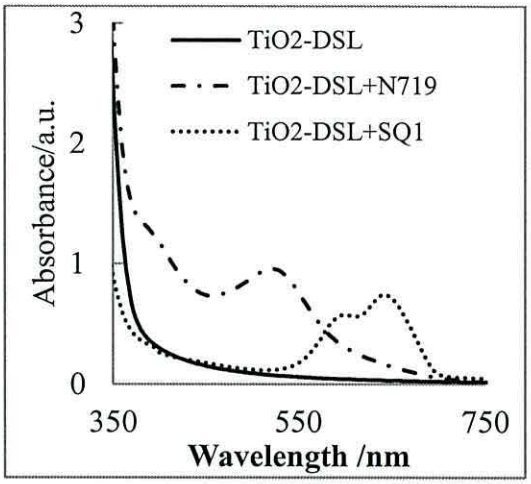

(d)

Figure 4.7: Absorbance UV-Vis spectra for (c) (solid line) P25 film, (dotted line) after SQ1 adsorbed and (dashed line) after adsorbed N719. (b) (solid line) DSL-18NRT films (dotted line) after SQ1 adsorbed SQ1 and (dashed line) after N719 adsorbed N719.

4.3.4 Effect of CDCA co-adsorbent on the co-sensitization of a mixture of SQ1:SQ2

Chenodeoxycholic acid (CDCA) has been reported as a co-adsorbent to minimize the formation of molecular aggregates on the surface of TiO_2 nanocrystalline films which also reduces dye loading.[16] This is because of the competitive process between dye molecules and co-adsorbent on the restricted TiO_2 surface. The effect of CDCA as the co-adsorbent when co-sensitizing SQ1 and SQ2 which both absorb at the same wavelengths at 636nm has been investigated (Table 4.3). Device A was dyed with 1ml of a SQ1:SQ2 1:1 v/v mix (concentration of each dye was 0.34 mM) giving η 2.9 % with J_{sc} = 8.44 mA.cm^{-2} and V_{oc} = 0.59 v and FF = 0.58. All the dyes were desorbed by Bu_4NOH (200 µl, 40 mM) and the device was re-dyed with the same SQ1:SQ2 solution (Device B) giving η 2.9% which is similar to the first device performance.

To test the effect of CDCA on cell performance, Device C was pump dyed with SQ1:SQ2 in 5 mM CDCA giving η of 3% and J_{sc} = 9.35 mA.cm^{-2} which are slightly higher than the device without 5 mM CDCA. Reasons for this could be that the

CDCA, which has a carboxyl group as shown in Figure 4.8, may fill any unoccupied sites on the TiO_2 and reduce charge recombination and/or dye aggregation. Desorption of the dyes followed by re-dyeing with same mix SQ1:SQ2 in 5mM CDCA gave η 3% and the J_{sc} increased to 10.49 $mA.cm^{-2}$ suggesting that the TiO_2 after washing and being neutralized by dilute hydrochloric acid may have had more positively charged dye sites The results show that cell performance has been slightly improved for co-sensitization of SQ1 and SQ2 with CDCA solution.

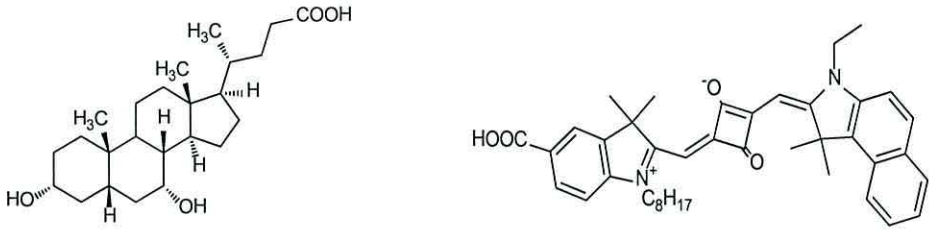

CDCA SQ2

Figure 4.8: Molecular structure of CDCA and SQ2 dye.

Table 4.3: I-V data of 1 of a DSL-18NRT Device (A) dyed with SQ1:SQ2 (1:1 0.34 mM) without CDCA, Device B dyed with mix SQ1:SQ2 without CDCA, Device C dyed with SQ1:SQ2 in 5 mM CDCA and Device D after desorption re-dyed with mix SQ1:SQ2 in 5 mM CDCA. (Approximate errors on devices are ± 10% of the values shown).

Device	η (%)	V_{oc} (V)	J_{sc} / $mA.cm^{-2}$	FF
A	2.9	0.59	8.44	0.58
B	2.9	0.57	9.16	0.56
C	3.0	0.57	9.35	0.57
D	3.0	0.57	10.49	0.49

4.3.5 Co-Sensitization by sequential dyeing

The previous experiment studied a mixed dye solution. In that case, the dye molecules probably diffuse between the TiO_2 particles and also in direct competition with each other. Here, sequential dyeing was studied to see if the order of dyeing is important. Figure 4.9 shows the I-V characteristics for the device dyed first with SQ1, then partially removed and then SQ2 added. The effect of ageing the device is also given Table 4.4. Device A was pump dyed with SQ1 (500 µl, 0.34 mM) in 10 mM CDCA giving η of 3.6%. SQ1 was then partially removed by Bu_4NOH (50 µl, 1 mM) Device B and the η dropped to 2.7% and J_{sc} decreased to 6.23 $mA.cm^{-2}$ because the dye loading was reduced. SQ2 (500 µl, 0.34 mM) was then added giving Device C and the η dropped to 2.2%. The reason may have been due to the aggregation of SQ2 with SQ1 because when dye was again partially removed by Bu_4NOH (50 µl, 1 mM) the η increased to 2.8% with slight increases in both of J_{sc} to 6.78 $mA.cm^{-2}$ and V_{oc} to 0.57v (Device D). The device was then sealed and measured with ageing. After six days the η reached to 3.1 % but after 40 days the η had dropped to 2.3% and J_{sc} decreased to 5.12$mA.cm^{-2}$ with consistent V_{oc} = 0.58v and FF = 70.

To see the effect of the order of dying another device was dyed with SQ2 and then SQ1 in the same manner as the previous experiment. Figure 4.10 shows the I-V characteristics for the device sequence dyed with SQ2, partially removed and then SQ1 added also the aged device (Table 4.5). Device A was pump dyed with SQ2 (500 µl, 0.34 mM) giving η of 2.4 % and parameters (J_{sc} = 6.59 $mA.cm^{-2}$, V_{oc} =0.55 and FF = 0.67). SQ2 was then partially removed with Bu_4NOH (50 µl, 1 mM), Device B, and the η increased to 2.7% with increasing both of J_{sc} to 7.49 $mA.cm^{-2}$ and V_{oc} to 0.57v possibly because of the aggregation of dye molecules was reduced by partial desorption. SQ1 (500 µl, 0.34 mM) in 10mM CDCA was then added (Device C) and the η increased to 3.4% and J_{sc} also increased to 9.28 $mA.cm^{-2}$. Although the cell performance improved η was still similar to the individual SQ1 device. However, after six days η had increased to 3.7% and J_{sc} = 9.45 $mA.cm^{-2}$ which is slightly higher than the individual dyes. The results from Table 4.4 and Table 4.5 might provide a conceptual basis for the design sequence dying for co-sensitization. Also, dye aggregation was found to be important. It was also found that this could be reduced by partial dye removal.

Table 4.4: I-V data of 0.9 cm^2 of a DSL-18NRT DSC dyed with SQ1 (500 µl, 0.34 mM) in 10 mM CDCA, partial removed by Bu_4NOH (50 µl, 1mM), SQ2 added (500 µl, 0.34 mM) in 10mM CDCA then partial removed by Bu_4NOH (50µl, 1mM). (Approximate errors on devices are ± 10% of the values shown).

Device	η (%)	V_{oc} (V)	J_{sc} /mAcm^{-2}	FF
A Dyed with SQ1	3.6	0.62	8.28	0.64
B Partial removed SQ1	2.7	0.59	6.23	0.66
C Re-dyed with SQ2	2.2	0.53	5.74	0.66
D Partial removal	2.8	0.57	6.78	0.65
The device after 1 day	3.0	0.59	7.02	0.66
The device after 2 days	3.2	0.58	7.72	0.65
The device after 3 days	3.2	0.59	7.44	0.66
The device after 6 days	3.1	0.58	7.28	0.67
The device after 40 days	2.3	0.58	5.15	0.70

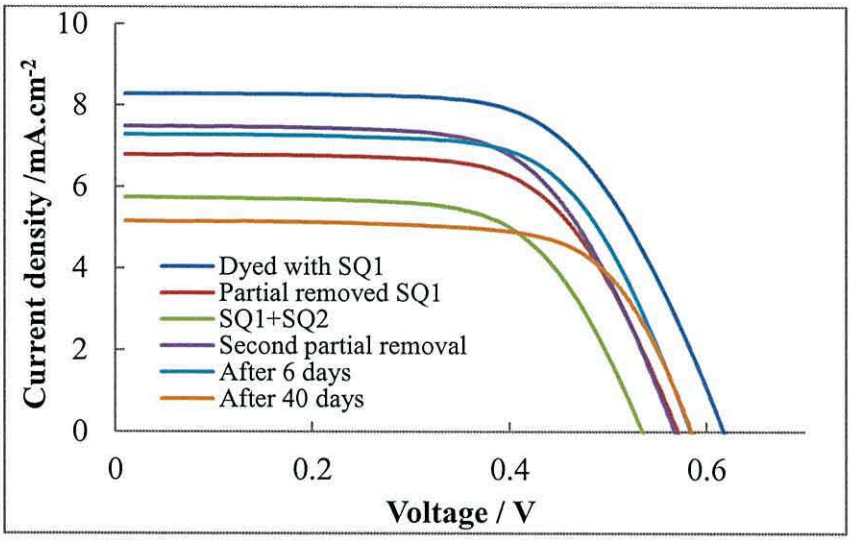

Figure 4.9: Photocurrent density-voltage characteristics for the sequential co-sensitization of SQ1 (500 µl, 0.34 mM) partial removal then after addition of SQ2 (500 µl, 0.34 mM) along with age of the device.

Table 4.5: I-V data of 1 cm^2 of a DSL-18NRT DSC dyed with SQ2 (500 µl, 0.34 mM) partial removed by Bu_4NOH (50 µl, 1mM), SQ1 added (500 µl, 0.34 mM) in 10 mM CDCA then partial removed by Bu_4NOH (50 µl, 1 mM). (Approximate errors on devices are ± 10% of the values shown).

Device	η (%)	V_{oc} (V)	J_{sc}/ $mA.cm^{-2}$	FF
E Dyed with SQ2	2.4	0.55	6.59	0.67
F Partial removal	2.7	0.57	7.49	0.64
G Re-dyed with SQ1	3.4	0.60	9.28	0.62
The device after 1 day	3.6	0.62	8.82	0.65
The device after 2 days	3.6	0.60	9.67	0.63
The device after 3 days	3.7	0.61	9.32	0.66
The device after 6 days	3.7	0.61	9.45	0.64
The device after 40 days	3.4	0.60	8.86	0.64

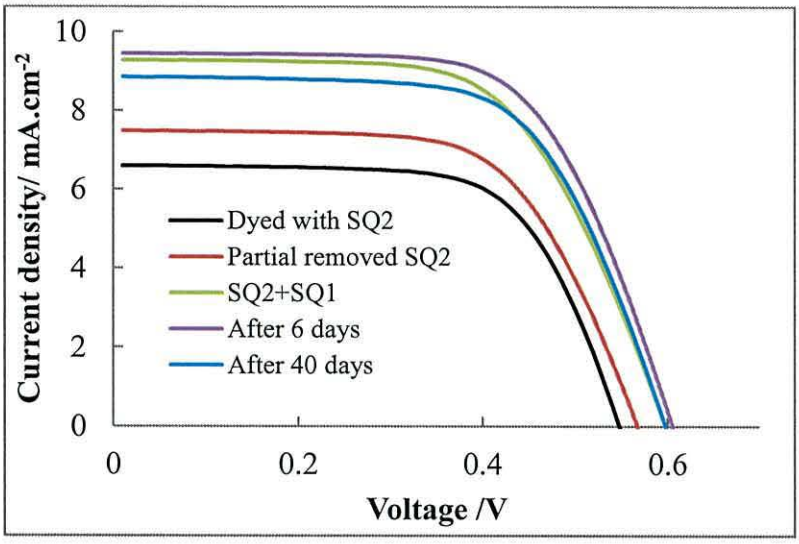

Figure 4.10: Photocurrent density-voltage characteristics for the sequential co-sensitization of SQ2 (500 µl, 0.34 mM), partial dye removal and then SQ1 addition (500 µl, 0.34 mM) along with ageing of the device.

4.3.6 Study of various additions of SQ1 for co-sensitizing SQ1with N719

Co-sensitization of two different dyes, Ru-bipy (N719) which absorbs in blue part of visible spectrum, and the organic dye (SQ1) which shows intense absorption in the red–NIR region to broaden the light absorption spectrum, have been studied. There is a big difference in the molar extinction coefficient of the dyes (14000 $M^{-1}.cm^{-1}$)[17] for N719 and (158500 $M^{-1}.cm^{-1}$)[18] for SQ1. Therefore the difference in the amount of adsorbed dye for co-sensitization is important. For this experiment, co-sensitization of N719 with SQ1 with different dye loadings of SQ1 was investigated and the I-V data are presented in Table 4.6. Device A was pump dyed with SQ1 (500 µl, 0.34 mM) in 10 mM CDCA giving η 3.5 %. SQ1was then partially removed by Bu_4NOH (50 µl, 1 mM) giving Device B. The η dropped to 2.3% and J_{sc} decreased to 6.71 $mA.cm^{-2}$ because the amount of adsorbed dye was reduced. The amount of partially desorbed SQ1 was measured as 9.5 $\mu g.cm^{-2}$ as shown by the UV-Vis spectra for the desorbed SQ1 by Bu_4NOH in Figure 4.11a. N719 (150 µl, 1 mM) was then added (Device C) and η increased slightly to 2.5% with a good FF = 0.75. However the J_{sc} was decreased to 5.31 $mA.cm^{-2}$which may be due to the adsorption behaviour of

N719 (it might be unable to form a monolayer on TiO_2 surface). Therefore N719 was selectively removed, as discussed in chapter three, using LiOH (50 µl, 100 mM) and the amount of desorbed N719 was measured to be 37.4 $\mu g.cm^{-2}$ as shown the UV-Vis spectra for N719 desorbed by LiOH solution (Figure 4.11b). The N719 (1 ml, 1 mM) was then added (Device D) and the co-sensitization of N719 with SQ1 led to an increase in η to 6.3 % with a big increase in J_{sc} 14.46 $mA.cm^{-2}$. Figure 4.12 shows the pictures of the device. Figure 4.12a shows that when SQ1 is added the device became dark blue. After the SQ1 was partially removed (Figure 4.12b) the device colour became faint blue the blue colour of the desorbed SQ1 can be seen in a vial in the same picture. After selective removal of 150 µl of N719 (Figure 4.12c) shows a blue colour device of SQ1 with a red colour of desorbed N719 in the vial. Finally, 1 ml of N719 was added which leads to a red N719 colour of the device (Figure 4.12d).

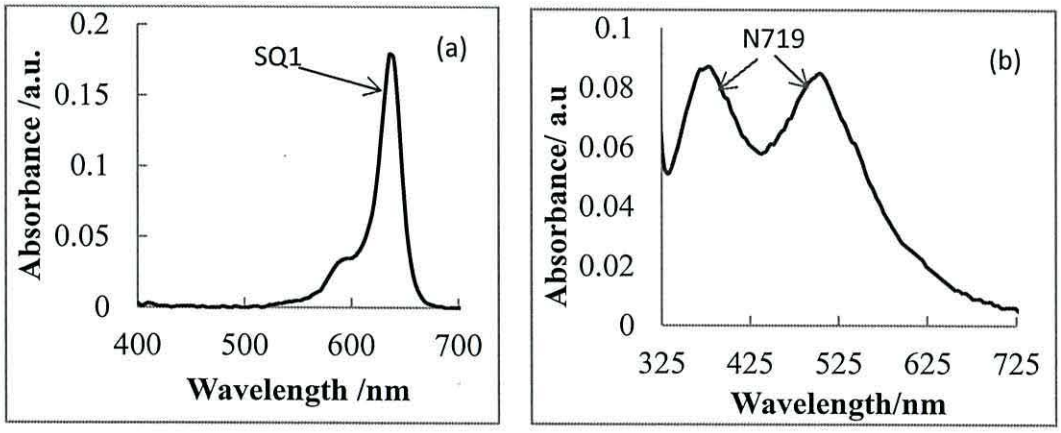

Figure 4.11: UV-Vis spectra for desorbed dyes (a) SQ1 partially desorbed by Bu_4NOH (50 µl, 1 mM) and (b) N719 desorbed by LiOH (50 µl, 100 mM).

Table 4.6: I-V data of 1 cm^2 device of DSL-18NRT dyed with SQ1 (500 µl, 0.34 mM). After partial SQ1 removed N719 was added then selectively removal and N719 re-added (1 ml, 1 mM). (Approximate errors on devices are ± 10% of the values shown).

	Device	η (%)	V_{oc} (V)	J_{sc}/mA.cm^{-2}	FF	Amount of desorbed dye /µg.cm^{-2}
A	Dyed with SQ1	3.5	0.61	8.78	0.65	
B	Partial removal by 1mM Bu_4NOH	2.3	0.56	6.71	0.61	9.5
C	After adding 150 µl N719	2.5	0.63	5.31	0.75	37.4
D	Re-dyed with N719	6.4	0.7	14.46	0.63	

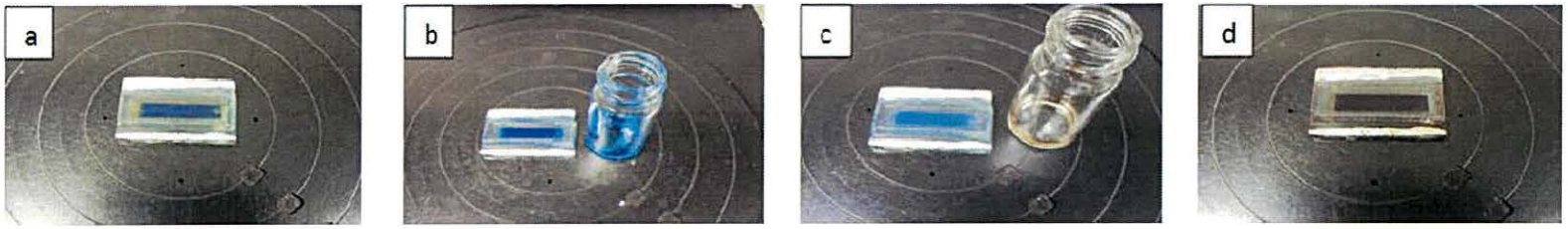

Figure 4.12: Photographs of the TiO_2 device (2 cm x 0.5 cm) showing (a) dyeing with SQ1 (b) after partial removal of SQ1 (c) after selective removal of N719 after 150µl N719 had been added along with a vial containing desorbed N719 and (d) adding 1ml of N719.

Figure 4.13 shows the external quantum efficiency (EQE) for co-sensitized TiO_2 with SQ1 and N719. The co-sensitized of SQ1+N719 device exhibited a broad response from 300 nm extending beyond 750 nm. Although the spectral response is rather low with a maximum EQE of 45% at 550 nm for N719 (I) there is a clear enhanced response from the device at 680 nm for the SQ1 (II).

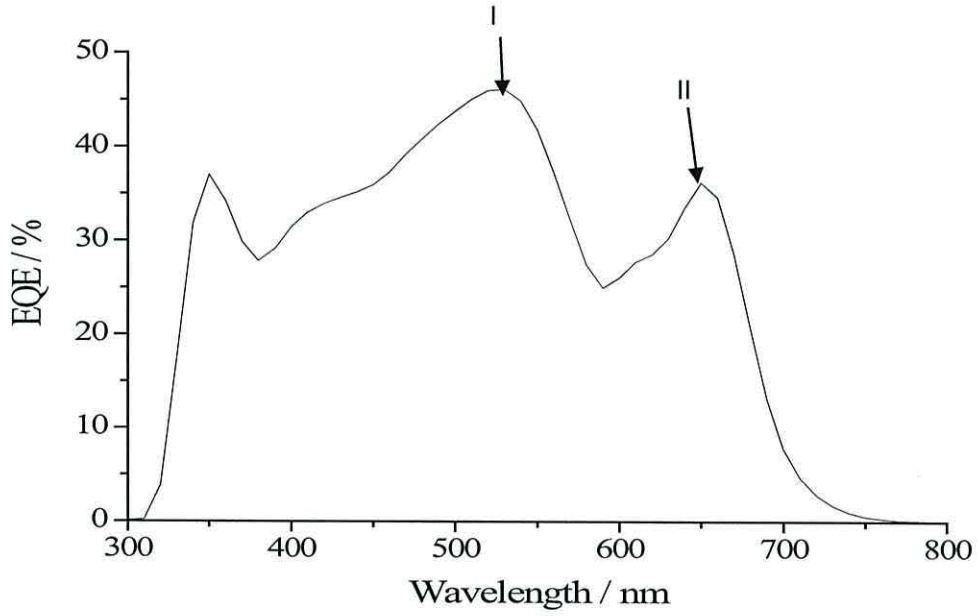

Figure 4.13: External quantum efficiency (EQE) *versus* wavelength, for Device D of sequential co-sensitization of SQ1 then N719.

The next experiment for co-sensitization was the stepwise dyeing of N719 in 10 mM CDCA and then SQ1 (Table 4.7). Device A was pump dyed with N719 (1 ml, 1 mM) giving η of 6.9%. N719 was then partially removed by Bu_4NOH (50 µl, 1 mM) giving Device B and η had dropped to 5.7%. It was assumed that this was because the N719 dye loading was reduced by partial removal which led decreased J_{sc} from 14.24 $mA.cm^{-2}$ to 12.29 $mA.cm^{-2}$. SQ1 (10 µl, 0.34 mM) in 10 mM CDCA was then added giving η 5.9% and J_{sc} increased to 14.59$mA.cm^{-2}$. The thinking here was that there are few available sites on TiO_2 for SQ1. However this small amount of SQ1 contributed to improved cell performance due to the high ε of SQ1. After selective

removal of N719 using LiOH (100 µl, 100 mM), Device D, η had dropped to 1.2% which was believed to be due only to adsorbed SQ1. Again the device was co-sensitized by adding N719 (1 ml, 1 mM) Device E giving η 7.0 % giving the highest J_{sc} (16.30 mA.cm^{-2}) suggesting that the titania film is sufficiently covered with N719 and suggesting that the order and method of co-sensitization is important. The process is illustrated by photographs as shown in Figure 4.14. This shows the device, when dyed with N719 (Figure 4.14a), appears red. When SQ1 was added (Figure 4.14b) the device colour became dark purple in line with co-adsorbed N719 and SQ1 on the TiO_2 surface. Thereafter, N719 was selectively removed (Figure 4.14c) showing a blue colour on the device indicating SQ1 remaining on the titania film along with a red solution for desorbed N719 in the vial. After adding 1 ml of N719 (Figure 4.14d) the SQ1 colour becomes no longer visible to the eye due to the N719 molecules. Therefore the device shows a red colour.

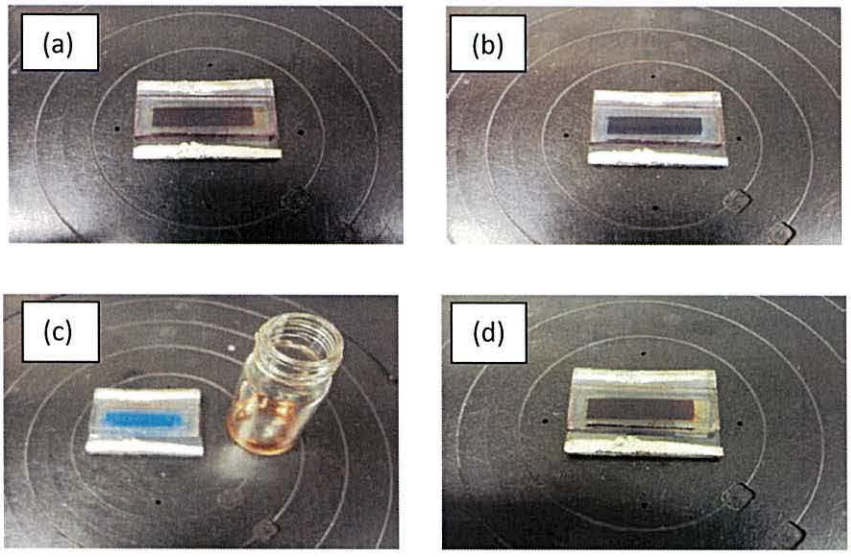

Figure 4.14: Photographs of the TiO_2 device (2 x 0.5 cm) showing (a) dyeing with N719 (1 ml, 1 mM) (b) after partial removal of N719 and addition of SQ1 (10 µl, 0.34 mM) in 10 mM CDCA (c) Selective removal of N719 by LiOH (100 µl, 100 mM) (d) re-dyeing with N719 (1 ml, 1 mM).

Figure 4.15 show the external quantum efficiency (EQE) for the co-sensitization N719 with small amount of SQ1 (Device E in Table 4.7). The data shows a step wise co-sensitization of N719 with 10 µl SQ1 device exhibits a broad response from 300 nm extending to 750 nm. Although the EQE_{max} for SQ1 is 35% at 650 nm (I) and for N719 is 45 % at 550 nm (II).

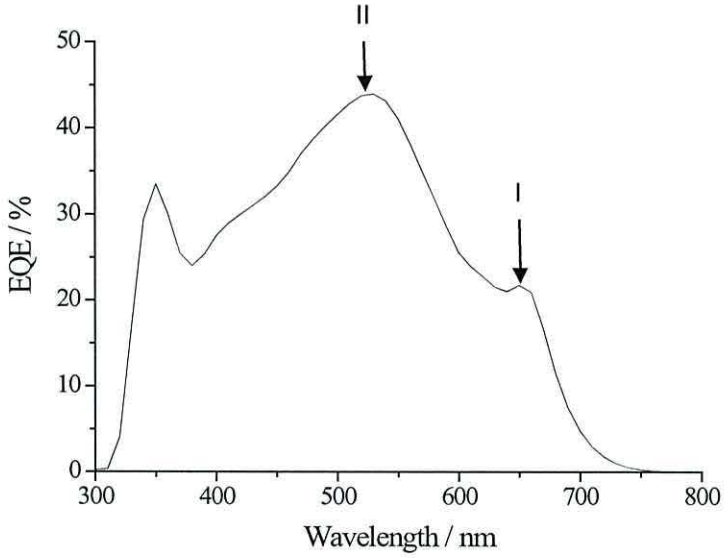

Figure 4.15: External quantum efficiency (EQE) *versus* wavelength for the Device E in Table 4.7 for a stepwise co-sensitization of N719 (1 ml, 1 mM) and then SQ1 (10 µl, 0.34 mM) in 10 mM CDCA ultra-fast dyed.

Table 4.7: I-V data of a 1 cm^2 device of DSL-18NRT dyed with N719 (1 ml, 1 mM), after partial removal of N719 then SQ1 (10 µl, 0.34 mM) was added, then after selective removal of N719, re-dyed with N719. (Approximate errors on devices are ± 10% of the values shown).

Device	η (%)	V_{oc} (V)	J_{sc} / $mA.cm^{-2}$	FF
A Dyed with N719	6.9	0.72	14.24	0.67
B Partial N719 removal	5.7	0.69	12.29	0.67
C 10 µl SQ1 added	5.9	0.67	14.59	0.61
D Selective N719 removal	1.2	0.72	2.33	0.71
E Re-dyed with N719	7.0	0.72	16.30	0.60

4.3.7 Co-sensitization with 6% SQ1: N719

The previous experiments studied the addition of different volumes of SQ1 for the co-sensitization of SQ1 with N719 and also the order in which dye was added. This experiment studied the mix of 6% SQ1:N719 by mixing volume ratio 1:4 from the stock solutions of 0.86 mM and 1.5mM for SQ1 and N719. The real concentration ratio of SQ1:N719 was calculated from the UV-Vis spectra of the mixed dye solution as shown in Figure 4.16a giving 6 % SQ1:N719. A smaller amount of SQ1 was used because it has a higher molar extinction coefficient than N719 and to balance the number of sorption sites to yield a complementary absorption spectrum.[19] To test this Device A was dyed with a mixed solution of 6% SQ1:N719 the I^-_3/I^- redox electrolyte was added giving η 7.2% and J_{sc} 15.99 mA.cm^{-2} with enhanced V_{oc} of 0.74V as compared to Device C in the previous experiment which was co-sensitized with SQ1 and N719 in a step wise manner. All the dyes were then desorbed by Bu_4NOH (200 µl, 40 mM). The UV-Vis spectrum was measured for the desorbed dye solution (as shown Figure 4.16b) which shows a peak at 636 nm due to SQ1 and two peaks at 512 nm and 370nm due to N719. The amount of each dye was measured to be 3.5 µg.cm^{-2} for SQ1 and 255 µg.cm^{-2} for N719. The device was then re-dyed the same solution of mix 6% SQ1:N719 (Device B) giving η of 7.0 % with slightly increased J_{sc} to 16.6 mA.cm^{-2}. After one day, the device was re-measured and gave η 7.1% showing a similar performance.

Table 4.8: I-V data of DSC device co-sensitizing with mix 6% SQ1:N719. (Approximate errors on devices are ± 10% of the values shown).

Device	η (%)	Voc (V)	Jsc / mA.cm^{-2}	FF
A Dyed with 6% SQ1:N719	7.2	0.74	15.99	0.60
B Re-dyed with 6% SQ1:N719	7.0	0.72	16.60	0.59
C Device after one day	7.1	0.73	15.61	0.63

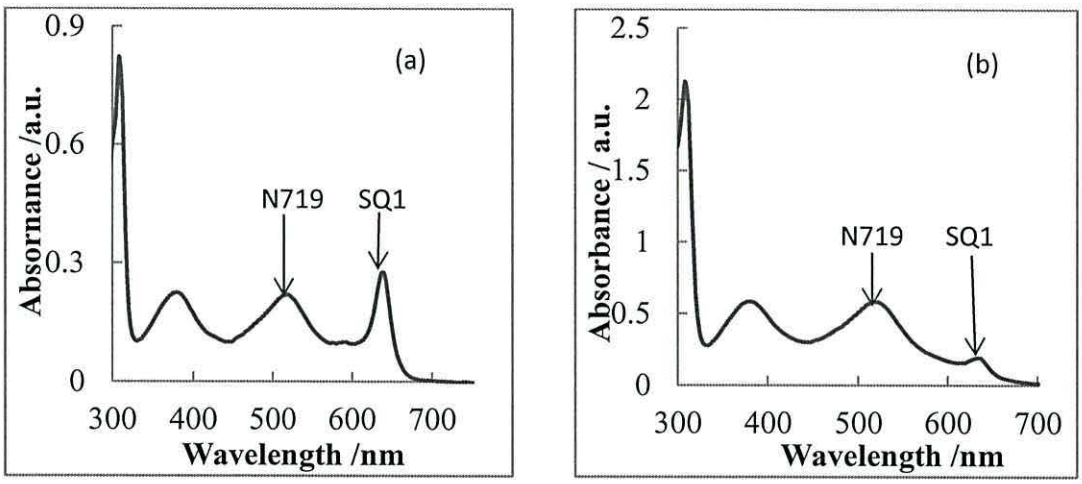

Figure 4.16: UV-Vis Spectra of (a) a mix of 6% (SQ1:N719) (0.86 mM:1.5 mM) before adsorption (b) mixed (SQ1:N719) solution after desorption from the device by Bu_4NOH solution

Figure 4.17 shows the external quantum efficiency (EQE) measurement for a device dyed with 6% SQ1:N719. The EQE at 680 nm is 13% for SQ1 (I) showing extended light harvesting from N719 alone (II) at 550 nm is 45%. The EQE generated at < 400 nm is due to light absorption by titania.

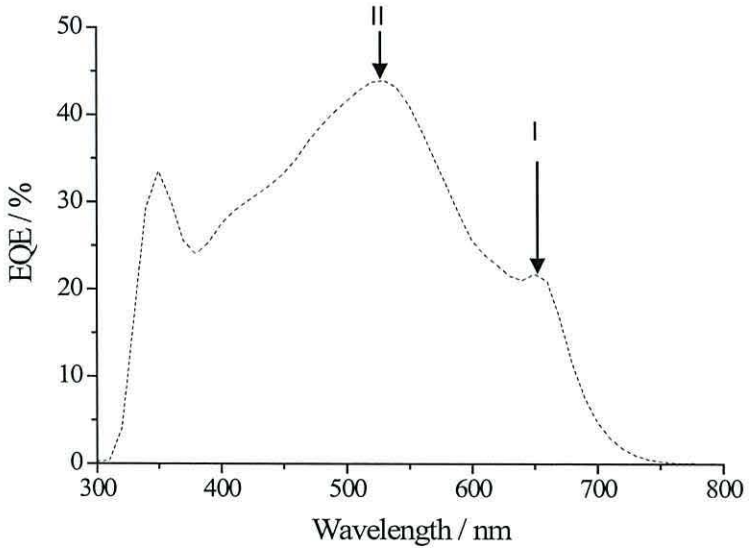

Figure 4.17: External quantum efficiency (EQE) *versus* wavelength for a device co-sensitized with 6 % SQ1: N719.

4.3.8 Co-sensitization of YD with N719

The previous experiment studied the co-sensitization of the metal complex N719 which has a maximum absorption at 532 nm with the organic dye SQ1 which shows absorption in the infrared region at 636 nm. This experiment studied the co-sensitization for N719 with a new yellow triphenylamine dye (YD) which has molar extinction coefficient 32300 $M^{-1}cm^{-1}$ and absorbs in the blue part of the visible spectrum at 384 nm as shown the UV-Vis spectra in Figure 4.18. The molecular structure of YD named 4-[2-(4-diphenylaminophenyl) vinyl] benzoic acid] is shown in Figure 4.19

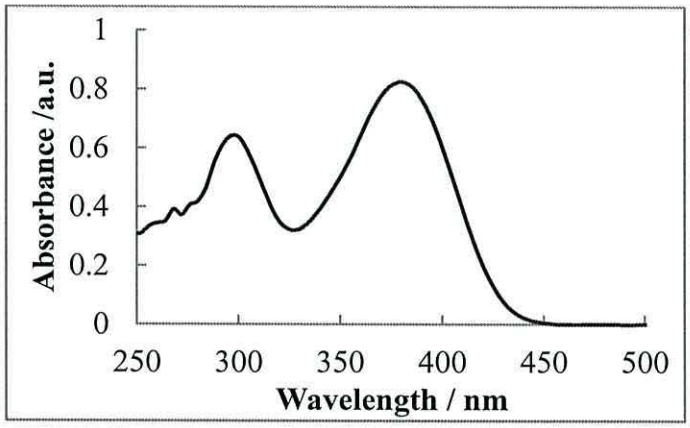

Figure 4.18: UV-Vis spectra for (0.25 mM) YD in ethanol.

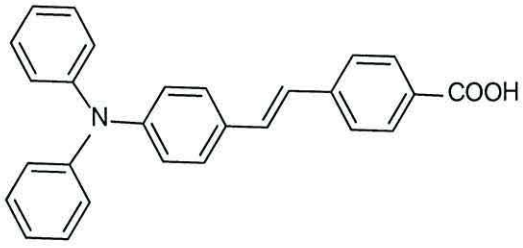

Figure 4.19: Molecular structure of 4-[2-(4-diphenylaminophenyl) vinyl] benzoic acid] YD.

The molar extinction coefficient of YD at the maximum absorption of 384 nm is 32000 $M^{-1}cm^{-1}$ which is believed to correspond to a π—π^* transition of the conjugated molecule. For the study, at first the device was ultra-fast dyed with YD (1.5 ml, 2.5 mM) in 5 mM CDCA followed by N719 (1 ml, 1 mM). The I-V curves

are shown in Figure 4.20 and the corresponding photovoltaic parameters are included in Table 4.10. Device A was pump dyed with YD (1.5 ml, 2.5 mM) in 5 mM CDCA to form a layer of YD chemisorbed on TiO_2 (Figure 4.21a) giving η 2.7%. This was followed by adding N719 (1 ml, 1 mM), Device B, and the device colour appeared dark red-green as shown in Figure 4.21b. The device was then measured and giving η of 6.7% with increased V_{oc} and J_{sc} of 0.76 V and 13.46 $mA.cm^{-2}$ respectively in line with the addition of N719 dye. Importantly, the co-sensitized solar cell shows a greater J_{sc} with higher η after one day (Device D) giving η 7.5% with a big increased in J_{sc} 15.06 to $mA.cm^{-2}$. These results show a superior performance for the co-sensitization of YD with N719 compared with that of individual YD or N719 dyed DSC devices. The amount of adsorbed dyes has been calculated. First, N719 was selective removal using LiOH (100 µl, 100 mM) then YD was desorbed using Bu_4NOH (100 µl, 40 mM). The UV-Vis spectra of the desorbed dyes solutions corresponding to separate dyes are shown in Figure 4.22. The amounts of desorbed dyes were then measured using molar extinction coefficient for each dye giving 57.3 $\mu g.cm^{-2}$ for YD and 216 $\mu g.cm^{-2}$ for N719.

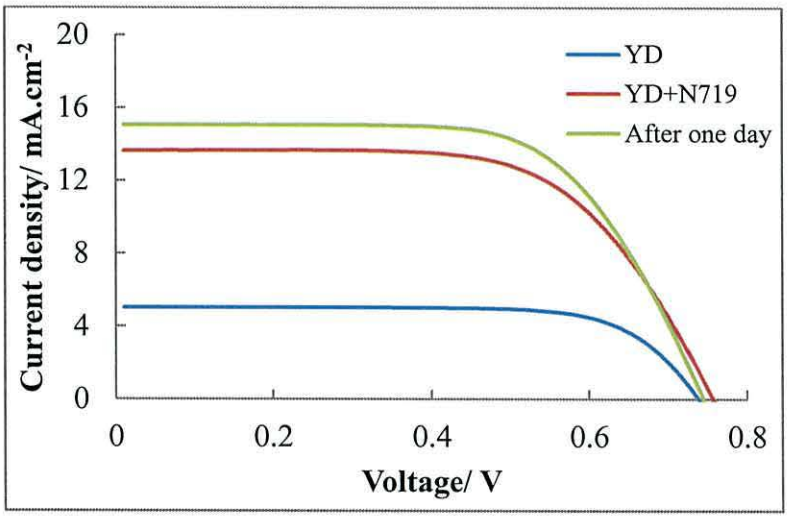

Figure 4.20: I-V curves under AM 1.5 full sunlight with a white background for sequence dyeing of co-sensitization YD (1.5 ml, 2.5 mM) in 5 mM CDCA with N719 (1 ml, 1 mM).

Table 4.10: I-V data of order dyeing in co-sensitizing TiO_2 with YD (1.5 ml, 2.5 mM) in 5 mM CDCA, followed by adding N719 (1 ml, 1 mM). (Approximate errors on devices are ± 10% of the values shown).

Device	η (%)	V_{oc} (V)	J_{sc} / mA.cm^{-2}	FF	Dye loadings μg.cm^{-2}
A Dyed with YD	2.7	0.70	5.42	0.71	57.3
B Added 1 ml N719	6.7	0.76	13.4	0.64	216
C Device after one day	7.5	0.74	15.06	0.65	

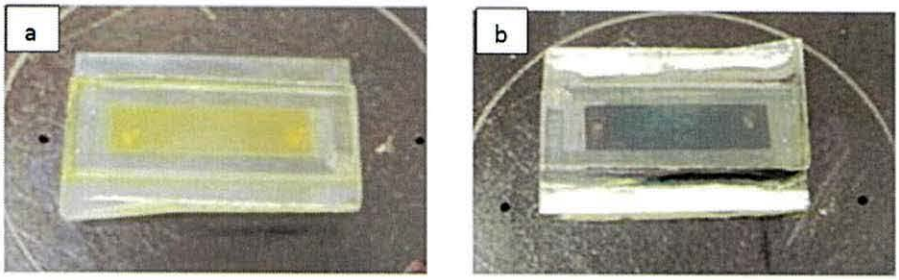

Figure 4.21: Photographs of TiO_2 device (2 x 0.5cm) showing (a) dyed with yellow dye (1.5 ml, 2.5 mM) (b) after adding 1 ml of N719 (1 ml, 1 mM) to the YD device.

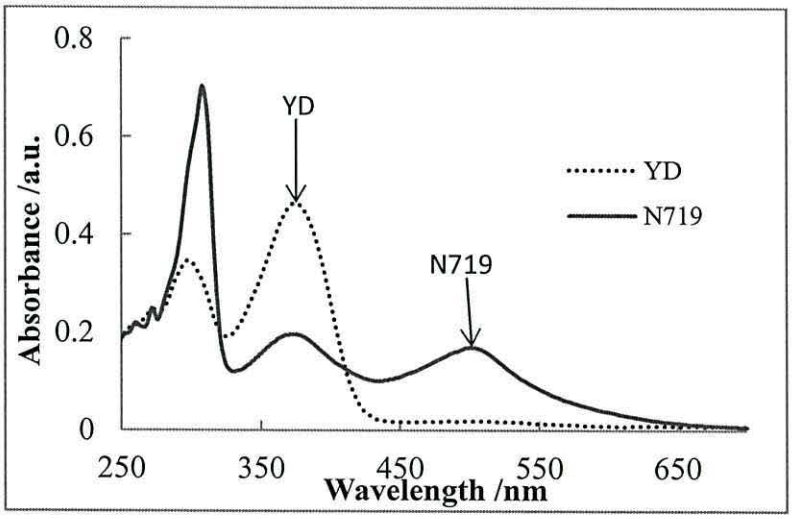

Figure 4.22: UV-Vis Spectra of desorbed (solid line) N719 by 100 mM LiOH and (dotted line) YD desorbed by 40 mM Bu_4NOH from Device C.

The next experiment studied the sequential dyeing of N719 and then YD to test the effect of the order of dyeing on the photovoltaic performance. The I-V curves of the device dyed with N719 then co-sensitized with N719 plus YD and the same device after one day are shown in Figure 4.23 and the corresponding photovoltaic parameters are in Table 4.11. Here Device A was pump dyed with N719 (1 ml, 1 mM) giving η 6.4%, but the device performance improved when YD (1.5 ml, 2.5 mM) in 5 mM CDCA was added Device B giving η 7.2% with J_{sc} increased to 15.63 $mA.cm^{-2}$. The device was then left in a dark place until the next day and re-measured (Device C). The η dropped to 6.7% but was still higher than N719 or YD dyed individually. N719 was then desorbed by LiOH (100 µl, 100 mM) and the YD was desorbed by Bu_4NOH (100 µl, 40 mM). The absorbance of each desorbed solution was measured as shown the UV-Vis spectra in Figure 4.24. The amounts of desorbed dyes solutions were calculated to be 206 $\mu g.cm^{-2}$ for N719 and 27 $\mu g.cm^{-2}$ for YD. In this case, the smaller amount of adsorbed YD which may explain the slightly lower efficiency of 6.7%.

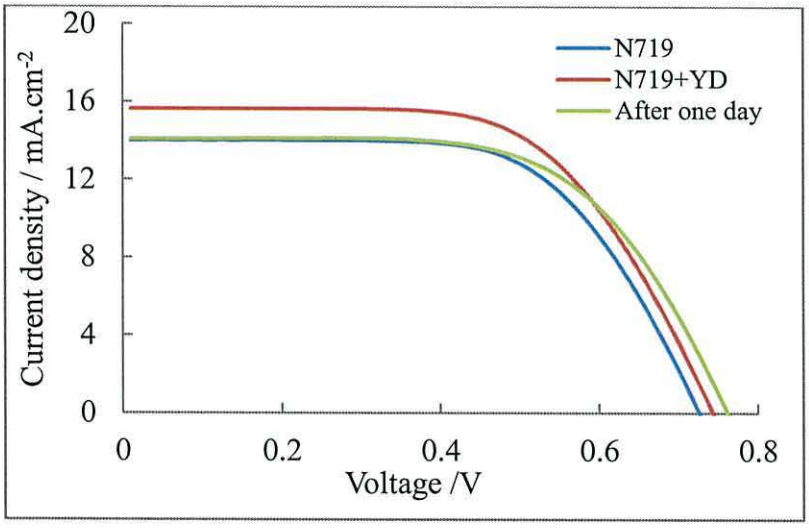

Figure 4.23: I-V curves under AM 1.5 for sequential dyeing of N719 (1ml, 1mM) with YD (1.5ml, 2.5mM) in 5mM CDCA.

Table 4.11: I-V data of order dyeing in co-sensitizing TiO_2 with N719 (1 ml, 1 mM), followed by adding (1.5 ml, 2.5 mM) in 5 mM CDCA. (Approximate errors on devices are ± 10% of the values shown).

Device	η (%)	V_{oc} (V)	J_{sc} / mA.cm^{-2}	FF	Dye loadings μg.cm^{-2}
A Dyed with N719	6.4	0.73	14.00	0.63	206
B Added 1 ml of YD	7.2	0.74	15.63	0.62	27
C Device after one day	6.7	0.76	14.08	0.63	

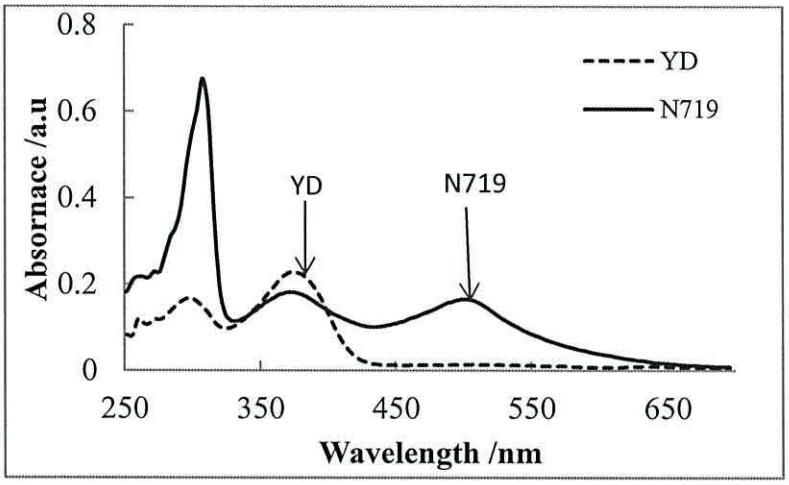

Figure 4.24: UV-Vis spectra of desorbed (solid line) N719 by 100 mM LiOH and (dotted line) YD by 40 mM Bu_4NOH from Device C.

4.3.9 Co-sensitization of SQ1 and YD

The previous experiments studied the co-sensitization and the effect of order of dyeing on the performance of YD with the metal complex N719. This experiment studied co-sensitization of the organic dyes; YD with SQ1. Table 4.12 shows the I-V data for the device co-sensitized with SQ1 and YD. The device was pump dyed with SQ1 (500 μl, 0.25 mM) in 5 mM CDCA giving blue colour for SQ1 molecules on the TiO_2 film (Figure4.25a). YD (1 ml, 2.5 mM) in 5 mM CDCA was added and the device changed colour to green as shown in (Figure 4.25b) giving η = 4%. Importantly, the co-sensitized device shows enhanced photovoltaic performance

relative to either of the single-dye systems (η = 3.5% for SQ1 and η 2.7% for YD). The dyes were then desorbed using Bu_4NOH (200 µl, 40 mM). The absorbance of the desorbed dye solutions was measured as shown in the UV-Vis Spectra in Figure 4.26. The amounts of desorbed dye were measured which was to be 13 $\mu g.cm^{-2}$ for SQ1 at 636 nm and 129 $\mu g.cm^{-2}$ for YD.

Table 4.12: I-V data of TiO_2 device sensitized with SQ1 (500 µl, 0.25 mM) in 5 mM CDCA followed by adding YD (1 ml, 2.5 mM) in 5 mM CDCA. (Approximate errors on devices are ± 10% of the values shown).

Device	η (%)	V_{oc} (V)	J_{sc} / $mA.cm^{-2}$	FF	SQ1 loading/ $\mu g.cm^{-2}$	YD loading/ $\mu g.cm^{-2}$
Dyed with SQ1	3.5	0.61	8.78	0.65		
Dyed with YD	2.7	0.70	5.45	0.71		
Dyed with SQ1 and YD	4.0	0.71	8.35	0.65	13	129

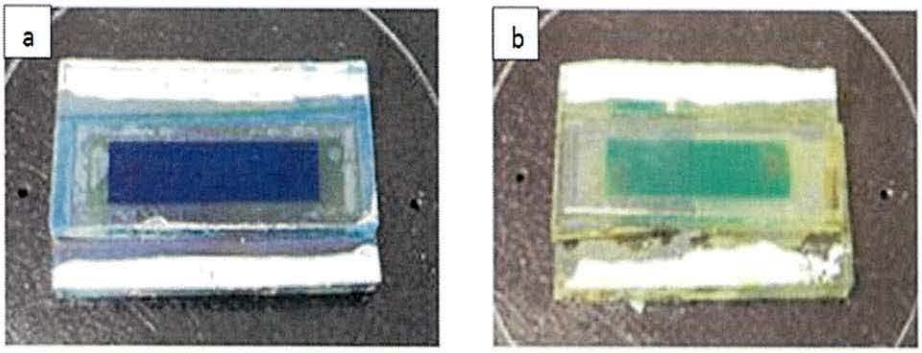

Figure 4.25: Photographs of TiO_2 device (2 x 0.5cm) showing (a) dyed with SQ1 (b) dyed with SQ1 and YD.

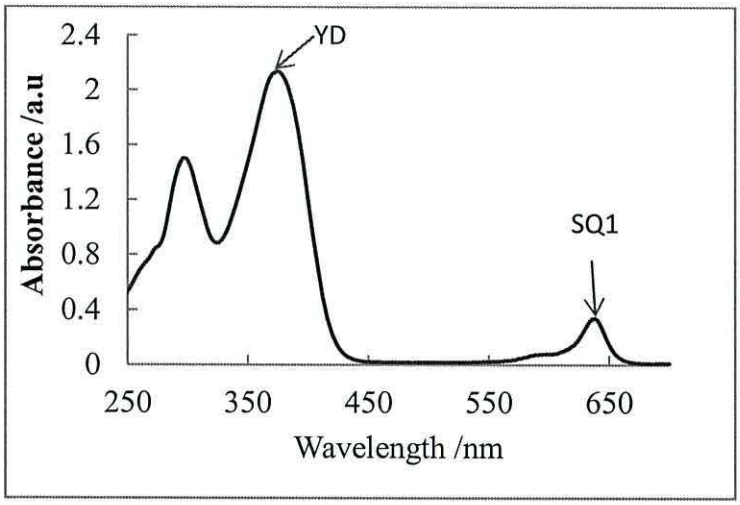

Figure 4.26: UV-Vis spectra of desorbed dye solutions a co-sensitized device of SQ1+YD desorbed by Bu_4NOH (200 µl, 40 mM).

4.3.10 Co-sensitized YD with D149

To try to enhance the device performance through ultra-fast co-sensitization, a combination of YD that absorbs at 385 nm was studied with the indoline dye (D149) which absorbs at 528 nm. To study this, a device was first dyed with each single dye and then co-sensitized by stepwise dyeing. The I-V curves are shown in Figure 4.27 and the corresponding photovoltaic parameters are included in Table 4.13. Device A was pump dyed with single dye D149 (1.5 ml, 0.5 mM) giving η 6.1%. The other device was dyed with YD (1 ml, 2.5 mM) in 10 mM CDCA, Device B, giving η 2.8% and the parameters (J_{sc} = 4.33 mA.cm^{-2}, V_{oc} =0.53V and FF = 0.60). After the electrolyte was removed by pumping 100 µl ethanol through a device cavity D149 (1 ml, 0.5 mM) was added giving Device C and the device performance improved (η = 6.7%, J_{sc}= 18.75 mA.cm^{-2}, V_{oc} = 0.63 and FF = 0.57) which is higher than either single dye.

Table 4.13: Detailed photovoltaic parameters of the devices based on individual D149 (1.5 ml, 0.5 mM), individual YD (1 ml, 2.5 mM) in 10 mM CDCA and co-sensitization with YD+D149. (Approximate errors on devices are ± 10% of the values shown).

Device	η (%)	V_{oc} (V)	J_{sc} / mA.cm^{-2}	FF
A Dyed with D149	6.1	0.64	17.69	0.54
B Dyed with YD	2.8	0.53	8.73	0.60
C D149 added	6.7	0.63	18.75	0.57
D After one day	6.8	0.64	18.23	0.58
E After five days	6.8	0.64	19.32	0.55

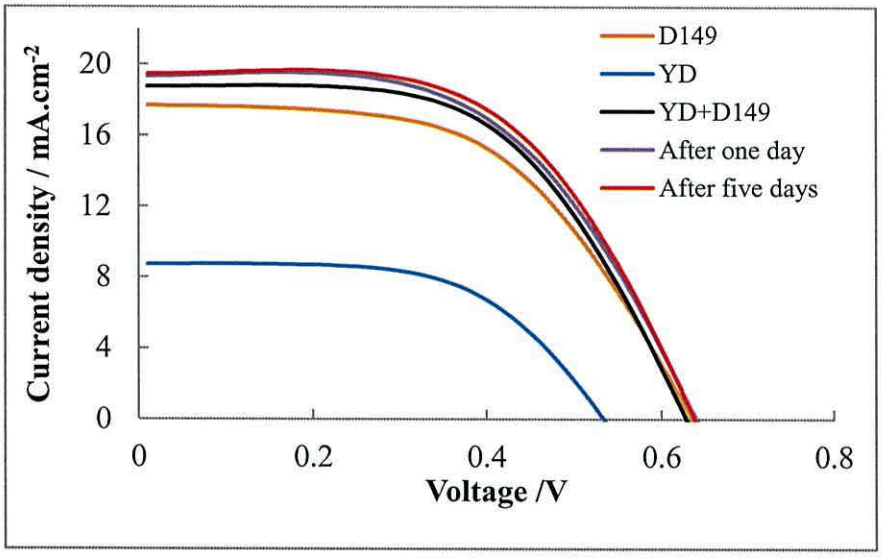

Figure 4.27: I-V curve of the devices dyed with individual dyes D149 (1.5 ml, 0.5 mM) and YD (1 ml, 2.5 mM) and also co-sensitized with YD+D149.

4.3.11 Co-sensitization N719 with varying ratios of D149

The next series of experiments aimed to study the effect of molar ratio on the co-sensitization of two dyes (N719 and D149) which absorb at similar wavelengths. These experiments studied the new approaches of selective removal for co-sensitization and step wise adsorption using mixed dye solutions in certain molar ratios.

4.3.11.1 Co-sensitization of N719: D149 (10:1)

Table 4.14 shows I-V data for a device after partial N719 removal and co-sensitized with small amount of D149, and the I-V curves are shown in Figure 4.28. Device A was pump dyed with N719 (1ml, 1mM) giving η 6%. The N719 was then partially removed by Bu_4NOH (50 µl, 1 mM) and η dropped to 5.5%. This process freed some sites to adsorb other dye molecules. D149 (100 µl, 0.5 mM) was then added giving Device C. The η slightly dropped to 5%. However, the J_{sc} increased to 13.73 $mA.cm^{-2}$. The efficiency dropped because the V_{oc} reduced from 0.73 V to 0.57 V. This was in line with D149 addition because D149 has a lower V_{oc} compared to N719.[20, 21] N719 was then selectively removed by LiOH (100 µl, 100 mM) giving Device D leaving just adsorbed D149 molecules giving η 3.2% and J_{sc} 9.1 $mA.cm^{-2}$ from the addition of D149 (100 µl, 0.5 mM). N719 (1 ml, 1 mM) was then added giving Device E which showed significant enhancement in the performance to give η 6.5%. The improved performance of the co-sensitized cell with D149+N719 is attributed to the combined enhancement in J_{sc} to 13.05 $mA.cm^{-2}$, V_{oc} to 0.74V and FF to 0.61.

Table 4.14: Detailed photovoltaic parameters of the devices based on individual N719 (1 ml, 1 mM), partial removed, then added D149 (100 µl, 0.5 mM) in 10 mM CDCA and after selective removal of N719 re-dyed with N719 (1 ml, 1 mM). (Approximate errors on devices are ± 10% of the values shown).

Device	η (%)	V_{oc} (V)	J_{sc} /$mA.cm^{-2}$	FF
A Dyed with N719	6.0	0.77	12.46	0.58
B Partially removed N719	5.5	0.73	11.43	0.60
C D149 100 µl added	5.0	0.57	13.73	0.58
D Selective removal of N719	3.2	0.58	9.10	0.55
E Re-dyed with N719	6.5	0.74	13.05	0.61

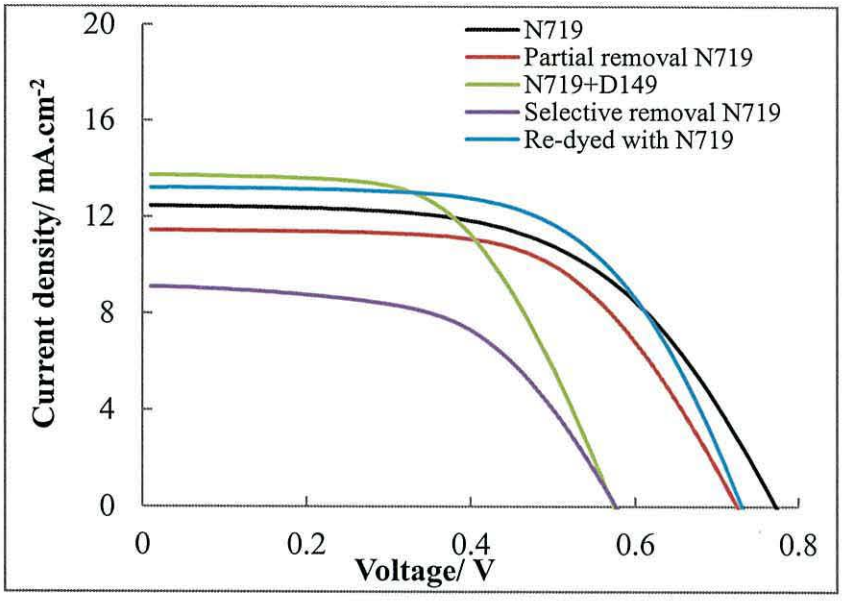

Figure 4.28: I-V data of DSC devices sensitized with N719, after partial removal of N719, after 100 µl D149 added, then selective removal of N719, and re-dyed with N719.

Figure 4.29 show the external quantum efficiency (EQE) measurement for a Device E which is dyed with a 10:1 v/v of a mixed N719:D149. The EQE_{max} is 10% at 650 nm (I) due to a small amount of D149 used, and the EQE max >35% at 550 for N719 (II). The EQE peak is in line with N719 alone that is mean the J_{sc} not affected by the small amount of D149.

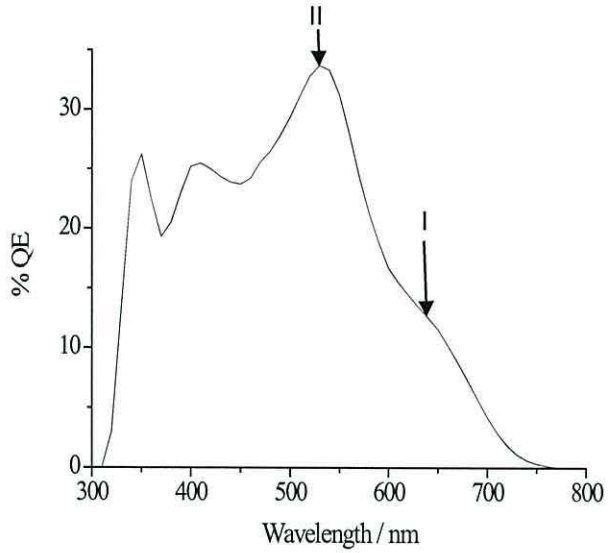

Figure 4.29: External quantum efficiency (EQE) *versus* wavelength of a device co-sensitized with a mix of N719:D149 by (volume ratio 10:1) from a stock solution 1 mM N719 and 0.5 mM D149 from device E.

4.3.11.2 Co-Sensitization N719:D149 (1:1)

A mixed of dye solution with a 1:1 volume ratio of D149 (1 ml, 0.5 mM) in 10mM CDCA and N719 (1 ml, 1 mM) was then studied (Table 4.15). Device A was dyed with N719:D149 (volume ratio 1:1) in 10 mM CDCA giving η 7.2%. To quantify the dye loading on the TiO_2 surface, N719 was desorbed by LiOH (100 ml, 100 mM). Then D149 was desorbed by Bu_4NOH (200 µl,40 mM) followed by acetone and ethanol. The amount of each desorbed dye was calculated to be 84 $\mu g.cm^{-2}$ for N719 and 52 $\mu g.cm^{-2}$ for D149. After the device rinsing, the device was re-dyed with the same mix N719:D149 (1:1), Device B, giving η 6.8% slightly lower than first dying due to lower J_{sc} which might suggest that the TiO_2 surface was not completely saturated.

Table 4.15: Detailed photovoltaic parameters of the device based co-sensitization with a mix of N179 (1ml, 1mM) with D149 (1ml, 0.5mM) in 10mM CDCA and after total dyes removed re-dyed with the same mix solution of N719:D149 (1:1). (Approximate errors on devices are ± 10% of the values shown).

Device	η (%)	V_{oc} (V)	J_{sc} /mA.c m^{-2}	FF
A Dyed with mix N710:D47	7.2	0.71	16.42	0.59
B Re-dyed with mix of N71:D149	6.8	0.71	15.30	0.60

Figure 4.30 show the external quantum efficiency (EQE) measurement for a Device B which was dyed with a 1:1 v/v of a mixed N719:D149. The device show broad response from 300 nm extending beyond 700 nm. The EQE is > 20 % at 650 nm which is higher than the device in the previous experiment due to more D149 is loading. Although the spectral response is rather low with a maximum EQE of 45 % at 550 nm for N719.

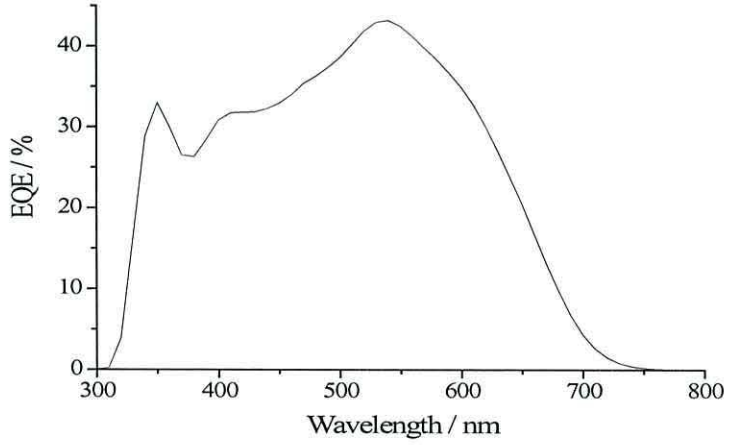

Figure 4.30: External quantum efficiency (EQE) *versus* wavelength for co-sensitized (N719+D149) (1:1) for the device B.

4.4.11.3 Co-sensitization N719:D149 (1:2)

Following the earlier experiments showing the photocurrent density of the device was increased by increasing the proportion of D149 dye in the dyeing solution. The next experiment doubled the N719:D149 ratio to 1:2 (Figure 4.31). The

corresponding photovoltaic parameters are included in Table 4.16. Device A was pump dyed with a 1:2 mixture of N719 (1 ml, 1 mM) and D149 (2 ml, 0.5 mM) in 10 mM CDCA. The device performance was η = 8.1% (J_{sc} = 18.31 mA.cm^{-2}, V_{oc} = 0.71 V and FF = 0.62). The N719 was then selectively removal by LiOH (100 µl, 100 mM), Device B, and the η dropped to 5.6% and both V_{oc} and J_{sc} also decreased to 0.66 V and 13.57 mA.cm^{-2}, respectively presumably in line with only D149 remaining adsorbed on the TiO_2 surface. The amount of desorbed N719 was calculated to be 65 µg. cm^{-2}. The device then re-dyed with the same mix solution of N719:D149 (volume ratio 1:2) Device C giving η 8% which is the similar performance of the first co-sensitization.

Table 4.16: Detailed photovoltaic parameters of the device based co-sensitization with a mix of N179 (1 ml, 1mM) with D149 (2 ml, 0.5 mM) in 10 mM CDCA and after selective removal of N719, re-dyed with the same mix solution of N719:D149 (1:2). (Approximate errors on devices are ± 10% of the values shown).

Device	η (%)	V_{oc} (V)	J_{sc} / mA.cm^{-2}	FF
A Dyed with 1:2 mix N719:D149	8.1	0.71	18.31	0.62
B Selective removal N719	5.6	0.66	13.57	0.63
C Re-dyed with mix N719:D149	8.0	0.71	18.32	0.61

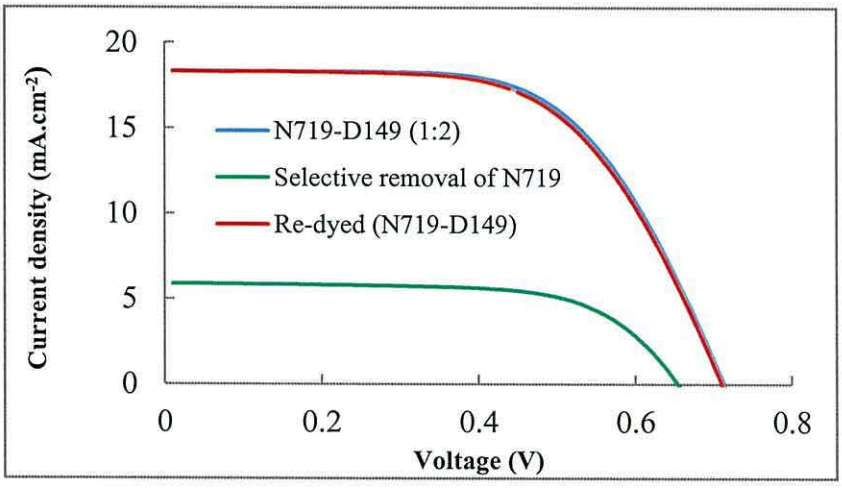

Figure 4.31: Photocurrent density-photo voltage curve of co-sensitized a mix 1:2 (N719:D149) under AM 1.5 G radiation.

4.3.11.4 Co-Sensitization N719:D149 (1:3)

The next experiment used a 1:3 v/v mixture of N719:D149. The I-V data are in Figure 4.32 and the corresponding photovoltaic parameters are included in Table 4.17. Device A was pump dyed with 1ml of a 1:3 v/v mixture of N719 (1 ml, 1 mM) and D149 (3 ml, 0.5 mM) in 10 mM CDCA giving η 7.5%. N719 was then selectively removed by LiOH (100 µl, 100 mM) (Device B) and the efficiency dropped to 4.7% in line with only D149 remaining adsorbed. The amount of desorbed N719 was to be 57 $\mu g.cm^{-2}$ which is less than the amount of N719 desorbed in previous experiment for using volume ratio 1:2 N719:D149 which is expected because the initial dyeing solution contained less N719. However, the η and J_{sc} of Device B were lower than for the 1:2 device after selective removal of N719 even through, in theory, there may be more D149 molecules still adsorbed. When the device was re-dyed with the same dye solution, Device C, the device performance improved to yield η = 8.2% (J_{sc} = 16.58 $mA.cm^{-2}$, V_{oc} = 0.71 V and FF = 0.63)

Table 4.17: I-V data for TiO_2 device after co-sensitization with a 1:3 v/v mixture of N179 (1 ml, 1 mM) with D149 (3 ml, 0.5 mM) in 10 mM CDCA then after selective removal of N719, and re-dyeing with the same mixed solution of N719:D149 (1:3) (Approximate errors on devices are ± 10% of the values shown).

Device	η (%)	V_{oc} (V)	J_{sc} / $mA.cm^{-2}$	FF
A Dyed with 1:3 mix N719:D149	7.5	0.70	15.81	0.61
B Selective removal N719	4.7	0.66	10.67	0.60
C Re-dyed with mix N719:D149	8.2	0.71	16.58	0.63

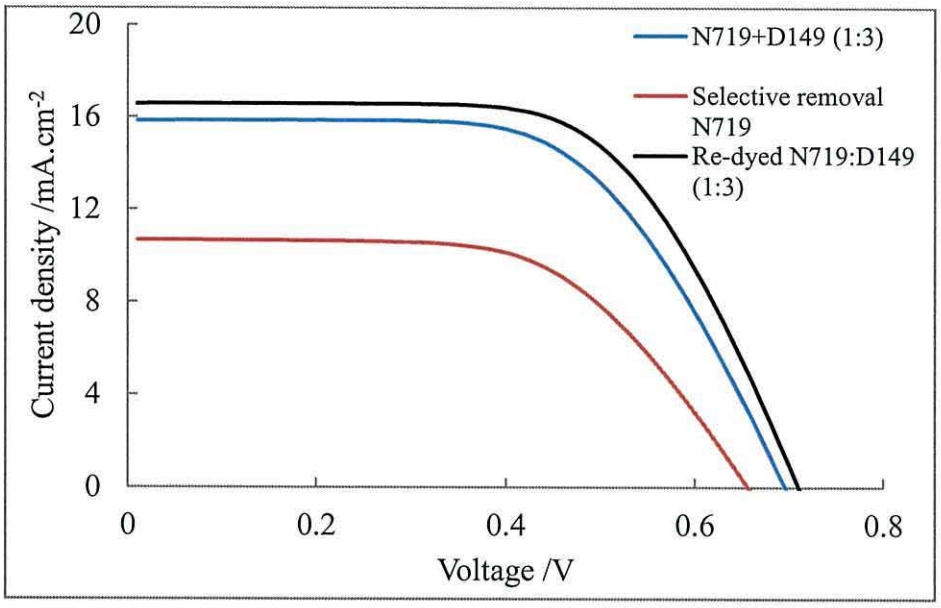

Figure 4.32: I-V data for a device co-sensitized with a mixture of 1:3 v/v N719:D149 from the stock solution N719 (1 ml, 1 mM) and D149 (3 ml, 0.5 mM). Device was dyed, N719 was selectively desorbed and the device re-dyed.

The results in Tables 4.14 – 4.17 show that the ratio of dyes in the co-sensitization of N719 and D149 is important to improve the cell performance. Although these two dyes absorbs at the same wave length. Their varying in molar extinction coefficients and spectral response mean that it was possible to harvest more light and it was found that the best ratio for mixing N719 with D149 1.2 1:2 for these solutions.

4.4 Co-sensitization with three dyes mix of N719:D149:SQ1

Sensitization with three dyes has been rarely studied to date and never using ultra-fast sensitization.[22] However high molar extinction coefficients of strongly absorbing dyes should give sufficient space on the surface of TiO_2 to allow absorption of other dyes with a complementary absorption. This aspect has been tested in this experiment based on the ultra-fast co-sensitization of three dyes; N719 and D149 which absorb at similar wavelengths at 530 nm and SQ1 which absorbs at 636nm as shown the UV/Vis spectra in Figure 4.33. The device was pump dyed with 1 ml dye solution containing three dyes of N719 (1 ml, 1 mM), D149 (1 ml, 0.5 mM) and SQ1(0.1 ml, 0.34 mM) in 10 mM CDCA. Table 4.18. The data show η 7.3% with (J_{sc} = 15.5 mA.cm^{-2}, V_{oc} = 0.71V and FF = 0.65) which is greater than those of DSCs

with any of the corresponding individual dyes. However, the cell performance is similar to the device that co-sensitized with a mix of N719:D149 (1:1 v/v). It might be that the co-sensitization is not affected by SQ1 or that the amount of SQ1 used in this experiment is too small as it is ten times less than N719 or D149.

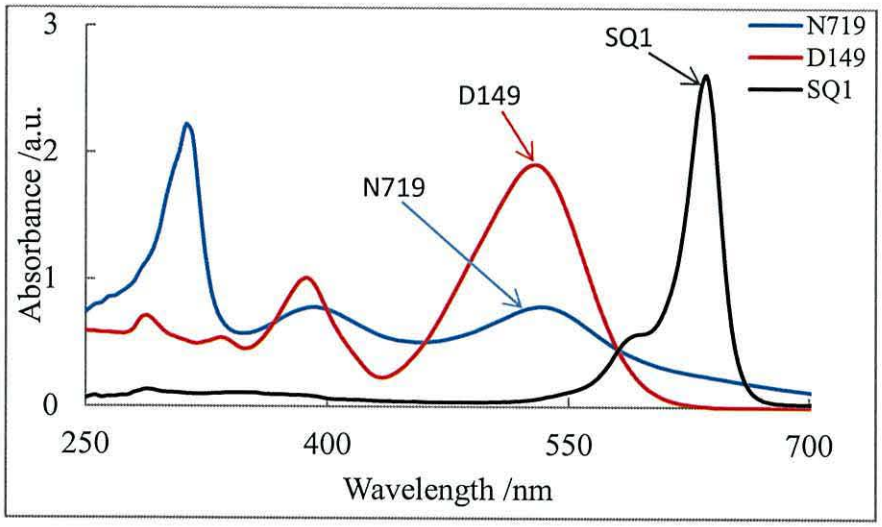

Figure 4.33: UV-Vis spectra of pure (blue line) N719 in *tert*-butanol : acetonitrile (1:1), (red line) D149 in *tert*-butanol : acetonitrile and (black line) SQ1 in ethanol.

Table 4.18: The I-V data of 0.975 cm^2 device of TiO_2 dyed with 1ml of a mix of (N719:D149:SQ1) in 10 mM CDCA by volume ratio (1:1:0.1). (Approximate errors on devices are ± 10% of the values shown).

Device	η (%)	V_{oc} (V)	J_{sc} /mA.cm^{-2}	FF
A Dyed with mix N719:D149:SQ1	7.3	0.71	15.51	0.65
B Dyed with N719	6.4	0.73	14.00	0.63
C Dyed with SQ1	3.5	0.61	8.78	0.65
D Dyed with D149	6.1	0.64	17.69	0.54

4.4.1 Co-sensitization of (N719:D131:SQ1)

To further study tri-sensitization, other dyes have been tested. In this experiment D149 was changed for another indoline dye (D131). The molecular structure of D131 is shown in Figure 4.34. D131 has a molar absorption coefficient (5 x 10^4 $M^{-1}cm^{-1}$) at 425nm.[23] It was chosen because indoline dyes have shown significantly higher molar extinction coefficients which facilitate light absorption in DSC. Figure 4.35 shows the I-V curves of sequential co-sensitization with three dyes N719:D131:SQ1 and the corresponding photovoltaic parameters are summarized in Table 4.19. Device A was pump dyed with D131 (1.5 ml, 0.1 mM) giving η 5.1%. For comparison with co-sensitization another device was dyed at first with N719 (1 ml, 1 mM) Device B giving η 6.4%. N719 was then partially removed by Bu_4NOH (50 µl, 1 mM) Device B1 and the efficiency dropped to 4.4% because some of the N719 was removed (62µg.cm^{-2}). A 300 µl of mix D131:SQ1 (which was mixed D131 (1 ml, 0.1 mM) with SQ1 (1 ml, 0.2 mM) was then pump dyed giving Device B2 and η increased slightly to 4.8% with greater J_{sc} (15.67 mA.cm^{-2}). However, the V_{oc} reduced to 0.55 which may have been due to later dye recombination. To study the effect of dye arrangement on the TiO_2 surface N719 was selectively removed by LiOH (100 µl, 100 mM), Device B3, giving η 3.2 % due to remaining D131+SQ1 and the amount of N719 desorbed was calculated to be 74µg.cm^{-2}. N719 (1 ml, 1 mM) was added a gain giving Device B4 and the η increased to 6.3% which is similar performance to the Device B for dyeing with individual N719 system.

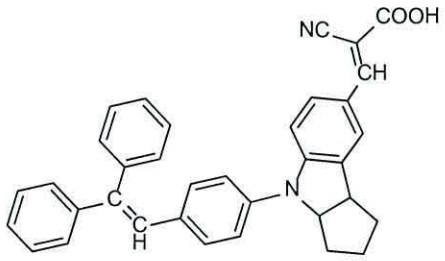

Figure 4.34: Molecular structure of the indoline dye (D131).

Table 4.19: The I-V data of 1 cm^2 device of DSL-18NRT paste dyed with N719 then after adding a mixed solution of D131:SQ1 (1:1) in 10 mM CDCA. (Approximate errors on devices are ± 10% of the values shown).

Device	η (%)	V_{oc} (V)	J_{sc} /mA.cm^{-2}	FF
A Dyed with D131	5.1	0.68	11.78	0.61
B Dyed with N719	6.4	0.77	15.03	0.56
B1 Partial dye removal	4.4	0.76	9.34	0.63
B2 D131:SQ1added	4.8	0.55	15.67	0.56
B3 Selective removal of N719	3.2	0.58	9.29	0.60
B4 Re-dyed with N719	6.3	0.76	14.34	0.58

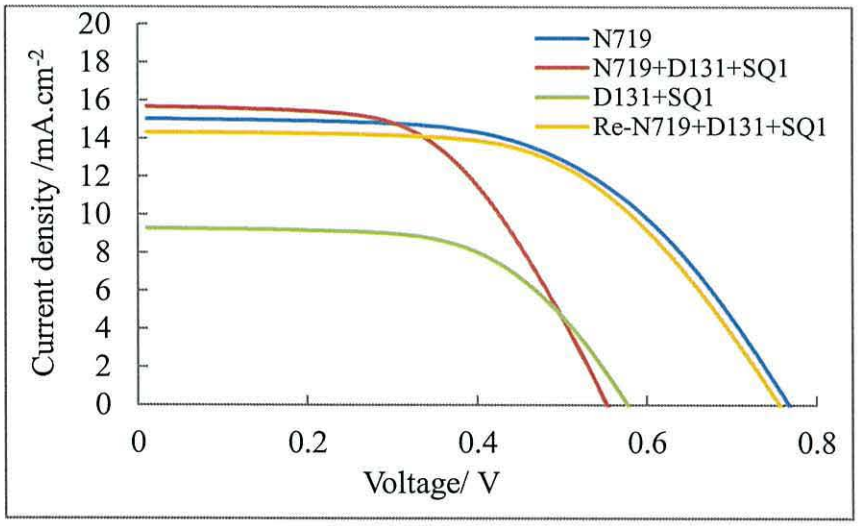

Figure 4.35: I-V data for stepwise co-sensitization of (N719:D131:SQ1) which was step wise dyed with N719 (1 ml, 1 mM) after partial removal of N719 after addition of then 300 µl of mixed D131 (1 ml, 0.1 mM) with SQ1 (1 ml, 0.2 mM).

4.4.2 Co-Sensitization of (N719: YD: SQ1)

In the next experiment to further study trisensitization, other dyes have been tested. In this experiment a step wise co-sensitization of SQ1, then YD and then N719 has been tested. Figure 4.36 shows the I-V curves of a device sequentially dyed in co-sensitization starting with SQ1 (500 µl, 0.34 mM) in 5 mM CDCA followed by

adding YD (1 ml, 0.25 mM) in 5 mM CDCA then after adding N719 (1 ml, 1 mM). The corresponding I-V data are included in Table 4.20. At first, Device A dyed with SQ1 (500 µl, 0.34 mM) gives η 2.6% using small amount of SQ1 to avoid saturation of the TiO_2 surface in order to leave free sorption sites. YD (1 ml, 0.25 mM) in 5 mM was then added (Device B) and the co-sensitized (SQ1+YD) yielded an enhancement in the device performance η = 4.1%, (J_{sc} = 8.46 mA.cm^{-2}, V_{oc} = 0.68V and FF = 0.66). When N719 (1 ml, 1 mM) was added (Device C) η 5.6%. However, this efficiency is not higher than N719 on its own. But after one day the device was re-measured and the η increased to 6.5% with improvements in both J_{sc} = 13.17 mA.cm^{-2} and V_{oc} = 0.71V. It is belived that co-sensitization of three dyes enhances photon absorption making the dye combination more effective than each individual dye. To test the dye loading for the co-adsorption of the three dyes, the N719 was selectively removed by LiOH (100 µl, 100 mM) then a mix of YD and SQ1 was desorbed by Bu_4NOH (200 µl, 40 mM). The absorbances of the desorbed dyes were measured using UV-Vis spectroscopy (Figure 4.37). The dye loadings were then determined as 15.59, 73.95, and 142.28 µg.cm^{-2} for SQ1, YD, and N719 respectively.

Table 4.20: I-V data of a TiO_2 device sequentially dyed starting with SQ1 (500 µl, 0.34 mM) in 5 mM CDCA, then added YD (1 ml, 0.25 mM) in 5 mM CDCA finally, added N719 (1 ml, 1 mM) in 5 mM CDCA. (Approximate errors on devices are ± 10% of the values shown).

Device	η (%)	Voc (V)	Jsc /mA.cm^{-2}	FF
A Dyed with SQ1	2.6	0.61	6.76	0.60
B YD added	4.1	0.68	8.46	0.66
C N719 added	5.6	0.73	12.01	0.60
D Device after one day	6.5	0.71	13.17	0.65

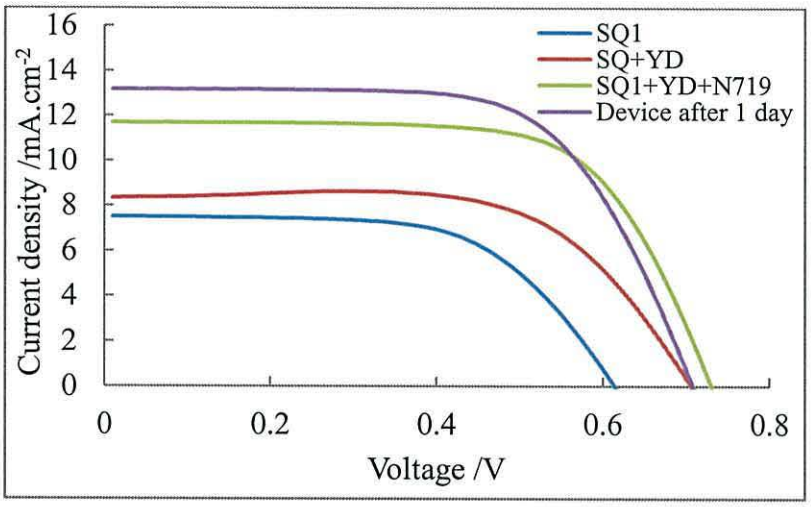

Figure 4.36: I-V data for step wise co-sensitization of (N719:YD:SQ1) which was step wise dyed with SQ1 (500 µl, 0.34 mM) then YD (1 ml, 0.25 mM) and then N719 (1 ml, 1 mM).

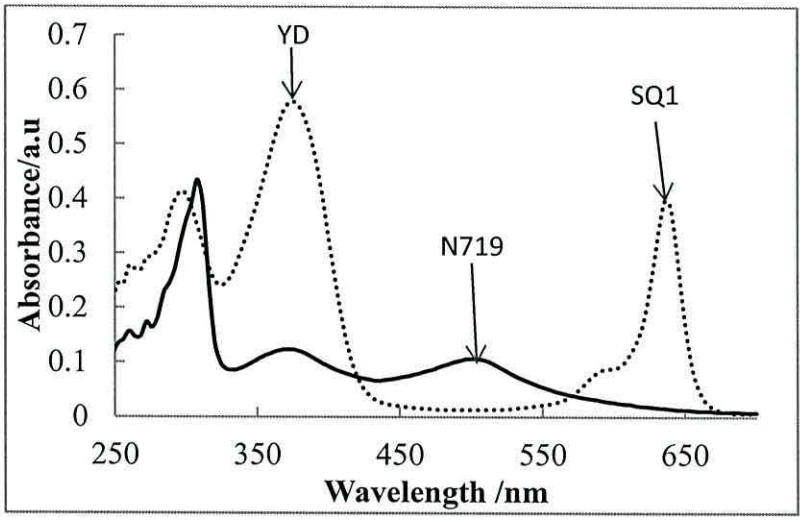

Figure 4.37: UV-Vis Spectra of dye solutions desorbed from the DSL-18NRT device film. The solid line is due to N719 desorbed by LiOH and the dashed line due to a mixture of yellow dye and SQ1 dyes desorbed by Bu_4NOH.

4.4.3 Co-Sensitization with YD:N719:D149

Another example of co-sensitization with three dyes was studied using sequential adsorptions of YD which is absorbs at 385nm with a mix of N719:D149 (1:1 v/v). The latter two dyes absorb light at a similar wavelength at 530 nm. The UV/Vis spectrum for each dye is shown in Figure 4.38.

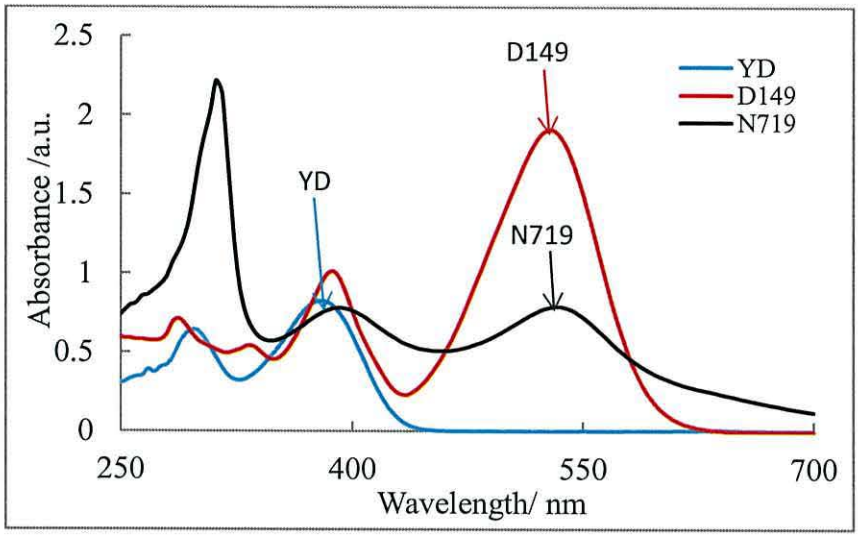

Figure 4.38: UV-Vis spectra of neat (black line) 1 mMN719 in *tert*-butanol: acetonitrile (1:1), (red line) 0.5 mM D149 in *tert*-butanol: acetonitrile and (blue line) 1.2 mM YD in ethanol.

Figure 4.39 shows the I-V curves for each dyeing step and the corresponding photovoltaic parameters are summarized in Table 4.21. Device A was pump dyed with YD (1.5 ml, 1.2 mM) in 10 mM CDCA giving η 2.6%. When a mix of N719:D149 (1:1) was added, Device B, the η increased to 6.9 % with improvements in both J_{sc} and V_{oc} (15.92 $mA.cm^{-2}$ and 0.72 V). After seven days Device E was re-measured and the device yielded significant performance, η = 7.5%, (J_{sc} = 15.9 $mA.cm^{-2}$, V_{oc} = 0.72V and FF = 0.65).

Table 4.21: The I-V data of 1 cm^2 DSL-18NRT device dyed with YD (1.5 ml, 1.2 mM) in 10 mM CDCA, then a 1:1 v/v of mixture N719:D149 added.dye then added 1ml of a mixed (D149:N719). (Approximate errors on devices are ± 10% of the values shown).

Device	η (%)	V_{oc} (V)	J_{sc} /mA.cm^{-2}	FF
A Dyed with YD	2.6	0.51	8.84	0.59
B (1:1 v/v) of N719:D149 added	6.7	0.72	15.92	0.59
C Device after one day	6.9	0.72	15.65	0.61
D Device after five days	7.2	0.73	15.80	0.62
E Device after seven days	7.5	0.72	15.90	0.65

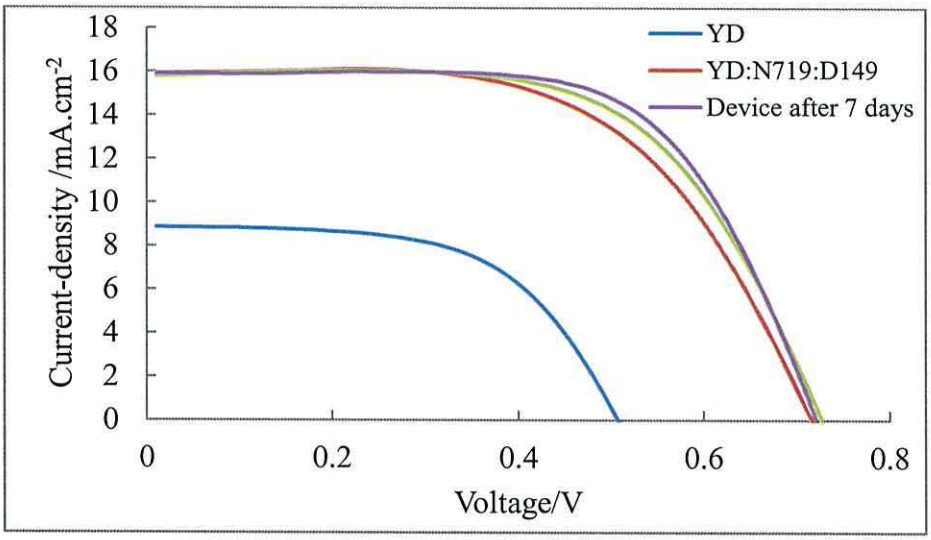

Figure 4.39: I-V data for step wise co-sensitization of (N719:D149:YD) which was step wise dyed YD (1.5 ml, 1.2 mM) the a 1:1 v/v mixture of D149 (1 ml, 0.5 mM) with N719 (1 ml, 1 mM) added.

4.4.4 Co-Sensitization with a mixture of (N719: YD: RD)

Another example of co-sensitization with three dyes was studied using stepwise sensitized YD then RD and then N719. Whilst triphenylamine YD absorbs at 386

nm and RD absorbs 405 nm both YD and RD have higher molar extinction coefficient (Ɛ for YD 32300 $M^{-1}cm^{-1}$ and for RD is 31600 $M^{-1}cm^{-1}$ at 405 nm).[24] Figure 4.40 shows the chemical structure of RD in addition to the carboxyl group has also a cyanoacrylate linker and slightly broader UV-Vis absorption.

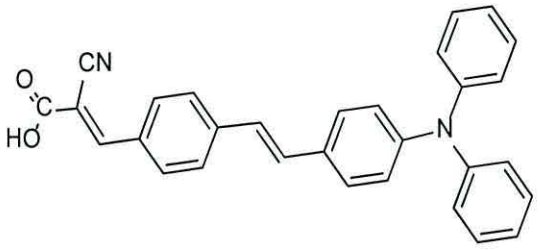

Figure 4.40: Molecular structure of (E)-2-cyano-3-(4-((E)-4-(diphenylamino)styryl)phenyl)acrylic acid RD

The experiment tested a device dyed with RD then another device was sequentially co-sensitisation dyed with YD, RD and N719 dyes. The I-V measurements for each step are shown in Figure 4.41 and the photovoltaic parameters are summarized in Table 4.22. Device A was pump dyed with RD (1 ml, 1.5 mM) in 5 mM CDCA giving η 4.6%. To quantify the dye loading, RD was then desorbed by Bu_4NOH (200 µl, 40 Mm) and the desorbed RD was calculated as 136.5µg.cm^{-2}. Another device was sequential co-sensitized starting by pump dyeing YD (1 ml, 1.2 mM) in 10 mM CDCA, Device B, giving η 2.5%. RD (100 µl, 1.5 mM) in 5 mM CDCA was added giving Device B1 and the η increased to 3.8% with higher J_{sc} (9.23 mM.cm^{-2}), due to the device being co-sensitized with both YD and RD. Although this efficiency is lower than the Device A which was only dyed with RD this may have been because only a small amount of RD was used to dye the device. However, it has helped the J_{sc} to increase to 9.23 mA.cm^{-2}. N719 (1 ml, 1 mM) was then added (Device B2) which yielded a significant enhancement in device performance (η = 6.4%, J_{sc} = 13.04 mA.cm^{-2}, V_{oc} = 0.73V). Figure 4.42 shows photographs of each step showing a yellow device from dyeing with YD (Figure 4.42a). Co-sensitization of result in mixed colours for instance co-sensitizing YD with RD (Figure 4.42b) gives a red colour and co-sensitizing with YD, RD and N719 produces a darker coloured film

than any of any of the dyes individually (Figure 4.42c). To quantify the dye loading on the TiO_2 surface in Device B2, N719 was desorbed first by LiOH (100 µl, 100 mM) and the residual RD and YD were desorbed together by Bu_4NOH (200 µl, 40 mM). Figure 4.43 shows the UV-Vis spectrum of the desorbed dye solutions for N719 and YD:RD. The amount of each dye was calculated, giving 139.3 $\mu g.cm^{-2}$ for N719, 30.35 $\mu g.cm^{-2}$ for both YD and RD.

Table 4.22: I-V data of DSL-18NRT device dyed with YD (1 ml, 1.2mM) in 10 mM CDCA then RD (100 µl, 1.5 mM) in 5 mM CDCA and then N719 (1 ml, 1 mM). (Approximate errors on devices are ± 10% of the values shown).

Device	η (%)	V_{oc} (V)	J_{sc} /mA.cm^{-2}	FF
A Dyed with RD	4.6	0.70	9.27	0.71
B Dyed with YD	2.5	0.71	4.77	0.73
B1 Added 100µl RD	3.8	0.66	9.23	0.63
B2 Added 1ml N719	6.4	0.73	13.04	0.63

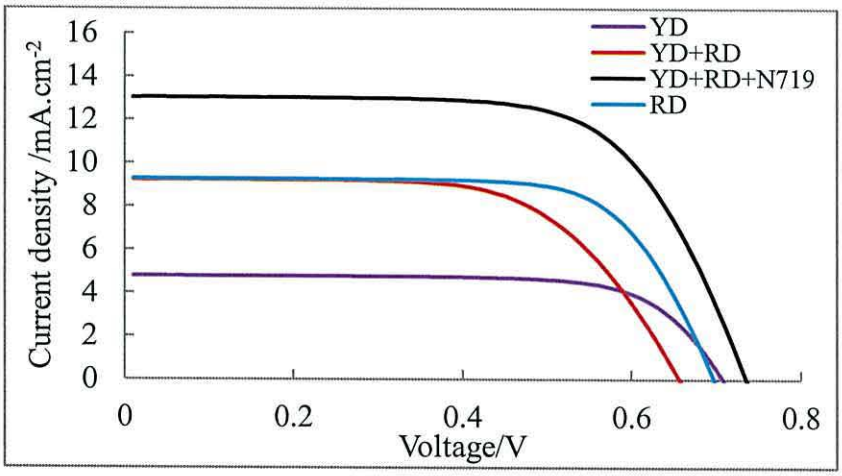

Figure 4.41: I-V data for step wise co-sensitization of (N719:RD:YD) which was step wise dyed YD (1 ml, 1.2 mM) in 10 mM CDCA then RD (100 µl, 1.5 mM) in 5 mM CDCA and then N719 (1 ml, 1 mM).

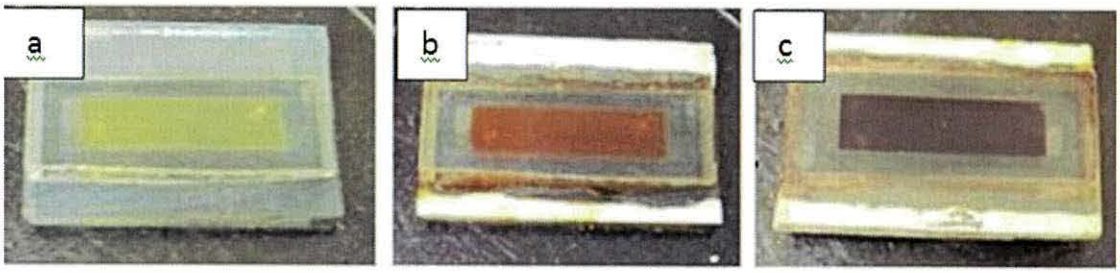

Figure 4.42: Photographs of DSC device dyed with (a) YD (1 ml, 1.2 mM) (b) YD with 100 µl RD added and (c) YD, 100 µl then RD added and then added N719.

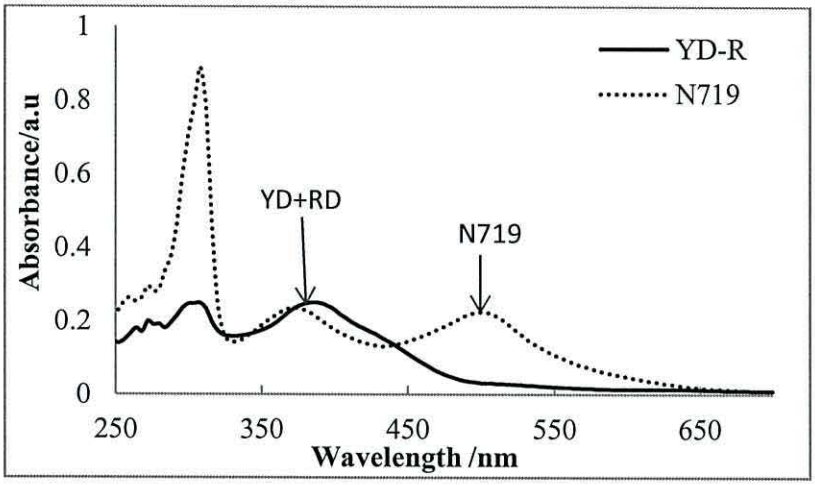

Figure 4.43: UV-Vis Spectra of N719 (dash line) desorbed by LiOH and a mixture of YD+RD (solid line) desorbed by Bu_4NOH.

The results from all previous experiments for co-sensitization with three dyes show that sequential ultra-fast co-sensitization is generally more successful than using a mixed dye solution containing three dyes. This is believed to be because step wise dyeing has more control on the quantity of dyes adsorbed in the process. In this process the dyes can be kept separately also small amount of dye using for dyeing DSC devices.

4.4.5 Co-Sensitization with four dyes (N719:D149:YD:SQ1) from a mixed solution

Studies of co-sensitization of four dyes was then attempted to try to further enhance light harvesting and to reducing the amount of dye used. To test this, a mixed of dye

solution was prepared using N719, D149 and YD in a same volume ratios with a small amount of SQ1 consisting of N719 (1 ml, 1 mM), D149 (1 ml, 0.5 mM), YD (1 ml, 1.2 mM) and SQ1 (100 µl, 0.25 mM). These dyes in this experiment absorbs the light at different wavelengths; the maximum absorption of SQ1 in ethanol is at 636nm, N719 and D149 in *tert*-butanol:acetonitrile absorb at 532 nm and YD in ethanol at 386 nm (Figure 4.44). Figure 4.45 the I-V data of a device co-sensitized with four dyes from a mixed solution and the photovoltaic parameters are summarized in Table 4.23 The data show η = 7.1% (J_{sc} = 16.54 mA.cm^{-2}, V_{oc} = 0.72V and FF= 0.60). Two days later the device was re-measured and the efficiency had increased to 8% with similar J_{sc} = 16.41 mA.cm^{-2} , but V_{oc} increased to 0.75 V. This might have been due to rearrangement of dye molecules and/or electrolyte ingress on the surface leading to better coverage of the surface of TiO_2 thus reducing the recombination.

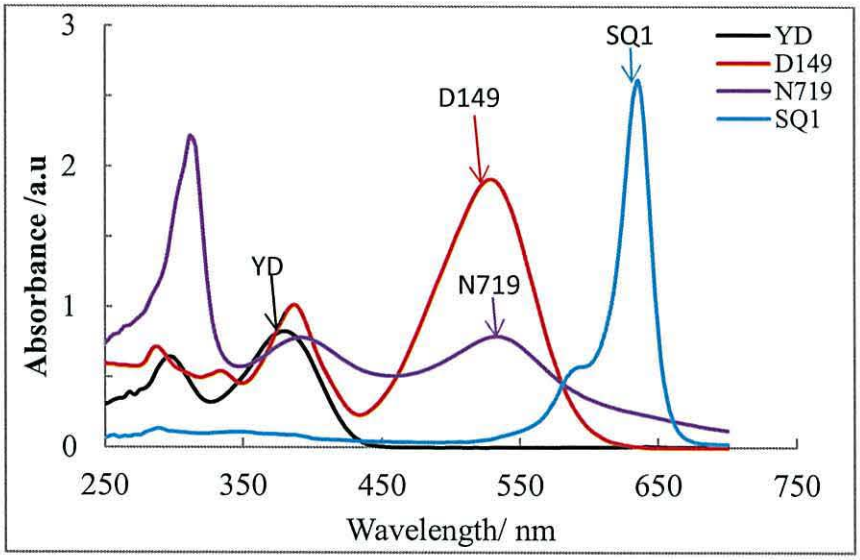

Figure 4.44: UV-Vis spectra of neat (1 mM) N719 in *tert*-butanol : acetonitrile (1:1) (purpule line), (0.5 mM) D149 in *tert*-butanol : acetonitrile (red line), (1.2 mM) YD in ethanol (black line) and (0.25 mM) SQ1 in ethanol (blue line).

Table 4.23: Photo-voltaic parameters of the TiO_2 device co-sensitized with a mix of four dyes by the volume ratios (1:1:1:0.1v/v) N719 (1 ml, 1 mM), D149 (1 ml, 0.5 mM), YD (1 ml, 1.2 mM) and SQ1 (100 µl, 0.25 mM). (Approximate errors on devices are ± 10% of the values shown).

Device	η (%)	V_{oc} (V)	J_{sc} /mA.cm^{-2}	FF
Mix of N719:D149:YD:SQ1	7.1	0.72	16.54	0.60
Device after one day	7.7	0.74	16.60	0.62
Device after two days	8.0	0.75	16.41	0.65

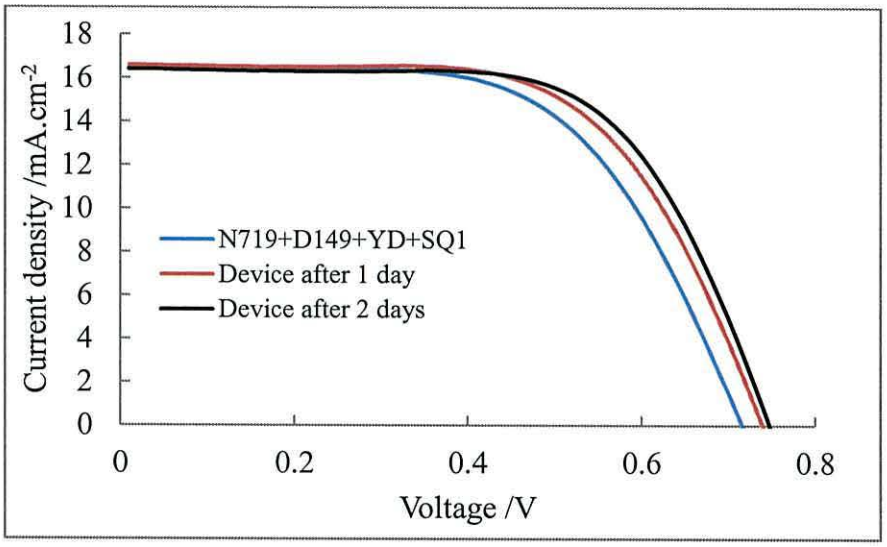

Figure 4.45: Photocurrent density-photo voltage curve of co-sensitized a mix of (N719:D149: YD: SQ1) by volume ration (1:2:1: 0.1) ml measuring for two days under AM 1.5 G radiation.

4.4.6 Stepwise co-Sensitization with four dyes (N719:D149: YD: SQ1)

The next experiment was designed to test the sequential co-sensitization and selective dye removal using the four the same dyes (N719, D149, YD and SQ1). Table 4.24 shows the photo-voltaic parameters for this stepwise approach of co-sensitization. Device A at first was pump dyed with N719 (1 ml, 1 mM) giving η 6.4%. After removal of the electrolyte, 200 µl of a mix of D149 (1 ml, 0.5 mM), YD (1 ml, 1.2 mM) and SQ1 (100 µl, 0.25 mM) with a volume ratio of 1:1:0.1 were added Device B and the efficiency slightly increased to 6.8% due increased J_{sc} due co-sensitization of the different dyes. However, the V_{oc} slightly decreased to 0.69 V. N719 was then selectively removed (Device C) and the efficiency dropped to 4.3%

which was believed to be due to the remaining D149: YD: SQ1. Re-dyeing the device with N719 (1 ml, 1 mM), Device D, yielded a significant enhancement in the device performance η = 7.3% (J_{sc} = 15.02 mA.cm^{-2}, V_{oc} = 0.7V and FF = 0.63) in line with increased light harvesting. After ageing the device for five days η was 7.1%. To quantify the dye loading the device N719 was selectively removed by LiOH (100 µl, 100 mM), a mix of YD and SQ1 was desorbed by Bu_4NOH (200 µl, 8 mM) and finally D149 was desorbed by Bu_4NOH (200 µl, 40 mM) followed by acetone and ethanol. The absorbance of the desorbed dye solutions are shown in Figure 4.46. The dye adsorptions were measured to be N719 = 197.5 µg.cm^{-2}, D149 = 8.06 µg.cm^{-2}, YD = 13.8 µg.cm^{-2} and SQ1= 1.1µg.cm^{-2}.

Table 4.24: Photo-voltaic parameters of TiO_2 sequentially ultra-fast co-sensitized with N719 (1 m,1 mM) and a mix of D149 (1 m, 0.5 mM), YD (1 ml, 1.2 mM and SQ1 (100 µl, 0.25 mM) and after selective removal of N719 re-dyed with N719 (1 ml, 1 mM). (Approximate errors on devices are ± 10% of the values shown).

Device	η (%)	V_{oc} (V)	J_{sc} /mA.cm^{-2}	FF
A Dyed with N719	6.4	0.71	12.76	0.64
B Added 200µl of mix (D149:YD:SQ1)	6.8	0.69	14.07	0.63
C After selective removal N719	4.3	0.66	8.62	0.68
D Re-dyed with N719	7.3	0.70	15.02	0.63
E Device after one day	7.4	0.71	14.78	0.63
F Device after two days	7.2	0.71	14.43	0.63
G The device after five days	7.1	0.71	14.02	0.65

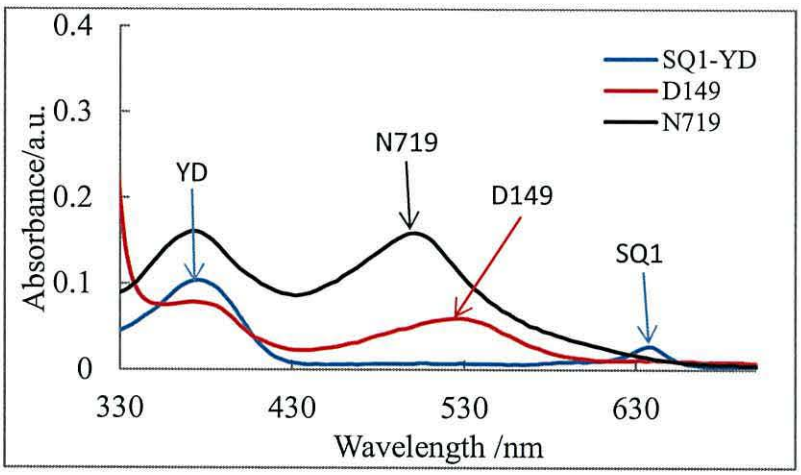

Figure 4.46: UV–Vis spectra of N719 desorbed by 100 mM LiOH (black line), and desorbed mix of SQ: YD by 8 mM Bu_4NOH (blue line) and D149 desorbed 40mM Bu_4NOH followed by acetone and ethanol (red line).

4.4.7 Co-Sensitization with a mix of D131:SQ1 and mix of D149:N719

The previous experiment studied sequential ultra-fast co-sensitization with four dyes N719, D149, YD and SQ1. However, YD was changed to D131 studies of co-sensitization using four dyes was then also attempted to try to further enhance light harvesting and reduce the amount of dye used and also to see the effect of the alternative dye. Table 4.26 shows the photovoltaic parameters of the device ultra-fast co-sensitized with a mix of SQ1 (1 ml, 0.25 mM) with D131 (1 ml, 0.5 mM) in 10 mM CDCA, Device A giving η 4.9%, (J_{sc} =10.46 mA.cm^{-2}, V_{oc} = 0.67 V, and FF = 0.71). This efficiency is higher than a device sensitized only with SQ1 dye but, similar to the efficiency yielded with individual D131 dye. The device was then co-sensitized by a 1:2 v/v a mix of N719 (1 ml, 1 mM) with D149 (2 ml, 0.5 mM) in 10 mM CDCA, Device C, giving a significant enhancement in the device performance to η 7.3%, (J_{sc} = 15.52 mA.cm^{-2}, V_{oc}= 0.7 V, and FF = 0.67). Figure 4.47(a) shows photographs of dyeing the steps. A green colour results as expected for co-sensitization of SQ1 and D131 and Figure 4.47(b) shows the dark colour as expected when a mix of N719:D149 was added.

To measure the dye loadings N719 was selectively removed by LiOH (100 µl, 100 mM) followed by a mix of D131 with SQ1 by Bu_4NOH (200 µl, 8 mM) and then D149 was desorbed by Bu_4NOH (200 µl, 40 mM) followed by acetone then ethanol. Figure 4.48 shows the UV-Vis spectra for each desorbed dye solution, and the amount of each dye was measured giving N719 =117.5 $\mu g.cm^{-2}$, SQ1= 6.79 $\mu g.cm^{-2}$, D131= 8.14 $\mu g.cm^{-2}$, D149 = 22.5 $\mu g.cm^{-2}$. The result shows the device performance improves by co-sensitization with four dyes and this reduces the loading of sensitizers used in the device and increases light harvesting capacity.

Table 4.25: Photo-voltaic parameters of a TiO_2 device sequentially ultra-fast co-sensitized with a mix of SQ1 (1 ml, 0.25 mM) with D131 (1 ml, 0.5 mM) in 10 mM CDCA and then mix of N719 (1 ml, 1 mM) with D149 (2 ml, 0.5 mM) in 10mM CDCA. (Approximate errors on devices are ± 10% of the values shown).

Device	η (%)	V_{oc} (V)	J_{sc} /mA.cm^{-2}	FF
A Dyed with mix of (SQ1:D131)	4.9	0.67	10.46	0.71
B Added 1ml of mix D149:N719 (2:1)	7.2	0.69	15.49	0.68
C The device after one day	7.3	0.70	15.52	0.67

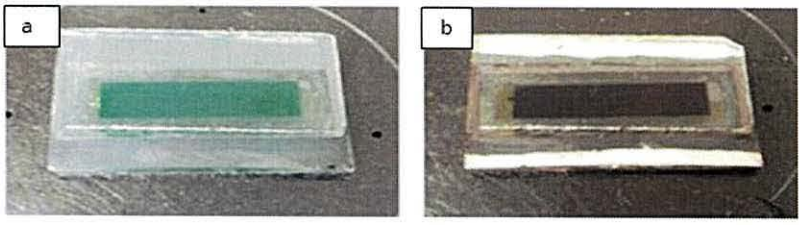

Figure 4.47: Photographs of device (2 x 0.5 cm) showing co-adsorption 1 ml of a mix SQ1 (1 ml, 0.25 mM) with D131 (1 ml, 0.5 mM) in 10 mM CDCA, (b) after adding 1ml of 1:2 v/v mix of N719 (1 ml, 1 mM) with D149 (1 ml, 0.5 mM) in 10 mM CDCA.

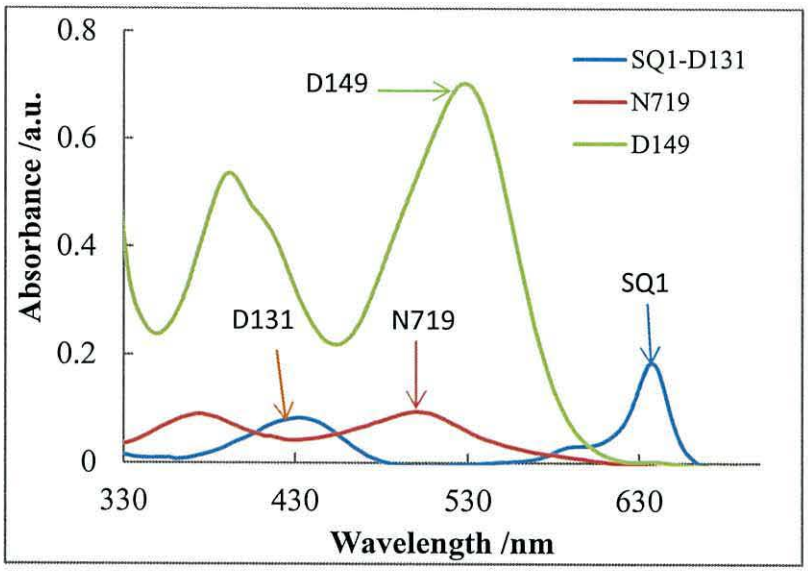

Figure 4.48: UV-Vis spectra of (red line) N719 desorbed by 100mM LiOH , (blue line) a mixture of SQ1:D131 desorbed by 8 mM Bu_4NOH, and (green line) D149 desorbed by 40 mM Bu_4NOH followed by 200 µl acetone.

4.5 Conclusions

In summary, co-sensitization of nanocrystalline TiO_2 with various sensitizers was tested for achieving enhanced power conversion efficiency compared with that of individually dyed DSCs. A cheap paste of P25 TiO_2 which was prepared in the laboratory was compared with commercial TiO_2 DSL-18NRT for co-sensitization studies with various dyes. The best efficiency was achieved with co-sensitization on DSL-18NRT, perhaps because it is more transparent or possibly due to a higher surface area.

This work has studied ultra-fast co-sensitization to maximize the light-harvesting DSC devices, using different methods; co-adsorption together, sequential adsorption, and changing the order of dye loading. Also ultra-fast co-sensitization for two, three and four dyes with complementary absorption spectra was studied. The work shows that there are two methods to co-sensitize either using a mixed dye solution with certain molar ratios of the dyes or sequential co-sensitization by adsorbing different dyes in a consecutive manner. Overall most devices showed significant improvements in the EQE spectra and photocurrents compared with devices based on individual dyes. It was found that the ratio of dyes in a mixed dye solution is

important. The best ratio for mixing SQ1with N719 to make co-sensitization was 6% SQ1:N719 (c/c) due to the big difference in molar extinction coefficients. It was also found that the best ratio for mixing N719 with D149 is mix N719:D149 (1:3). However, the molar extinction coefficient for D149 is higher than N719.

Sequential ultra-fast co-sensitization was also investigated for two or more dyes. The results show that the sequential ultrafast co-sensitization with YD then N719 achieved η = 7.4% which is higher than the co-sensitization by the order N719 then YD (6.7%). The selective removal of dyes such as desorbed N719 by LiOH and organic dye by Bu_4NOH and D149 by concentrated Bu_4NOH followed by acetone and ethanol have been used to balance the loading amount of dyes in co-sensitization and this process also provides an alternative choice for changing the sensitizers in the device. Ultra-fast co-sensitization with three or four dyes using either sequential or stepwise method has been also studied. The results show that a significant improvement in device performance either with three dyes or four dyes.

4.6 References

1 J. H. Yum, S. R. Jang, P. Walter, T. Geiger, F. Nuesch, S. Kim, J. Ko, M. Grätzel and M. K. Nazeeruddin, *Chemical Communications*, 2007, 4680-4682.

2 Q. Shen, Y. Ogomi, B. W. Park, T. Inoue, S. S. Pandey, A. Miyamoto, S. Fujita, K. Katayama,T. Toyoda and S. Hayase, *Physical Chemistry Chemical Physics* , 2012, **14**, 4605-4613.

3 A. Hagfeldt, G. Baschloo, L. Sun, L. Kloo, H. Petterson, *Chemical Reviews*, 2010, **110**, 6595-6663.

4 K. M. Lee, Y. C. Hsu, M. Ikegami, T. Miyasaka, K. R. Justin Thomas, J. T. Lin and K. C. Ho, *Journal of Power Sources*, 2011, **196,** 2416-1421.

5 M. Kimura, H. Nomoto, N. Masaki and S. Mori, *Angewandte Chemie*, 2012, **124**, 4447-4450.

6 D. Kuang, P. Walter, F. Nuesch, S. Kim, J. Ko, P. Comte, S. M. Zakeeruddiin, M. K. Nazeeruddin, and M. Grätzel, *Langmuir*, 2007, **23**, 10906-10909.

7 Y. Chen, Z.Zeng, C. Li, W. Wang, X. Wang, and B. Zhang, *New Journal of Chemistry,* 2005, **29**, 773-776.

8 C. M. Lan, H. P. Wu, T. Y. Pan, C. W. Chang, W. S. Chao, C. T. Chen, C. L. Wang, C. Y. Lin, and E.W. G. Diau, *Energy and Environmental Science*, 2012, **5**, 6460-6464.

9 B. E. Hardin, H. J. Snaith, and M. D. McGehee, *Nature Photonics*, 2012, **6**, 162-169.

10 J. N. Clifford, A. Forneli, H. Chen, T. Torres, S. Tan, and E. Palomares, *Journal of Materials Chemistry,* 2011, **21**, 1693-1696.

11 P. J. Holliman, M. L. Davies, A. Connell, B. V. Velasco, and T.M Watson, *Chemical Communications*, 2010, 46, 7256-7258.

12 R. Y. Ogura, S. Nakan, M. Morooka, M. Orihashi, Y. Suzuki, K. Noda, *Applied Physics Letters*, 2009, **94**, 073308.

13 H. Choi, S. Kim, S. O. Kang, J. Ko, M. S. Kang, J. N. Clifford, A. Forneli, E. Palomares, M. K. Nazeeruddin, M. Grätzel, *Angewandte Chemie International Edition*, 2008, **47**, 8259-8263.

14 C. Reichardt, *Chemical Reviews*, 1994, **94**, 2319-2358.

15 X. Liu, and K. Thomas, *Chemical Communications*, 1996, 1435-1436.

16 J. H. Yum, S. J. Moon, R Humphry-Baker, P. Walter, T. Geiger, F. Nuesch, M. Grätzel, and M. K. Nazeeruddin, *Nanotechnology*, 2008, **19**, 424005.

17 P. Wang, C. Klein, R. Huphry-Baker, S. M. Zakeeruddin, M. Grätzel, *Journal of American Chemical Society*, 2005, **127**, 808-809.

18 J. H. Yum, P. Walter, S. Huber, D. Rentsch, T. Geigar, F. Nuesch, F. De Angelis, M. Grätzel, M. K. Nazeeruddin, *Journal of American Chemical Society,* 2007, **129**, 10320-10321.

19 N. Robertson, *Angewandte Chemie International Edition*, 2008, **47**, 1012-1014.

20 Y. Ren, Y. Z. Zheng, J. Zhao, J. F. Chen, W. Zhou, X. Tao, *Electrochemistry Communications*, 2012, **16**, 57-60.

21 M. K. Nazeeruddin, F. D. Angelis, S. Fantacci, A. Selloni, G. Viscardi, P. Lisk, S. Ito, B. Takeru, M. Grätzel, *Journal of American Chemical Society,* 2005, **127**, 16835-16847.

22 P. J. Holliman, M. Mohsen, A. Connell, M. L. Davies, K. AL-Salihi, M. B. Pitak, G. J. Tizzard, S. J. Coles, R. W. Harrington, W. Clegg, C. Serpa, O. H. Fontes, C. Charbonneau, M. J. Carnie, *Journal of Materials Chemistry*, 2012, **22**, 13318-13327.

23 T. Horiuchi, H. Miura, K. Sumioka, S. Uchida, *Journal of American Chemical Society*, 2004, **126**, 12218-12219.

24 S. Hwang, J. H. Lee, C. Park, H. Lee, C. Kim, C. Park, M-H. Lee, W. Lee, J. Park, K. Kim, N- G. Park, and C. Kim, *Chemical Communications*, 2007, 4887-4889.

Chapter Five Study of Kinetics of Dye-sensitization for DSC Devices

5.1 Introduction

Dye loading using either single or multiple dyes as a function of sensitization time can have a significant effect on DSC device performance.[1] This chapter presents the results of experiments conducted to investigate rate constants for the adsorption of the yellow triarylamine dye (YD) using either passive or ultra-fast dyeing on TiO_2 surfaces, as well as studying the adsorption of mixed dye solutions (N719:YD or N719:SQ1) on TiO_2 photo-electrodes in DSC.

5.2 Previous work on the Kinetics of dye adsorption on TiO_2

The adsorption of dye molecules on TiO_2 nanoparticles in DSC photo-electrodes plays a crucial role for DSC efficiency and stability.[2] The interaction between the TiO_2 semiconductor and the dye photo-sensitizer has been studied in the literature using UV-Vis, Raman, resonance Raman, and ATR-FTIR spectroscopy to investigate the nature of binding on the TiO_2 films.[3] The results have shown that adsorption occurs *via* formation of ester-like linkages.[4] For instance, the coordination of photosensitizing Ru-(bipy) dyes on TiO_2 has been investigated by Finnie *et al.*, who suggested three possible carboxylate binding modes unidentate, bidentate or bridging as illustrated in Figure 5.1.[5]

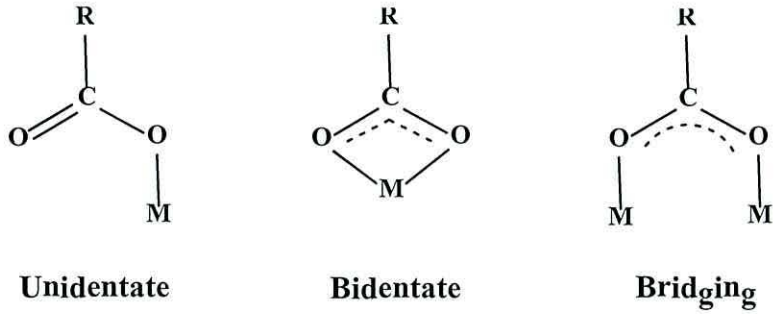

Figure 5.1: Three possible carboxylate coordination modes.5

In DSC devices dye chemisorption on the TiO_2 is preferred over physisorption because the latter does not enable efficient electron transfer into the metal oxide

substrate.[6] TiO_2 surfaces with full monolayer dye coverage have also been reported to be preferable over partially covered surfaces for several reasons: i) full coverage of the substrate or saturation by dye molecules increases the electron transfer, ii) complete dye layers reduce recombination losses by physically separating the electrolyte solution from the titania surface, and iii) full coverage maximizes light absorption efficiency, as well as the photoelectron injection efficiency.[7] Surface coverage, θ can be defined as the number of adsorbate atoms per unit area (N_{ads}) compared to the number of surface atoms per unit area (N_s). This can be is expressed as.[8]

$$\theta = \frac{N_{ads}}{N_s} \qquad 5.1$$

Using this expression, the maximum amount of adsorbate in a monolayer is when θ=1. However, this does not indicate how quickly adsorption occurs. Prediction of chemical kinetics is significant for designing adsorption systems and explaining the rate of chemical reactions. The kinetics of dye sorption can be illustrated as two steps, the kinetics of the rate of surface reactions and the rate of diffusion which in the mesoporous TiO_2 films is the rate controlling step.[9] Pseudo-first and second order equations and intraparticle diffusion have been used to examine the mechanism of dye sorption from solution.[10] Lagergren's paper expressed the pseudo-first order rate equation for the liquid-solid adsorption system[11] as follows:

$$\frac{dq_t}{dt} = k_1 (q_e - q_t) \qquad 5.2$$

Where q_e and q_t are the amounts of dye adsorbed at equilibrium and at time (t) respectively, and k_1 is the rate constant of the pseudo first-order reaction.

On integration, this gives

$$-ln (q_e - q_t) = k_1 t + constant \qquad 5.3$$

After integration by applying the conditions (q_t =0, at t =0, and q_t =q_t , at t =t) and Eq. 5.3 becomes

$$constant = -ln\, q_e \qquad 5.4$$

Substituting Eq. 5.4 into Eq. 5.3 we obtain;

$$-ln\,(q_e - q_t) = k_1 t - \ ln\ q_e \qquad 5.5$$

Rearranging Eq. 5.5 for the logarithms and linearized data gives:

$$\log(q_e\ - q_t) = \log(q_e) - \frac{k_1}{2.303} t \qquad 5.6$$

By comparison, the pseudo-second order kinetic rate equation is described as[12]:

$$\frac{dq_t}{dt} = k_1\,(q_e\ - q_t)^2 \qquad 5.7$$

Integrating Eq. 5.7 for the boundary conditions t = 0, to t = t and qt = 0 to $q_t = q_t$ gives:-

$$\frac{t}{q_t} = \frac{1}{k_2 q_e^2} + \frac{t}{q_e} \qquad 5.8$$

Where q_e is the amount of sorbate adsorbed at equilibrium, t is the reaction time, q_t is the amount of sorbate adsorbed at time t and k_2 is the equilibrium rate constant of pseudo-second order sorption. Using this equation, plotting $1/q_t$ *versus* t will give a straight line with slope $1/ q_e$ and intercept $1/k_2 q_e^2$ which can be used to calculate the equilibrium rate constant (k_2).

5.3 Aim of study

The aim of the work in this chapter was to investigate the rates of dye adsorption on TiO_2 photo-electrodes to understand the mechanisms controlling dye loadings. Other aims included studying dye loadings *versus* time by ultra-fast dyeing, and the kinetics of co-adsorption using more than one dye.

5.4 Results and discussion.

5.4.1 Kinetics of passive adsorption of YD on TiO_2.

An initial study was carried out into kinetic studies for the sensitizer adsorption onto TiO_2 DSC devices using adsorption of the yellow triphenylamine dye, 4-[2-(4-diphenylaminophenyl)vinyl]benzoic acid (YD) shown by the chemical structure in Figure 5.2. The COOH group of YD can interact with O-H groups on the surface of TiO_2. The rate of reaction by passive adsorption has been investigated to compare with the adsorption rate constant by ultra-fast dyeing.

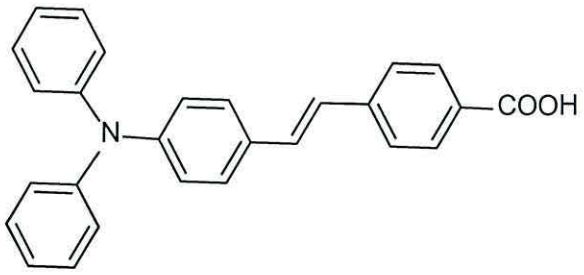

Figure 5.2: Chemical structure of (E)-4-(4-(diphenylamino)styryl)benzoic acid (YD).[13]

The amount of YD dye loaded onto TiO_2 films as a function of time was obtained by measuring the absorbance of the amount of desorbed dye from TiO_2 at various times. To start with, an initial YD concentration of 1.2 mM was used and TiO_2 films were passively dyed. To do this, several TiO_2 films (2 x 0.5 cm) were sintered at 450 ^{0}C for 30 minutes. After being cooled these were immersed in a pot containing YD (100 ml, 1.2 mM). At fixed times, the TiO_2 films were removed, and the amount adsorbed of dye was calculated by desorption using 40 mM of Bu_4NOH. The YD loadings were plotted against time and Figure 5.3 shows that passively dyeing YD was faster in the initial stages, then showed a decreasing pattern and finally became constant showing saturation of the TiO_2 film occurs after *ca.* 6 h after upon which the dye loading remains reasonably constant at 75μg.cm^{-2}. The amount of dye desorbed was calculated using the molar extinction coefficient of YD after measuring the absorbance of each desorption solution as shown in Figure 5.4. The dye loadings were measured by dye desorption from TiO_2 surface in alkali solution. Therefore the amount of dye adsorbed into TiO_2 film (cm^2) can be calculated by the following equation.

$$Q_e = \frac{C_e}{A} x\, V \qquad 5.9$$

Where Q_e the amount of adsorbed dye ($\mu g.cm^{-2}$), C_e is the concentration of dye desorption ($\mu g.ml^{-1}$), V volume of alkaline used for desorption (ml) and A is the surface area of the TiO_2 film (cm^2).

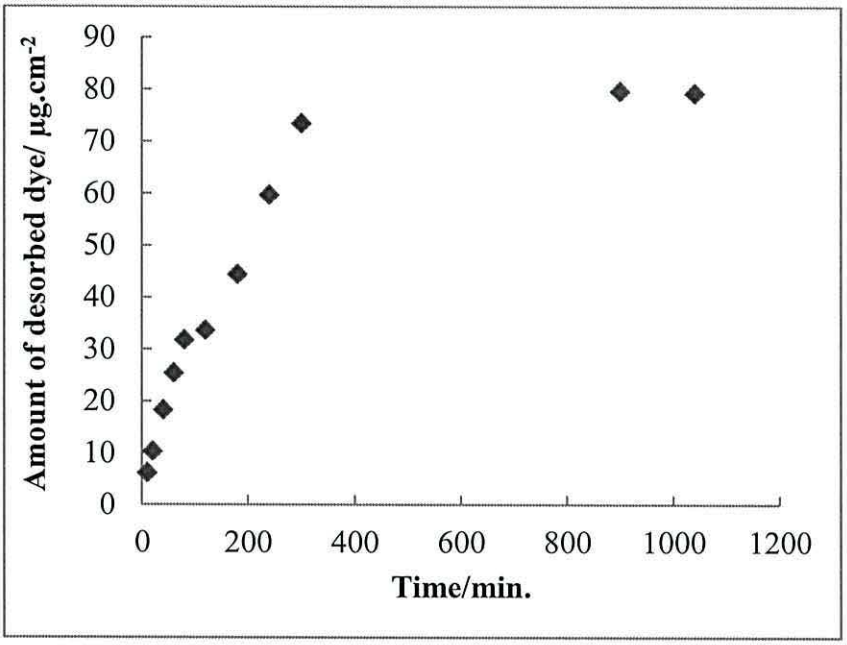

Figure 5.3: Effect of contact time of dyed of yellow triphenylamine dye (1.2 mM) passively dyed on TiO_2 films (0.5 x 2 cm) measured by desorption using in Bu_4NOH (40 mM) followed by UV-visible spectroscopy measuring at 385nm.

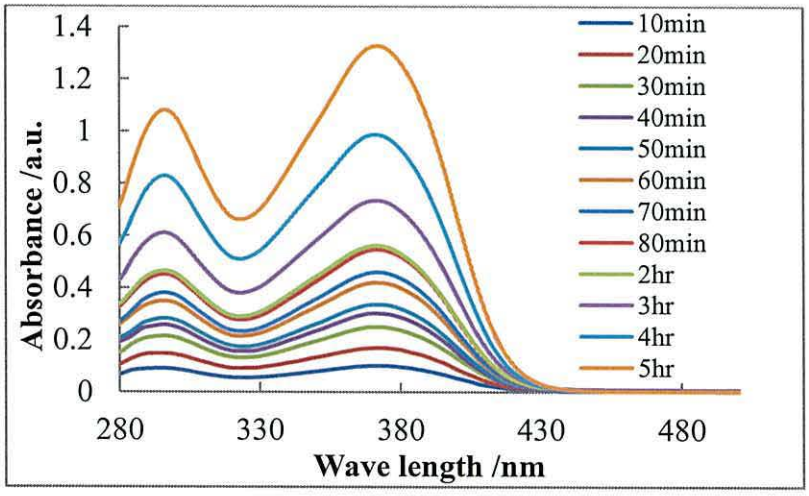

Figure 5.4: UV-Vis Spectra of desorbed yellow dye at various dyeing times using passive dyeing.

The adsorption kinetics for YD adsorption on TiO_2 can be expressed by the concentration change with time (t), according to the equation:

$$\frac{d[YD:TiO_2]}{dt} = k[TiO_2]^n[YD]^m \qquad 5.10$$

Where k is reaction constant and n and m represent the reaction order. The $[TiO_2]$ represents the concentration of the adsorption sites in the TiO_2 film which can be expressed as $[TiO_2:YD]_\infty - [TiO_2:YD]_t$ where $[TiO_2:YD]_\infty$ represents the saturated amount of the adsorbed dye. And $[TiO_2:YD]_t$ represent the concentration of dye adsorbed at time t, Thus, the concentration of $[YD]$ can be set constant because of almost no change during the adsorption, therefore Eq. 5.10 can be rewritten as follows;

$$r = \frac{d[YD:TiO_2]}{dt} = -\frac{d([TiO_2:YD]_\infty - [TiO_2:YD]_t)}{dt} \qquad 5.11$$

And rate of reaction equal to:

$$r = k[TiO_2]^n[YD]^m = k[TiO_2] = k([TiO_2:YD]_\infty - [TiO_2:YD]_t)^n \qquad 5.12$$

By combination equation 5.11 with equation 5.12 we can obtain equation 5.13

$$\frac{d[YD:TiO_2]}{dt} = k([TiO_2:YD]_\infty - [TiO_2:YD]_t)^n \qquad 5.13$$

The maximum amount of adsorbate which is adsorbed in first layer is usually called the monolayer and when the TiO_2 surface is fully covered by dye molecules θ =1. The coverage TiO_2 surface can be expressed by θ which is defined as $[TiO_2:YD]_t/[TiO_2:YD]_\infty$ and the uncovered TiO_2 surface at period times is (1- θ). Therefore the pseudo-first order reaction can be written as the following equation:

$$-\frac{d(1-\theta)}{dt} = k_1(1-\theta) \qquad 5.14$$

Integrating (Eq. 5.12) for the boundary conditions

$$ln(1-\theta) = k_1 t \qquad 5.15$$

The coverage θ is the fractional number of adsorbed molecules per unit area on the TiO_2 surface which can be calculated from Equation 5.1. The reaction rate of the first order reaction for the YD adsorption can be obtained from Eq.5.15. The amounts of YD passive dyed on TiO_2 films with dyeing times and the parameters θ which is the ratio of the amount of desorbed dye at time = t to the maximum amount of desorbed dye , and then t/qt with ln(1- θ) were found and are listed in Table 5.1

The first order rate constant was determined from the plot between $ln(1-\theta)$ *versus* adsorption time for the passive adsorption of YD on TiO_2 films as shown in Figure 5.4. This gives a slope equal to (–k) which is 6.7 x 10^{-3} min^{-1}.

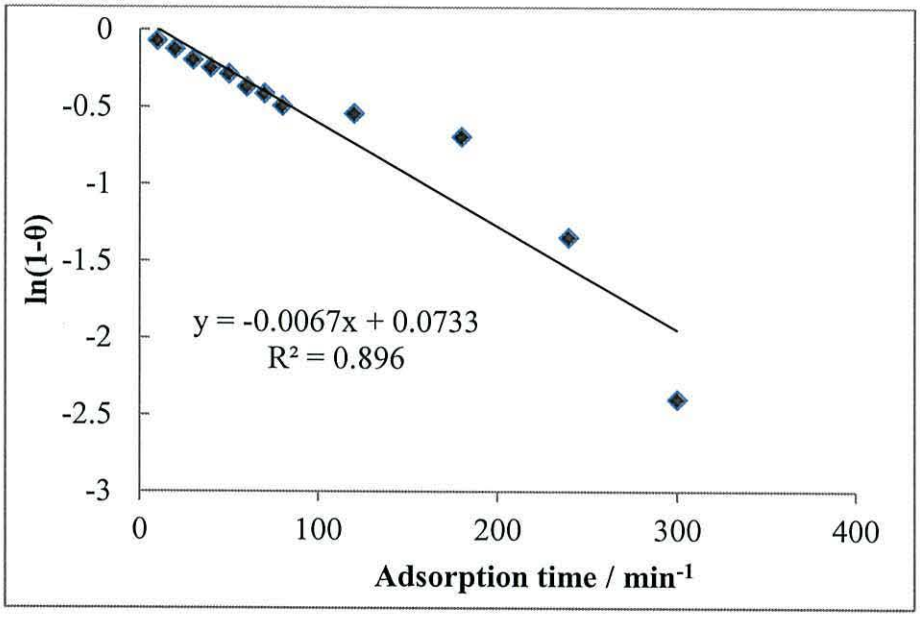

Figure 5.4: Dye coverage (θ) *versus* adsorption time for (1.2 mM) of yellow dye based on pseudo-first order reaction.

As discussed previously the pseudo-second order kinetics may be expressed in a linear form using Eq. 5.5. The parameter t/qt from Table 5.1 for the passive desorption of YD on TiO_2 was plotted *versus* time (Figure 5.5) which gives an equilibrium adsorption capacity q_e (determined from the slope) of 87.7 μg.cm^{-2}. The second order constant k_2 was determined from the intercept as 9.8 x 10^{-5} cm^2.μg^{-1}.min^{-1}. The correlation for passive dyed YD onto TiO_2 films were R^2 = 0.896 from the first order model and R^2 = 0.981 from second order was indicating a better fit for the latter. This suggests that the adsorption does depend on the initial concentration of YD.

Table 5.1: The data of the amount of YD loaded passively on TiO_2 at interval time with kinetic parameters.

Dyeing time (min.)	Abs.	conc.of YD $mg.L^{-1}$	q_t	θ	$1-\theta$	ln(1-θ)	t/q_t
10	0.101	1.22	6.10	0.07	0.93	-0.07	1.64
20	0.170	2.05	10.28	0.12	0.88	-0.13	1.94
40	0.302	3.65	18.25	0.22	0.78	-0.25	2.19
60	0.420	5.07	25.39	0.31	0.69	-0.37	2.36
80	0.526	6.36	31.80	0.39	0.61	-0.50	2.51
120	0.557	6.73	33.67	0.42	0.58	-0.54	3.56
180	0.735	8.88	44.43	0.50	0.5	-0.70	4.05
240	0.987	11.93	59.67	0.79	0.26	-1.35	4.02
300	1.215	14.69	73.45	0.91	0.09	-2.40	4.08
900	1.318	15.93	79.63	0.99	0.01	-4.60	11.30
1040	1.311	15.85	79.25	0.98	0.02	-3.91	13.60

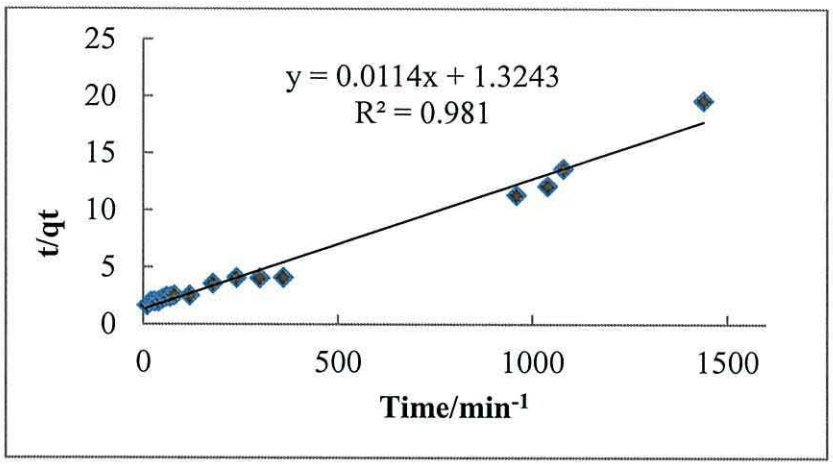

Figure 5.5: Plot of t/q_t *versus* time (minutes) based on pseudo-second order reaction model for the adsorption of YD (1.2 mM) passively dyed on TiO_2

5.4.2 Kinetic study of ultra-fast dyeing YD on TiO_2.

The rate of adsorption YD on TiO_2 photo-electrode as a function of time has also been studied using the ultra-fast dyeing method to compare with the rate of adsorption by passive dyeing, and also to study the effect of dyeing time on DSC cell performance. In this case YD (1.5 ml, 1.5 mM) was pumped through the device cavity on a hotplate at 50 °C for various periods of time. The amount of dye sorption was measured at different times by desorbing the dye using $Bu_4NOH_{(aq)}$ followed by UV-Vis spectroscopy, (Figure 5.6).

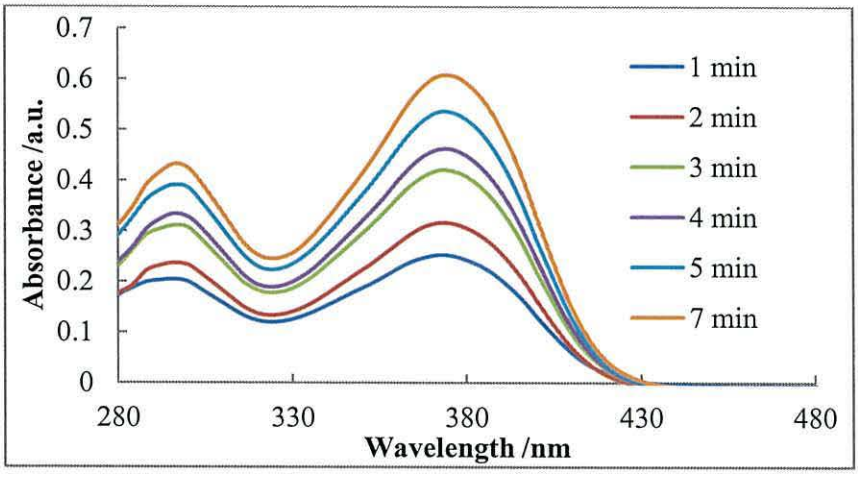

Figure 5.6: UV-Vis spectra of YD solutions desorbed from TiO_2 photo-electrodes by Bu_4NOH after fast-dyeing for the time periods shown.

The amounts of adsorbed dye ($\mu g.cm^{-2}$) after different periods of fast dyeing (0-10 minutes) were plotted *versus* time minutes as shown in Figure 5.7 for the ultra-fast sorption of YD on TiO_2 film in DSC device. The YD surface coverage on TiO_2 at different times was calculated by the fractional amount of dye uptake at specific time with the maximum amount of dye adsorption at equilibrium, and all experimental data are presented in Table 5.2. The result shows the amount of adsorbed YD on TiO_2 working electrode increased fastest in initial stages. However, the TiO_2 surface did not saturate by ultra-fast dyeing presumably because more dyeing time was needed.

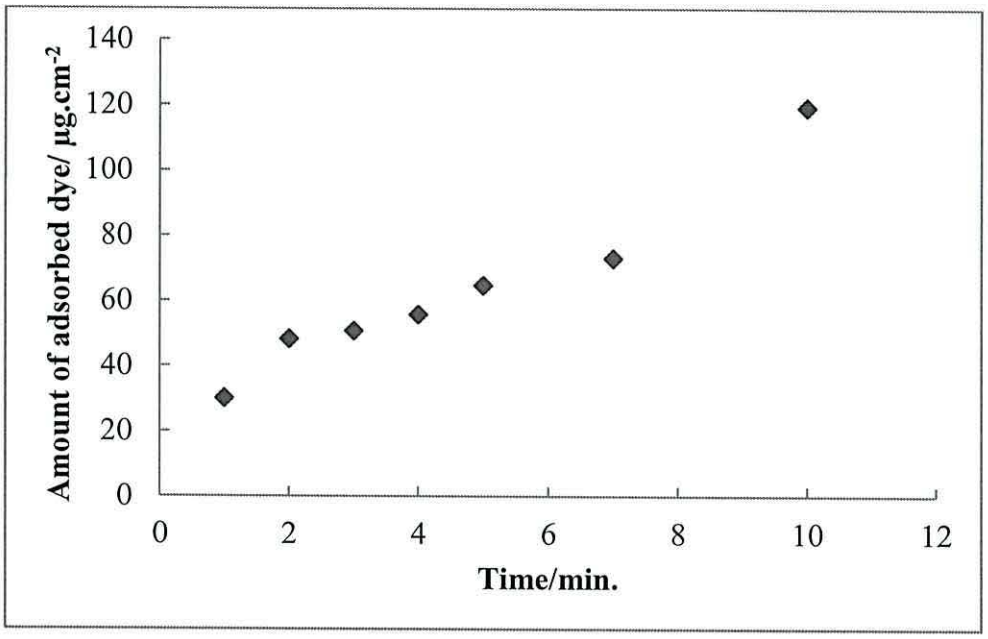

Figure 5.7: Graph to show adsorbed dye versus time for ultra-fast dyeing of YD (initial conc. = 1.5 mM) on TiO_2 measured by desorption in Bu_4NOH solution.

Table 5.2: Experimental data for the kinetic study of ultra-fast dyeing of YD 1.5 mM on 1 cm^2 of DSL-18NRT film measured by desorption using Bu_4NOH solution.

Time (min.)	Abs.	Con. $mg.L^{-1}$	q_t /$\mu g.cm^{-2}$	θ	1-θ	ln(1-θ)	t/qt
1	0.253	3.06	30.6	0.25	0.75	-0.29	0.032
2	0.316	3.82	38.2	0.32	0.68	-0.39	0.052
3	0.42	5.07	50.7	0.42	0.58	-0.54	0.059
4	0.461	5.57	55.7	0.46	0.54	-0.62	0.071
5	0.535	6.47	64.7	0.54	0.46	-0.78	0.077
7	0.606	7.30	73.0	0.61	0.39	-0.94	0.095
10	0.987	11.93	119.3	1.00	0.00	E	0.083

The kinetic rate constant for the sorption of YD on TiO_2 by ultra-fast dyeing was calculated from the data in Table 5.2 using Eq. 5.15 for the pseudo-first order kinetic model. Figure 5.8 shows plot of $ln(1-\theta)$ *versus* time (min) which gives a slope equal to (–k) which is 11.1 $x10^{-2}$ min^{-1} with a coefficient correlation (R^2 = 0.989). In this case, suggest that the adsorption of YD on TiO_2 particles by ultra-fast dyeing depends on the initial concentration of YD.

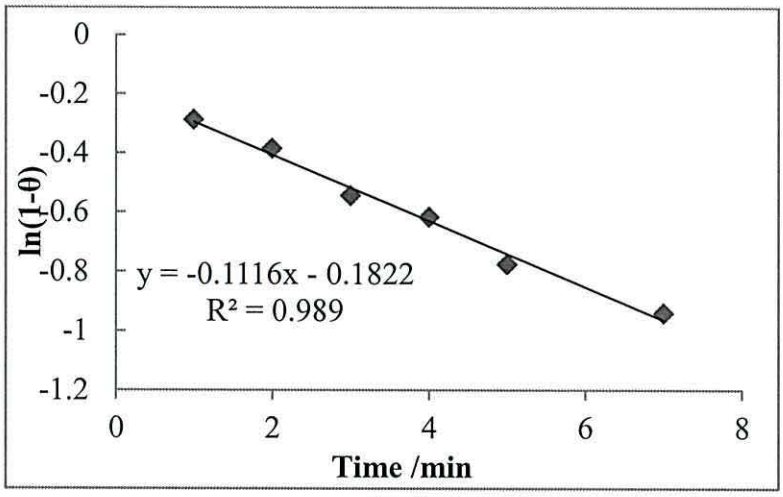

Figure 5.8: Plot of ln (1- θ) *versus* time (min) using a pseudo-first order model for YD (1.5 mM) ultra-fast dyed on TiO_2 film.

The adsorption of YD on TiO_2 may also be described by a pseudo-second order model, shown in linearised form in Eq. 5.8. Hence, as discussed earlier, a plot of t/qt against t should give a linear relationship as shown in Figure 5.9 which gives a coefficient correlation (R^2 =0.970). The rate constant k_2 from the slope gives 3.5 x 10^{-3} $cm^2.\mu g^{-1}.min^{-1}$ and the adsorption capacity at equilibrium q_e was calculated from the intercept as 101.01 $\mu g.cm^{-2}$.

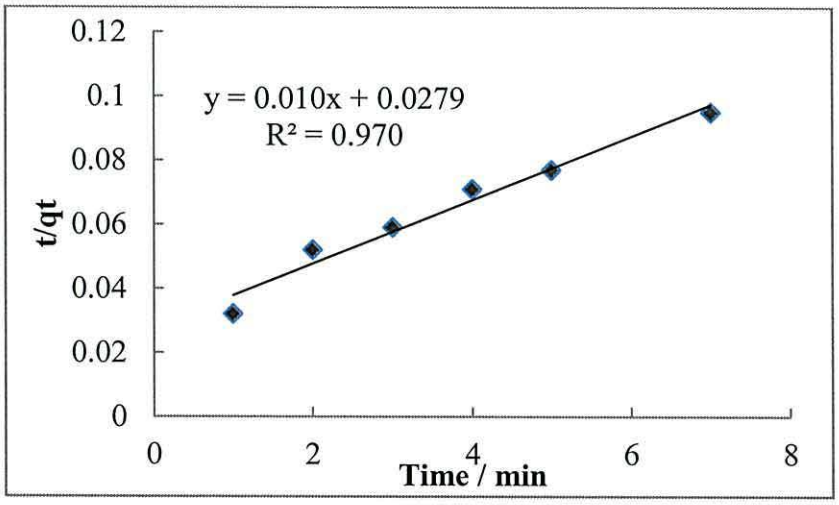

Figure 5.9: Plot of t/qt versus time (t) for the pseudo-second order model for YD (1.5 mM) ultra-fast dyed on TiO_2 films.

All kinetic parameters determined for the pseudo-first order and pseudo second order models applied to the passive adsorption YD and ultra-fast adsorption on TiO_2 with correlation coefficients are described in Table 5.3. The data shows that the adsorption of YD on TiO_2 films by passive adsorption most closely follows a pseudo-second order model giving a rate constant k_2 =9.8 x 10^{-5} $cm^2.\mu g^{-1}.min^{-1}$ with an equilibrium adsorption capacity equal to 87.72 $\mu g.cm^{-2}$. By comparison, the sorption of YD by ultra-fast dyeing gave similar correlation coefficients for both a pseudo-first order or pseudo second order model. The rate of pseudo-first order and pseudo second order rate constants for the ultra-fast adsorption of YD were determined from Figures 5.8 and 5.9 to be 11.16 x 10^{-2} min^{-1} and 3.5 x 10^{-3} $cm^2.\mu g^{-1}.min^{-1}$, respectively. The calculated equilibrium adsorption capacity of YD by ultra-fast adsorption is higher than passive adsorption.

Table 5.3: Kinetic parameters for either passively dyed, or ultra-fast dyed YD on DSL-18NRT TiO_2 films.

Adsorption method	Pseudo-first order		Pseudo-second order		
	k_1/min^{-1}	R^2	k_2 /cm^2. μg^{-1}. min^{-1}	R^2	q_e/ $\mu g.cm^{-2}$
Passive adsorption	6.7 x10^{-3}	0.896	9.8 x 10^{-5}	0.981	87.72
Ultra-fast adsorption	11.16 x10^{-2}	0.989	3.5 x 10^{-3}	0.970	101.01

5.4.3 Photovoltaic measurements of sensitization YD.

The I-V data for YD dyed DSC devices were measured as a function of dyeing time, (Figure 5.10), and the corresponding dye loading was measured by desorbing with 40 mM Bu_4NOH followed by UV-visible spectroscopy (Table 5.4). The data show that the efficiency increased with dye loading as shown in Figure 5.10 and J_{sc} increased with increasing dye loading on the TiO_2 surface as shown in Figure 5.11. The reason

is that more dye molecules on the TiO_2 surface leads to a more complete monolayer of chemisorbed dye molecules which led to more electron injection into the TiO_2 conduction band. On the other hand, the V_{oc} and fill factor do not appear to be so strongly influenced by dye loading.

Table 5.4: I-V data for a DSL-18NRT device dyed with YD (1.5 mM) in 10 mM CDCA with the amount of desorbed dye by $\mu g.cm^{-2}$ at interval time in fast dyeing. (Approximate errors on devices are ± 10% of the values shown).

Time (min)	η (%)	V_{oc} (V)	J_{sc} /mA.cm^{-2}	FF	Amount of desorbed dye /μg.cm^{-2}
1	1.16	0.62	2.81	0.66	30.6
2	1.45	0.62	3.48	0.67	38.2
3	1.62	0.63	3.82	0.66	50.7
4	1.97	0.65	4.56	0.66	55.7
5	2.10	0.65	4.88	0.66	64.7
7	2.21	0.66	5.18	0.64	73.2
10	2.81	0.61	6.92	0.67	119.3

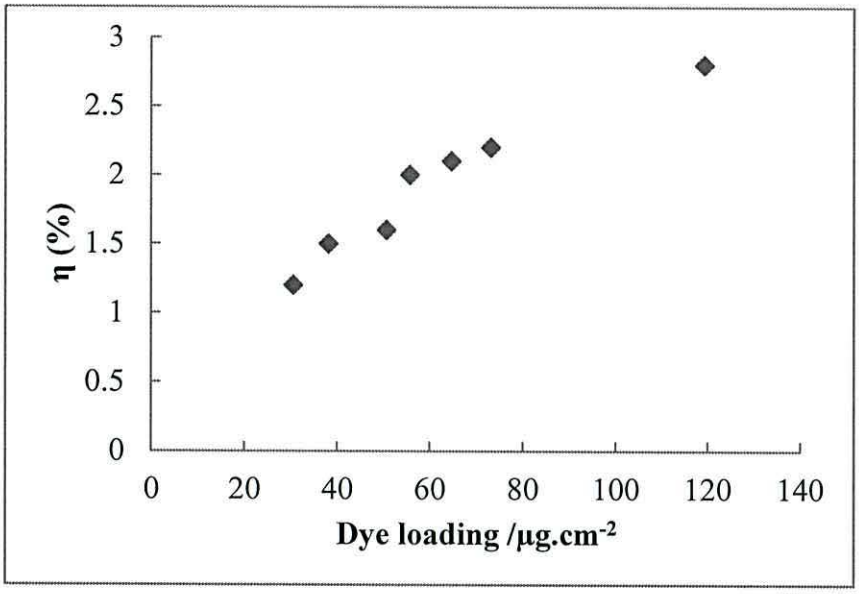

Figure 5.10: Plot η *versus* dye loading at different dyeing time for ultra-fast dyed YD.

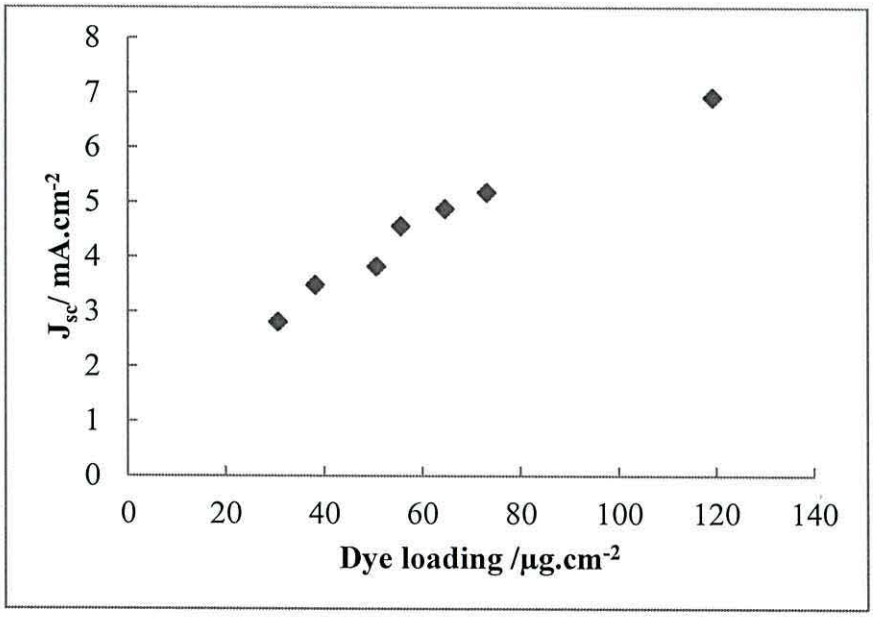

Figure 5.11: Plot J_{sc} *versus* dye loading at different dyeing time for ultra-fast dyed YD.

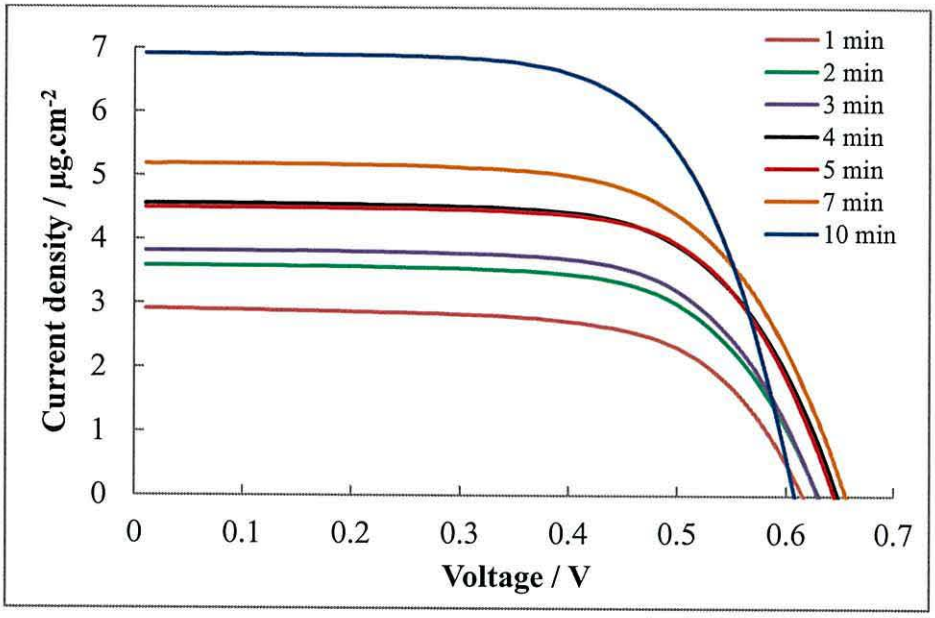

Figure 5.10: I-V data for ultra-fast YD (1.5 mM) sensitized DSC device measured at different dyeing times.

The results show that it is possible to study the kinetic of YD adsorption by ultra-fast dyeing on TiO_2 DSC device, then using Bu_4NOH for desorption. These data were useful in the context of the co-sensitization of YD with N719 in the following section. Therefore, the data were useful to study the effect of competitive of dye adsorption in a mixed dye solution onto TiO_2 film.

5.5 Kinetics of co-adsorption of mixed YD and N719 solution by ultra-fast dyeing on TiO_2.

Co-sensitization is an effective approach to enhance the photovoltaic properties of the DSC through a combination of two or more dyes sensitized together on a semiconductor film. Therefore a kinetic study for co-adsorption of more than one dye on TiO_2 film is important. Because the competition between the dyes molecules into the sites of TiO_2 reduces the equilibrium time which effects on the device performance.

5.5.1 Study of the effects of dyeing time

The dye uptake of mixed N719:YD solutions by ultra-fast dyeing as a function of time has been studied by the selective removal of the dyes after different dyeing times. Figure 5.11 shows a plot of the amount of adsorbed dye ($\mu g.cm^{-2}$) *versus* time using a solution containing N719 (1 ml, 1 mM) mixed with YD (1 ml, 1.5 mM) in 10 mM CDCA giving (1:1.5 c/c) N719:YD by the concentration ratio. The dye solution was pumped through a device cavity for various times at flow rate 100 $\mu l.min^{-1}$. After each minute of dyeing redox electrolyte (I_3^-/I^-) was added for I-V measurements. To quantify dye loading at a various times, after each minute of dyeing and I-V measurements, the electrolyte was removed by ethanol (as discussed in chapter three). The dye was then desorbed using alkali solution, so the absorbance of the desorbed dye solution was the measured using UV-visible spectrophotometer.

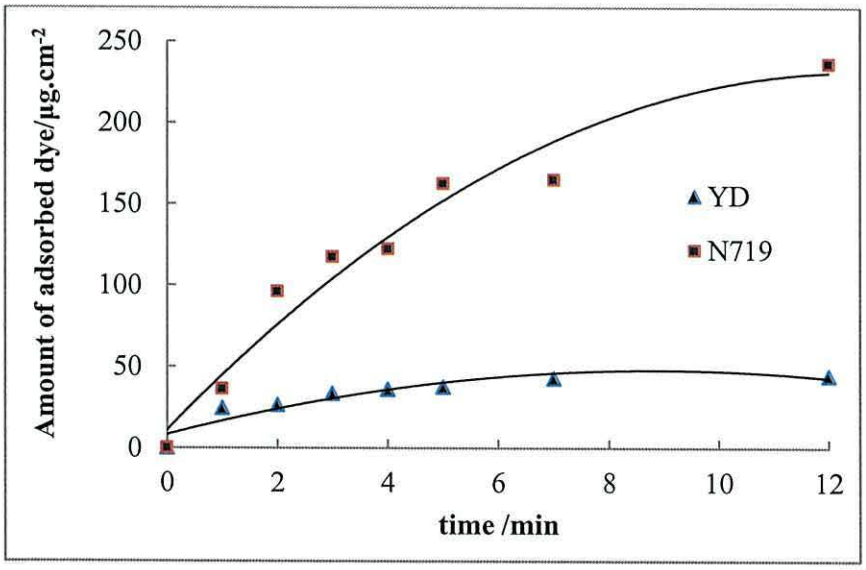

Figure 5.11: Effect of contact time for the ultra-fast dyeing of mix N719: YD (1:1.5 mM) on $1cm^2$ of TiO_2 film, measured by selectively desorption with N719 desorbed by LiOH (100 mM) and YD desorbed using *t*-Bu_4NOH (40 mM).

In these measurements N719 was removed by 0.1 M LiOH after each dyeing time and the UV-vis absorbance measured for the desorbed dye solutions. Figure 5.12 shows the UV-Vis spectra for $LiOH_{(aq)}$ desorbed N719 at different dyeing times.

Because YD was not removed by LiOH, the YD loading was desorbed with 40 mM $Bu_4NOH_{(aq)}$ and the UV-vis spectra are presented in Figure 5.13.

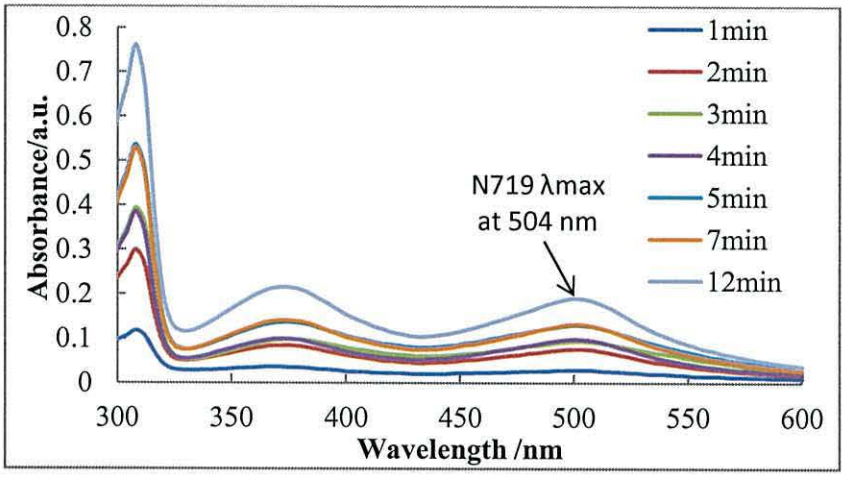

Figure 5.12: UV-Vis spectra for N719 desorbed by LiOH (100 mM) from a 1 cm^2 of DSL-18NRT device after dye uptake from a mixed N719:YD (1mM : 1.5 mM) in 10 mM CDCA solution at the dyeing times shown.

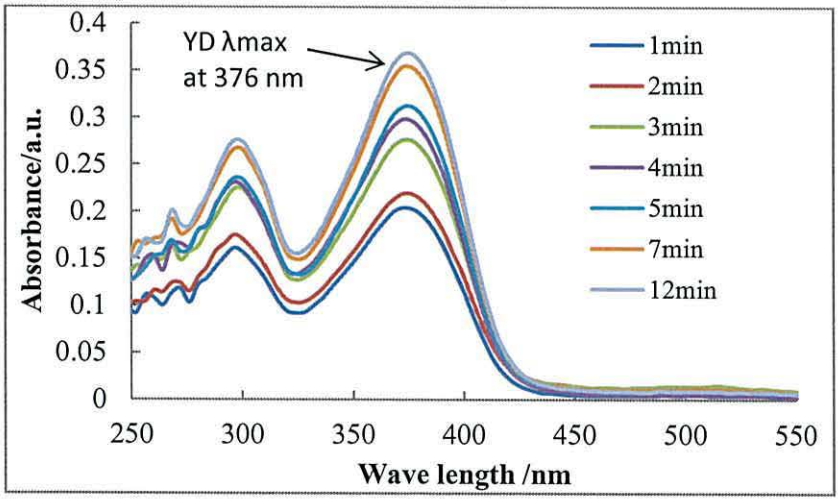

Figure 5.13: UV-Vis spectra of YD desorbed by $Bu_4NOH_{(aq)}$ from a 1 cm^2 of DSL-18NRT device which had been ultra-fast dyed from a mixed N719 (1 ml, 1 mM) : YD (1ml, 1.5 mM) in 10 mM CDCA solution at the dyeing times shown.

5.5.2 Determination of rate constants for N719: YD co-sensitization.

To determine the rate constants for the adsorption of N719 and YD from mixed solutions onto TiO_2 surfaces by ultra-fast dyeing was found by selective desorption. The kinetics of each dye was studied separately. The concentrations of N719 and YD dyes desorbed at varying time were determined from the UV-Vis spectra of each of N719 in Figure 5.15 and YD as shown in Figure 5.13. The amounts of desorbed N719 and YD dye (q_t) at the specific time were measured by the Eq. 5.9. The surface coverage θ at every time was calculated by divided the amount of dye desorbed to the maximum amount of desorbed dye. The desorbed dye concentrations and surface coverage θ and the amount of dye desorbed values were found and are listed in Table 5.5 for YD adsorption and in Table 5.6 for N719 adsorption on TiO_2 surface.

The dye uptake data from the ultra-fast adsorption of mixed solution of N719:YD (1 mM:1.5 mM) has been modelled using pseudo first-order and second order models. The data from the calculations to determine the rate constants for the pseudo-first order model for YD and N719 are shown in Tables 5.5, and 5.6, respectively. These data were used to plot $\ln(1-\theta)$ *versus* time giving a rate constant, k_1 equal to 0.173 min^{-1} for N719 adsorption and 0.396 min^{-1} for YD adsorption.

Table 5.5 : Kinetic data for the ultra-fast dyeing of YD on a TiO_2 film from a mixed solution of N719 (1ml, 1 mM) :YD (1 ml, 1.5 mM) in 10 mM CDCA.

Dyeing Time (min)	Abs	Conc. of YD $mg.L^{-1}$	qt/ $\mu g.cm^{-2}$	θ	1-θ	ln(1-θ)	t/qt
1	0.204	2.4	24.6	0.15	0.54	-0.78	0.04
2	0.219	2.64	26.4	0.40	0.59	-0.89	0.08
3	0.276	3.33	33.3	0.49	0.75	-1.39	0.09
4	0.298	3.60	36.0	0.51	0.81	-1.66	0.11
5	0.311	3.76	37.6	0.68	0.84	-1.83	0.13
7	0.354	4.28	42.8	0.70	0.96	-3.22	0.16
12	0.367	4.43	44.3	1.00	0.00	E	0.27

Table 5.6: Kinetic data for the ultra-fast dyeing of N719 on a TiO_2 film from a mixed solution of N719 (1ml, 1 mM) :YD (1 ml, 1.5 mM) in 10 mM CDCA.

Dyeing Time (min)	Abs	conc. of N719 $mg.L^{-1}$	qt/ $\mu g.cm^{-2}$	θ	1-θ	ln(1-θ)	t/qt
1	0.029	3.63	36.3	0.15	0.85	-0.16	0.027
2	0.077	9.63	96.3	0.40	0.60	-0.51	0.020
3	0.094	11.75	117.5	0.49	0.51	-0.67	0.025
4	0.098	12.25	122.5	0.51	0.49	-0.71	0.032
5	0.230	16.25	162.5	0.68	0.32	-1.14	0.013
7	0.132	16.50	165.0	0.70	0.30	-1.2	0.040
12	0.189	23.63	236.2	1.00	0.00	E	0.050

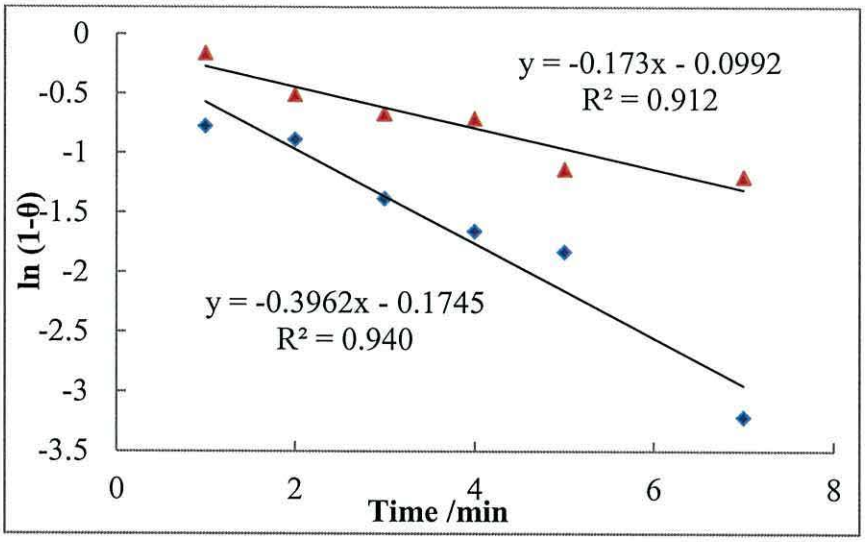

Figure 5.14: Plot ln(1-θ) *versus* time (min) based on a pseudo-first order model for the ultra-fast dyeing of a mixed N719:YD solution (1 mM:1.5 mM), (red triangles) show N719 data, and blue squares show YD data.

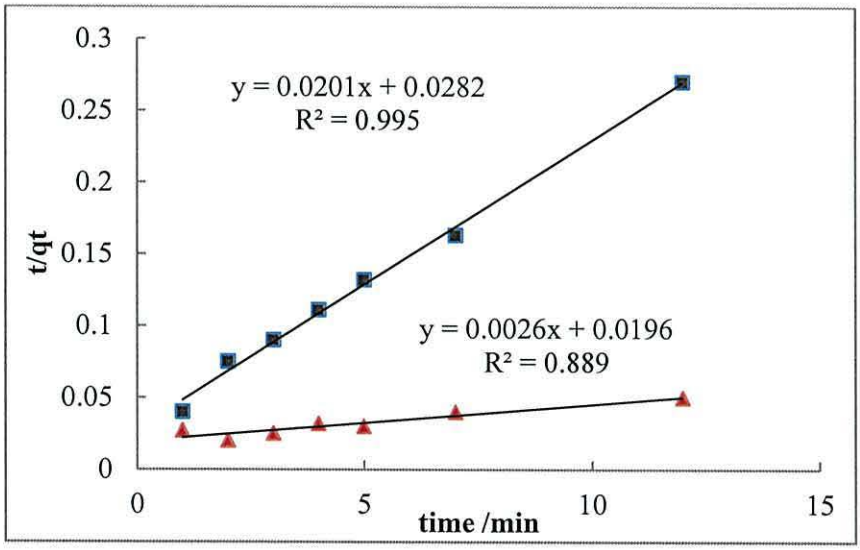

Figure 5.15: Plot (t/qt) *versus* time (min) based on a pseudo-second order model for the ultra-fast dyeing of a mixed N719: YD solution (1 mM:1.5 mM) , blue squares show N719 data, and red triangles show YD data.

To investigate the mechanism of adsorption of a mixed solution of N719:YD on TiO_2, a pseudo-second order model was also fitted to the experimental data in Tables 5.5 and 5.6. The plot t/qt *versus* t gives a slope and intercept which were used to

determine pseudo-second order rate constant k_2 and equilibrium adsorption capacity of YD and N719 loading on TiO_2 in the same device.

All the kinetics parameters for the two different models are listed in Table 5.7. The data show that N719 gives a slightly better fit to the pseudo-first order model with a better correlation coefficient for this plot. The data showed YD a slightly better compliance with the pseudo-second order model which is reflected by the higher correlation coefficient for a linear plot of t/qt *versus* t. The results show a value of q_e (49.75 $\mu g.cm^{-2}$) for YD sorption from the pseudo-second order which is slightly higher than the experimental data that was calculated to be 44.3 $\mu g.cm^{-2}$. But N719 shows calculated value of q_e (384.6 $\mu g.cm^{-2}$) which is higher than the experimental value which is equal to (236.25 $\mu g.cm^{-2}$), which suggests incomplete N719 coverage by ultra-fast adsorption.

Table 5.7: Kinetic parameters for the ultra fast dyeing of a mixed N719: YD (1mM:1.5 mM) by the same volume in 10 mM CDCA at room temperature.

Dye	Pseudo-first order		Pseudo-second order		
	k_1/min^{-1}	R^2	k_2 /cm^2. μg^{-1}. min^{-1}	$q_e/\mu g.cm^{-2}$	R^2
YD	0.396	0.940	1.4×10^{-2}	49.75	0.995
N719	0.173	0.912	3.4×10^{-4}	384.6	0.889

5.5.3 Effect of adsorption time of mixed N719:YD solutions on DSC device performance.

DSC device performance as a function of dyeing time has also been investigated, since it has been shown that the amount of dye uptake varies with time. Table 5.8 shows the photovoltaic parameters for a TiO_2 device dyed with mix N719:YD solution (1 mM:1.5 mM) by ultra-fast dyeing at different dyeing times. The results show that the efficiency increases with dyeing time presumably due to increasing dye loading. This leads to increasing J_{sc}, because the dye loading increased by the

adsorption time. Figure 5.16 show I-V curves for different dyeing times for the sensitized a mixed N719:YD solution (1 mM:1.5 mM) in 10 mM CDCA.

Table:5.8: I-V data of 1cm^2 DSL-18NRT device of TiO_2 ultra-fast dyed with a mixed N719:YD solution (1mM:1 mM) in 10 mM CDCA as a function of time after each desorption using LiOH (100 µl, 100 mM) for desorbing N719 and Bu_4NOH (200 µl, 40mM) for desorbing YD. (Approximate errors on devices are ± 10% of the values shown).

Time	η (%)	V_{oc} (V)	J_{sc} /mA.cm^{-2}	FF	qt N719 /µg.cm^{-2}	q_t of YD/ µg.cm^{-2}
1	3.23	0.67	7.37	0.65	36.3	24.6
2	4.24	0.60	11.02	0.64	96.3	26.4
3	4.68	0.64	11.55	0.63	117.5	33.3
4	4.86	0.60	12.99	0.62	122.5	36.0
5	5.31	0.63	13.18	0.64	162.5	37.6
7	5.87	0.62	15.32	0.62	165.0	42.8
12	7.07	0.71	15.76	0.63	236.3	44.3

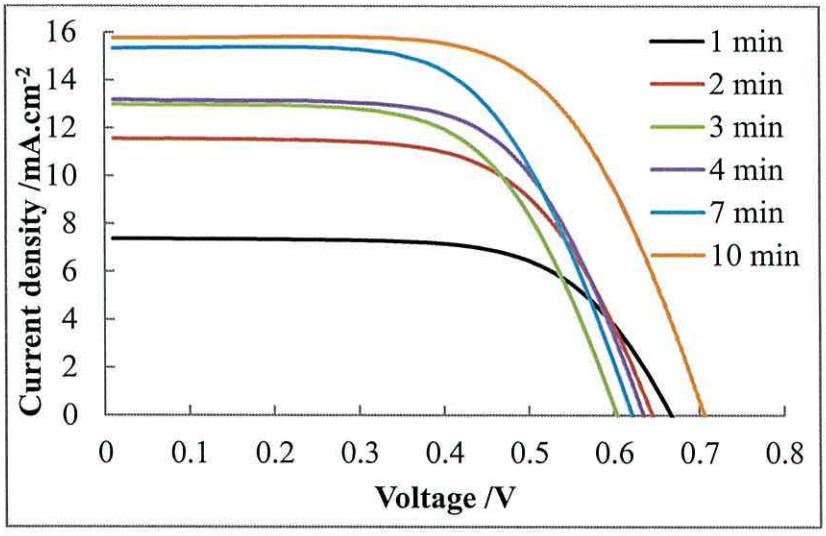

Figure 5.16: I-V data for a DSC device ultra-fast dyed with a mixture of N719: YD (1 mM:1.5 mM) as a function of dyeing time.

5.6 A study of the Kinetics of ultra-fast adsorption of 6.4 % SQ1: N719 on TiO_2 photo-electrodes.

5.6.1 Effect of contact time.

A mixed SQ1:N719 solution was prepared by mixing SQ1 (2 ml, 0.24 mM with N719 (3 ml, 2.5 mM). The final concentration of each dye was calculated theoretically, giving 0.096 mM for SQ1 and 1.5 mM for N719 and the ratio of SQ1:N719 was calculated to be (6.4% SQ1 c/c). But the real concentration for each dye was determined from the UV-Vis spectrum of the final solution (Figure 5.17). By using the molar extinction coefficient for each dye, which were determined in chapter three, the SQ1 concentration was determined from the peak at 636 nm to be 0.1 mM, and the N719 concentration was measured at 530 nm giving 1.8 mM. In this case the concentration ratio for SQ1:N719 was measured to be 5% which was used in this experiment. The dye uptake from this solution was then studied to try to understand the mechanism of mix SQ1:N719 loading on TiO_2 surfaces. The 5% SQ1:N719 was chosen because co-sensitizing TiO_2 by this ratio of dye has previously given best device efficiency.[14]

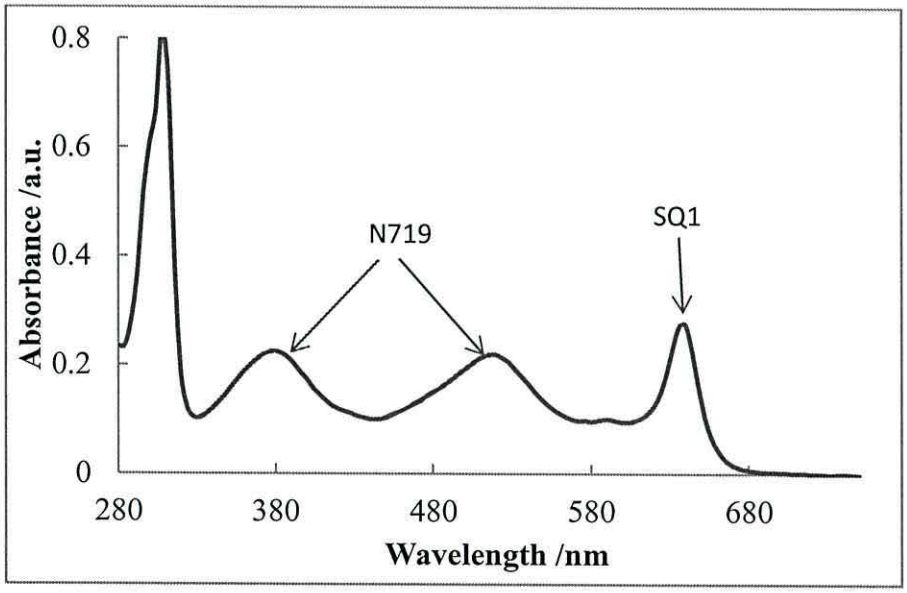

Figure 15.17: UV-Vis spectrum of the mixed stock solution 5 % SQ1:N719 (0.24 mM: 2.5 mM) diluted 100 times used for kinetic study of ultra-fast dyeing.

The ultra-fast adsorption of 5% SQ1:N719 at different dyeing times was then examined by measuring the dye loadings using selective desorption. First dye solution was pump dyed through a device cavity for a period of times at a rate 100 $\mu l.min^{-1}$. Then after each minute I_3^-/I^- electrolyte was added and the I-V was measured. To quantify dye loading after each minute, the N719 was desorbed using LiOH (100 µl, 100 mM), followed by desorbing SQ1 using Bu_4NOH (100 µl, 40 mM). The UV-visible spectrum for the dyes desorption were measured using UV-visible spectroscopy. Figure 5.18 shows the UV-Vis spectra of the N719 desorbed by LiOH with different time and Figure 5.19 shows the UV-Vis spectra of the SQ1 desorbed by Bu_4NOH at different dyeing times. The amount of dye adsorption for each dye at the specific time was then calculated from the absorbance of desorbed dye solution using the molar extinction coefficient of each dye. The surface coverage θ has also been estimated from the ratio of equilibrium maximum adsorption to the adsorption at time t. Thus, all the kinetic parameters of N719 adsorption from a mixed 5 % SQ1:N719 solutions are listed in Table 5.9, and the kinetic parameters for SQ1 are listed in Table 5.10.

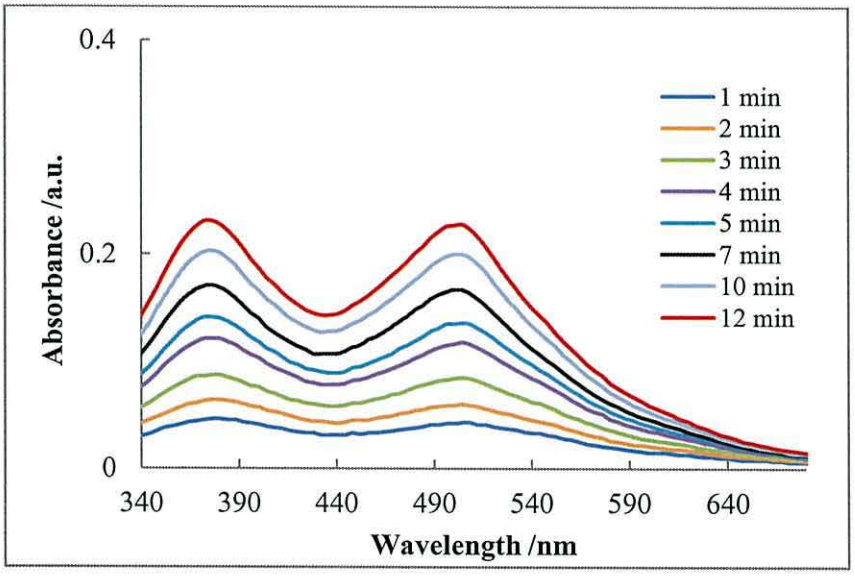

Figure 5.18: UV-Vis spectra for N719 desorbed N719 by LiOH (100 mM) from a DSL-18NRT device for different ultra-fast dyeing times as shown. Initial dyeing was from a 5% SQ1:N719 solution

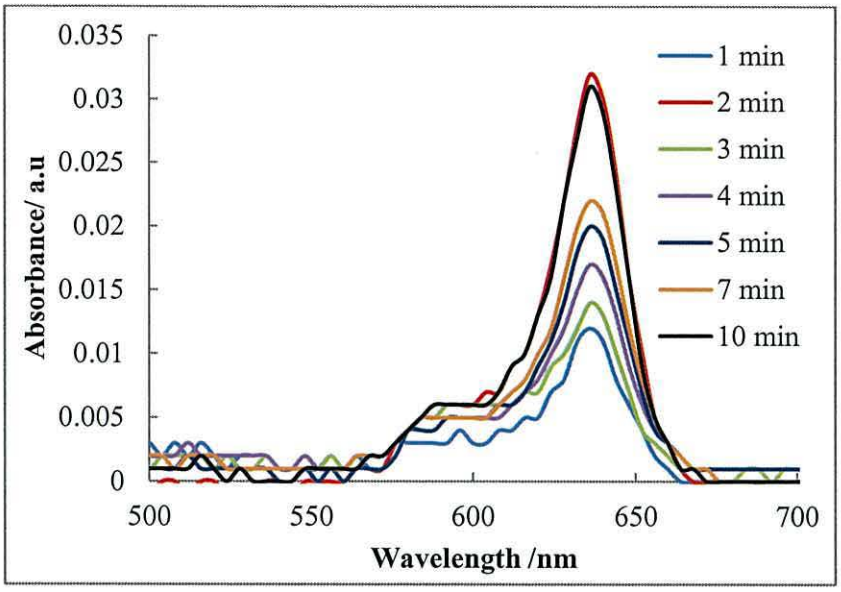

Figure 5.19: UV-Vis spectra for SQ1 desorbed by Bu_4NOH (40 mM) from a DSL-18NER device for different ultra-fast dyeing times as shown. Initial dyeing was from a 5% SQ1:N719 solution (2 ml, 0.24 mM: 3 ml, 2.5 mM).

Table 5.9: Kinetic data for N719 ultra-fast dyed from a mixed 5% SQ1:N719 (0.24 mM:2.5 mM) solution on a $1cm^2$ DSL-18NRT device.

Dyeing time (mins)	Abs	C_e for N719 ($mg.L^{-1}$)	q_t for N719 $\mu g.cm^{-2}$	θ	1-θ	ln(1-θ)	t/qt
1	0.039	4.87	48.75	0.17	0.83	-0.19	0.020
2	0.061	7.50	75.00	0.26	0.74	-0.30	0.026
3	0.085	10.62	106.20	0.37	0.63	-0.46	0.028
4	0.118	14.75	147.50	0.51	0.49	-0.71	0.027
5	0.136	17.00	170.00	0.59	0.41	-0.89	0.029
7	0.151	18.87	188.75	0.66	0.34	-1.08	0.037
10	0.166	20.87	208.75	0.73	0.27	-1.31	0.047
12	0.021	25.00	250.00	0.87	0.13	-2.04	0.048
16	0.231	28.85	285.00	1.00	0.00	E	0.059

Table 5.10: Kinetic data for SQ1 ultra-fast dyed from a mixed 5% SQ1:N719 (0.24 mM: 2.5 mM) solution on 1 cm^2 DSL-18NRT device.

Dyeing time (min)	Abs.	C_e for SQ1 ($mg.L^{-1}$)	q_t for SQ1 $\mu g.cm^{-2}$	θ	1 - θ	ln(1-θ)	t/q_t
1	0.011	0.044	0.44	0.37	0.63	-0.462	2.27
2	0.014	0.052	0.52	0.44	0.56	-0.579	3.84
3	0.017	0.062	0.62	0.52	0.48	-0.733	4.83
4	0.020	0.074	0.74	0.62	0.38	-0.967	5.4
5	0.022	0.081	0.81	0.68	0.32	-1.139	6.17
7	0.027	0.098	0.98	0.83	0.17	-1.77	7.14
10	0.031	0.114	1.14	0.96	0.04	-3.21	8.77
12	0.031	0.115	1.15	0.97	0.03	-3.506	10.43
16	0.032	0.118	1.18	1	0	E	13.55

The effects of dyeing time on the ultra-fast adsorption of N719 on TiO_2 are shown in Figure 5.20. The dye was rapidly adsorbed in the first 5 minutes because the dye molecules can find more unoccupied sites on the TiO_2 surface at the beginning of the adsorption. Then the adsorption rate gradually shows and reached a loading of 285 $\mu g.cm^{-2}$ after 16 min. However, according to the theoretical maximum sorption for N719 the TiO_2 surface does not appear to saturate by ultra-fast dyeing in this time frame. The effect of dyeing time on the adsorption of SQ1 from a mixed 5 % SQ1:N719 solution is shown Figure 5.21. The data show that the SQ1 dye was rapidly adsorbed in the first 5 minutes, and then the adsorption rate also decreased because there was no more space on theTiO_2 surface for dye to adsorb on it. However, the TiO_2 surface did not reach saturation by ultra-fast dyeing. The maximum amount of SQ1 adsorption by ultra-fast dyeing from mixed 5% SQ1:N719 was 1.18 $\mu g.cm^{-2}$, and the adsorption of mixed dye solution probably due to the particle charges.[15]

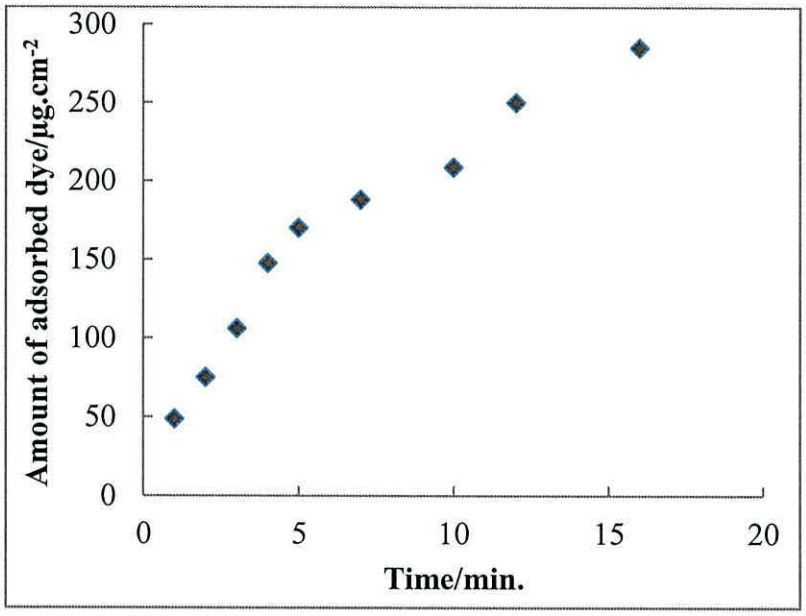

Figure 5.20: Effect of contact time for N719 ultra-fast from a mixed 5% SQ1:N719 (0.24 mM, 2.5 mM) solution on 1cm^2 of TiO_2 films, measured by selectively desorption of N719 by LiOH (100 mM).

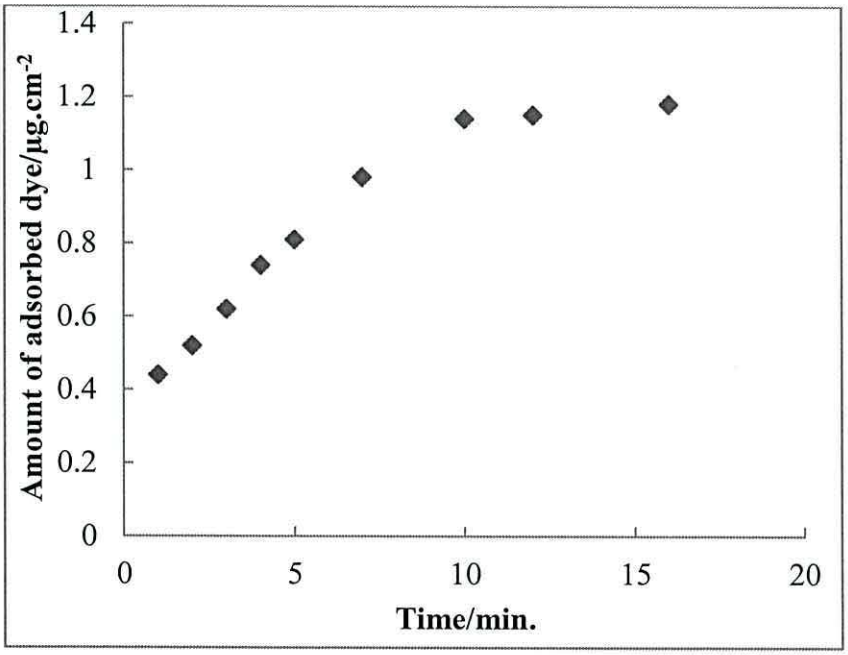

Figure 5.21: Effect of contact time for SQ1 ultra-fast dyed from a mixed 5% SQ1:N719 dye solution on 1cm^2 of TiO_2 films, measured by selectively desorption, of SQ1 by Bu_4NOH (40 mM).

5.6.2 Comparison of kinetic models for ultra-fast adsorption of N719 and SQ1 from a mixed 5 % SQ1:N719 solution.

Kinetic data for N719:SQ1 were analyzed using pseudo first-order and pseudo second order equations as discussed previously for N719:YD. For the determination of adsorption rate constants using the different kinetic models, the data in Tables 5.9 and 5.10 were used. The first-order rate constants were determined from a plot between ln(1-θ) *versus* time, (Figure 5.22) which shows k_1 equal to 0.153 min^{-1} for N719 and 0.301 min^{-1} for SQ1. The first-order rate constants for mixed 5% SQ1:N719 adsorption are similar to rate constants of mixed YD:N719 adsorption by ultra-fast dyeing which are qual to 0.173 min^{-1} for YD and 0.396 min^{-1} for N719.

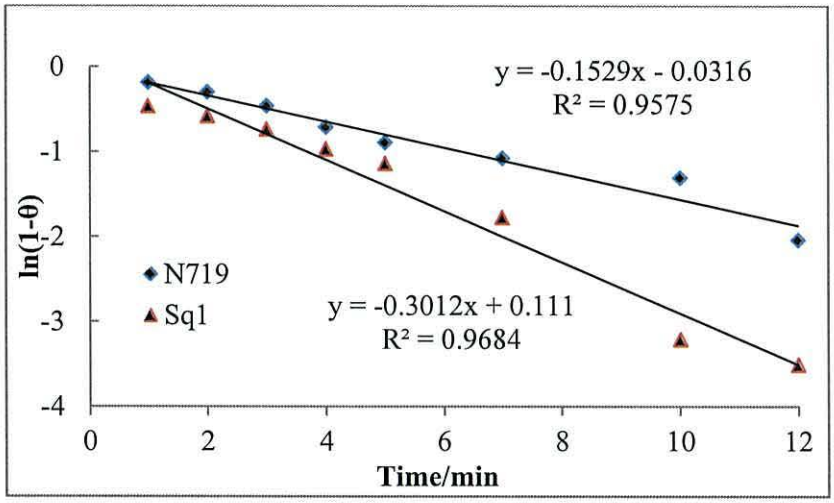

Figure 5.22: Plot of ln(1-θ) *versus* time based on a pseudo first order model for the ultra-fast dyeing of a mixed 5% SQ1:N719 (0.24mM:2.5 mM), [red triangles are for SQ1 , and blue squares are for N719].

The pseudo-second order kinetic model applied was also studied to determine the adsorption rate constants using the data in Tables 5.9 and 5.10. The second order rate constants were estimated from the plot of t/qt *versus* time (t). Figure 5.23 presents plot of the pseudo-second order kinetic for N719 adsorption and Figure 5.24 shows the equivalent data for SQ1 adsorption on TiO_2.

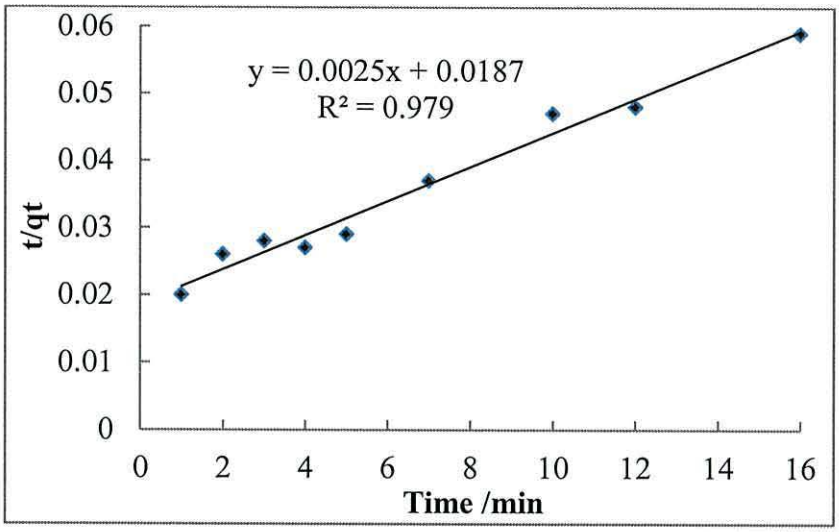

Figure 5.23: Plot of t/qt against time according to the pseudo- second order kinetic model for the ultra-fast adsorption of N719 from a mixed SQ1:N719 (0.24 mM: 2.5mM) solution on TiO_2.

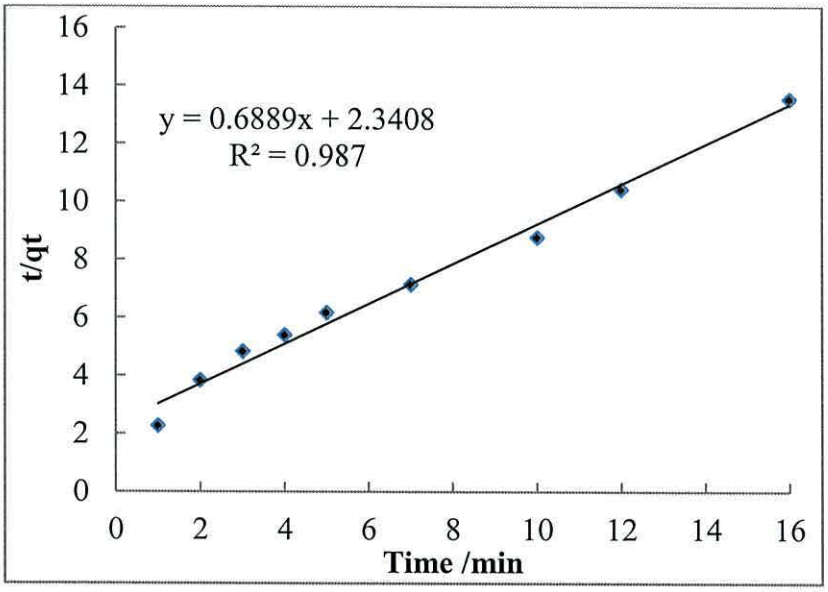

Figure 5.24: A Plot of t/qt *versus* time (minutes) according to the pseudo- second order kinetic model for the ultra-fast adsorption of SQ1 from a mixed 5% SQ1:N719 (0.24 mM: 2.5 mM) on TiO_2.

All kinetic parameters were determined for the pseudo-first and pseudo-second order plots and the data are presented in Table 5.11. The calculated value of q_e for SQ1 adsorption using the pseudo-second order model (1.45 $\mu g.cm^{-2}$) is in agreement with experimental data (1.18 $\mu g.cm^{-2}$) with (R^2 =0.987). However the calculation of q_e for N719 adsorption is 400 $\mu g.cm^{-2}$from the pseudo-second order model which is higher than experimental data (285 $\mu g.cm^{-2}$). This means the surface of TiO_2 does not reach saturation by ultra-fast dyeing for N719. The result shows a better linearity was obtained for the pseudo-second order model of the N719 and SQ1 adsorption on TiO_2 in a mixed 5% SQ1:N719. The rate constant k_2 of SQ1 is higher than k_2 of N719, which suggest that the adsorption of SQ1 on TiO_2 surfaces is faster than the loading N719 on the TiO_2 surface.

Table 5.11: Kinetic parameters for the ultra-fast adsorption of a mixed solution of 5%SQ1:N719 with initial concentration [N719 (3 ml, 2.5 mM) and SQ1 (2 ml, 0.24 mM)] in 10 mM CDCA at room temperature.

Dye	Pseudo-first order		Pseudo-second order		
	k_1 (min^{-1})	R^2	k_2 / $cm^2\mu g^{-1}$ min^{-1}	q_e/ $\mu g.cm^{-2}$	R^2
N719	0.153	0.958	3.3×10^{-4}	400.00	0.979
SQ1	0.301	0.968	0.203	1.45	0.987

5.6.3 Effect of adsorption time of 5%SQ1:N719 on DSC device measurements.

The cooperation of squaraine dyes which harvest red and near-IR light, and Ru(II) polypyridine complexes which absorbs blue and green light efficiency can lead to a more panchromatic sensitizing system for DSCs than for individual dyes[16]. The chemical interaction between the dye molecules and TiO_2 surface is important for the development efficiency in DSCs. Since the dye loading on TiO_2 surface depends on adsorption time, therefore the device performance should also vary with adsorption time. Figure 5.25 shows photocurrent-voltage curves for a TiO_2 device

dyed with 5% SQ1:N719 as a function of time. The relevant photovoltaic parameters are listed in Table 5.12. The data show that efficiency increases with increasing adsorption time due to increasing photocurrent density as a result of increasing dye uptake. Figure 5.26 shows the pictures of TiO_2 device dyed with 5 % SQ1:N719 over time. The device shows a blue colour during the first three minutes of dyeing, which suggests SQ1 adsorption is faster than N719. After five minutes, the device colour from becomes dark violet, because the amount of N719 adsorbed increases with increasing time.

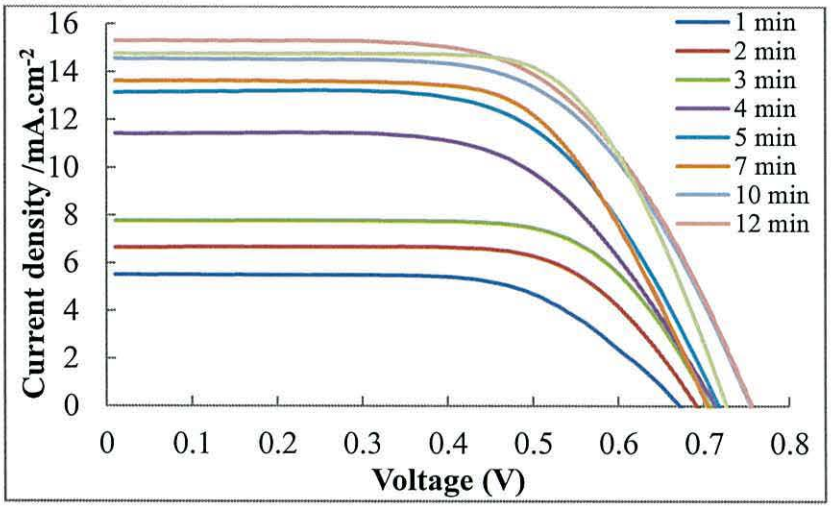

Figure 5.25: I-V data for ultra fast dyed DSC with a mix of 5% SQ1:N719 (0.24 mM :2.5 mM) solution as a function of dyeing time.

Table 5.12: Photovoltaic parameters for 1cm^2 of DSL-18NRT device ultra-fast dyed with a mix of 5% SQ1:N719 (0.24 mM: 2.5 mM) as a function of time. (Approximate errors on devices are ± 10% of the values shown).

time	η (%)	V_{oc} (V)	Jsc/ mA.cm^{-2}	FF	q_t N719/μg.cm^{-2}	q_t SQ1/μg.cm^{-2}
1	2.2	0.63	5.05	0.68	48.7	0.44
2	2.4	0.71	5.12	0.67	75.0	0.52
3	3.3	0.72	6.69	0.67	106.2	0.62
4	5.5	0.75	11.22	0.65	147.5	0.74
5	5.8	0.75	11.62	0.66	170.0	0.81
12	7.0	0.74	14.45	0.66	250.0	1.15
16	7.3	0.75	14.92	0.67	285.0	1.18

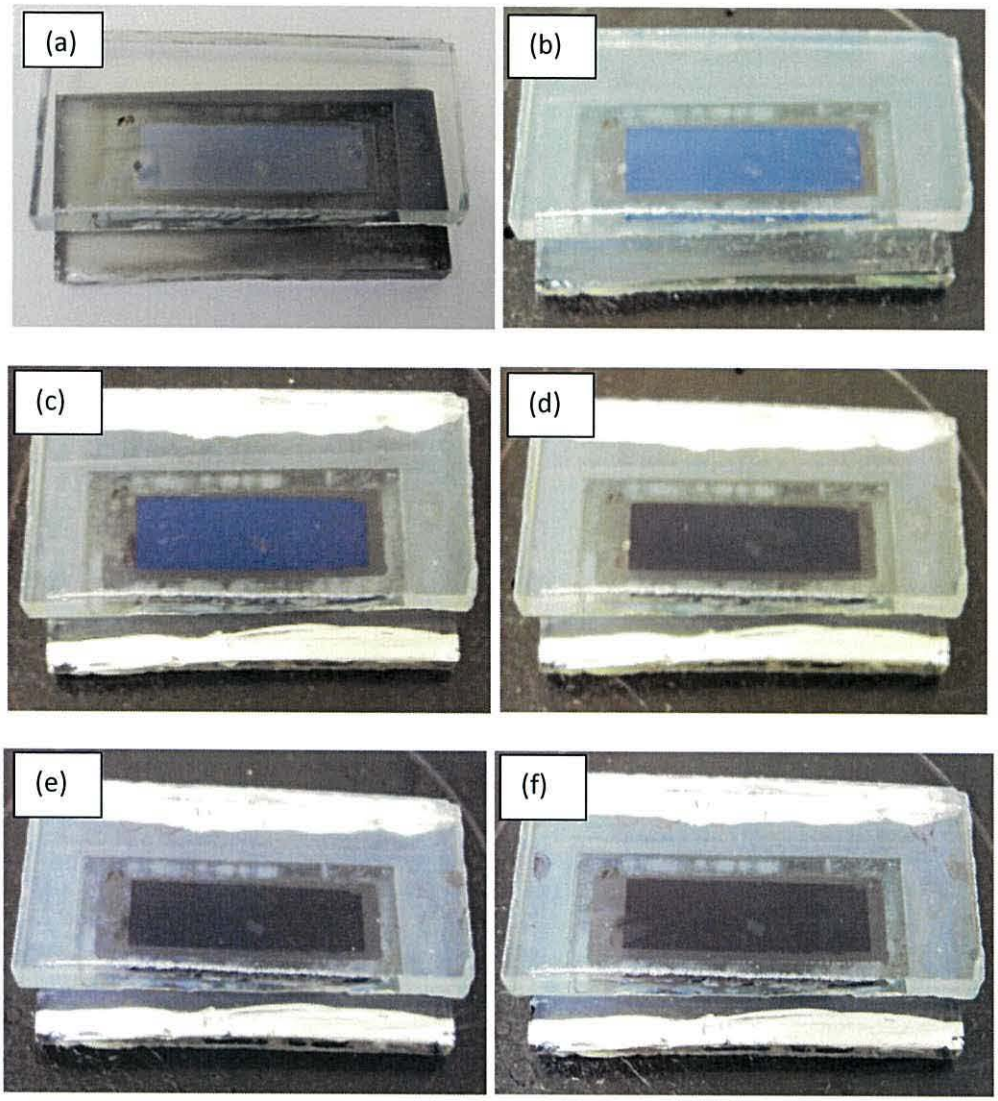

Figure 5.26: Photographs of a TiO_2 device (dimensions 0.5cm x2 cm) ultra-fast dyed with 5% SQ1: N719 solution (0.24mM: 2.5 mM) at different dyeing times (a) before dyeing (b) after 1 minute (c) after 3 minutes (d) after 5 minutes (e) after 10 minutes (f) after 16 minutes.

5.7 Conclusions

This chapter reports studies of the kinetics of dye sorption on TiO_2 surfaces from single and multiple dye solutions. The rate constants of YD adsorption by passive adsorption as well as ultra-fast dyeing have been found showing that the adsorption by passive dyeing follows a pseudo-second order model, whilst ultra-fast dyeing follows a pseudo-first order model. However, q_e by ultrafast adsorption is higher than the q_e by passive dyeing which may suggest that the pressure by pumping helps

to adsorb more dye molecule on the TiO_2 surface. A procedure for studying the kinetics of multiple dye sorption in a mixed N719:YD has been developed and studied using the selective removal of N719 by $LiOH_{(aq)}$ followed by desorption of YD using $Bu_4NOH_{(aq)}$ solution. The YD most closely followed a pseudo- second order model but N719 most closely followed pseudo-first order model suggesting that the shape and size of dye molecules may have affected adsorption. The kinetics for a mixed 5 % SQ1:N719 by ultra-fast dyeing on the TiO_2 device has also been studied using two different kinetic models. The adsorption of SQ1 and N719 onto TiO_2 from a mixed dye solution both followed a pseudo-second order model. The rate constant for each was determined to be 0.203 $cm^2\mu g^{-1}$ min^{-1} for SQ1 and 3.3 x 10^{-4} $cm^2\mu g^{-1}$ min^{-1} for N719. The effects of dyeing times on the photovoltaic measurements also have been studied for single and multiple dyes using ultra-fast dyeing technique suggesting that and the efficiency and photo-current increased with increasing dye loading because more dye molecules adsorbed on the TiO_2 surface leads to higher and more efficient electron injection to the TiO_2 conduction band. The data in this chapter show that the kinetics adsorption of mixed dye solutions can be successfully studied using ultra-fast selective desorption.

5.8 References

[1] B.E. Hardin, E. T. Hoke, P. B. Armstrong, J. H. Yum, P.Comte, T. Torres, J. M. J. Frechet, M. K. Nazeeruddin, M. Grätzel, M. D. McGehee, *Nature Photonics,* 2009, **3**, 406-411.

[2] V. Gusak, L. P. Heiniger, M. Grätzel, C. Langhammer B. Kasemo, *Nano Letters*, 2012, **12**, 2397-2403.

[3] A. H. Goff, S. Joiret, P. Falaras, *Journal of Physical Chemistry B*, 1999, **103**, 9569-9575.

[4] K. E. Lee, M. A. Gomez, S. Elouatik, G. P. Demopoulos, *Langmuir*, 2010, **26**, 9575-9583.

[5] K. S. Finnie, J. R. Bartlett, J. L. Woolfrey, *Langmuir*, 1998, **14**, 2744-2749.

[6] F. Hirose, K. Kuribayashi, M. Shikaka, Y. Narita, Y. Takahashi, Y. Kimura, M. Niwano, *Journal of Electrochemical Society*, 2009, **156**, B987-B990.

[7] L. E. Gibbings, V. Johansson, R. B. Walsh, L. Kloo, J. S. Quinton, G. G. Andersson, *Langmuir*, 2012, **28**, 9431-9439.

[8] E. M. McCash, in *Surface Chemistry*, 2001, Oxford University Press, Inc., NewYork, pp53-122.

[9] W. Rudzinski, W. Plazinski, *Environmental Science and Technology*, 2008, **42**, 2470-2475.

[10] Y. S. Ho, *Water Research*, 2006, **40**, 119-125.

[11] Y. S. Ho, *Scientometrics,* 2004, **59**,171-177.

[12] Y. S. Ho, and G. Mckay, *Journal of Chemical Engineering.,* 1998, **70**, 115-124.

[13] P. J. Holliman, M. Mohsen, A. Connell, M. L. Davies, K. AL-Salihi, M. B. Pitak, G. J. Tizzard, S. J. Coles, R. W. Harrington, W. Clegg, C. Serpa, O. H. Fontes, C. Charbonneau, M. J. Carnie, *Journal of Materials Chemistry*, 2012, **22**, 13318-13327.

[14] P. J. Holliman , M. L. Davies, A. Connell, B. V. Velasco, T. M. Watson, *Chemical Communications*, 2010, **46**, 7256-7258.

[15] J. D. Macedo, N. B. D. Junior, L. E. Almeida, E. F. D. Vieira, A. R. Cestari, I. D. Gimenez, N. L. V. Carreno, L. S. Barreto, *Journal of Colloid and Interface Science*, 2006, **298**, 515-522.

[16] C. Li, W. Wang, X. Wang, B. Zhang, and Y. Cao, *Chemical Letters*, 2005, **34**, 554-555.

Chapter six Conclusion

6.1 General conclusion and future work

The present study focused on the development of environmentally sustainable and low cost dye sensitized solar cells (DSCs). A summary of important conclusions, primarily based on the results presented in this thesis and the scope of future work for the device performance in DSCs.

6.2 Ultra-fast selective dyeing, desorption and re-dyeing

In summary, a novel adsorption, desorption and re-dyeing method using ultra-fast technique has been investigated. Mesoporous TiO_2 was prepared and the adsorption of N719 and SQ1 dyes on the as-prepared TiO_2 was studied. The equilibrium data have been analyzed using Langmuir and Freundlich isotherms and characteristic parameters for each isotherm have been determined. The Freundlich isotherm has been shown to give the best agreement for the SQ1 adsorption and the Langmuir isotherm fits better for the adsorption of N719. Desorption and ultra-fast re-dyeing through DSCs device has also been studied using different alkali solutions. Bu_4NOH has been used as the best alkaline for desorbing both of Ru-bipyridyl and organic dyes from the TiO_2 devices because the ability to removing both of Ru(II) complexes and organic dyes from TiO_2 device without any damage in TiO_2 films. The procedure was then developed to remove only partial amounts of dye by controlling the volume and concentration of Bu_4NOH. Ultra-fast re-dyeing with same dye or different dyes into the same device was then studied and formed to be successful. A new method for the highly selective removal of multiple dyes N719, SQ1 and D149 from a phoro-electrode was also studied. The result of this and the data shows that there is potential to reduce the amount of dye used within a photo-electrode with relatively less effect on device performance with obvious benefits for reducing cost. The method is also very versatile enabling ultra-fast re-dyeing for a wide range of

DSC dyes leading to ultra-fast multiple sensitizations of metal oxide photo-electrode films. Bu_4NOH has been chosen among different alkaline solutions as the best alkalis to remove the dye from TiO_2 surface without destroy the performance of the device. The dye loadings was also calculated for adsorbed on a TiO_2 photo-electrode and the result shows that the amount of N719 loaded is more than SQ1 loaded suggests that due to the deference in the shapes of N719 and SQ1 molecules which N719 show octahedral and SQ1 is linear. The dark current for the DSC device was also measured when dyeing, desorbed and re-dyed then compared with the device measurement in illuminated. The result shows an increased recombination of photo-generated carriers can lead to a significant loss in J_{sc} and V_{oc} increase in dark saturation current suggests that it takes time for dye molecules to absorb photon, so it might also take time for dye molecules to transfer those electrons to the carrier molecules. Other than that the TiO_2 particles in the carrier molecule would trap the electron this it might have delay the current. The device error also was studied for re-dyeing a device with N719 giving η of 4.6 ±1%. Re-using the device after re-dyeing as well as achieved the similar performance with the first dyeing. Selective removal also has been concluded for co-adsorption of different dyes on TiO_2. LiOH solution was successfully used to selective removal N719 from the device and also it is possible to selective removal SQ1 from the device dyed with SQ1 and D149 using dilute Bu_4NOH. This technique helps to improve DSC devices by co-sensitization method.

6.3 Ultra-fast co-sensitization

Chapter four in this thesis deals with the ultra-fast co-sensitization for two, three and four dyes with complementary absorption spectra on TiO_2 film to further enhance the light–harvesting ability DSC. Because using two methods to make a co-sensitization: co-sensitized in mixed dye solution with certain molar ratios of the dyes and sequential ultra-fast co-sensitization by adsorbed different dyes in a consecutive manner. Systems showed significant improvements in the active spectra and photocurrents compared with the cells based on individual dyes with most experiments. It was found that the ratio of dyes in mixed dye solution is important, the best ratio for mixing SQ1with N719 to make co-sensitization is 6% SQ1:N719

due to big differences in molar extinction coefficients which and the device is giving η 7.1% this performance superior to that of either individual device made from N719 (η = 6%) and SQ1 (η= 3.5%). It was found also the best ratio for mixing N719 with D149 is mix (1 mM) N719: (0.5 mM) D149 (1:3 v/v) showed an enhanced performance η = 8.2% relative to those of their individual dyes. Sequential ultra-fast co-sensitization was investigated to compare the adsorption power and order of dyeing effect in co-sensitization of two or more dyes. The results showing that the sequential ultrafast co-sensitization with order dye adsorption by YD then N719 achieved η = 7.4% which is higher than the co-sensitization by the order N719 then YD giving 6.7%. the selective removal of dyes such as desorbed N719 by LiOH and organic dye by Bu_4NOH and D149 by concentrated Bu_4NOH followed by acetone and ethanol have been used to balance the loading amount of dyes in co-sensitization and the process also provides an alternative choice for changing the sensitizers in the device. The ultra-fast co-sensitization with three dyes of mix N719:D149:SQ1 (1:1:0.1) was successfully, improved the device performance yielded (η =7.3%, J_{sc} = 15.5 mA.cm-2, V_{oc} = 0.71V and FF =0.65) over the individual sensitized SQ1, N719 and D149 devices with improvements in both J_{sc} and V_{oc}. We have briefly summarized the data for ultra-fast co-sensitization with two, three and four dyes into TiO_2 devices using different methods in the following Table 6.1.

Table 6.1: The I-V data for the device co-sensitized with different dyes of two, three and four dyes using ultra-fast dyeing.

Device Co-sensitized	η (%)	Voc/V	Jsc/mA.cm^{-2}	FF
N719 + Hf-SQ1	5.1	0.74	9.57	0.66
SQ2 +SQ1	3.4	0.6	8.86	0.64
6 % SQ1:N719	7.1	0.73	15.61	0.63
YD + N719	7.5	0.74	15.06	0.65
SQ1 + YD	4.0	0.71	8.35	0.65
D149 + YD	6.8	0.64	19.32	0.55
N719 +D149 (1:2)	8.1	0.71	18.31	0.62
N719 +D149 (1:3	8.2	0.72	16.58	0.63
N719:D149:SQ1	7.3	0.71	15.51	0.65
N719:D131:SQ1	6.3	0.76	14.34	0.58
N719:YD:SQ1	6.5	0.71	13.17	0.65
N719:YD: D149	7.5	0.72	15.90	0.65
N719:YD:RD	6.4	0.73	13.04	0.63
N719:D149:YD:SQ1	8.0	0.75	16.41	0.65
N719:D149:YD:SQ1	7.4	0.71	14.78	0.63
N719:D131:D149:SQ1	7.3	0.70	15.52	0.67

6.4 Kinetics study

This study demonstrated that the kinetic of dye sorption on TiO_2 surface were investigated using selective desorption in the process. The rate constant of YD adsorption by passively adsorption, also by ultra-fast adsorption methods were found both adsorptions follow to pseudo second order, however q_e by ultrafast adsorption is higher. The kinetic of multiple dye sorption of mix N719:YD and a mix of 5 % SQ1:N719 by ultra-fast adsorption on the device of TiO_2 films were investigated. It was found YD follow both of pseudo first order and pseudo second models in a mix dye solution, but N719 was fellow pseudo first order model. The results also show that both of pseudo first order and pseudo second models were fitted with the co-adsorption of N719 and SQ1 in a mix of 5% SQ: N719 dye solution A novel method

also has been developed to drive kinetic information about co-adsorption of multiple dyes on TiO_2 photo-electrode in DSC. The procedure is based on selective removal of dyes and quantifies the dyes loading separately. This approach enables processes to control dyes loading on TiO_2 which leads to DSC performance with co-sensitization.

6.5 Recommendations and future work

The DSCs are attractive renewable energy and all aspects related to DSCs have been subjected to improvement. However the work in this thesis needs more development and more characterization. Suggesting to study selective desorption for different sensitizers with different catalysts in detail which has a highly versatile applications. Sensitizers considered a heart of DSC device and the adsorption of dye on a semiconductor play an important role into the DSC performance. The DSC performance preferred one layer of dye adsorbed on wide band gap semiconductor of high surface area TiO_2 nanoparticles. This occurs when the dye molecules chemisorbed on the TiO_2 surface. Therefore it is necessary to study the factors affecting on the dye adsorption such as effect of solvent, temperature, surface area and ionic strength.

The DSC general use a solvent electrolyte based on acetonitrile or 3-methoxypropionitrile (MPN) and I^-/I_3^- redox couple electrolyte and have impressive energy conversion efficiencies reaching around 11%. However, some problems still exist for liquid electrolytes such as difficulty of sealing and leakage, and volatilization of the organic solvent. Thus, identifying redox shuttles to replace I^-/I_3^- is one of the most important problems in advancing DSC.

The other effective part in DSCs is semiconductor metal oxide usually used TiO_2. The dye coverage can be optimized by use of small amount of TiO_2 particle with high internal surface area by tuning the TiO_2 layer thickness. Thus, preparation a paste of layer double hydroxide helps to sintering in low temperature and also to improve J_{sc} with co-sensitization for light harvesting at different wavelengths.

Appendix

Appendix 1 Calibration curve data for N719 in ethanol λmax 532 nm.

Conc. N719/ $mg.L^{-1}$	Abs. at λmax 532nm
0	0
5	0.053
10	0.106
20	0.208
30	0.342
40	0.422
50	0.575
60	0.674

Appendix 2 Calibration curve data for SQ1 in ethanol at λmax 636 nm.

Conc. SQ1/ $mg.L^{-1}$	Abs. at λ max 636 nm
0	0
0.08	0.025
0.1	0.037
0.2	0.061
0.3	0.089
0.4	0.108
0.6	0.154
0.8	0.208
1.0	0.257
1.2	0.339
1.4	0.390

Appendix 3 Calibration curve data for N719 in 40 mM Bu_4NOH at 512 nm and 636 nm.

Conc. of N719 mg/L	Abs. at 512 nm	Abs. at 636 nm
0	0	0
5	0.037	0.005
10	0.073	0.008
20	0.154	0.016
30	0.235	0.021
40	0.325	0.030
50	0.422	0.039
60	0.523	0.045
70	0.663	0.062

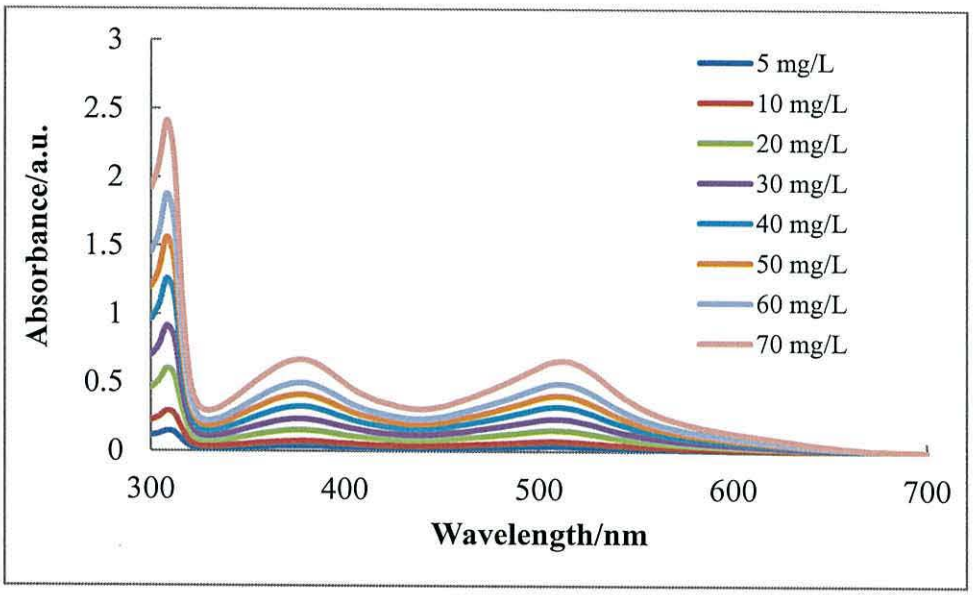

UV-Vis spectrum for different concentration of N719 in *tert*-butanol ammonium hydroxide

Appendix 4 Calibration curve data for N719 dye in 0.1M LiOH at 504 nm.

Conc. of N719 mg.L-1	Abs. At 504 nm
1	0.010
3	0.029
5	0.038
10	0.075
20	0.155
30	0.234
40	0.322
50	0.401
60	0.483
70	0.641

Appendix 5 Calibration Curve for YD in ethanol

Conc. of YD $mg.L^{-1}$	Abs at 380 nm
0.5	0.03
1	0.074
2	0.156
3	0.224
4	0.301
5	0.399
6	0.482
7	0.565
8	0.623
9	0.746
10	0.817

Appendix 6 Calibration curve data for D149 in *tert*-Butanol:Acetonitrile (1:1) at λmax 532 nm.

Conc. D149/ $mg.L^{-1}$	Abs. at λmax 532 nm
0	0
1	0.088
2	0.176
3	0.334
4	0.387
5	0.459
6	0.598
7	0.687
8	0.812
9	0.942
10	1.012

Appendix 7 Data of the amount of desorption N719 and SQ1 in different % SQ1:N719 by *tert*-Butyl ammonium hydroxide.

Desorbed dye	No.of TiO_2 film	5% SQ1:N719	10% SQ1:N719	20% SQ1:N719	40% SQ1:N719	50% SQ1:N710	60% SQ1:N719
N719	1	161.05	159.32	161.87	158.12	125.62	118.12
	2	158.25	154.25	158.25	146.56	130.11	113.75
	3	163.75	148.55	147.23	150.46	127.25	123.31
	Average	161.02	154.04	155.78	151.71	127.66	118.39
SQ1	1	0.85	2.23	4.91	8.28	10.59	12.42
	2	1.1	1.95	5.12	10.11	11.55	10.35
	3	1.2	2.40	3.55	6.45	7.32	14.77
	Average	1.05	2.19	4.53	8.28	9.82	12.51